YUTO S. TANAKA
EDITOR

DIAMOND-LIKE CARBON FILMS

MATERIALS SCIENCE AND TECHNOLOGIES

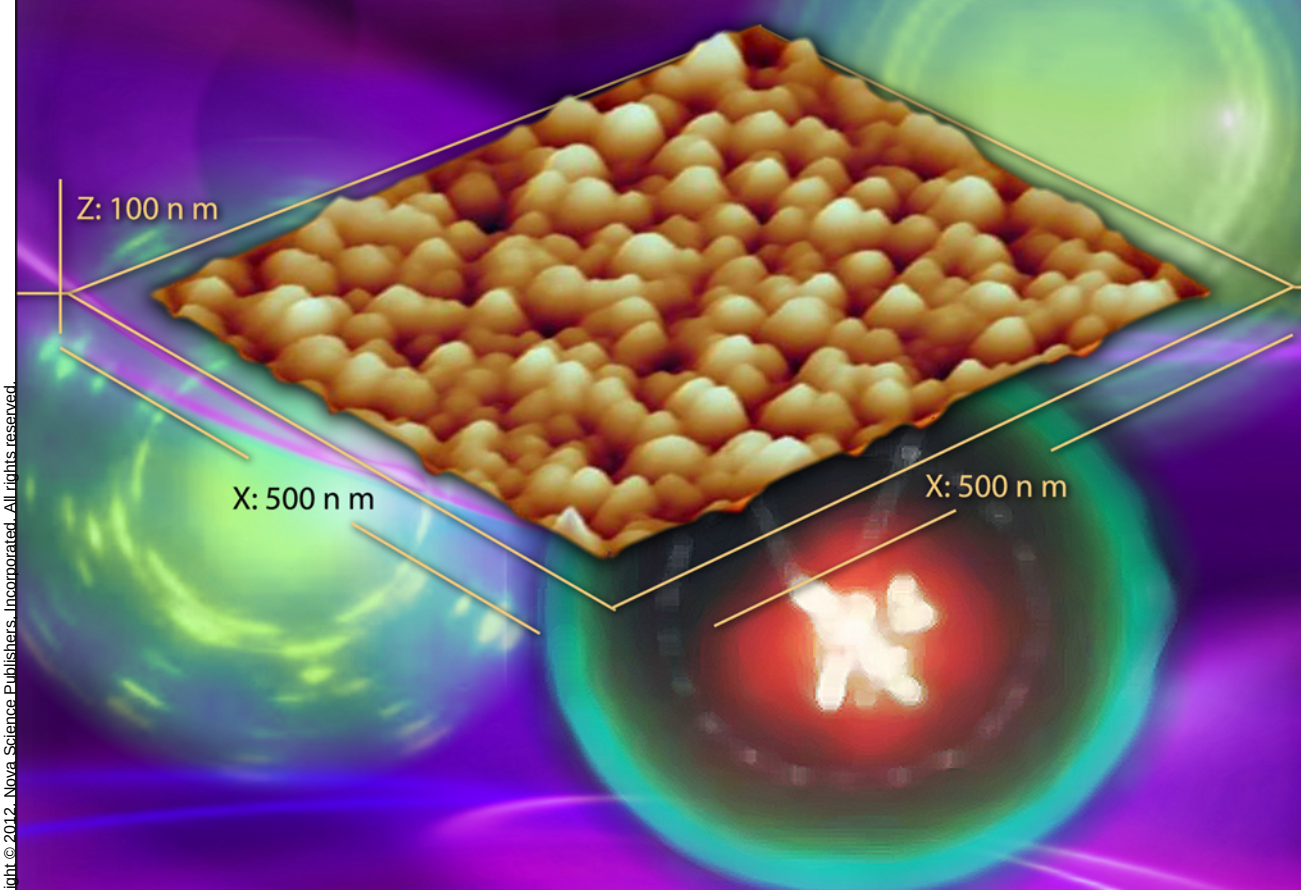

NOVA

Copyright © 2012. Nova Science Publishers, Incorporated. All rights reserved.

Copyright © 2012. Nova Science Publishers, Incorporated. All rights reserved.

Diamond-Like Carbon Films, Nova Science Publishers, Incorporated, 2012. ProQuest Ebook Central,

MATERIALS SCIENCE AND TECHNOLOGIES

DIAMOND-LIKE CARBON FILMS

No part of this digital document may be reproduced, stored in a retrieval system or transmitted in any form or by any means. The publisher has taken reasonable care in the preparation of this digital document, but makes no expressed or implied warranty of any kind and assumes no responsibility for any errors or omissions. No liability is assumed for incidental or consequential damages in connection with or arising out of information contained herein. This digital document is sold with the clear understanding that the publisher is not engaged in rendering legal, medical or any other professional services.

Copyright © 2012. Nova Science Publishers, Incorporated. All rights reserved.

Diamond-Like Carbon Films, Nova Science Publishers, Incorporated, 2012. ProQuest Ebook Central,

MATERIALS SCIENCE AND TECHNOLOGIES

Additional books in this series can be found on Nova's website
under the Series tab.

Additional E-books in this series can be found on Nova's website
under the E-books tab.

Copyright © 2012. Nova Science Publishers, Incorporated. All rights reserved.

Diamond-Like Carbon Films, Nova Science Publishers, Incorporated, 2012. ProQuest Ebook Central,

MATERIALS SCIENCE AND TECHNOLOGIES

DIAMOND-LIKE CARBON FILMS

YUTO S. TANAKA
EDITOR

Copyright © 2012. Nova Science Publishers, Incorporated. All rights reserved.

Nova Science Publishers, Inc.
New York

Diamond-Like Carbon Films, Nova Science Publishers, Incorporated, 2012. ProQuest Ebook Central,

Copyright © 2012 by Nova Science Publishers, Inc.

All rights reserved. No part of this book may be reproduced, stored in a retrieval system or transmitted in any form or by any means: electronic, electrostatic, magnetic, tape, mechanical photocopying, recording or otherwise without the written permission of the Publisher.

For permission to use material from this book please contact us:
Telephone 631-231-7269; Fax 631-231-8175
Web Site: http://www.novapublishers.com

NOTICE TO THE READER

The Publisher has taken reasonable care in the preparation of this book, but makes no expressed or implied warranty of any kind and assumes no responsibility for any errors or omissions. No liability is assumed for incidental or consequential damages in connection with or arising out of information contained in this book. The Publisher shall not be liable for any special, consequential, or exemplary damages resulting, in whole or in part, from the readers' use of, or reliance upon, this material. Any parts of this book based on government reports are so indicated and copyright is claimed for those parts to the extent applicable to compilations of such works.

Independent verification should be sought for any data, advice or recommendations contained in this book. In addition, no responsibility is assumed by the publisher for any injury and/or damage to persons or property arising from any methods, products, instructions, ideas or otherwise contained in this publication.

This publication is designed to provide accurate and authoritative information with regard to the subject matter covered herein. It is sold with the clear understanding that the Publisher is not engaged in rendering legal or any other professional services. If legal or any other expert assistance is required, the services of a competent person should be sought. FROM A DECLARATION OF PARTICIPANTS JOINTLY ADOPTED BY A COMMITTEE OF THE AMERICAN BAR ASSOCIATION AND A COMMITTEE OF PUBLISHERS.

Additional color graphics may be available in the e-book version of this book.

LIBRARY OF CONGRESS CATALOGING-IN-PUBLICATION DATA

Diamond-like carbon films / editor, Yuto S. Tanaka.
p. cm.
Includes bibliographical references and index.
ISBN 978-1-61324-909-3 (eBook)
1. Diamonds, Artificial. 2. Diamond thin films. I. Tanaka, Yuto S.
TP873.5.D5D58 2011
667'.9--dc23
2011017300

Published by Nova Science Publishers, Inc. + New York

Copyright © 2012. Nova Science Publishers, Incorporated. All rights reserved.

Diamond-Like Carbon Films, Nova Science Publishers, Incorporated, 2012. ProQuest Ebook Central,

CONTENTS

Preface		**vii**
Chapter 1	Advanced Pulsed Arc Technique of Fabrication of DLC Films and Their Technical and Medical Applications *N. Chekan*	**1**
Chapter 2	Peculiarities of Ion-Beam Synthesis of Carbon-Based Phases *D. I. Tetelbaum, A. N. Mikhaylov and A. I. Belov*	**39**
Chapter 3	Electron Field Emission Properties of Nonmetal and Metal Doped Diamond Like Carbon *Sk. Faruque Ahmed*	**63**
Chapter 4	Internal Stress of Hydrogenated Diamond-Like Carbon Films *Masahito Ban*	**95**
Chapter 5	Diamond-Like Carbon Films Improve their Properties with the Incorporation of Crystalline Diamond Particles *F. R. Marciano, E. C. Almeida, R. P. C. Costa, D. A. Lima-Oliveira, A. O. Lobo, E. J. Corat and V. J. Trava-Airoldi*	**119**
Chapter 6	DLC Thin Films Growth in Thermionic Vacuum Arc Technologies: TVA and GTVA *Rodica Vladoiu, Victor Ciupina, Mirela Contulov, Virginia Dinca, Aurelia Mandes and Madalina Prodan*	**141**
Chapter 7	Hard Cr-Containing Diamond-Like Carbon Films in Mid-Frequency Dual-Magnetron Sputtering *Yu Xiang, Wang Cheng-biao, Liu Yang and Yu De-yang*	**151**
Chapter 8	A Diamond-Like Carbon Film Applied as an Alignment Layer for LCDs *Yoshimine Kato*	**181**
Index		**199**

Copyright © 2012. Nova Science Publishers, Incorporated. All rights reserved.

Diamond-Like Carbon Films, Nova Science Publishers, Incorporated, 2012. ProQuest Ebook Central,

Copyright © 2012. Nova Science Publishers, Incorporated. All rights reserved.

Diamond-Like Carbon Films, Nova Science Publishers, Incorporated, 2012. ProQuest Ebook Central,

PREFACE

This book presents current research from across the globe in the study of diamond-like carbon films. Topics discussed include the peculiarities of ion-beam synthesis of carbon-based phases; electron field emission properties of nonmetal and metal doped diamond like carbon; internal stress and its reduction of hydrogenated diamond-like carbon thin films deposited by plasma CVD methods; incorporating crystalline diamond particles in diamond-like carbon films to improve their properties and diamond-like carbon films applied as an alignment layer for LCDs.

Chapter 1 - Cathodic arc plasma deposition can be used to obtain many metastable materials including non-hydrogenated DLC films. Despite the advantages of cathodic arc plasma deposition, it has not been largely used by industry due to reliability concerns that have evolved concerning the direct current (DC) powered cathodic arc processes. A pulsed arc method, which is the subject of this chapter, offers improved reliability, high level of plasma ionization and high energy of plasma particles, rather low content of graphite macroparticles in plasma stream that makes this deposition technology compatible with the commercial requirements like those satisfied by CVD technique whereas produce hydrogen free DLC films having high density and excellent hardness performances which related to the first type of DLC materials.

Chapter 2 - Ion implantation is a versatile and widespread approach for the synthesis of various materials. Recently, a particular interest has arisen in the application of ion beams to the fabrication of carbon-based nanostructures for the needs of nano-, optoelectronics and photonics. A distinctive peculiarity of the ion synthesis is its strongly expressed non-equilibrium character resulting in multiform structural transformations in the ion-implanted solids. In the present chapter, the principle of structural compliance of the new and parent phases has been, for the first time, formulated that allows to interpret and predict a type of the ion-induced transformations. The structural classification of the types of ion-beam induced phase transformations is suggested. The peculiarities of ion-beam synthesis and transformations are illustrated on several examples of carbon and carbon-rich phases: the face-centered cubic carbon, ion-synthesized films of SiC and Al_4C_3, etc. The literature and original data on the ion-beam synthesis of silicon carbide and other carbon-rich nanoclusters, mainly in SiO_2 matrix, are analyzed in comparison with similar nanostructures prepared by other techniques. It is concluded that the principle of structural compliance can be applied to some features of the ion synthesis of SiC and C nanoclusters, too. Special attention is paid to luminescent properties of the carbon-based nanostructures and to the relation of luminescence

Copyright © 2012. Nova Science Publishers, Incorporated. All rights reserved.

Diamond-Like Carbon Films, Nova Science Publishers, Incorporated, 2012. ProQuest Ebook Central,

bands to a phase composition of the layers. Some unsolved problems and the ways of further investigations are discussed.

Chapter 3 - Diamond like carbon (DLC) can be defined as a metastable phase of amorphous carbon (a-C) or hydrogenated amorphous carbon (a-C:H) containing a significant fraction of sp^3 hybridization. DLC has some extreme properties like diamond, such as high mechanical hardness, chemical inertness, dielectric strength, low wear and friction, optical transparency in the visible and infrared region, high electrical resistivity, high thermal conductivity and low electron affinity. Instead of these interesting properties, DLC films have several inherent problems, such as their high internal stress and low thermal stability. The high intrinsic stress generated in the film causes some serious problems in various applications of this material, like degradation of electrical and optical properties and leads to peel off the films from the substrate and poor adhesion. The ratio of sp^2/sp^3 carbon atoms is one of the most important factors determining the quality of the DLC films, which can be changed by incorporating different metal or nonmetal into DLC matrix. Metal and nonmetal doped DLC films have been an interesting field since last few years because, they have a great potential for solving some of the major drawbacks of pure DLC films. Various attempts have been made to dope DLC films with different nonmetals and metals such as nitrogen, iodine, boron, phosphorous, fluorine, gold, silver, titanium, tin, cupper etc. and the doping effects of these elements have been extensively investigated in terms of the chemical, electrical, optical and mechanical properties of DLC films. Doping of different elements in the DLC films reduced residual internal stress without sacrificing the hardness, leads to good adhesion to metal alloys, steels and glasses, improved high temperature stability, reduced hydrogen loss, graphitization and resistance to oxidation. Due to these noble properties of doped DLC, it has been studied in the last few years and has potential applications in many areas, such as electronic applications, solar cells, photoluminescence cells, optoelectronic devices, field effect transistor and high-temperature engineering materials. In this chapter, work done on synthesis, characterizations and electron field emission properties of metal or nonmetal doped DLC and diamond like nanocomposite materials will be discussed.

Chapter 4 - This paper reviews recent studies on an internal stress and its reduction of hydrogenated diamond-like carbon (DLC) thin films deposited by plasma CVD methods. Especially, focused on the DLC thin films prepared using CH_4 or C_6H_6 with varying deposition parameters by an electron-beam-excited plasma (EBEP) CVD system, the correlations between the internal stress and the structural properties such as the film density, total, bonded and unbound hydrogen contents, sp^3 ratio and graphite crystallite are discussed. As the result, it is found that the fraction of unbound hydrogen to total hydrogen content is the most influential factor for the compressive stress. The result implies that the insertion of unbound hydrogen, suggested to be into the disordered microstructure of graphite crystallites, can contribute to an increase in volume, and the strains by the expansion induce the compressive stress. Moreover, the internal stress reduction by incorporation of silicon into the DLC thin film is described. The Si-containing DLC thin films are deposited using $CH_4 + SiH_4$ by the EBEP-CVD system. From the relationships between the internal stress and the structural properties, it is found that Si-H bonds formed by silicon incorporation can play the role of reducing the compressive stress. It can be explained that the formation of Si-H bonds causes the relaxation of a three-dimensional rigid network of DLC thin film and the reduction in unbound hydrogen.

Copyright © 2012. Nova Science Publishers, Incorporated. All rights reserved.

Diamond-Like Carbon Films, Nova Science Publishers, Incorporated, 2012. ProQuest Ebook Central,

Chapter 5 - Diamond-like carbon (DLC) has been widely studied due to its mechanical properties such as low friction coefficient, high hardness, and high adherence on different substrate materials. The unique combination of chemical and mechanical properties of DLC films has opened the possibilities for the electrochemical applications of these film materials. In this chapter, a review of DLC films with extremally high hardness and very resistant to corrosion by incoporating crystalline diamond (CD) particles during the deposition process will be presented. These films were for the first time developed in our laboratories and the characterization performed will be also showed. The studies carried out in our laboratories show CD-DLC films improving DLC and stainless steel electrochemical corrosion resistance. CD-DLC prevented aggressive ions from attacking metallic surfaces, becoming a potential candidate for an anti-corrosion material in industrial applications, like pipelines in petroleum industry. It was also investigated the influence of the diamond particle sizes on the electrochemical corrosion resistance of these films. The electrochemical parameters obtained from the potentiodynamic polarization curves and the impedance were correlationated with the qualitative sp3/sp2 ratio of the CD-DLC films obtained from Raman scattering spectroscopy. The results show that both protection efficiency and impedance increase with the decrease of ID/IG ratio. It means the increase of sp3 bonds in DLC films reduce its electrochemical corrosion, improving the electrochemical protection efficiency and the impedance. In addition, diamond crystallites bigger than the DLC grain size reduced the pitting corrosion, which is an indication of the chemical inertness of the CD-DLC coatings to the Cl^- ions. The tribological behavior of these films under aggressive solution was also investigated. The presence of bigger CD particles increased the film roughness. In addition, these CD particles demonstrated to reduce DLC friction and wear. CD-DLC(500nm) films presented the lowest friction coefficient and wear rate under 5% NaCl saline solution. This result suggests the potential use of these films in aggressive environment even when suffer friction.

Chapter 6 - This work presents the comparative results concerning the surface free energy information processing, the reflective index, the hardness, and the morphology to provide a coherent description of the Diamond like Carbon films synthesized by Thermionic Vacuum Arc (TVA) and Gaseous Thermionic Vacuum Arc (GTVA). While in the TVA method the anode is solid, being suitable for deposition of the practically any solid material, the GTVA method enables the growth of DLC coatings using CH4 as gas precursor, in vacuum conditions. The main operational differences as well as the similarities between the two technologies are pointed out in this chapter, underlying the advantages in the development of advanced materials.

Chapter 7 - Diamond-like carbon (DLC) films have been extensively studied over the last two decades and applied as a good candidate for various sliding machine compnents and cutting tools, etc, due to their unique combined properties of high hardness, smooth surface and chemical inertness. Their inherent high compressive stresses induced during synthesis of their diamondlike content (sp3 carbon bonding), resulting in a low adhesion strength (especailly with ferrous substrates) and a thickness limit of 1μm, and their thermal stability, thermally unstable beyond 350 oC, are two major drawbacks of DLC films. Thereby, many scientific researches in the past decade have been concentrated on synthesizing metal-containing DLC (Me-DLC) films to overcome the two major drawbacks and, in turn, to improve the mechanical and sliding tribological behavior of DLC films. A number of studies

Copyright © 2012. Nova Science Publishers, Incorporated. All rights reserved.

Diamond-Like Carbon Films, Nova Science Publishers, Incorporated, 2012. ProQuest Ebook Central,

on synthesis and characterization of Me-DLC films have been conducted, and their studies mainly emphasized on Ti, W, Ta, and Cr containing DLC, especially on Ti and W. Although chromium has been used as carbide former and possesses attractive properties of combined hardness and ductility, available work in this area is still rather lacking and it is even rarer in mid-frequency dual-magnetron sputtering deposition. The purpose of this chapter is to intiate a systematic study of the processing-structure-property relationship in hard Cr-DLC films by a mid-frequency dual-magnetron sputtering system. The overall objective is to illustrate how to use methods of multilayer, gradient transitional layer, and doping to alleviate the two drawbacks, and then to synthesize an adherent thick Cr-DLC films of hard-and-lubricated property (micorhardness > 20 GPa, coefficient of friction < 0.2). This chapter is divided into four sections. Section 1 deals with using the system to prepare the Cr-DLC films that exhibited some combined superior properties: high hardness of 30~46 GPa, good adhesion of critical load of 50~65 N, and friction coefficient about 0.1 in air condition. Section 2 deals with comparing the mechanical and tribological propertis of some Cr-DLC films whose puttering sources had three optional power modes of continuous DC, pulsed DC and AC (40 kHz). Section 3 deals with a Cr-DLC film whose thickness up to 6 μm. Section 4 deals with the infulence of synthesizing method, Cr content, C/Cr nanocrystalline size, on the micorstructure and properties of hard Cr-DLC nanocompoiste films. In some cases, the presentation of experimental results is accopanied by a brief intorduction of the technique, so that non-experts will also be able to understand the main message of the proposed case.

Chapter 8 - Diamond-like carbon (DLC) films have been applied as an alignment layer for liquid crystal displays (LCDs). There are two ways to align the DLC films for liquid crystals (LC). One way is to use non-contact alignment processes on DLC such as ion beam (IB) or linearly polarized UV light. The other way is to use novel self-aligned DLC film. No alignment processes such as rubbing or atomic beam bombardment or UV irradiation on DLC are necessary. In other words, DLC itself is self-aligned for LC as deposited. In the first section, a DLC film which uses an additional alignment process is described, and in the second section a self-aligned DLC film without an alignment process is described. The DLC films which are used with non-contact alignment processes were deposited by chemical vapor deposition (CVD) or reactive DC magnetron sputtering on indium tin oxide (ITO) transparent electrodes on a glass. For this alignment process the DLC films can contain no or some hydrogen. The mechanism of liquid crystals (LC) alignment appears to be due to the C=C π bonds (sp^2) orientation of the alignment layer. Therefore, with the non-contact alignment processes π bonds on the DLC surface remain more in one direction. As a result, LC aligns on the DLC films. Many amorphous, transparent, and electrically insulated films were investigated, and DLC films were the first to be optimized. On the other hand, the self-aligned DLC films were deposited without hydrogen by using a DC magnetron in-line sputtering system only. The LC director alignment direction seems to be parallel to the substrate movement that is parallel to the magnetic field of the cathode and perpendicular to the plasma track line on the target during the in-line sputtering. The alignment mechanism of this DLC film seems to be related to the DLC crystalline structure that relates to the anisotropy of the π bonds orientation.

Copyright © 2012. Nova Science Publishers, Incorporated. All rights reserved.

Diamond-Like Carbon Films, Nova Science Publishers, Incorporated, 2012. ProQuest Ebook Central,

In: Diamond-Like Carbon Films
Editor: Yuto S. Tanaka
ISBN: 978-1-61324-791-4
© 2012 Nova Science Publishers, Inc.

Chapter 1

ADVANCED PULSED ARC TECHNIQUE OF FABRICATION OF DLC FILMS AND THEIR TECHNICAL AND MEDICAL APPLICATIONS

N. Chekan
Plasmoteg Research and Engineering Center of the Physical Technical Institute of the National Academy of Sciences of Belarus

Cathodic arc plasma deposition can be used to obtain many metastable materials including non-hydrogenated DLC films. Despite the advantages of cathodic arc plasma deposition, it has not been largely used by industry due to reliability concerns that have evolved concerning the direct current (DC) powered cathodic arc processes. A pulsed arc method, which is the subject of this chapter, offers improved reliability, high level of plasma ionization and high energy of plasma particles, rather low content of graphite macroparticles in plasma stream that makes this deposition technology compatible with the commercial requirements like those satisfied by CVD technique whereas produce hydrogen free DLC films having high density and excellent hardness performances which related to the first type of DLC materials [1].

1. DESIGN AND OPERATING PRINCIPLES OF THE PULSED PLASMA SOURCE

A pulsed arc plasma source developed in the PLASMOTEG Engineering Center is a new generation of such kind of plasma sources designed by Maslov and the others [2]. An outward appearance of the plasma source is given in Figure 1. The plasma source consists of the two main parts: (A) anode unit and (B) cathode unit. The basic element of the cathode unit is the main flange assembly. A bellows assembly is fixed on 'the atmospheric side' of the last one. The power feedthrough is cooled using water jacket placed on its atmospheric sides. This power feedthrough serves to provide a positive voltage on the ignition cathode unit. The main cathode output is mounted on the bellows assemble. The detachable main cathode is another

Copyright © 2012. Nova Science Publishers, Incorporated. All rights reserved.

Diamond-Like Carbon Films, Nova Science Publishers, Incorporated, 2012. ProQuest Ebook Central,

electrode of the couple of the main electrodes of the plasma source. It is a graphite consume electrode placed at the end of the plasma source. There is a possibility of axled moving of the main cathode but-and-ben. The moving is achieved by one of the two gear electric motors those are parts of the drive assemble. The cathode displacement is checked by the cathode position sensor. Another electrical motor is assigned to rotate an arbor and a gear unit placed on the 'vacuum part' of the arbor.

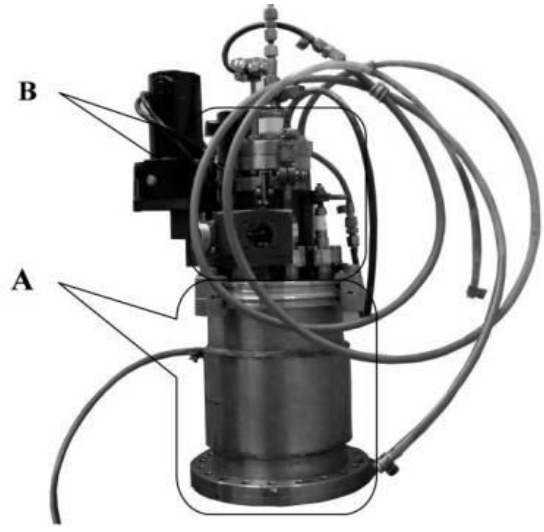

Figure 1. Pulsed arc carbon plasma source and its main parts: (A) anode unit and (B) cathode unit.

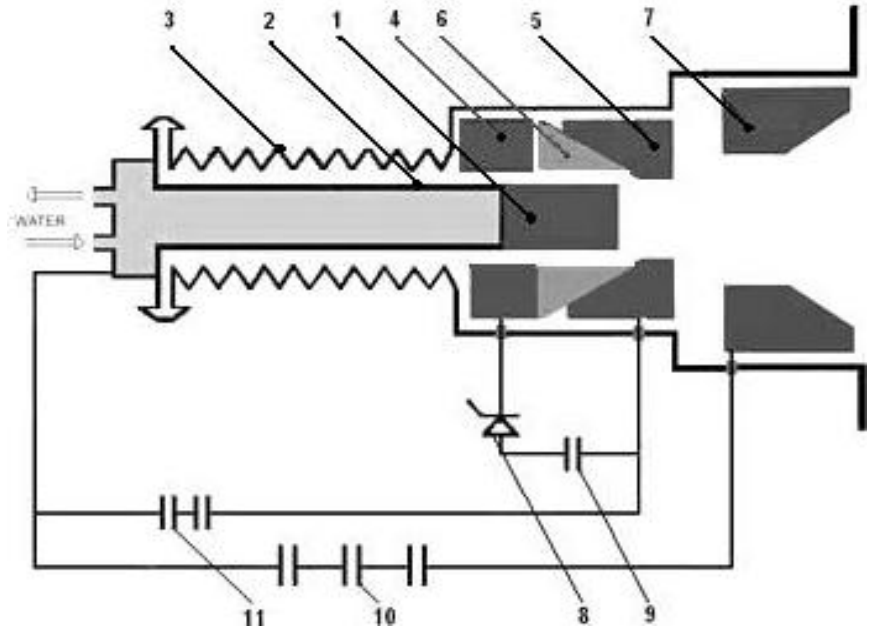

Figure 2. Draft diagram of the pulsed plasma source and its wiring diagram: (1) graphite cathode, (2) water cooled cathode holder, (3) bellow, (4) rotated ignition electrode, (5) stationary ignition electrode & auxiliary cathode, (6) ceramic insulator, (7) anode, (8) ignition thyristor, 9) ignition capacitor, (10) main capacitor bank, (11) auxiliary capacitor bank.

Copyright © 2012. Nova Science Publishers, Incorporated. All rights reserved.

Diamond-Like Carbon Films, Nova Science Publishers, Incorporated, 2012. ProQuest Ebook Central,

Plasma source work is based on evaporation and ionization of the material ejected from cathode spots while an arc discharge takes place. The plasma source is working in mode of the periodic arc discharge. To ignite the arc discharge in vacuum it is necessary to create a precursor density plasma. For this purpose, plasma source is equipped with a special ignition system. The main part of the system is a bearing assembly. The assembly consists of an ignition insulator and an ignition anode. An especial feature of this assemble is a hoop-like rotation of one of the ignition electrodes around the ceramic insulator that provides a high probability of an arc discharge following an ignition impulse as well as a uniform erosion of the graphite cathode.

The operation principles can be understood from the plasma source diagram in Figure 2. The ignition discharge in the located contact occurs after an actuating pulse is applied to the thyristor. The thyristor is located in the ignition unit of the power supply/control system set. Resistance of the located contact must be in the range from 1 Ω to 1500 Ω. A precursor plasma is generated as result of the ignition discharge.The plasma spreads in the gap between the main cathode and the auxiliary anode. It forms a conductive medium to get an auxiliary intense discharge to provoke arc spots on the cathode working surface. The intensive carbon evaporation from the cathode spots and ionization, the vapor created, leads to power arc between the main cathode and the main ring-like anode due to a discharge of the main capacitor bank. These processes repeated periodically with the use of actuating pulses to the thyristor. The pulse-periodic carbon plasma flows were generated as a result of arc sputtering of graphite cathode in vacuum (for residual pressures of down to 5 10^{-3} Pa) with the use of four-electrode arc system with a self-recovering thin-film conductor of the ignition device (discharge current of 4-10 kA, duration of pulses of 100-200 μs and the pulse repetition rate of up to 30 Hz). The carbon plasma generated at that is used to deposit diamond-like films.

The Main Result of the DLC Film Deposition by Pulsed Arc Technique

The designed plasma source was mounted onto vacuum machine UVNIPA 1-001 (Kvartz plant, Russia). It is a special vacuum machine to deposit DLC films in combination with refractory metals. In typical case of arc DLC technology, vacuum chamber is exhausted up to base pressure of 5×10^{-3} Pa, then an argon ion cleaning of WC-Co substrate was done within 15 minutes using a high energetic ion beam issued by a high voltage ion source at substrate bias of 1.5 kV. The deposition rate is about 600 nm per hour at the discharge impulse repetition rate of 5 Hz for non-rotated substrate placed in the center of the vacuum chamber (30 cm away from plasma source) is reached. The film density was evaluated by gravimetric measurement of 2.85…3.05 g/$cm^{3/}$. The film morphology examined by AFM is given in Figure 3. The film has very smooth surface with a low value of raphes parameters Ra = 0.2 nm, Rv-p = 16.0 nm on base distance of 5 μm.

The film structure revealed by X-ray photoelectron spectroscopy and Raman spectroscopy (XPS) is as almost four-fold coordinated sp^3 sites similar to diamond. In this sp^3 hybridized bond matrix, there are some a little amount of sp^2 bonded carbon atoms. As a typical C1s XPS peak and Raman spectrum is plotted in Figure 4 and Figure 5, respectively. The XPS spectra is combined by thee peaks placed at binding energy of 284.4, 285.3, and 288.6 eV corresponding sp^2, sp^3, and C-O bond respectively [3]. The content of sp^2 and sp^3

Copyright © 2012. Nova Science Publishers, Incorporated. All rights reserved.

Diamond-Like Carbon Films, Nova Science Publishers, Incorporated, 2012. ProQuest Ebook Central,

bond in this DLC film is about 47.4 and 44.3 %. Oxygen presence on the film surface mainly leads to formation of C-O bonds in quantity of 8.3%. If we take into account low film depth involved in XPS analyze, no more than few nanometers, as well as the fact that an upper layer of a DLC film is rich in graphite-like phase [4] then an actual ratio of sp^3 /sp^2 in the film is more higher in comparison with that determined by the XSP method.

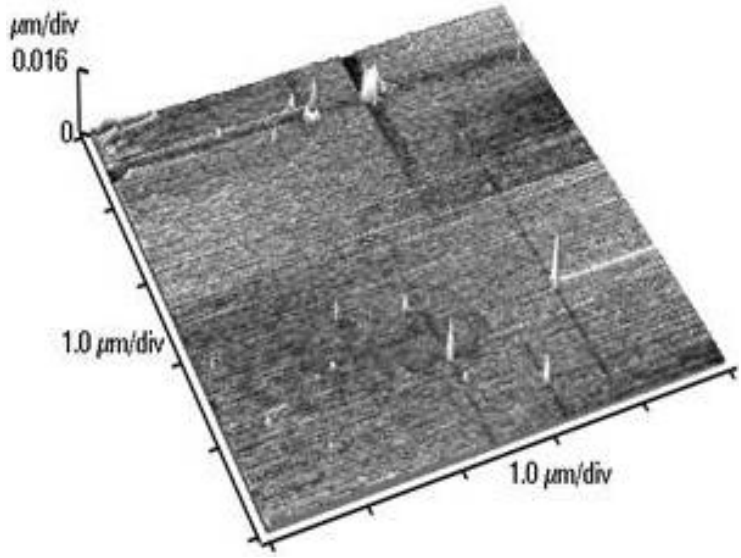

Figure 3.AFM image of the DLC film on silicon wafer.

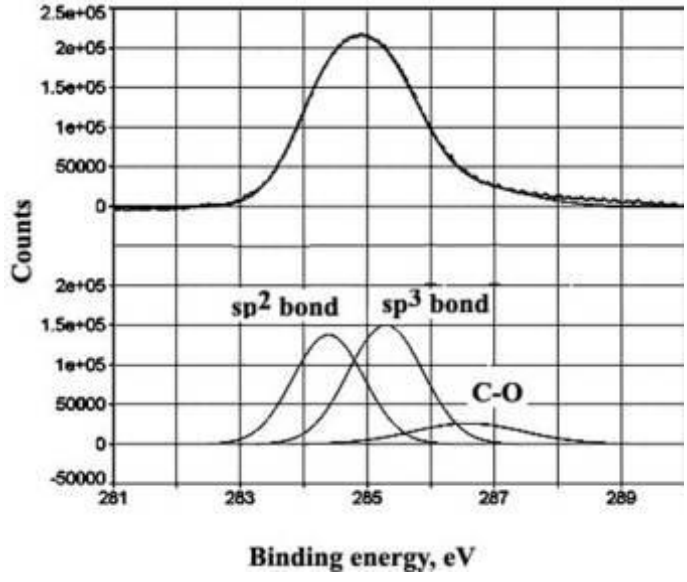

Figure 4.C1s XPS spectra of the DLC film prepared by the pulsed arc.

Copyright © 2012. Nova Science Publishers, Incorporated. All rights reserved.

Diamond-Like Carbon Films, Nova Science Publishers, Incorporated, 2012. ProQuest Ebook Central,

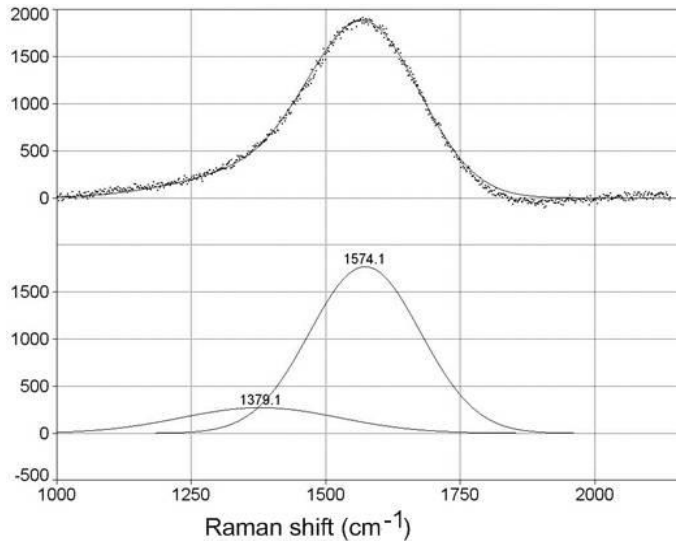

Figure 5. Raman spectra of DLC film deposited at discharge voltage of 300 V.

Raman spectrum of the DLC film deposited on a silicon substrate at the main discharge voltage of 300 V and capacitor bank capacity of 2400 μF is well symmetric one. Its deconvolution in D-peak located at 1376.9 cm^{-1} and G-peak located at 1565.4 cm^{-1} gives a possibility to estimate quality of a DLC films. One can see very low D-peak intensity, $I_{D,}$ in comparison with G-peak intensity, I_G. The I_D/I_G rate is 0.12. This parameter's value is an evidence of high content of diamond-type bonds in the DLC films which reached over 85% [5].

Among the mechanical properties of thin solid films, hardness and elastic modulus as well as toughness are the most important and valuable characteristics. The pulsed arc gives a possibility to deposit a very hard DLC coating without acceleration carbon ions using substrate bias. This circumstance is very important in many practical cases of film thickness homogeneity requirement for articles having sharp edges, prominences, protrusions.

One can see super hard evidence of these films in Figure 6 showing results of the hardness and elastic modulus determination by the nanoindentation test of the DLC film of 1 μm in thickness deposited on WC-Co substrate. The most meaningful hardness measurement is achieved at the indentation depth not more than 10% of the film thickness but more than 5% to avoid the influence of mistakes due to diamond pyramid tip deformation [6] and overcome a softer upper layer formed on the DLC film surface [7]. Reasoning from those the most reliable hardness for this film is about 85 GPa. Only few ion extract deposition methods yield such high hardness parameter for the tetrahedral amorphous carbon that belongs to the first type of DLC materials [8].The elastic modulus of the DLC film is close that of the natural diamond and its value is 970 GPa.

Toughness of solid films is very important parameter for their mechanical application. A possibility of a film to withstand again cracking formation under mechanical load is characterized by a combined parameter including hardness, H, elastic modulus, E, and Poisson's ration, ν: $H^3/(E/(1-\nu^2))^2$ Taking into account that ν = 0.2 for ta-C films [9], this parameter is 0.6 i.e. the DLC films exhibit the enough resistance to plastic deformation and crack formation [10].

Copyright © 2012. Nova Science Publishers, Incorporated. All rights reserved.

Diamond-Like Carbon Films, Nova Science Publishers, Incorporated, 2012. ProQuest Ebook Central,

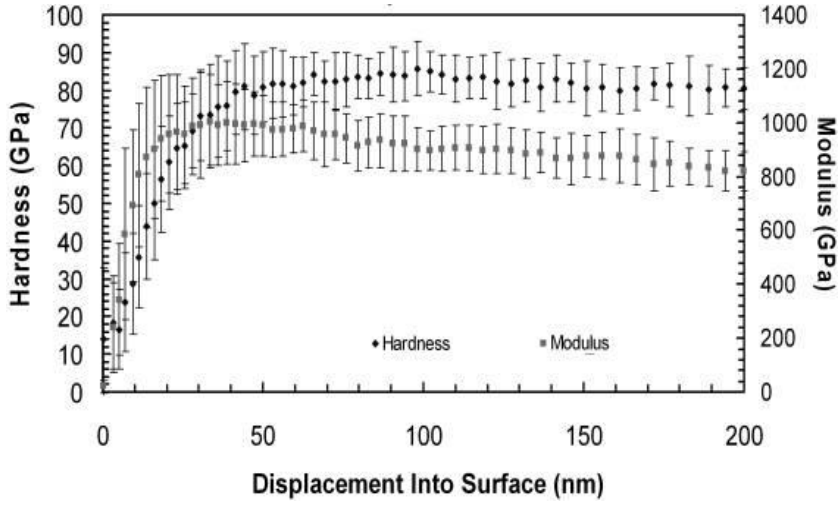

Figure 6. DLC hardness and elastic modulus determination by the nanoindentation method.

2. PLASMA SEPARATION

The big disadvantage of diamond-like carbon coatings deposited by arc methods is rather big carbon macroparticle content. Macroparticles are one of the components of cathode erosion at arc discharge. They are formed at the edges of cathode spots due to high plasma pressure in the strike of a cathode spot and they possess modified graphite structure. Graphite particle sizes are scaled from nanometer to micrometer. This quality failure is a serious obstacle to apply them in many areas like precision mechanics, MEMS, medicine solar cell. In medical implant application, they can act as nucleus of an undesirable protein and thrombocyte clots. Thus, the problem of macroparticles removal from plasma stream is quite topical.

There are some approaches to diminishing macroparticles number in plasma stream such as: a decrease of carbon macroparticles emission intensiveness by increasing velocity of travel of cathode spots on the cathode surface. It can be achieved by the influence of magnetic fields on cathode discharge area [11]; a decrease of carbon macroparticles flow density by using a short-time pulse vacuum-arc discharge causing decomposition of cathode spots into great number of small cathode spots, which quickly travel on the cathode surface [12]; an increase of relation of condensed ion flow density to carbon macroparticles flow density using magnetic focusing of plasma stream [13]; However, the most efficient way to remove theseparticles out of plasma stream is magnetic separation using magnetization of plasma and changing its movement trajectory which does not coincide with carbon macroparticles movement[14]. For practical purposes the used system of separation should be maximally efficient. To quantitatively estimate the efficiency of separation so called system coefficient, k, is used. It is a ratio of separated ion flow I_F to arc ion flow I_A [12].

The most wide-spread is the system of separation using toroidal magnetic tube [15]. A toroidal type separator usually has a form of a 45-90° curved magnetic tube with round or rectangular cross section. The separator with more complex shape as ‘S’ and double ‘S’ was used in the work [16]. A key problem of all the curved magnetic separators is low value of k.

Copyright © 2012. Nova Science Publishers, Incorporated. All rights reserved.

Diamond-Like Carbon Films, Nova Science Publishers, Incorporated, 2012. ProQuest Ebook Central,

Efficiency of plasma transfer in the systems with double curve of plasma-pipe is extremely low, and only 5÷8 % of input ion flow go to output plane of the separator. The power full water cooled 90°-curved separators generate magnetic fields of the high magnitude about 100 mT provide up to 30% of plasma transport effect [17].

Plasma separators can be placed outside and inside of a vacuum chamber. The latter are called separators of open type. They are used for quite big size vacuum chambers.

As it was mentioned above, the most wide-spread separators of plasma are curvilinear ones curved for 90^o (quarter-toroidal separators). Physical principle of their action is as follows: magnetized electrons while spiraling along curved field lines of the magnetic field due to coulomb interaction carry relatively heavy ions, for which Larmor radius is big and can exceed the diameter of the separator, with them. Neutral particles (graphite macroparticles and neutral carbon atoms) are not deflected by the magnetic field, they subside in special traps and on the walls of the separator and removed at a maintenance procedure.

In the pulsed cathode-arc plasma sources the feeding of magnetic deflective system is reasonable to be implemented in short periods of time of pulse discharge while a generation and injection of plasma takes place. Thus, it is reasonable to use inner a few-coil separators powered by the arc discharge current i.e. included in-turninto the chain of the main discharge. This system was designed at the PLASMOTEG Engineering Center (Belarus) and then was mounted on the special vacuum machine VDU-CI equipped with 4 pulsed arc carbon plasma sources described above.

The sketch of the 90^o-bended plasma separator is shown in Figure 7a. Structurally a corpse (1) of the separator represents itself a pipeline with 200 mm in diameter out of stainless steel direct-axis curved for 90^o, equipped with two flanges (2) for fixing to the vacuum chamber (3), and the source of pulse plasma (4). Structure of flanges is designed to make a separator be isolated from a pulse plasma accelerator and from a vacuum chamber in order to bias it. A negative bias voltage may be changed in the range of 20-80 V. There is a magnetic system inside the corpse of a separator consist of 9 copper coils (5). The cooper coils have a special geometrical form to reflect back the impacting macro particles.

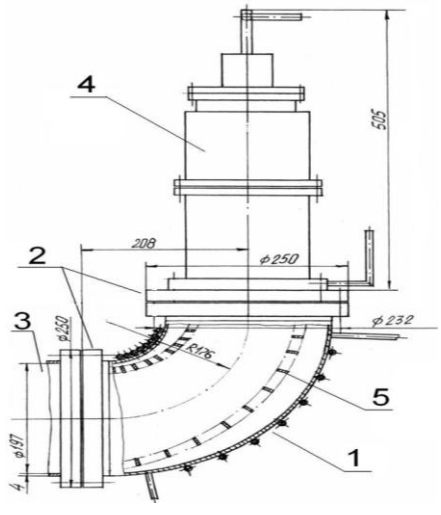

(a)

Figure 7. (continued)

Copyright © 2012. Nova Science Publishers, Incorporated. All rights reserved.

Diamond-Like Carbon Films, Nova Science Publishers, Incorporated, 2012. ProQuest Ebook Central,

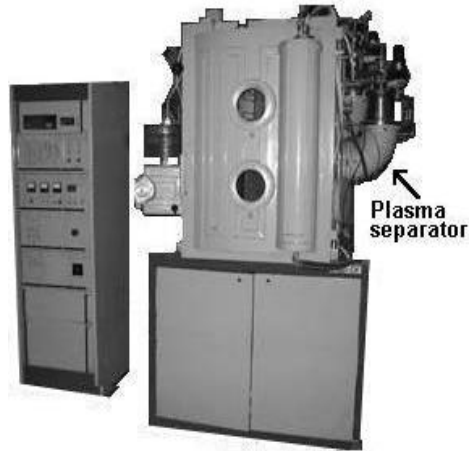

(b)

Figure 7.(a)Sketch of the 90^o -bended plasma separator attached to the pulsed arc source and (b) its appearance on vacuum machine VDU-CI: 1) separator corpse 2) electrically insulated flanges to fix to vacuum chamber (3) and arc source (4), 5) copper coil.

Magnetic field analyses and features of plasma transport through a curved separator. In this section, the magnetic fields and their influence of plasma travel are examined using as example of a 9-coil separator with inner diameter 115 mm and length of axial line 475 mm, which is uniformly curved for 90^o (Figure 7 b) close to that mounted onto vacuum machine VDU-CI which was manufactured as a pilot project by Smargon Plant of Optical Machine-Building (Belarus).

There are some problems with description magnetic field configuration of a curved solenoid consist of a few coil because of the low symmetry of such object. In this approach a special curvilinear coordinates were involved to describe magnetic field 'from first principles'.

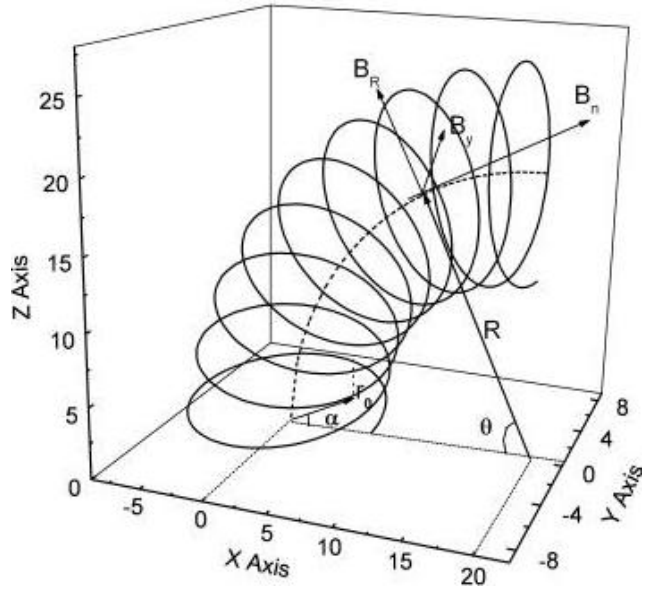

Figure 8.Scheme of quarter-toroidal small-coil plasma separator and main coordinates for it description.

Copyright © 2012. Nova Science Publishers, Incorporated. All rights reserved.

Diamond-Like Carbon Films, Nova Science Publishers, Incorporated, 2012. ProQuest Ebook Central,

A mathematical expression describing the form of the spiral with radius r_s, that is uniformly curved in one plane and that has radius of curvature of axial line R(see Figure 8), can be written down in the parametric form as follows:

$$x = R - (R - r_s \cos\alpha)\cos\left(\frac{\alpha}{4n}\right)$$
$$y = r_s \sin\alpha$$
$$z = (R - r_s \cos\alpha)\sin\left(\frac{\alpha}{4n}\right) \quad (1)$$

where n is a number of spiral coils, α is an angle between axis x and direction for projection of a point of non-curved spiral onto XY plane ($0 \le \alpha \le 2\pi n$).

An element of the coil of separator dl in the distance that is given by vector D creates magnetic magnetic field strength***dB***

$$d\vec{B} = \frac{\mu_0}{4\pi} I \frac{d\vec{l} \times \vec{D}}{D^3}, \quad (2)$$

where μ_0 is magnetic permeability of vacuum, I is a current in the separator.

To simplify the further calculations the coordinates of arbitrary point A(X,Y,Z), in which a magnetic field is calculated, as well as the coordinates of the spiral are useful to set parametrically as follows:

$$\mathrm{X} = \mathrm{R} - (\mathrm{R} - \mathrm{r}\cos(\beta + \delta))\cos\left(\frac{\beta}{4\mathrm{n}}\right)$$
$$\mathrm{Y} = \mathrm{r}\sin(\beta + \delta)$$
$$\mathrm{Z} = (\mathrm{R} - \mathrm{r}\cos(\beta + \delta))\sin\left(\frac{\beta}{4\mathrm{n}}\right) \quad (3)$$

This form of coordinates presentation enables research of a magnetic field along a virtual spiral of radius r having a step that equals the step of the real spiral with current and identically curved. Parameter δ is an angle of the set phase displacement of the "coordinate" spiral. New coordinates r, β and δ definitely determine the position of any point of the space. In the chosen curvilinear system of coordinates vector ***D***will be determined by the expression as follows:

$$\vec{D} = r_0 \begin{Bmatrix} \cos\tilde{\alpha}(a - \cos\alpha) - \cos\tilde{\beta}(a - \rho\cos(\beta + \delta)); \\ \rho\sin(\beta + \delta) - \sin\alpha; \\ \sin\tilde{\alpha}(\cos\alpha - a) + \sin\tilde{\beta}(a - \rho\cos(\beta + \delta)) \end{Bmatrix}, \quad (4)$$

Copyright © 2012. Nova Science Publishers, Incorporated. All rights reserved.

Diamond-Like Carbon Films, Nova Science Publishers, Incorporated, 2012. ProQuest Ebook Central,

where $a = R / r_0$ is aspect relation, $\rho = r/r_0$ is reduced "radial" distance, $\tilde{\alpha} \equiv \alpha/4n, \quad \tilde{\beta} \equiv \beta/4n$

Due to the peculiarities of geometry of a curvilinear separator, to be evident it is advisable to divide the magnetic induction vector into three orthogonal components: normal component B_n tangentially directed to the axial line, radial component B_R directed round radius R, and component B_y along axis Y (Figure 8). The first of these components is the most important one for the operation of a separator. It ensures the movement of plasma along the separator. As it will be seen from the further analysis the other two components are small in comparison with B_n. Out of (2) taking into account the chosen geometry of the separator we have the expressions of vector ***B*** components with the accuracy of multiplier $\frac{\mu_0}{4\pi} I \frac{1}{\vec{D}^3}$ as:

$$\begin{aligned} dB_n &\propto \left(dl \times D\right)_n = (dl \times D)_x \sin\tilde{\beta} + (dl \times D)_z \cos\tilde{\beta}; \\ dB_R &\propto \left(dl \times D\right)_R = (dl \times D)_z \sin\tilde{\beta} - (dl \times D)_x \cos\tilde{\beta} \\ dB_y &\propto \left(dl \times D\right)_y \end{aligned}, \qquad (5)$$

Expressions (1 - 3) enable calculating the components of a magnetic field induction vector created by a curved spiral:

$$\vec{B}_i = \frac{\mu_0}{4\pi r_0} I \int_0^{2\pi n} \frac{f_i(\alpha)}{F(\alpha)^{3/2}} d\alpha \;, \qquad (6)$$

where i = n, R, z,

$$\begin{aligned} f_n = {} & (\rho\sin(\beta+\delta) - \sin\alpha)\left[\tfrac{1}{4n}(a-\cos\alpha)\sin\left(\tilde{\alpha}-\tilde{\beta}\right) - \sin\alpha\cdot\cos\left(\tilde{\alpha}-\tilde{\beta}\right)\right] + \\ & + \cos\alpha\left[a - \rho\cos(\beta+\delta) - (a-\cos\alpha)\cos\left(\tilde{\alpha}-\tilde{\beta}\right)\right]; \end{aligned}$$

$$\begin{aligned} f_R = {} & (\rho\sin(\beta+\delta) - \sin\alpha)\left[\tfrac{1}{4n}(a-\cos\alpha)\cos\left(\tilde{\alpha}-\tilde{\beta}\right) + \sin\alpha\sin\left(\tilde{\alpha}-\tilde{\beta}\right)\right] + \\ & + (a-\cos\alpha)\cos\alpha\sin\left(\tilde{\alpha}-\tilde{\beta}\right); \end{aligned}$$

$$\begin{aligned} f_z = {} & \tfrac{1}{4n}\left[(a-\cos\alpha)^2 - (a-\cos\alpha)(a-\rho\cos(\beta+\delta))\cos\left(\tilde{\alpha}-\tilde{\beta}\right)\right] + \\ & + (a-\rho\cos(\beta+\delta)\sin\left(\tilde{\alpha}-\tilde{\beta}\right) \end{aligned}$$

$$\begin{aligned} F = {} & 1 + \rho^2 - 2\rho\left(\sin\alpha\sin(\beta+\delta) + \cos(\beta+\delta)\cos\alpha\cos\left(\tilde{\alpha}-\tilde{\beta}\right)\right) + \\ & + 2a(a-\cos\alpha-\rho\cos(\beta+\delta))\left(1-\cos\left(\tilde{\alpha}-\tilde{\beta}\right)\right), \end{aligned}$$

The results of numerical integration (6) as graphs are shown in Figure 9. Figure 9(a) represents a dependence of specific (per an ampere) value of the normal component of the vector of magnetic induction on the angle θ in the different distances from the separator axis

Copyright © 2012. Nova Science Publishers, Incorporated. All rights reserved.

Diamond-Like Carbon Films, Nova Science Publishers, Incorporated, 2012. ProQuest Ebook Central,

indicated in the Figure8 in relative (r/r_0) values for the separator with inner diameter 115 mm. The negative sign corresponds to a distance in the direction of concave (pressed) side of the separator and the positive sign corresponds to a distance in the direction of convex (stretched) one.Occurrence of components B_y and B_R inside the separator is caused by low density of coils and its curvature. These components cause a drift of electrons and ions to the walls of the separator and a decrease its transfer capability. As it can see in these figures, the normal component of the vector $\boldsymbol{B}$ exceeds in value the two other components in the whole separator space except for the areas near the input/output of the separator where the radial component is comparable with the normal one, however, $B_R$quickly goes down at the output of the separator.

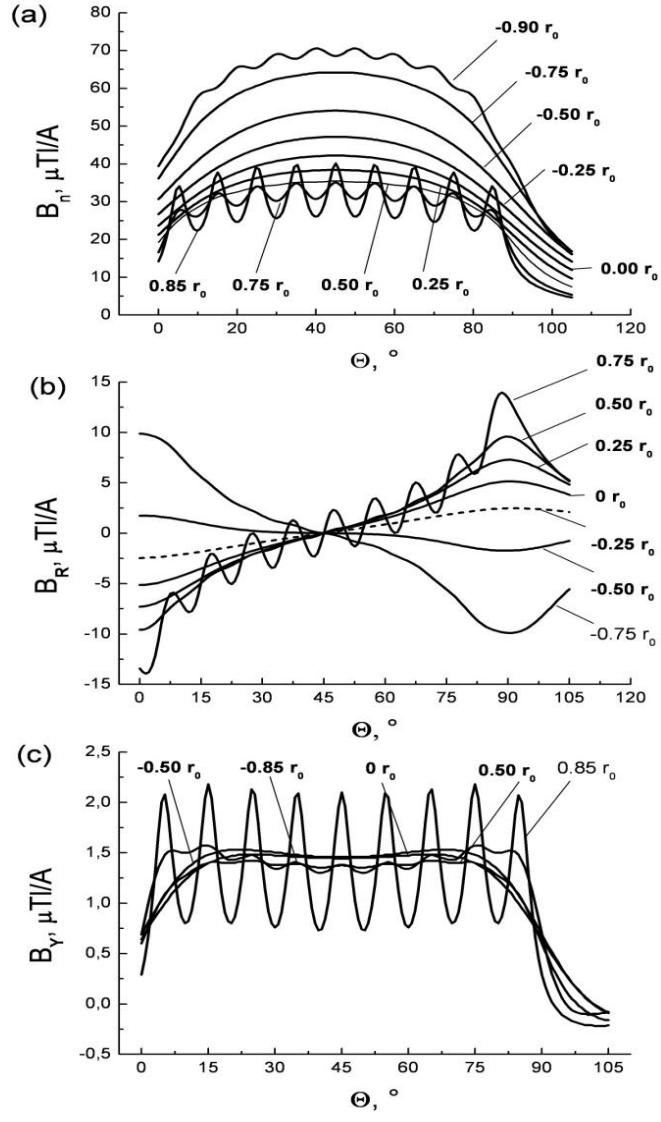

Figure 9.(a) Normal, (b) radial and (c) and (c) Z component of the magnetic in side if the separator at different distance from separator center represented in its radius rate in convex direction ("+") and concave direction ("-").

Copyright © 2012. Nova Science Publishers, Incorporated. All rights reserved.

Diamond-Like Carbon Films, Nova Science Publishers, Incorporated, 2012. ProQuest Ebook Central,

Further on the main attention will be drawn to the analysis of the normal component of vector ***B***. Normal component *Bn*significally changes along the axis of the separator. The value of magnetic field induction at input and output of the separator amounts at 54 % from the corresponding value in its centre. The largest non-uniformity of the field is in the area near the concave (inner) side of the separator. In immediate proximity of the separator's coils an oscillate character of changing of *Bn* appears being caused by prevailing influence of the magnetic field of the nearby local current areas. Oscillations of *Bn* go down while approaching the separator's axial line and they practically disappear in distances comparable with intervals between the coils amounted at 13 mm and 30 mm for inner (concave) and outer (convex) sides of the separator, correspondingly.

The obtained expressions in explicit form for the components of magnetic field strengthsallow constructing a figure of field lines of the separator's magnetic field represented in Figure10. In spite of small quantity of the separator's coils the field lines practically coincide with concentric circles of the radii of the separator's curvature, except for the areas in immediateproximity from the separator's coils and at its input and output. An angle φ between the axial and field lines, passing through the separator, draws the attention. For the chosen configuration of the separator it is 10˚. In the result of it there should be displacement of the centre of deposited coating. A difference in density of the magnetic lines indicates a gradient of the magnetic field in the direction of radius of curving R from outer to inner side of the separator. Figure 11 shows a dependence of magnetic field size and its gradient in the centre of the separator on diameter of its coils $2r_0$. Unlike an extensive separator with high density of coils, the magnetic field strength of a small-coil separator varies with the change of coil diameter. A more sensitive parameter in this relation is a gradient of value of magnetic induction vector. The gradient causes a drift of electrons and ions in the direction of the normal to the plane passing through vector ***B*** and *grad B*, i.e. in the direction of axis Y to the walls of the separator and it can decrease transfer capability of such kind of separators.

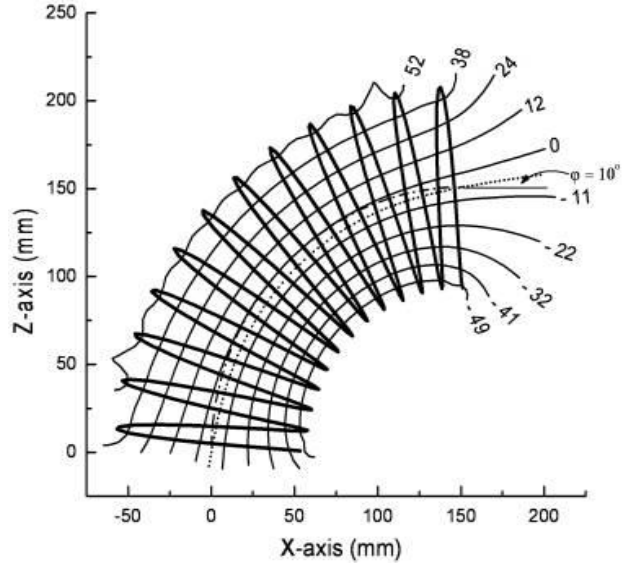

Figure 10. Magnetic field lines of a low-coil separator.

Copyright © 2012. Nova Science Publishers, Incorporated. All rights reserved.

Diamond-Like Carbon Films, Nova Science Publishers, Incorporated, 2012. ProQuest Ebook Central,

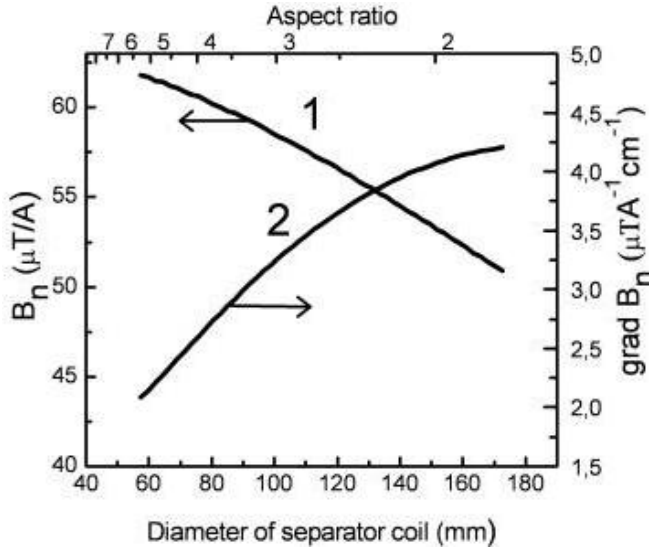

Figure 11. Dependenceof(1) magneticinductionvector value and (2) gradient of magnetic field on separator coil diameter.

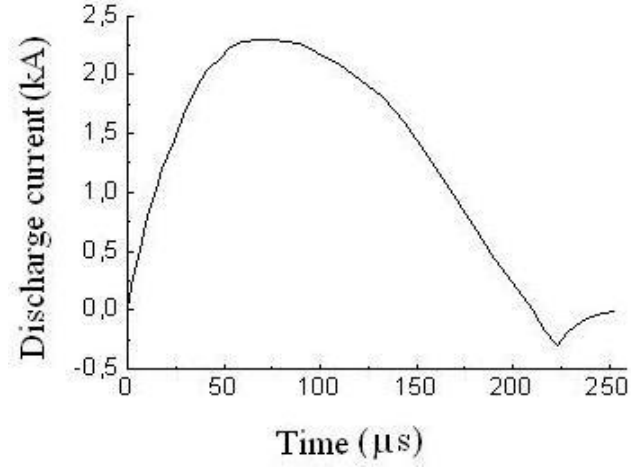

Figure 12. Oscillogram of the arc discharge current.

Thus, separator's magnetic field configuration is such as there should be displacement of plasma stream in the both direction of outer side of the separator and perpendicularly to the axis of the separator. This phenomenon was for the first time described by researchers from the Fraunhofer Institute [18] without explanation of the physical reasons for its appearance.

To create more uniform magnetic field one should use narrower separators. Narrow separators are more preferable for one more reason: the field strength there is higher. Thus, for a separator to be operated efficiently, a diameter of input cavity of a separator should slightly exceed a diameter of end anode of plasma source i.e. diameter $2r_o$ should be chosen using the criterion as follows:

$$V_{dr}\tau/2r_o<<1, \quad (3.7)$$

Copyright © 2012. Nova Science Publishers, Incorporated. All rights reserved.

Diamond-Like Carbon Films, Nova Science Publishers, Incorporated, 2012. ProQuest Ebook Central,

where V_{dr} is velocity of lateral drift of plasma particles, τ is duration of discharge pulse that approximately corresponds to the time of plasma presence in the separator.

In reality at designing a separator it is necessary to take into account a natural plasma beam divergence in a solid angle before its entering the separator caused by gas-thermal expansion of plasma and electrostatic interaction of charged particles.

At pulse feeding of a separator with passing current of arc discharge of 2.2 kA, the normal component of magnetic induction vector runs up to very high values as 50 mT at input/output and 100 mT in the centre. Knowledge of magnetic field size allows estimating Larmor radius, r_L, of electrons and ions in plasma of pulsed arc discharges. According to the probe plasma diagnostics described below, the velocity of plasma flow reaches value of 2 kilometers per a second that is much more than the quasi-equilibrium thermal velocity of carbon ions, whereas electrons are spread toward the substrate with velocity that is more much then ion velocity – their velocity of progressive motion is over 15 kilometers per a second. Using these data and calculated data of the magnetic field value for electrons we have r_L = 0.8 μm while radius of the single-charged ions of carbon is about 2.5 mm, i.e. in the magnetic separator there is strong magnetization of electrons and relatively weak magnetization of ions. Any way the Larmor radius of the carbon ions is much less than separator inner dimensions. Thus the both electron components and ion component are magnetized. It means that the carbon plasma can be effectively guided by the magnetic field yielded by a discharge current.

According to [19], a magnetic field of about 80 mT is necessary for both efficient plasma separation and achievement of high transfer capability. At the maximum value of the discharge current of 2.2 kA, magnetic field is varied from 50 up to 100 mT depending on the coordinate inside of the separator. If it is possible to suppose a linear dependence of the plasma transport through the separator on of magnetic induction vector magnitude, we can estimate its value. The oscillogram of discharge current is shown in Figure 12, from that a mean value of discharge current is 1.26 kA, an averaged value of $B_n$along the axial line at this current is 57 mT. For this value of magnetic field, the separator's transparence represented by the system coefficient is expected to be about 35 %.

The experiments of plasma separation were carried out. Efficiency of a separator was estimated by determination of a ratio of deposited film mass value with a separator, M_1 to that without separator, M_2:

$$k_m = \frac{M_1}{M_2} \cdot 100\% ,$$

Depositions of DLC films occur onto thin aluminium foils having a big area enough to collect all carbon particles of the plasma stream. From the point of the technology of depositing coatings, the proposed criterion of plasma transport efficiency, i.e. transport of mass instead of transfer of ions, seems to be more preferable. Its value determines the most important technological parameter that is coating deposition velocity, while ion current, because of the existence of double and even triple ionized carbon ions as well as some amount of neutral carbon atoms, does not linearly depend on a volume of carbon stuff transferred through the separator.

Copyright © 2012. Nova Science Publishers, Incorporated. All rights reserved.

Diamond-Like Carbon Films, Nova Science Publishers, Incorporated, 2012. ProQuest Ebook Central,

DLC film mass was estimated using weighing of the samples before and after deposition with accuracy of 0.1 mg. Some results obtained in the experiments are shown in Table 1.

Table 1. Efficiency of transfer capability of a separator

Main discharge voltage (Volt)	Mass of film (mg)		Efficiency of plasma transport (Percent)
	With separator	Without separator	
200	14.7	4.4	30
250	18.3	5.9	32
300	21.6	6.3	29
350	22.7	6.2	27
400	24.4	7.0	29

Efficiency of mass transfer of a separator depends on voltage of the main discharge tailoring the energy of carbon ions has non-monotonous character. The best mass transfer was achieved at voltage being 250 V. At voltage more than 250 V a number of high-energy particles rises and the movement of them practically is not controlled by the separator. From the other hand, the rise of voltage is accompanied by a rise of current causing an increase of vector of magnetic induction, and, it consequently leads to a rise of drift of plasma to the walls of the separator. The mean value of separator operation efficiency is about 30 % and it significantly exceeds the results usually obtained at using multi-coil separators of plasma fed with DC current [20].

Distribution of plasma stream density was determined according to change of thickness of carbon coating deposited on a substrate located perpendicularly to the axis of the separator at its output. As a substrate an aluminum foil of 50 μm in thickness fixed on round holder with diameter 300 mm was used. Diagrams of the thickness level of coatings obtained at the main discharge voltage ranging from 200 to 400 V are shown in Figure 13. For orthogonal axes X-Y shown in the diagram the coordinate system is chosen, in which *X* axis is directed towards outer radius of the separator's curvature, and axis *Y* is directed along the normal of the plane, in which the axial line of the separator (the plane of the separator's curvature) is situated.

The thickness level diagrams significantly differ from those of non separated plasma (Figure13f): they transform from concentric circles into eccentrically located ellipses with distorted forms. This is an evidence of the disturbance of axial symmetry of the plasma stream caused by the non-uniform magnetic field.

The second feature of the separated plasma is that a magnetic field created by a curvilinear separator produces remarkable focusing of pulse arc plasma stream. Judging by distribution of coating thickness, the area of the biggest density of plasma stream is dislocated with regard to the centre of the output window of the solenoid towards the outer radius of the separator for a distance of 50÷60 mm in Y axis. The field lines of separator at its output is somehow turned towards the its outer wall by 10 . However, it effects to shift the plasma stream $100 \times \text{tng}10^{o} = 18$ mm (100 mm is distance between the separator output and substrate).

Thus, the main contribution into the evident "radial" plasma shift is rendered by along a curved trajectory [21]. The plasma drifts along *X* axis almost similar to that of the centrifugal drift but caused by the gradient of the magnetic field inside of separator. The experimentally

Copyright © 2012. Nova Science Publishers, Incorporated. All rights reserved.

Diamond-Like Carbon Films, Nova Science Publishers, Incorporated, 2012. ProQuest Ebook Central,

revealed direction of plasma drift coincides with the direction of vector B×gradB, the calculated value of which is $5 \cdot 10^{-2}$ T^2/m. This value is quite big to cause an evident drift of moving carbon ions [22]. Hereby, the results of the theoretical analysis are proved about a possibility of gradient plasma drift in a low-coil separator which deleteriously influence a plasma transport.

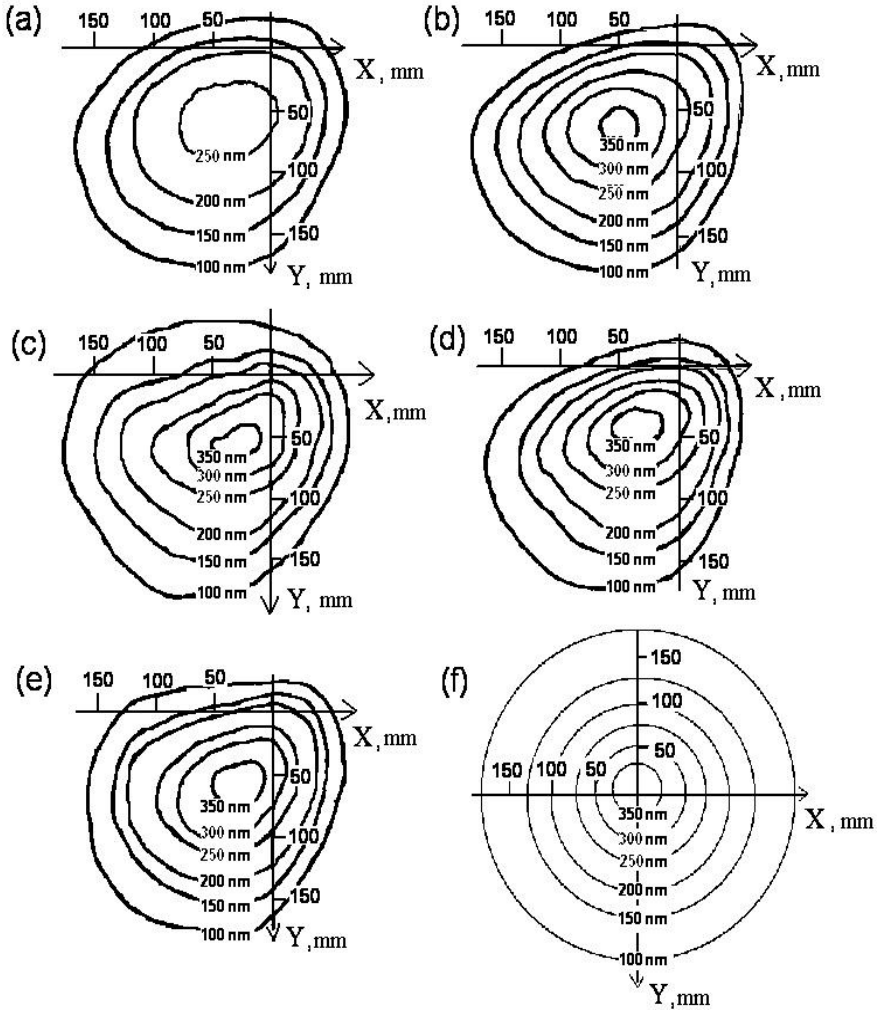

Figure 13. Diagram of the film thickness distribution over the substrate surface and duaxialshift thickness peak ad the main voltage of (a) 200 V, (b) 250 V, (c) 300 V, (d) 350 V, (e) 400 V, and (f) uniform distributed thickness of a film deposited without separation.

*Efficiency of Macroparticles Removing.*A typical picture of surface of DLC thin film deposited by pulsed arc technique is presented in Figure 14. There are a lot of randomly distributed over the film surface large and small carbon particles.

The particles have sizes several tens micrometers as a maximum. The lowest limit of the particles sizes lies in nanometer scale. Defectiveness of coatings was determined by a mean number of well-distinguishable macroparticles with linear size more than 1 μm within eyeshot

Copyright © 2012. Nova Science Publishers, Incorporated. All rights reserved.

Diamond-Like Carbon Films, Nova Science Publishers, Incorporated, 2012. ProQuest Ebook Central,

of the metallographic microscope at zooming 400^x. The data of macroparticles in DLC coatings separately for large (more than 5μm) and little macroparticles are given in Table 2.

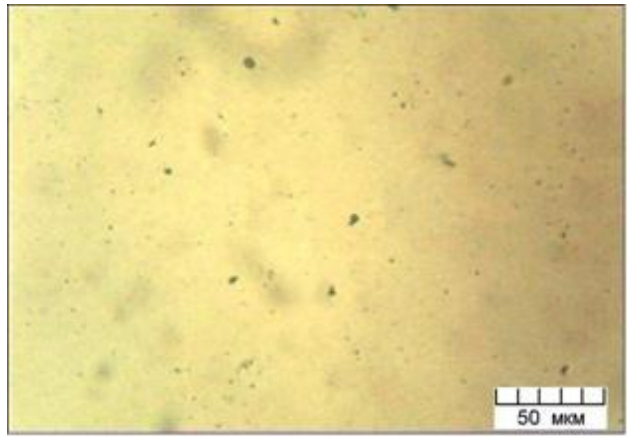

Figure 14. Picture of the DLC film containing carbon macroparticles.

The table data are obvious evidences of macroparticles problem in arc deposition technique. The total area occupied by these defects can reach 15-20% that deteriorates greatly the excellent performances of DLC material. The quantity of the large macroparticles increases of almost linear with increase in the main discharge voltage whereas a more power tendency is observed for the little macroparticles. Is this respect, a lower voltage is preferable one in order to obtain more perfect film surface. The used separator removes all large particles and sinks a number of small macroparticles more than one order of the magnitude. The most probable reason for the small macroparticle transport through the separator out of the line-of-sight with regards to the cathode is that the particles in plasma acquire an electric charge and their motion inside the separator is controlled by local electric fields of plasma; and it forces them to move together with plasma as a comprehensive whole. Besides, high velocity of macroparticles leads to their reiterated reflections from the walls of a vacuum chamber and to their deposition on a substrate. In the separated stream a part of large macroparticles is significantly decreased, while density of particles with size less than 100 μm does not practically change.

Table 2. Number of carbon macroparticles onto DLC film surface without and with separation

Film thickness (nm)	Main discharge voltage (Volt)	Separation	Density of carbon particles (mm^{-2})	
			Large particles (more than 5 μm)	Little particles (1…5 μm)
150	200	no	1320	4080
150	300	no	1800	5100
150	400	no	2280	7500
210	200	yes	-	120
200	300	yes	-	200
220	400	yes	-	180

Copyright © 2012. Nova Science Publishers, Incorporated. All rights reserved.

Diamond-Like Carbon Films, Nova Science Publishers, Incorporated, 2012. ProQuest Ebook Central,

*Structure of DLC films.*The magnetic separator not only effectson macroparticles removing but film structure and formation of sp^3 hybridized bonds due to change of plasma density and energy of carbon particles as well as pulse duration enhancement because of an inductivity of separator connected consequently in the discharge circuit. Figure 15 shows Raman spectra of DLC films obtained without separation (a, c, e) and with separation (b, d, f) of the carbon arc plasma at different values of the main discharge voltage.

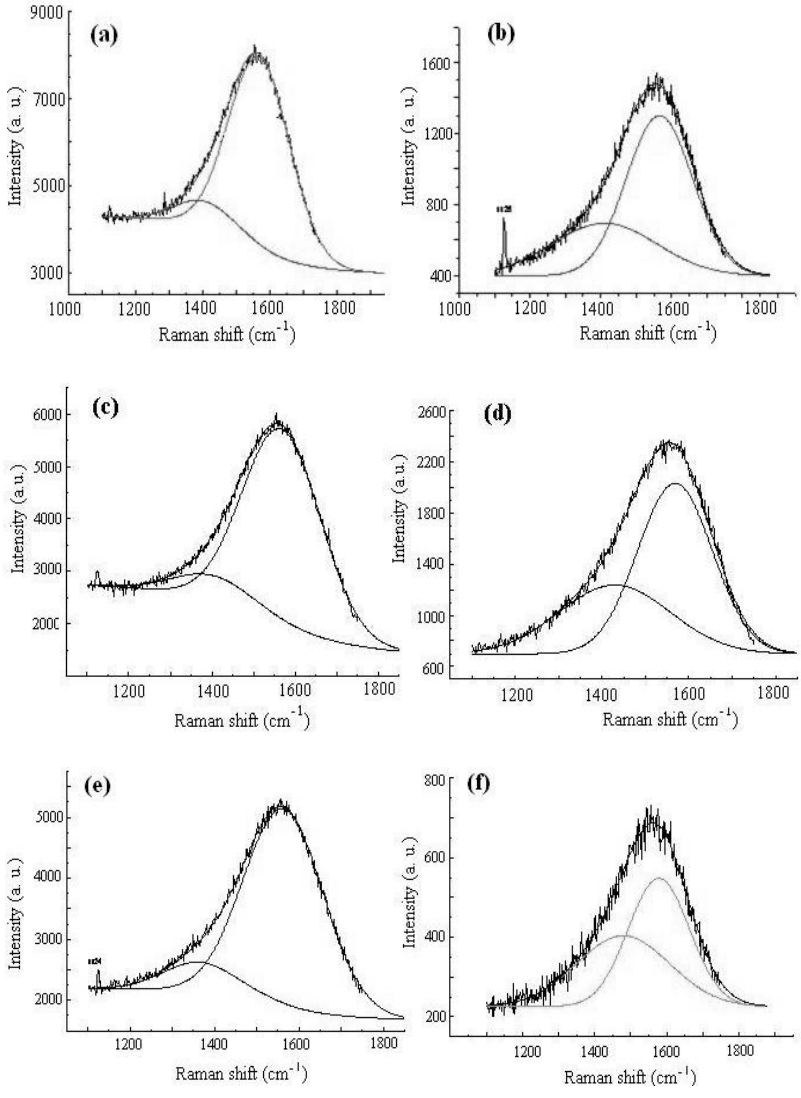

Figure 15. Raman spectra of DLC films obtained (a, c, e) without plasma separation and (b, d, f) with plasma separation at different value of the main discharge voltage: (a, b) 200 V, (c, d) 300V and (e, f) 400 V.

The parameters of D- and G-peak as result of the Raman spectra deconvolution are listed in Table 3. The Raman spectra are typical ones acquired from ta-C films those are characterized almost symmetrical peak near 1560 cm^{-1} [23] The usage of the separator gives some changes of Raman spectra: there is a shift D and G peak towards higher value of the

Copyright © 2012. Nova Science Publishers, Incorporated. All rights reserved.

Diamond-Like Carbon Films, Nova Science Publishers, Incorporated, 2012. ProQuest Ebook Central,

wave vector and the increase in relatively intensity of D-peak. These both features are clear evidences of the enhancement of sp^2-bonded carbon in DLC films. [24]. One of the causes of the film quality deterioration is a decrease of plasma stream density having passed the separator that decreases the rate of non-equilibrium of the deposition process and diminishes the probability of formation of a meta-stable diamond-like phase.

Table 3. Parameters of Raman spectra of DLC films obtained from non-separated and separated plasma stream

Discharge voltage, V	Non-separated plasma stream				Separated plasma stream			
	D-peak (cm^{-1})	G-peak, (cm^{-1})	Width of G-peak (cm^{-1})	I_D/I_G	D-peak, (cm^{-1})	G-peak (cm^{-1})	Width of G-peak (cm^{-1})	I_D/I_G
200	1384	1562	214	0.13	1410	1565	223	0.33
300	1370	1560	221	0.12	1429	1569	203	0.40
400	1368	1560	223	0.15	1479	1579	200	0.55

The Raman study revealed a strong dependence of the ratio of D-peak intensity to G-peak intensity, I_D/I_G, on the main voltage value in the case of separated plasma and its absence for non-separated plasma An increase in the voltage of the main discharge in range from 200 to 400 V causes I_D/I_G ratio is changed from 0.33 to 0.55. It is difficult to understand the observed a relative decreasing in the content of four-fold bonds at increasing in main discharge voltage. The higher discharge voltage the higher is both carbon particles energy and discharge current going through the separator which enhances plasma transport. Both these circumstances are positive in sp^3 bond formation. In the other hand, high current leads to focusing plasma stream. As a result, there is a local short time overheating of substrate that provokes graphitization of a growing film.

The other possible cause of the phenomena is that a separator changes the ratio of the high energetic particles to low energetic ones: the higher velocity of carbon ion the worse it under the guidance by magnetic and electrical fields generating in a separator. The high energetic particles play a key role in formation diamond-like phase [25].

Thus, separation of carbon plasma stream leads to formation of diamond-like coatings with a lower containment of "diamond" phase that in coatings obtained in straight plasma stream. At that, in contrast to straight stream for separated stream there is a clear tendency of an increase of a rate of graphitization of diamond-like carbon coatings with the growth of the main discharge voltage.

Comparative tribology.Friction coefficient of DLC films grown on polished substrates made of M2 steel was under study using a tribometer with operation scheme "pin-disc". As a rider was involved a diamond tip of 6.35 mm in diameter that loaded with 1 N. A sliding speed was 6 cm/s.

Figure 16 shows the dynamics of friction coefficient for DLC films obtained at different discharge voltages both in non-separated and in separated pulse plasma streams. One can see that the films obtained with plasma separation demonstrate stable and lower friction coefficient about 0.1 independently of the value of discharge voltage due to smooth film

Copyright © 2012. Nova Science Publishers, Incorporated. All rights reserved.

Diamond-Like Carbon Films, Nova Science Publishers, Incorporated, 2012. ProQuest Ebook Central,

surfaces and relatively high fraction of graphite-like phase in these films. The most difference in the friction coefficient value reveals a film obtained at low discharge voltage (see Figure 1a) indicating an importance of separation of low energetic plasma.

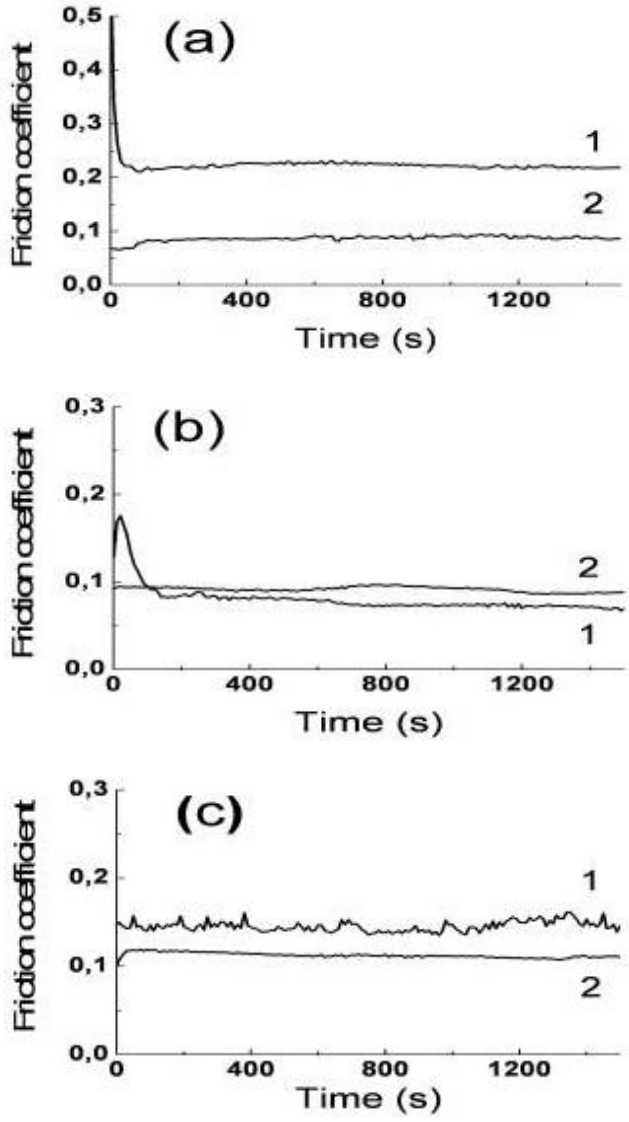

Figure 16. Friction coefficient for DLC film obtained from (1) non-separated and (2) separated plasma at different discharge voltage as: (a) 200 V, (b) 300 V, and (c) 400 V.

In order to determine an influence of the fiction on the film structure in a wear track area there was a Raman investigation. It was revealed that there is no modification of phase composition of surface layers for all deposited films reasoning from that the Raman spectra before wearing becomes practically coincident those after wearing as it is indicated in Figure 17.

Thus, the experiment has not revealed graphitization processes of the tribolayer in contrast with other studies (see for example [26]. One of the cause of this phenomena is that a

Copyright © 2012. Nova Science Publishers, Incorporated. All rights reserved.

Diamond-Like Carbon Films, Nova Science Publishers, Incorporated, 2012. ProQuest Ebook Central,

diamond rider was used is this study unlike convenient studies involved steel riders. As it know well transition metals like Co, Ni, Fe effect catalytically on transformation diamond-like phase to graphite-like phase [27].

In the friction processes under the research there was an abrasive wear and no delamination of diamond-like carbon film was observed. Friction coefficient of carbon coatings against diamond rider is below than ~ 0.1 due to the super high hardness of films (HV 6000) and high smoothness of the surface (Ra ~ 1 nm).

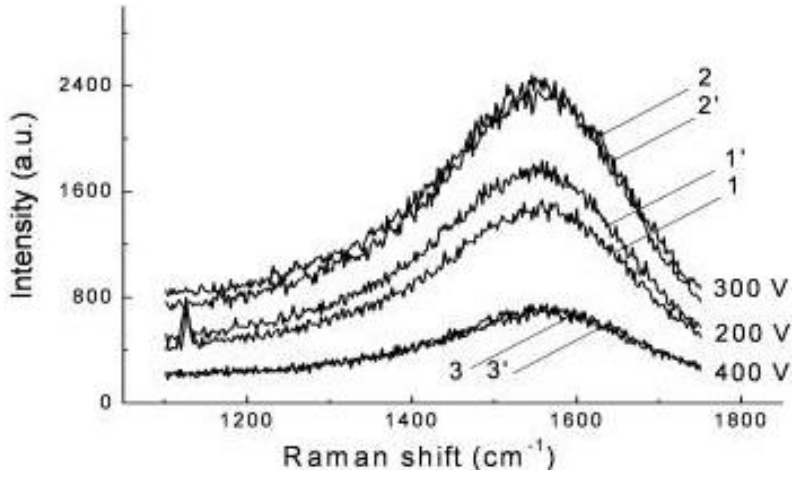

Figure 17. Raman spectra of DLC films before (1, 2, 3) wearing and (1', 2', 3') after wearing which were deposited at discharge voltage of (1,1') 200, (2,2') 300 and (3,3') V.

3. SPECTROSCOPIC AND PROBE DIAGNOSTICS OF CARBON PLASMA

Plasma characteristics like, density, ionic and electronic temperature, particle energy, speed of plasma flow play a key role in the formation of DLC films. The main methods of arc plasma diagnostics namely Langmuir probes and optics spectroscopy was used to study thecathodic arc carbon plasma. The first one gives a possibility to perform a diagnosis of ion and electron components of plasma whereas second one reveals ionization state of carbon particles and dynamic temperature of plasma. There is some difficulty to test the pulsed plasma because of crosstalk disturbances of a Langmuir probe signal due to the strong electromagnetic induction of pulsed discharge current. Moreover plasma parameters are not the same for discharge impulses followed one after another. When studying the arc sputtering of graphite cathode in vacuum it was found that integrated radiation intensity in fixed spatial point of the plasma flow can vary by a factor of ten in spite of steady current characteristics of the discharge in question. The light pulse may be bell-shaped or may have strong fluctuations of intensity at a frequency of 100-200 kHz due to formation and decay of cathode spot groups with lifetime of 5-10 μs. At the same time the topology of electrode spots on the cathode surface and an anode attachment region vary from impulse to impulse while emission spectrum of the discharge for ultraviolet and visual wavelength ranges remains invariable. Thus only a statistical approach is possible in this case for diagnose of the pulsed plasma.

Copyright © 2012. Nova Science Publishers, Incorporated. All rights reserved.

Diamond-Like Carbon Films, Nova Science Publishers, Incorporated, 2012. ProQuest Ebook Central,

Plasma Spectroscopy. Emission spectra of plasma were obtained by diffraction spectrometer MS 3504 based on Cherny-Turner scheme and registrated by CCD detector TCD (Toshiba) when observing both longitudinally and transversely to plasma flow and averaging over several thousands of pulses. The probe potential was measured by means of high-impedance tester and normalizing differential amplifier. The signal from amplifier output was transmitted to an analog-to-digital converter with conversion frequency of 10^7 s^{-1} and then processed by computer. Data recording process was triggered by plasma generator synchronizing pulse.

Plasma emission spectra were studied for various energies put in the pulsed arc discharge. The spectral range under investigation was 200 to 1000 nm. The qualitative analysis of spectra (Figure 18) has shown that the basic radiating components of plasma are lines of atoms, ions and second-order ions of carbon (CI, CII, and CIII) as well as molecular bands of C_2 Swan system. Besides, there are hydrogen atomic lines (H_a and Hp) and weak lines of atomic oxygen (OI) and molecular bands of CH and CN in the spectra.

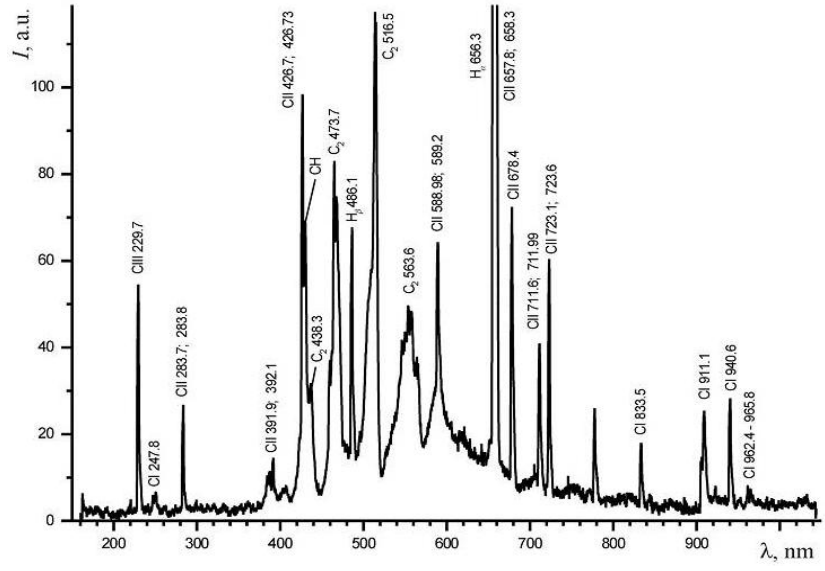

Figure 18. Carbon plasma emission spectrum in the range of 200-1000 nm.

The ratios of spectral components, present in the spectrum, describe the physical conditions of the discharge. The range of 250 to 300 nm in the obtained spectrum is the most informative. There is CIII line at 229.7 nm (excitation energy is 18.09 eV), CII lines at 283.7 and 299.3 nm (excitation energies are 16.33 and 22.19 eV respectively), and CI line at 247.8 nm (excitation energy is 7.68 eV) in this spectral range. The ratios of intensities of these components reflect changes in the discharge conditions including the ratio of concentrations of charged components and populations of their excited levels.

Assuming that populating of levels is due to electron impact and electron energy distribution is maxwellian function it is possible to estimate the excitation temperature T_{ex} of carbon atoms from relative intensities of CII lines at 283.7 and 299.3 nm having difference of excitation energies about 6 eV. Obtained data for three values of main discharge capacitor voltages 250, 300 and 350 V give values of $T_{ex}$of 1.72, 2.09 and 2.87 eV, respectively.

Copyright © 2012. Nova Science Publishers, Incorporated. All rights reserved.

Diamond-Like Carbon Films, Nova Science Publishers, Incorporated, 2012. ProQuest Ebook Central,

The spectral distribution of radiation differs appreciably in various spatial zones of the discharge. Three reference spatial zones of radiation are observed as they pictured in Figure 19: (I) cathode spots on the cathode surface with the continuous spectrum of highly heated graphite; (II) area of diffuse-reddish radiation near the cathode spots caused by emission of carbon ions and hydrogen atoms; and (III) blue-green radiation in the inter electrode gap near the anode attachment due to emission of molecular carbon C_2. There are many cathode spots simultaneously existing while the arc discharge operates. The spots appear as a result of splitting a precursor spot due to a huge discharge current reached over 2500 A in a peak. The spots have much more drift velocity in comparison with those of DC arc. In that way the injection of carbon particles in the plasma steam is dropped.

It was found out that integrated intensity of carbon plasma emission is proportional to a squared energy supplied to the discharge irrespective of combination of capacity storage parameters, while the spectral distribution of emission at the given discharge energy practically does not depend on the main discharge capacitor voltage over the range of 212…424 V examined in this study as it can be seen in Figure 20, in which the spectral distribution of carbon plasma emission for two energies of pulsed cathodic discharges, 54 J and 27 J, but different combinations of both capacity of the main capacitor bank, 600 μF and 1200 μF, and main discharge voltage, 424 V and 300 V, provided these energies are shown.

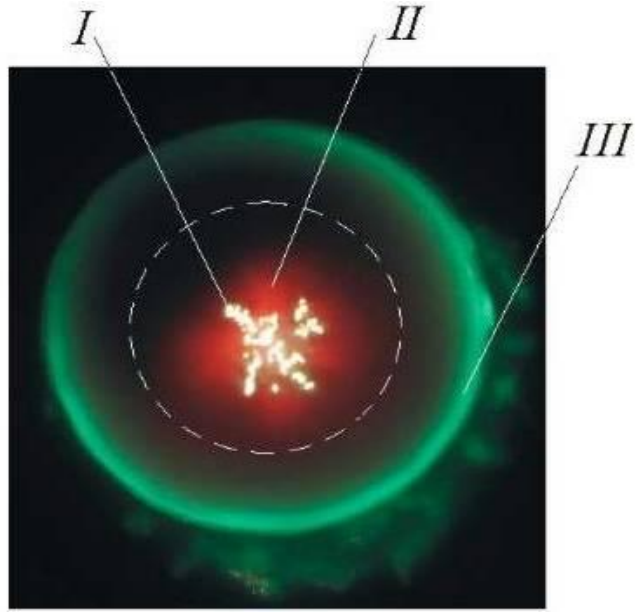

Figure 19. Discharge pattern near the cathode surface (a cylindrical cathode outline is shown by dashed line).The characteristic spatial zones of the discharge are: (I) cathode spots, (II) C and H ion light emission, and (III) carbon dimer light emission.

From detailed analysis of the registered emission spectra, C_2 molecule band of Swan system at 516.5 nm was chosen as pyrometric band. Spectral sensitivity and amplitude characteristic of spectrometer registration path were taken into account. From comparison of rotational structures of calculated and experimentally measured spectra of the molecular band at 516.5 nm, the gas-kinetic temperature of plasma near substrate was found to be about 1000 K.

Copyright © 2012. Nova Science Publishers, Incorporated. All rights reserved.

Diamond-Like Carbon Films, Nova Science Publishers, Incorporated, 2012. ProQuest Ebook Central,

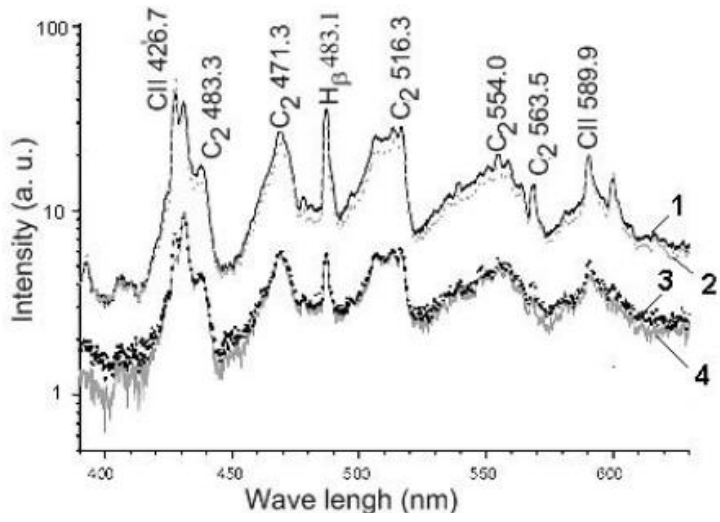

Figure 20. Spectral distribution of carbon plasma emission near the substrate for various discharge energies as: (1, 2) 54 J and (3,4) 27 J at the next discharge parameters: (1) 1200 μFand 300 V, (2) 600 μFand 424 V, (3) 600 μFand 300 V, (4) 1200 μF and 212 V.

Langmuire probe diagnostics of the carbon plasma. During the discharge a substrate is subjected to action of charged particles. The charge and energy of the particles determine the substrate floating potential in each phase of the discharge. Measurements of substrate floating potential $U_f$were carried out together with the main discharge current*I* (Figure 21).

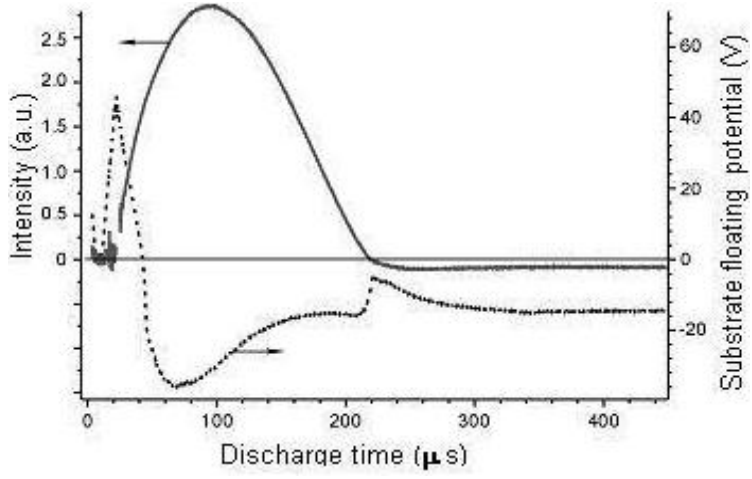

Figure 21. Time dependences of main discharge current and probe potential near the substrate for main voltage of 250 V.

To measure the gas-kinetic temperature *T*g (or temperatures of neutral component) of plasmas, well-shaped molecular bands of C2, present in the emission spectra of the arc in question, were used. Determination of gas-kinetic temperature from rotational temperature *T*rot of molecules is the most widespread technique for *T*g monitoring.

Copyright © 2012. Nova Science Publishers, Incorporated. All rights reserved.

Diamond-Like Carbon Films, Nova Science Publishers, Incorporated, 2012. ProQuest Ebook Central,

The rotational temperature characterizes distribution of excited molecules on rotational levels of the upper excited state of vibronic transition under study. Such distribution is established rapidly, so the rotational temperature is close to gas-kinetic temperature of molecules. Excited state distribution of molecules influences directly the relevant intensity distribution in the molecular band, including rotational structure of the spectrum in question. As a result the ratio of emission intensities in various parts of rotational spectrum within one band, corresponding to transition between selected vibration levels, may serve as a quantitative characteristic of rotational temperature.

It was ascertained that the substrate is under accelerating potential of -15…-25 V during the discharge, and the value of potential is essentially independent of the main discharge energy.

To determine the electron energy distribution function the dependences of probe current I_p on a bias voltage U_b were registered during the discharge impulse [28]. Each recording cycle was performed at fixed capacitor voltage of the main discharge. The measurements for each value of $U_b$were repeated many times with synchronous recording of discharge current to improve the reliability of results. The recording parameters such as zero level position and sensitivity of measuring path were taken into account. Then all registered functions $I_p(t)$ were synchronized to eliminate uncertainty of the main discharge starting time after synchronizing pulse. Thus, the matrix of probe current at different bias voltages for various time points was obtained. The probe current at different value of bias voltage is shown in Figure 22.

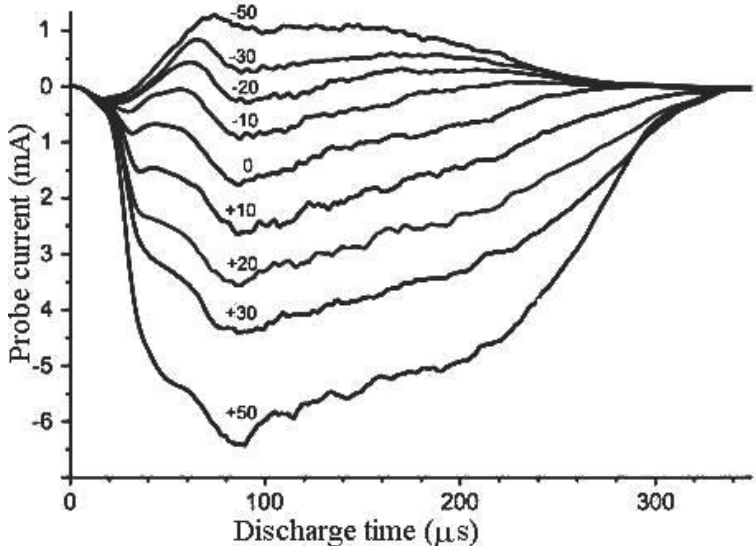

Figure 22. Probe current for a bias voltage indicated.

The electron probe current is a difference between total probe current and ion saturation current, $Ie = Ip - Ii$. It was found that dependences of logarithm of Ie on bias voltage look like a straight line, so the electron energy distribution is a maxwellian function. The plasma electron temperature (in electronvolt) may be estimated from the ratio [28]

Copyright © 2012. Nova Science Publishers, Incorporated. All rights reserved.

Diamond-Like Carbon Films, Nova Science Publishers, Incorporated, 2012. ProQuest Ebook Central,

$$T_e = \left(\frac{\partial \ln I_e}{\partial U_b} \right)^{-1}$$

The electron temperature varies slightly during the impulse and amounts to about 50 eV for maximum of the discharge current**.** From the value of the electron saturation currentthe lower value of electron density in plasma was estimated to be 2×10^{11} cm^{-3}.

It was revealed that delay period of the probe electron current concerning the main discharge does not exceed 15 μs for negative or small positive bias voltages. At the same time, the delay period of the probe ion current amounts to ~ 100 μs for high positive biases (> 15 V). Thus, some polarization of the plasma flow takes place when velocity of high-energy electrons comprises 35 km/s, and velocity of ions, which is identified with the plasma flow velocity, is equal to about 20 km/s. From this it follows, taking into account the results of temperature measurements, that energy of thermal motion of electrons exceeds considerably the energy of their ordered motion, and the energy of ordered motion of ions is four times as much as their thermal energy.

Conclusion. From the obtained optical emission spectra of a pulsed cathodic-arc vacuum discharge were revealed that the basic radiating components of plasma are lines of atoms, ions and second-order ions of carbon (CI, CII, and CIII) as well as molecular bands of C_2 Swan system. The integrated intensity of carbon plasma emission is proportional to a squared energy supplied to the discharge irrespective of combination of capacity storage parameters. The value of gas-kinetic temperature of plasma near the substrate was determined to be about 1000 K. Langmuire probe testing of the plasma of cathodic arc discharge shown that substrate was under accelerating potential of -15…-35 V during the discharge, and the value of potential does not depend on the main discharge energy. The electron energy distribution function is maxwellian with electron temperature of ~ 50 eV. The pulsed plasma source provides an acceleration of plasma plum up to 20 km per second.

4. A NOVEL COMBINED PVD-CVD METHOD OF DLC FILM DEPOSITING

Tetrahedral amorphous carbon (ta-C) obtained by the pulsed arc technique demonstrates specific characteristics as compared to natural diamond. However, high internal stress, rather low range of thermal stability equal up to 400°C and low growth rate of this excellent carbon material as well as its non-uniformity in thickness on deposition on large substrates are regarded as the main obstacles to a wide industrial application.

A novel method of diamond-like carbon film deposition, which allows overcoming aforementioned problems in many respects, has been developed. Its essence is ina combined method that involves a pulse cathode arc deposition (PVD method) and carbon plasma enhanced chemical vapor deposition (PECVD) in order to improve an actual deposition technique and DLC films performances as well.

Owing to using a special-purpose design of the Hall plasma source, carbon plasma spreads towards a substrate at a speed of about 20 kilometers persecond. Then they are accelerated by a floating potential about 35 V near the substrate. With that they received a

Copyright © 2012. Nova Science Publishers, Incorporated. All rights reserved.

Diamond-Like Carbon Films, Nova Science Publishers, Incorporated, 2012. ProQuest Ebook Central,

total energy of 60 eV that is sufficient to cause destruction of any hydrocarbon molecule at impact with a carbon ion. The technique enables avoiding the sophisticated RF or MW plasma activation as well as substrate bias and substrate heating.

Acetylene is one of the most commonly used hydrocarbon gas in PECVD process due to its low ability to form polymer-like condensate and it is almost environmentally friendly. The experience in the combined method development has been entirely acquired by applying this gas.

Theoretical approach. One of the most probable ways to form DLC coatings as a result of interaction of the carbon plasma with hydrocarbon gas is excitation and destruction of the gas molecules directed towards a substrate to form a DLC film. Thus, there are two kind of deposited particle namely ions ejected by the arc discharge and radicals of acetylene. As result, the deposition rate should be increased in comparison with the arc burning in vacuum. Based on Ervin's and Gronert's researches on the bond energy of acetylene molecule [29], it is possible to image the next plasmachemical reaction :

$$H\text{-}C{\equiv}C\text{-}H \rightarrow H\text{-}C + H\text{-}C \qquad (9.9) \qquad (1)$$

$$H\text{-}C \rightarrow H + C \qquad (4.2) \qquad (2)$$

$$H\text{-}C{\equiv}C\text{-}H \rightarrow H\text{-}C{\equiv}C + H \qquad (5.7) \qquad (3)$$

$$H\text{-}C{\equiv}C \rightarrow H\text{-}C + C \qquad (7.7) \qquad (4)$$

$$H\text{-}C \rightarrow C + H \qquad (4.2) \qquad (5)$$

$$C{\equiv}C \rightarrow C + C \qquad (8.4) \qquad (6)$$

All these reactions are exothermal ones (the absorbed energiesare given in brackets).In accordance with (1-6), a minimal energy needed for acetylene molecule decomposition is 5.7 eV. Energy for the full molecule desay is 17.5 eV following the lessenergy-consumingchain of the reactions: (3.3) → (3.4) → (3.5).As it was determined by spectroscopic and Langimuar probe investigations electrone component of the pulsed arc plasma is about 2×10^{13} cm^{-3}.Electronshave energy about 50 eV and they may play a role in exitation or decomposition of the hydracarbon molecules. But at low pressure acetylene gas ranged from 0.01 to 1 Pa, a possibility of electron-acetylene molecule impact at characteristic distance in several dozen cantimeters inside of a vacuum chamber is very low.Taking into account that singly ionized carbon ions is a dominant component of the plasm, an assumption of the same ion density is reasonable. Their energies are in the range 50...60 eV depending on the initial voltage of the main discharge.One carbon ion is able to cause full decomposition of three C_2H_2 molecules or a partial decomposition of ten molecules acoordingly to reaction (3). The last process is more preferable due to its lowest energy consumption.C-H radical has high chemical activity and they easy to be adsorbed by a substrate. The collision number that leads to molecule decomposition imposes a constraint on the acetylene partial pressure upper limit.

Optimal acetylene pressure, *p*, may be calculated on the basis of the mean freepath carbon ion in this gas. The data of C_2H_2 molecule dimension obtained from TEM

Copyright © 2012. Nova Science Publishers, Incorporated. All rights reserved.

Diamond-Like Carbon Films, Nova Science Publishers, Incorporated, 2012. ProQuest Ebook Central,

investigation of the acetylene adsorption on palladium is given in reference [30]. It has longitudinaldimension of 0.32 nm and transversedimension of 0.13 nm.The collision number of C^+ ion with C_2H_2 particles passing distance *L is*:

$$N = \frac{\sqrt{2}}{4}\pi L\left(D_{C^+} + D_{C_2H_2}\right)^2 \frac{P}{kT}$$

where $D_C{}^+$and D_{C2H2} is diameter of carbon ion and overage size of acetylene molecule, respectively, T is absolute temperature, *k* is Boltzmann constant.The pulsed arc deposition process runs at room temperature of 300 K.At distance of 30 cm between cathode and vacuum chamber center is about 30 cm the overage collision number of 10 reached at the acetylene gas pressure about 1 Pa. Anyhigher pressure does not provide an increase in deposition rate but leads to dissipation energy of carbon ions of the cathodic arc plasma and deterioration of DLC film quality.The lower limit of the acetylene pressure of 0.1 Pa was estimated taking into account only a collision of a carbon ion with the gas molecule before reaching a substrate.

*Spectroscopic diagnostic of plasma at acetylene gas presence.*In order to better understand deposition phenomena in the case of combined PVD-CVD technique, spectroscopic investigation was carried out like those described in the previous section. In a series of experiments the acetylene gas filled the vacuum chamber to the pressure in the range of 0.1~1.5 Pa.

The chamber was preliminary pumped out to residual pressure of $\cdot 10^{-3}$ Pa. Silicon substrates were cleanedbefore deposition by argon ions of 2 keV energy. The main voltage was applied between an anode and a cathode of the arc source with the magnitude of 300 V and the capacitor bank provided the discharge power about 100 J. The duration of discharge impulses did not exceed 300 μs at pulse repetition of 1.5 per second. Letting the acetylene vapor into vacuum chamber led to dramatic increase of intensities of Swan system whereas intensities of other radiating components almost did not changed. For example, intensity of molecular cant C_2 at 563.55 nm increased by factors of 6, 8, and 11 when reaching the hydrocarbon partial pressure of 0.2, 0.5, and 1.0 Pa, respectively. The behavior of the intensity ratio is illustrated in Figure 23.

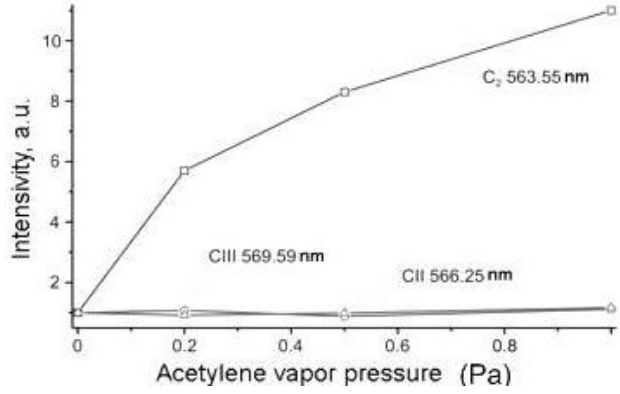

Figure 23. Dependence luminescence intensity of carbon ion CII, CIII and molecular carbon C_2 on acetylene vapor pressure in vacuum chamber.

Copyright © 2012. Nova Science Publishers, Incorporated. All rights reserved.

Diamond-Like Carbon Films, Nova Science Publishers, Incorporated, 2012. ProQuest Ebook Central,

At the same time, emission spectra of C_2H_2 molecules were not observed. The increase of acetylene pressure in the range from 0.2 Pa to 1.0 Pa resulted in increasing the intensity of H_β and H_β spectral lines 2 to 3 times as compared to the vacuum condition whereas the luminescence level of CH radicals remained almost the same. The enhancement of luminescence of C_2 cants is indicative of changes in the plasma composition caused by increase of hydrocarbon molecules. In this respect the main result of the collisions of carbon plasma particles with hydrocarbon molecules is destruction of C-H bonds in acetylene molecule and formation of C_2 radicals. These results are in a good agreement with the analyses based on bond dissociation energy (BDE) of acetylene molecule that was done above.

*Types of chemical bonds.*X-ray photoelectronic spectroscopy (XPS) with MgK-characteristic radiation of 1253.6 eV, and Raman spectroscopy with a wave length of 514.5 nm were used for characterization of film compositions and obtaining the information of carbon atomic bonds. C1s core level spectra for the deposited DLC films at different acetylene pressures revealed four different Gauss-Lorenz fit components with binding energies of 284.4 – 284.8 eV, 284.9 – 285.2 eV, 286.0 – 286.9 eV, and 287.3 - 287.7 eV. Based on the experimental data given in references [3] the components having these binding energies are attributed to sp^2 bond, sp^3 bond, C-O, and C=O, respectively. The quantity of chemical bonds derived from the fitting peak areas is expressed in percentage and given in Table 4. The data of the table shows the effectiveness of the pulsed arc method for DLC film deposition since it provides a high content of 4-fold coordinated sp^3 sites.

Table 4. Bond content for DLC coatings

	Bond content, % (Binding energy, eV)			
Acetylene pressure, Pa	Without acetylene	0.3	0.6	1.0
sp^2 bonded C	12.5 (284.4)	30.1 (284.5)	8.8 (284.5)	17.4 (284.8)
sp^3 bonded C	81.3 (285.0)	63.8 (285.2)	74.4 (285.0)	61.4 (284.9)
C-O	2.0 (286.9)	2.1 (286.7)	9.7 (286.3)	14.5 (286.0)
C=O	4.2 (287.7)	4.1 (287.7)	7.1 (287.3)	6.7 (287.6)
sp^2/sp^3	0.15	0.47	0.12	0.28

The ratio of sp^2 bonds to sp^3 bonds is about 0.15 for the DLC films deposited in vacuum with zero substrate bias. The ratio for the bulk film material must be even lower since an upper film layer of DLC film is enriched by sp^2 bonds as it was demonstrated clearly in [4, 7]. Presence of acetylene vapor in a vacuum chamber leads to some decrease in content of the four-fold σ-bonds depending on the gas pressure. However, the tendency shows a non-monotonic character, perhaps as a result of the two main concurrent processes.

The presence of hydrocarbon molecules in a vacuum chamber yields a lot of low energy carbon particles deposited on a substrate that adversely affects a sp^3 bond creating. An opposite trend is connected with free hydrogen released as a result of acetylene molecules

Copyright © 2012. Nova Science Publishers, Incorporated. All rights reserved.

Diamond-Like Carbon Films, Nova Science Publishers, Incorporated, 2012. ProQuest Ebook Central,

decomposition - the hydrogen can terminate of sp^3 dangling bonds on the growing film surface and stabilize them effectively.

Table 4 also shows that the increase in acetylene pressure up to 1.0 Pa in vacuum chamber leads to increase of oxygen contents in DLC film more than 3 times. Oxygen, in turn, actively promotes the coating graphitization, i.e. it is the additional factor of growth of sp^2 bonds content in DLC films.

Raman spectra of a DLC film obtained in acetylene at pressure of 0.3 Pa are given in Figure 24. The spectra generally exhibit a broad intensity distribution at around 1560 cm^{-1}.A low intensive shoulder at 1360 cm^{-1} only slightly disturbs the peak symmetry. Such Raman spectrum shape is typical for the high-quality diamond-like carbon films having a large content of sp^3 bonds [5]. DLC films deposited in acetylene atmosphere reveal some more skewness of Raman spectra in comparison with that of the films deposited in vacuum, their peak positions are shifted towards a low frequency as well.

The deconvolution of D- and G band from a broad Raman spectrum is shown in Figure 24, too.For DLC films deposited in vacuum and those deposited in acetylene at pressure 0.3 Pa, the ratio of integral intensity for D- and G-peak, I_D/I_G, considerably differs and takes 0.12 and 0.29, respectively, while G-peak positions coincide practically for both Raman spectra (1565.4 and 1564.3 cm^{-1}). Acetylene presence leads to widening D-peak at half high from 170.1 to 293.4 cm^{-1}, and does not affect width of G-peaks which remains practically invariable (224.6 and 228.3 cm^{-1}). These results mean that graphite phase in a film deposited with acetylene is increased due to growth of a number of small graphite clusters in the amorphous sp^3 matrix.

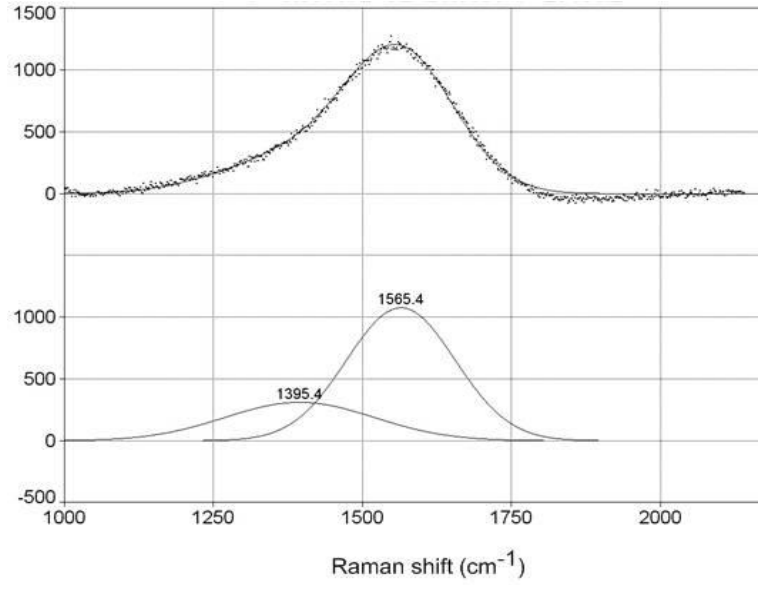

Figure 24. Raman spectrum of DLC film deposited at acetylene pressure of 0.3 Pa.

*Mechanical properties.*To determine deposition rate an amount of a deposited carbon material was determined by weighing the aluminum foils 30 μm thick before and after DLC film deposition after 1500 discharge impulses. The accuracy of weight determination was of 0.1 mg. The substrates were placed in vacuum chamber at a distance of 30 cmaway from a

Copyright © 2012. Nova Science Publishers, Incorporated. All rights reserved.

Diamond-Like Carbon Films, Nova Science Publishers, Incorporated, 2012. ProQuest Ebook Central,

plasma source output normally to the plasma flow. The thickness of a coating was determined using interferometer MII-4. The hardness and elastic constants were measured by nano-indentation using Berkovich diamond tip.

There is a nearly linear dependence of the DLC film deposition rate on acetylene vapor pressure as seen in Figure 25. Its means that the amount of activated acetylene radicals directed by the arc plasma towards the substrate depends in direct ratio of the quantity of collisions between carbon ions emitted by arc and acetylene molecules. The experience with the combined PVD-CVD technique allows to draw a conclusion that it gets an increase of DLC film deposition rate by a factor of 5…8 in comparison with the vacuum pulsed arc technique.

Increase content of the graphite-like phase in a DLC film follows the dropping film hardness as far as the vapor pressure increases. The tendency leads to very soft DLC films obtained at acetylene gas pressure higher that 1 Pa. (Figure 25). Technological compromise between high deposition rate and low hardness could be achieved at the gas pressure ranging from 0.3 to 0.8 Pa.

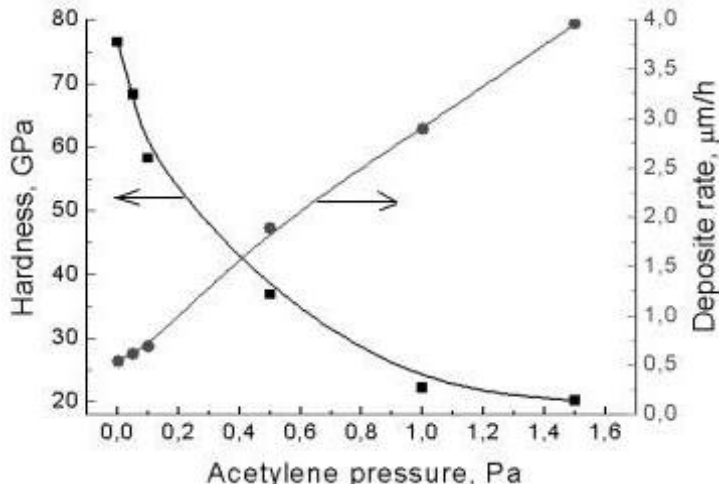

Figure 25. Dependence of hardness and growth rate on acetylene vapor pressure.

Figure 26 demonstrates the dependence of a surface roughness on acetylene pressure. Remarkable change of the roughness is observed above acetylene pressure of 1.0 Pa. Such roughness changing behavior is commonly observed for CVD methods of thin film deposition [12, 13].

*Tribological testing.*The tribological properties of DLC coatings were investigated by the tribometer pin-on-disk scheme. The ball 5.51 mm in diameter made of bearing steel was used as a counterbody. The load force was 0.4 N, and RPM 120 that provided the relative speed was 7.16 m/min. Friction tracks ware observed by the Hitachi S-900 scanning electronic microscopy.

The dependence of frictioncoefficient, *f,* on the number of sliding cycles for DLC films deposited in vacuum and an acetylene atmosphere at pressure 0.5 Pa is shown in Figure 27. For comparison, the friction curve for silicon wafer without a coating is presented, too. The friction coefficient, *f,* is relatively high bytribolayer formation during 30 min. After this time

Copyright © 2012. Nova Science Publishers, Incorporated. All rights reserved.

Diamond-Like Carbon Films, Nova Science Publishers, Incorporated, 2012. ProQuest Ebook Central,

value*f* is stabilized for the sample (1) at the level of 0.25 while for the sample (2) the friction coefficient slowly decreases and achieves value of 0.06. Such low dry friction coefficient is there only for a hard layered lubricant based on molybdenum disulfide orgraphite.

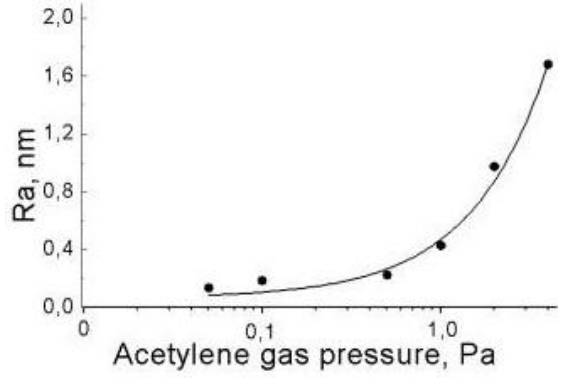

Figure 26. Dependence of roughness of coating surface on acetylene pressure.

It is necessary to note that without coating the friction coefficient of the steel ball against a silicon plate is 1.15. The observation of friction tracks after 7 hours of sliding test (Figure 28 a) has revealed weak abrasive wear of DLC films deposited by the combined method in comparing with that for the vacuum deposited DLC films.In the latter case the fatigue wear takes place and it is expressed in the fragmental delaminating of coating from the substrate as it is shown in the SEM image in Figure 28 b. In this way an abrasive wear of the steel rider is strongly increased. Similar results have been reported in [25]. The wear track analysis revealed no abrasive particles of the steel rider in the case of DLC films deposited by the combined technique. A converse effect is observed for the DLC film obtained by the pure PVD method. Figure 30 demonstrates energy dispersive x-ray (EDX) microanalysis spectra that consist of iron peak and oxygen peak. Content of Fe and O is in ratio 1:3 in accordance with the peak intensities of these elements. Possibly it denotes formation of iron hydrate $Fe(OH)_3$ on the steel ball surface.

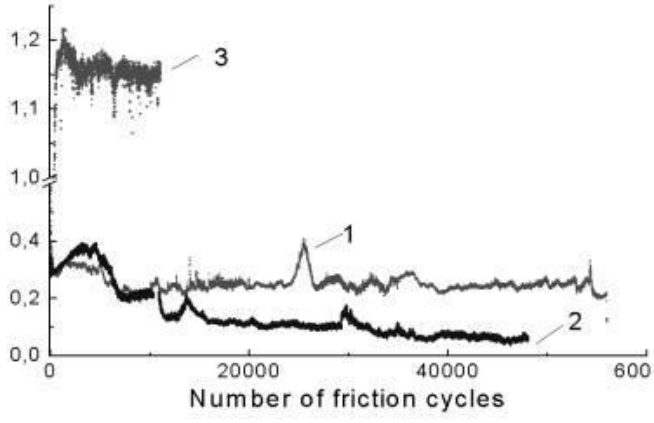

Figure 27. Evolution of the friction coefficient vs. number of sliding cycles for DLC film (1) deposited in vacuum and (2) acetylene at pressure of 0.5 Pa. For comparison: (3) is a sliding curve for uncoated silicon.

Copyright © 2012. Nova Science Publishers, Incorporated. All rights reserved.

Diamond-Like Carbon Films, Nova Science Publishers, Incorporated, 2012. ProQuest Ebook Central,

It is necessary to note that without coating the friction coefficient of the steel ball against a silicon plate is 1.15. The observation of friction tracks after 7 hours of sliding test (Figure 28 a) has revealed weak abrasive wear of DLC films deposited by the combined method in comparing with that for the vacuum deposited DLC films.In the latter case the fatigue wear takes place and it is expressed in the fragmental delaminating of coating from the substrate as it is shown in the SEM image in Figure 28 b. In this way an abrasive wear of the steel rider is strongly increased. Similar results have been reported in [25]. The wear track analysis revealed no abrasive particles of the steel rider in the case of DLC films deposited by the combined technique. A converse effect is observed for the DLC film obtained by the pure PVD method. Figure 30 demonstrates energy dispersive x-ray (EDX) microanalysis spectra that consist of iron peak and oxygen peak. Content of Fe and O is in ratio 1:3 in accordance with the peak intensities of these elements. Possibly it denotes formation of iron hydrate $Fe(OH)_3$ on the steel ball surface.

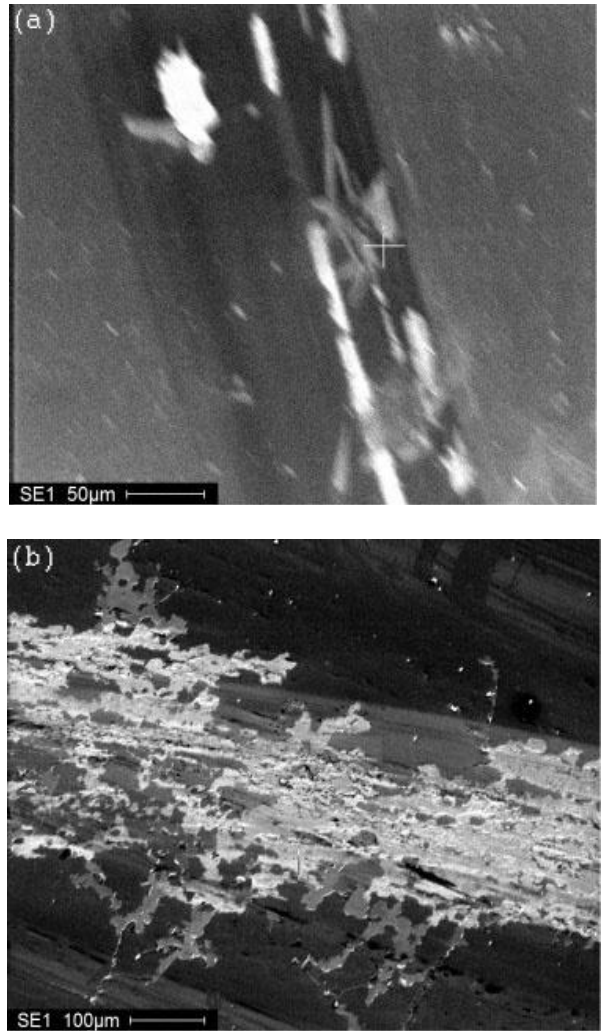

Figure 28. Friction tracks after 7 hours of sliding test for DLC coating deposited (a) at acetylene presence and (b) in vacuum.

Copyright © 2012. Nova Science Publishers, Incorporated. All rights reserved.

Diamond-Like Carbon Films, Nova Science Publishers, Incorporated, 2012. ProQuest Ebook Central,

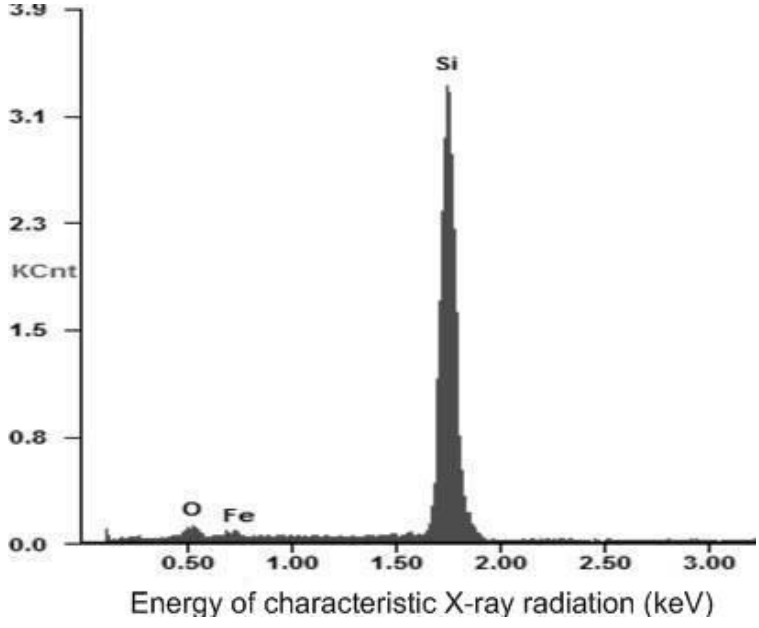

Figure 29. EDX microanalysis spectra of the weartrack for DLC film deposited in vacuum (PVD method).

*Industrial application the combined PVD-CVD method in DLC coating deposition.*The newly developed method has been applied in some areas of modern industry and medicine. A successful usage of the combined PVD-CVD technology is described in this section in several examples.

The novel technique was used for improvement functional performances and life spans of micro drills and routers of tungsten carbide for the processing of printed-circuit-boards. Figure 30 b shows drills of diameter of 0.25 mm with length of a working part 3.8 mm (Kyocera Tycom Corp., USA) with DLC films of 0.3μm in thickness. The TEM picture of cross-section of a DLC coating on WC-Co drill is pictured in Figure 31 b. One can see a well adhered DLC film to substrate. There are no swellings and delaminations but only perfect interface between a substrate and coating. Drilling and cutting tests showed that the DLC coatings increased wear resistance of the micro drills and routers 1.5…2 times as much; there were no sticking problems, and excellent quality of holes and grooves when printed-circuit-board processing was observed.

Deposition of DLC coatings on pistons of diesel engines for trucks (Figure 30 a)given a possibility to reduce the friction coefficient of cylinder-sleeve and to diminish wear of a pistons surface at the stage of engine run-in.

A technology developed for the obtaining those coatings on the operate surfaces of molds and dies used for plastic good fabrication be found to be more effective as galvanic chrome technology. DLC coatings hinder from plastic sticking to a mold surface, increase its life time essentially and they may play a role of solid lubricants successfully in many cases when it is impossible to use an oil lubricant for the moving parts of complicate molds and dies like these showed in Figure 30 c. That is because of prevention of any contaminations of manufacturing articles.

Copyright © 2012. Nova Science Publishers, Incorporated. All rights reserved.

Diamond-Like Carbon Films, Nova Science Publishers, Incorporated, 2012. ProQuest Ebook Central,

Figure 30. Industrial application if the combined PVD-CVD method to deposit DLC films onto (a) engine piston, (b) WC-Co microdrills, (c) plastic mold, (d) germanium lens for IR-optics,(e) space optical devices, and (f) artificial heart valve.

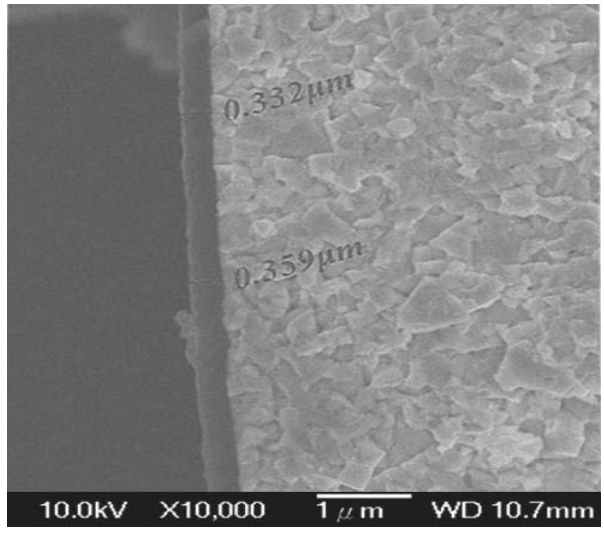

Figure 31. SEM image of the cross-section of DLC coating of 0.35 μm in thickness on WC-Co substrate.

Copyright © 2012. Nova Science Publishers, Incorporated. All rights reserved.

Diamond-Like Carbon Films, Nova Science Publishers, Incorporated, 2012. ProQuest Ebook Central,

DLC films exhibit considerable promise as materials for IR antireflection coatings to be used in optical devices as well as for absorbing coatings of body in order to guard against stray light in optical The PVD-CVD technology is very attractive to deposit such kind coatings owing to high uniformity of coating thickness and possibility to its controlling to several nanometers which is conditioned by a discrete impulse mode of DLC film deposition. The bilateral DLC coatings deposited on germanium windows (Figure 30 d) increase their light transmission from 0.45 up to 0.95 for wave length of 10 μm.

DLC coatings were also investigated concerning their application for bodies of optical mounted on artificial Earth satellites. Figure30 (e) shows one of the optical devices having a body and frames that made of invar (Ni-36% -Fe) and coated with DLC films. These films were deposited at special conditions of PVD-CVD process in order to have a high light absorption and low thermal expansion coefficient.

As it is know well that DLC films possess an excellent chemical inertness and low permeability for other chemical elements. Combination of these properties with perfect mechanical and tribological performances makes DLC films one of the best biocompatible coatings for medical implants. They were applied to coat bodies of PLANIX-T artificial heart valves (ELECTRONMASH Plant, Belarus) after all necessary technical and medical testing (see Figure 30 f). The DLC coatings were tested as biocompatible coating of bone implants which temporally inserted in a human bogy, too. They prevent adsorption of osteoblasts and implants can be easy removed after knitting of a brooked bone. As it was recently demonstrated [31]. The application of titanium implants with DLC doped by silver hasinhibiting influence on growth of some tumors, in particular, on C6neoplastic rat glioma. These data are new and they open furtherpossibility for application of DLC:Ag composite in medicine.

*Conclusion.*A high deposition rate of diamond-like carbon coatings is the main advantage of recentlydeveloped novel combined PVD-CVD method. The deposition rate exceeds in several times that achieved by pulsed cathodic arc burned in vacuum due to formation of C_2 radicals as a result of acetylene molecule rupture in collisions with the carbon plasma particles. The chemical bond structure, hardness and other properties like roughness, compressive stress etc. lie between those of ta-C coatings and hydrogenated DLC coatings. The performance may differ with changing acetylene pressure in a vacuum chamber. With development of this method, opportunities for technical application essentially widen. Essentially with this new method, it is able to obtain all types of DLC coatings beginning from hydrogenized a-C:H deposited at a high hydrocarbon gas pressure to tetrahedral amorphous carbon (ta-C) deposited at a low gas pressure and room temperature without substrate bias.

REFERENCES

[1] Ohtake N., Saito H. Classification of DLCs (temporary). International Session on DLC, JNDF, Chiba, Japan, 2009.

[2] Goncharenko V.P., Kolpakov A.J., Maslow A.I. Method of forming diamond-like carbon coating. *US Patent* 6261424B1, 2001.

Copyright © 2012. Nova Science Publishers, Incorporated. All rights reserved.

Diamond-Like Carbon Films, Nova Science Publishers, Incorporated, 2012. ProQuest Ebook Central,

[3] Me`rel P., Tabbal M., Chaker M., Moisa S., Margot J., *Applied Surface Science*, 136, (1998), 105.

[4] C. A. Davis, K. M. Knowles, G. A. J. Amaratunga. Cross-sectional structure of tetrahedral amorphous carbon. *Surface and Coatings Technology* 316 (1995) 76-78.

[5] Ferrari A.C., Determination of bonding in diamond-like carbon by Raman spectroscopy, *Diamond and Related Materials*, 11 (2002) 1053-1061.

[6] Oliwer W.C. Measurement of hardness and elastic modulus byinstrumented indentation: Advances in understanding and refinements to methodology. *J. Mater. Res*., 19 (2004) 3-20.

[7] Liu D., Benstetter G., Lodermeier E., Akula I, Dudarchyk I. SPM investigation of diamond-like carbon and carbon nitride films. *Surf. Coat. Tech.* 173 (2003) 194-203.

[8] Ohtake N., Saito H. Classification of DLCs, Japan New Diamond Forum, Chiba, Japan, 2009

[9] Cho, Sungwoo; Chasiotis, Ioannis; Friedmann, Thomas A.; Sullivan, John P. Young's modulus, Poisson's ratio and failure properties of tetrahedral amorphous diamond-like carbon for MEMS devices, *J. Micromechanics and Microengineering* 15 (2005) 728-735.

[10] Musil J., Jirout M. Toughness of hard nanostructured ceramic thin films. *Surf. and Coat. Tech*., 201, (2007), 5148–5152.

[11] Bernard F., Coll B.F., Sanders D.M. Design of vacuum arc-based sources. *Surf. Coat. Technol*. 81, (1996), 42-51.

[12] Anders A. Approaches to rid cathodic arc plasmas of macro- and nanoparticles: a review. *Surf. Coat. Technol*. 120 (1999) 319-330.

[13] Keidar M., Beilis I., Boxman R.L., Goldsmith S. Transport of macroparticles in magnetized plasma ducts. *Proc. 12th Int. Symp. on Plasma Chem.*, 3 (1995) 1367-1370.

[14] Boxman R.L., Goldsmith S. Macroparticle contamination in cathodic arc coatings: generation, transport and control. *Surf. Coat. Technol*. 52 (1992) 39-50.

[15] Aksenov I.I., Belous V.A., Padalka V.G. Transport of plasma streams in a curvilinear plasma-optics system. *Sov. J. Plasma Phys*. 4 (1978) 425-430.

[16] Anders S., Anders A., Dickenson M.R., MacGill R., Brown I.G. S-shaped magnetic macroparticle filter for cathodic arc deposition. *IEEE Trans. Plasma Sci.* 25 (1997) 670-674.

[17] Anders A., Anders S., Brown I.G. Transport of vacuum arc plasmas through magnetic macroparticle filters. *Plasma Sources Science and Technology* 4 (1995) 1-12.

[18] Witke T., Schuelke T., Schultrich B., Siemroth P., Vetter J. Comparison of filtered high-current pulsed arc deposition HCA with conventional vacuum arc methods. *Surf. Coat. Technol*. 126 (2000) 81-88.

[19] Polo M.C., Andujar J.L., Hart F., Robertson J., Milne W.I. Preparation of tetrahedral amorphous carbon films by filtered cathodic vacuum arc deposition. *Diam. Relat. Mater*. 9 (2000) 663–667.

[20] Zhang, T., Zeng Z.M., Tian X.B., Tang B.Y., Chu P.K. Mechanism of enhanced plasma transport of vacuum arc plasma through curved magnetic ducts. *J. Vac. Sci. Technol*. 17, (1999) 3074-3076.

[21] Boxman, R.L., Martin P.J., Sanders D. Handbook of vacuum arc science and technology. Noyes, New York, 1996 P. 520.

Copyright © 2012. Nova Science Publishers, Incorporated. All rights reserved.

Diamond-Like Carbon Films, Nova Science Publishers, Incorporated, 2012. ProQuest Ebook Central,

[22] Artsimovich A.A., Sagdeyev R.Z. Physics of plasma for physicists. Moscow, Atomizdat, 1979, P. 148.

[23] Chu P.K., Li L. Characterization of amorphous and nanocrystalline carbon films. *Materials Chemistry and Physics* 96, (2006), 253-277.

[24] Zhang S., Zeng X.T., Xie H., Hing P. A phenomenological approach for the Id/Ig ratio and sp3fraction of magnetron sputtered a-C films. *Surface and Coatings Technology* 123 (2000) 256–260.

[25] McKenzie, Muller D., Paithorpe B.A. et al. Properties of tetrahedral amorphous carbon prepared by vacuum. *Diamond and Related Materials* 1 (1991) 51-59.

[26] Bui Xuan Lam. Diamond-like carbon coating for tribologycal application. *Science and Technology Development*11(2008) 100-108.

[27] Yudasaka M., Kikuchi R. Graphitization of carbonaceous materials. In: Yoshimura S, Chang R.P.H, editors. Supercarbon: synthesis, properties, and applications. Berlin, Springer, 1998, P. 99-105.

[28] L. Schott. Electric probes Plasma diagnostics. W. Lochte-Holtgreven editor. North-Holland, Amsterdam, 1968, P.29-32.

[29] ErvinK. M., GronertS., BarlowS.E., GillesM. K.,. HarrisonA. G, BierbaumV. M., DePuyC. H., Lineberger W.C., EllisonG.B. Bond Strengths of Ethylene and Acetylene. *J. Am. Chem. Soc.* 112 (1990) 5750-5759.

[30] Dunphy J.C., Rose M., Behler S., Ogletree D.F., Salmeron M. Acetylene structure and dynamics on Pd(111). *Physical Review* B. Number 20. 57 (1998) 705-708.

[31] N.M. Chekan, N.M. Beliauski a, V.V. Akulich a, L.V. et al. Biological activity of silver-doped DLC films. *Diamond and Related Materials* 18 (2009) 1006-1009.

Copyright © 2012. Nova Science Publishers, Incorporated. All rights reserved.

Diamond-Like Carbon Films, Nova Science Publishers, Incorporated, 2012. ProQuest Ebook Central,

In: Diamond-Like Carbon Films
Editor: Yuto S. Tanaka
ISBN: 978-1-61324-791-4
© 2012 Nova Science Publishers, Inc.

Chapter 2

PECULIARITIES OF ION-BEAM SYNTHESIS OF CARBON-BASED PHASES

D. I. Tetelbaum, A. N. Mikhaylov and A. I. Belov
Physico-Technical Research Institute of Lobachevsky State University of Nizhny Novgorod, Nizhny Novgorod, Russia

ABSTRACT

Ion implantation is a versatile and widespread approach for the synthesis of various materials. Recently, a particular interest has arisen in the application of ion beams to the fabrication of carbon-based nanostructures for the needs of nano-, optoelectronics and photonics. A distinctive peculiarity of the ion synthesis is its strongly expressed non-equilibrium character resulting in multiform structural transformations in the ion-implanted solids. In the present chapter, the principle of structural compliance of the new and parent phases has been, for the first time, formulated that allows to interpret and predict a type of the ion-induced transformations. The structural classification of the types of ion-beam induced phase transformations is suggested. The peculiarities of ion-beam synthesis and transformations are illustrated on several examples of carbon and carbon-rich phases: the face-centered cubic carbon, ion-synthesized films of SiC and Al_4C_3, etc. The literature and original data on the ion-beam synthesis of silicon carbide and other carbon-rich nanoclusters, mainly in SiO_2 matrix, are analyzed in comparison with similar nanostructures prepared by other techniques. It is concluded that the principle of structural compliance can be applied to some features of the ion synthesis of SiC and C nanoclusters, too. Special attention is paid to luminescent properties of the carbon-based nanostructures and to the relation of luminescence bands to a phase composition of the layers. Some unsolved problems and the ways of further investigations are discussed.

Copyright © 2012. Nova Science Publishers, Incorporated. All rights reserved.

1. INTRODUCTION

The synthesis of nanocrystalline phases of group IV of the periodic system attracts great attention, mainly due to a hope to produce effective sources of light emission for

Diamond-Like Carbon Films, Nova Science Publishers, Incorporated, 2012. ProQuest Ebook Central,

optoelectronic devices compatible with silicon technology. This hope was largely excited in the early 1990s by the L.T. Canham's discovery [1] of bright luminescence of porous silicon which in fact, is a collection of the oxidized silicon nanocrystals (SiO_2:nc-Si system). This finding manifests the role of low-dimensional effects in the improvement of optical properties as the bulk silicon displays poor light-emission properties being the indirect-bandgap semiconductor. This role is associated with the fundamental Heisenberg uncertainty relation: $\Delta x \cdot \Delta p \geq h$. The smaller the size of a crystal, the larger the value of Δp and the probability of quasi-direct radiative transitions.

The Canham report stimulated numerous investigations of not only porous Si, but all kinds of the SiO_2:nc-Si system synthesized by various methods. Systems of nanocrystals or nanoclusters of other IV-group species, in particular, carbon and silicon carbide also became of interest some time later [2]. It is important for optoelectronic applications that C and SiC nanostructures display the room-temperature luminescence in a broad UV-visible spectral domain, in contrast to Si nanocrystals emitting light in the red and near-IR range of the spectrum. High melting temperature and better chemical stability are the recognized advantages of the SiC-based materials working in aggressive environments. To some extent, this also applies to carbon nanoclusters, although their properties (especially in dielectric matrices) are less studied than those of SiC.

Ion implantation seems to be one of the most appropriate methods to synthesize the thin layers or inclusions of chemical compounds that is fully relevant to a case of the formation of systems of the IV-group nanoinclusions in dielectric matrices. Among the benefits of this method are high controlability of the fabricated material properties and, especially, perfect compatibility with the traditional microelectronic technology. There are several ion-beam-based approaches to form carbon-containing nanostructures, such as the ion-beam synthesis of SiC phase that is transformed to a porous layer by anodic etching [3, 4], implantation of carbon into a single-crystal silicon with subsequent oxidation [5], implantation or Si^++C^+ into SiO_2 with subsequent phase separation during high-temperature annealing, etc [6].

An essential peculiarity of the processes taking place at the ion implantation of solids is their highly expressed non-equilibrium character. Such non-equilibrium processes at ion implantation often give rise to the formation of some phases that do not correspond to phase diagram and sometimes to the previously unknown substances or allotropic forms. The question, which phase and why it is synthesized, is of great scientific and practical interest. Here, we formulate the so-called *principle of structural compliance*, which may be useful for explanation of the peculiarities of ion synthesis and prediction of phase composition of the ion-synthesized materials.

In the present chapter, we start with short consideration of the principle of structural compliance. Then, we describe the results of ion-beam synthesis of the carbon-based and some other phases illustrating the principle. The main part of the chapter is devoted to the ion-synthesized silicon carbide and carbon nanoclusters in SiO_2. For the comparison, the literature data on the carbon-based nanostructures fabricated by other techniques is shortly described. Special attention is paid to the luminescent characteristics of nanoclusters because of their potential application in optoelectronics. In summary, some unsolved problems and tasks for further research work in this field are indicated.

Most of the analyzed experimental data is original, but the results of other authors are also discussed. However, our study does not claim to be the exhaustive literature review. The main goal of the chapter is to analyze the structural aspects of ion synthesis and its

Copyright © 2012. Nova Science Publishers, Incorporated. All rights reserved.

Diamond-Like Carbon Films, Nova Science Publishers, Incorporated, 2012. ProQuest Ebook Central,

capabilities for the fabrication of light-emitting materials on the basis of carbon and carbon-rich phases.

2. THE PRINCIPLE OF STRUCTURAL COMPLIANCE AT PHASE TRANSFORMATION UNDER ION IRRADIATION

The main distinction of structural and phase transformations at ion irradiation (implantation) compared to those at thermal annealing is the strong non-equilibrium character of the processes. There are two extreme approaches to the consideration of such processes. These approaches have been marked already at early stage of ion implantation research. The first approach is formulated by Brinkman [7] and is known as a model of displacement spikes (displacement cascades). This model fixes attention on the giant supersaturation of a solid by the point defects (vacancies and interstitials) in the regions along ion paths. Point defect concentration can approach a high value – up to tens of atomic percents, therefore this circumstance should affect strongly the structural and phase transformations either during irradiation or after it.

The influence of radiation defects is especially strongly expressed in the amorphization phenomenon. Ion irradiation may induce such a high defect concentration that the free energy of crystalline state becomes larger than that of amorphous phase (of the same chemical composition) and it becomes energetically favorable for a solid to transform into an amorphous state with a lack of localized point defects typical of crystalline state. The supersaturation with point defects at ion irradiation makes a thermodynamic stimulus not only for amorphization but for other kinds of structural and phase transformations, as well. For such transformations, point defects usually are not inherited by a newly formed phase. Then, the transformation decreases the free energy of a system. Therefore, transformations (such as solid solution decomposition) often become possible in such macroscopic conditions when they could not take place under the thermodynamic equilibrium.

The second approach is based on the representation of a region excited by ion penetration in terms of the temperature elevation – the model of thermal spike (F. Seitz [8]). According to this model, the temperature in a thermal spike center can approach to ~ 10^3 K. Although the lifetime of a thermal spike is very small (10^{-12}-10^{-10} s), such a high temperature (and the related high pressure) can induce structural and phase transformation, in particular, the formation of non-equilibrium phases. Local melting and subsequent quick solidification of the thermal spike regions can also cause the amorphization of semiconductors and dielectrics.

We will not go into a detailed consideration of the mentioned above models. It is, however, worth to note that these models cannot explain all of the features of structural and phase transformations under ion irradiation. The following regularity is often observed: *from various possible phases, such a phase is formed, the structure of which can be obtained from that of the parent phase by means of relatively small transformation, or which can be structurally better accommodated to the parent phase.* We nominate this regularity *'the principle of structural compliance'.*

P.V. Pavlov [9, 10, 11] was the first who had attracted attention to the fact that from the two allotropic forms of silicon nitride (α–Si_3N_4 and β–Si_3N_4), only α–Si_3N_4 is always formed at the ion implantation of nitrogen into Si. He explained this fact by the easier transformation

Copyright © 2012. Nova Science Publishers, Incorporated. All rights reserved.

Diamond-Like Carbon Films, Nova Science Publishers, Incorporated, 2012. ProQuest Ebook Central,

of the initial structural skeleton of Si to α–Si_3N_4 rather than to β–Si_3N_4. Namely, the transformation into α–Si_3N_4 can be provided by mutual rotation of tetrahedrons constituting the silicon skeleton and subsequent substitution of a fraction of Si atoms by nitrogen ones. Meanwhile, the synthesis of β–Si_3N_4 requires a more radical transformation of the Si skeleton. Such a situation is characteristic for many other cases of ion synthesis, especially at room-temperature and low-temperature implantation. This feature was called the *"structural adaptation"*. The principle of structural compliance is the generalization of this rule to a wider class of ion-induced transformations; this principle permits to explain and often to predict a type of the transformations. Another demonstration of this principle is the formation of a phase, crystalline lattice of which can be epitaxially (or endotaxially) accommodated with the parent phase.

Of course, not all of the cases of ion-induced structural and phase transformations can be described by the principle of structural compliance. So, high temperature and high pressure in thermal spikes can promote the formation of phases with a structure that cannot be considered in the frame of this principle.

Taking into account the above mentioned remarks, the classification of processes at ion synthesis can be carried out if we consider various kinds of the atomic configuration reconstructions.

a *Inculcation.* The skeleton of initial structure is preserved; the implanted atoms are placed in the interstitial positions. Ion synthesis of SiO_2 by O^+ implantation into Si is an example of such a process: the implanted oxygen atoms are placed between each two Si atoms. (The ion-synthesized silicon oxide is usually amorphous, therefore the stage of silicon amorphization must be involved in this transformation).

b *Substitution.* The implanted atoms take positions at the sites of initial lattice. This kind of reconstruction is revealed e.g. at the ion synthesis of ternary $A_{III}B_V$ semiconductors (such as the synthesis of $Al_{1-x}Ga_xAs$ by Al implantation into GaAs).

c *Sliding.* These transformations can occur by mutual displacements (sliding) of the adjacent atomic planes, with the implanted atoms locating into the interstitial positions of the transformed lattice. This kind occurs e.g. at the ion synthesis of some nitrides (carbides) by nitrogen (carbon) implantation into transitional metals with the closely packed crystalline lattices (such as Ta, Nb, Ni, Co).

d *Three-dimensional lattice reconstruction*. In these cases, the configuration of atoms is dramatically changed, the principle of compliance can then occur (as for the Si_3N_4 synthesis) but it is not mandatory. The above mentioned case of Si_3N_4 synthesis [9, 10, 11] can serve as an example of this kind of reconstruction.

The (c) type is characteristic for substances that are plastic at the irradiation temperature; for semiconductors implanted at an elevated temperature ("hot implantation"); for metals irradiated at room or elevated temperature. The (d) type usually takes place for substances with covalent bonds, such as diamond-like semiconductors irradiated at room or lower temperature.

Copyright © 2012. Nova Science Publishers, Incorporated. All rights reserved.

Diamond-Like Carbon Films, Nova Science Publishers, Incorporated, 2012. ProQuest Ebook Central,

3. EXPERIMENTAL EVIDENCES OF THE PRINCIPLE OF STRUCTURAL COMPLIANCE AT ION SYNTHESIS OF CARBON-RICH OR OTHER BULK PHASES

Due to a strong non-equilibrium character of the processes at ion irradiation of solids, the phases can be formed that are difficult or even impossible to obtain by other (more equilibrium) methods. It is the principle of structural compliance that often makes it possible to explain the appearance of one or another phase. Below, several examples of synthesis of such phases observed by us are presented, and their structural interpretation is given.

3.1. Carbon Phase with the Face-Centered Cubic Structure Formed under Irradiation of Graphite Films

The carbon films were deposited by pyrolysis of acetylene on the Al_2O_3 ceramic substrate – for the measurements of electrical conductivity, and on the oxidized silicon substrate – for the electron diffraction study. The deposition temperature was 600 °C. As-deposited films showed a structure of graphite with various level of disorder. The films were irradiated by N^+, Ne^+, Ar^+ ions with energies of 50-80 keV at the ion current density of 10 μA/cm^2 in a vacuum of ~ $3 \cdot 10^{-4}$ Pa and at elevated temperatures – in the range of 150-200 °C.

It is found that no measureable changes in the disorder level are observed after the irradiation of the deposited graphite films with N^+ and Ne^+ ions. After irradiation with Ar^+ ions to a dose of $3 \cdot 10^{16}$ cm^{-2}, in addition to polycrystalline rings, the electron diffraction pattern reveals a broad halo corresponding to the most intense ring of the original graphite film. This is an indication of the irradiation-induced amorphization of the film. At the higher ion doses, electron diffraction patterns show the polycrystalline structure.

Electron diffraction data shows for the irradiated films that there is a transformation of graphite into a new phase [12]. A system of the diffraction lines gives a set of inter-atomic distances (*d*) that does not match any known carbon phase, however, it is in well agreement with the assumption that carbon forms the face-centered cubic (FCC) phase unknown before. The values of inter-atomic distances (*d*), diffraction lines intensities (*I*), crystallographic indices (*hkl*) and lattice parameters (*a*) calculated for the assumed FCC phase of carbon are given in Table 1.

The first ring with d = 0.348 nm is not identified. It is probably related to a residual, strongly distorted graphite phase (for the original graphite phase, the most intense diffraction ring corresponds to d = 0.339 nm).

Formation of the FCC-phase under ion irradiation of graphite conforms with the principle of structural compliance. Transformation of the graphite structure to the structure of FCC-carbon may be represented in the following way. The graphite lattice consists of the hexagonal atomic planes. Under ion irradiation, the hexagon centers in all of the planes are occupied by carbon atoms displaced from the lattice sites resulting in the formation of the close-packed planes which alternate accordingly the ABABAB… package. The mutual pairwise shift (sliding) of the adjacent close-packed planes (having (111) indices in the FCC structure) and a change in distance between them leads to the formation of the FCC phase (the package of the ABCABC… type).

Copyright © 2012. Nova Science Publishers, Incorporated. All rights reserved.

Diamond-Like Carbon Films, Nova Science Publishers, Incorporated, 2012. ProQuest Ebook Central,

The formation of other (known) carbon phases from the parent graphite phase would require more radical transformation of atomic configurations and that's why it does not occur in the given conditions.

It is worth noting that the lattice parameter of the irradiated film is not constant and can vary from test to test in the range of 0.369-0.392 nm. In principle, the new phase may represent not the pure carbon but some chemical compound with impurity atoms (e.g. oxygen) due to the film contamination during implantation in the conditions of a rather bad vacuum. However, no impurity was found (by Auger spectrometry) with the concentration higher than sensitivity of the method (~ 1 at.%). (Probably, the implanted Ar atoms were desorbed due to heating of the film by the ion beam).

Increase in both resistivity and hardness of the irradiated graphite film is observed with an elevation of the ion dose (Figure 1). Such a behavior is typical of the amorphous diamond-like carbon phase, which may also be responsible for the increase in hardness. However, this is in contradiction with the electron diffraction data. Identification of the new phase as some hydrocarbon is also less probable because the hydrogen accumulation in high quantity is not expected for high temperatures provided by the ion-beam heating. The obtained phase is neither a 'metallic' modification of carbon [13], as the formation of this phase would result in a decrease of resistivity. Thus, the new carbon phase is certain to be the FCC allotropic form of carbon unknown before.

Table 1. Electron diffraction data for the graphite films irradiated with Ar^+ ions

d (nm)	0.348	0.226	0.195	0.138	0.118	0.113
I	strong	very strong	weak	strong	medium	weak
hkl	-	(111)	(200)	(220)	(311)	(222)
a (nm)	-	0.391	0.390	0.390	0.391	0.391

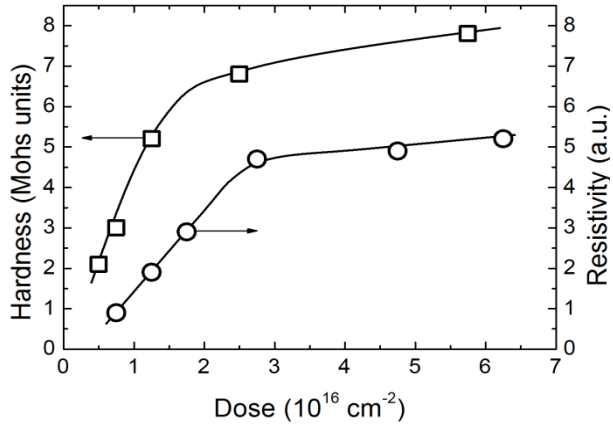

Figure 1. Dose dependencies of hardness (on the Mohs scale) and resistivity of graphite films irradiated by N^+ ions (50 keV).

The question arises how the binding of tetravalent C atom with 12 nearest neighborhoods could be realized in the FCC lattice (characterized by a coordination number n = 12)? It seems that this situation is possible in the case of quantum resonance between the three states of sp^3 type, each of them corresponding to a given carbon atom bound to four neighborhoods

Copyright © 2012. Nova Science Publishers, Incorporated. All rights reserved.

Diamond-Like Carbon Films, Nova Science Publishers, Incorporated, 2012. ProQuest Ebook Central,

[14]. The presence of sp^3-bonds (as in diamond and diamond-like carbon) explains high resistivity and hardness of the irradiated carbon films.

As a reason for the abovementioned variation of lattice parameters, the high and variable concentration of vacancies may be considered. Indeed, the pointed above occupation of the centers of hexagonal cells in the graphite planes by the self-interstitials should be accompanied by the generation of vacancies that partially undergo radiation annealing (recombination). Completeness of the annealing depends on the temperature during irradiation. The residual vacancy concentration may vary from case to case as a result of the temperature variation due to a poor thermal contact between a substrate and a sample holder.

Finally, it should be questioned why no transition to diamond-like modification is observed at ion irradiation, in contrast to the case of magnetron sputtering when the diamond-like structure of carbon films is related to the presence of ion bombardment during the deposition process. The transition from graphite to diamond-like modification is possible due to high temperatures and pressures in thermal spikes, but this possibility depends on the duration of the thermal spike cooling down, which, in turn, is determined by the conditions of heat conductivity. These conditions may differ in our case from those for the diamond-like film deposition and provide the formation of the other carbon phase. However, this is a speculative conclusion that requires further investigations.

3.2. Ion Synthesis of Silicon Carbide by Carbon Implantation in Si

Numerous investigations have been devoted to the ion synthesis of silicon carbide. Here, we report only on our own results.

The Si (111) surface was implanted with C^+ ions (40 keV, $6 \cdot 10^{16}$ cm^{-2}) and thereafter was annealed at different temperatures for 1 hour. A broad infrared absorption band at around 700-860 cm^{-1} related to the Si-C bond vibrations [15] is observed in the as-implanted layers. The band gets narrower and shifts to the shorter wavelengths with annealing. After annealing at 900 °C, it becomes typical of the crystalline SiC with a maximum at 810 cm^{-1}.

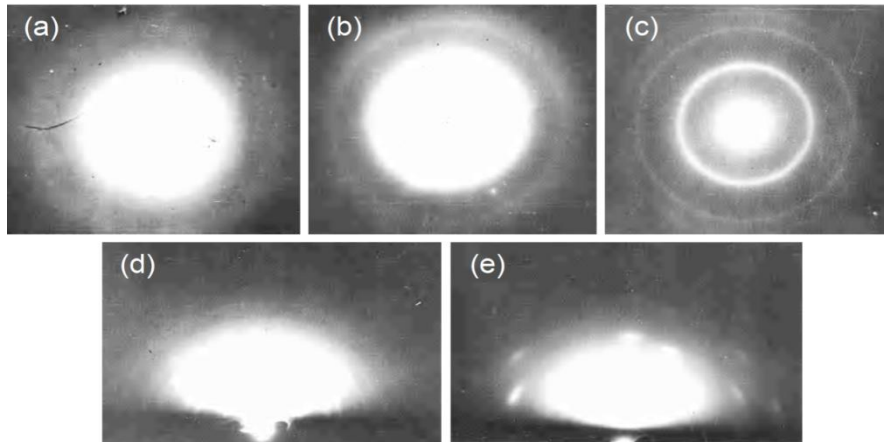

Figure 2. Electron diffraction patterns from SiC layers synthesized by C^+ implantation (40 keV, $6 \cdot 10^{15}$ cm^{-2}) at room temperature (a – no annealing, b – annealing at 700 °C, c – annealing at 900 °C), at 600 °C with no annealing (d) and at 850 °C with no annealing (e).

Copyright © 2012. Nova Science Publishers, Incorporated. All rights reserved.

Diamond-Like Carbon Films, Nova Science Publishers, Incorporated, 2012. ProQuest Ebook Central,

Electron diffraction data (Figure 2) confirms the formation of amorphous SiC phase after the room-temperature C^+ implantation as well as its transition to the polycrystalline phase after annealing at 900 °C. The electron diffraction patterns have shown that silicon carbide crystallizes in the cubic modification (β-SiC). It is known that most of the SiC polytypes have a hexagonal lattice. The formation of cubic SiC can be explained on a basis of the principle of structural compliance: the β-SiC structure is obtained from the Si structure by the substitution of half the Si atoms by the carbon ones. The given principle is also supported by the fact that, when Si is amorphized by the room-temperature implantation, the SiC phase is also amorphous. In the case of 'hot' implantation, when Si is not amorphized, the synthesized silicon carbide has crystalline structure even without annealing [16].

3.3. Ion Synthesis of Al_4C_3, AlN and AlB Phases

Aluminum films were deposited on a cleavage of NaCl and irradiated with C^+, N^+ or B^+ ions with energy of 40 keV, doses in the range of $(3\text{-}7)\cdot10^{17}$ cm^{-2} at ion current density of 16 $\mu A/cm^2$. Two kinds of original films were used – with the polycrystalline (no preferred grain orientation) and textured (grain-oriented) structure. The films preserved their type of the structure after C^+ or N^+ implantation (Figure 3). This fact is one of the demonstrations of the principle of structural compliance and evidences that the new phase grains grow endotaxially with respect to the grains of initial phase.

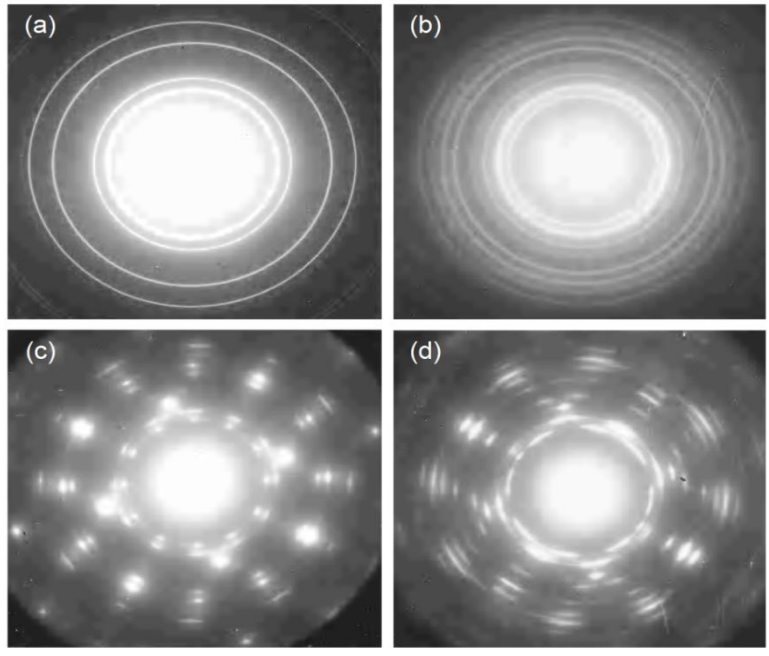

Figure 3. Electron diffraction patterns from the originally polycrystalline (a, b) and grain-oriented (c, d) Al films before (a, c) and after (b, d) N^+ ion implantation (40 keV, $3\cdot10^{17}$ cm^{-2}).

Copyright © 2012. Nova Science Publishers, Incorporated. All rights reserved.

Diamond-Like Carbon Films, Nova Science Publishers, Incorporated, 2012. ProQuest Ebook Central,

The electron diffraction data [17] shows that equilibrium phases of Al_4C_3 and AlN form under C^+ and N^+ implantation, respectively, whereas *an unknown before* phase of AlB with a structure of NaCl type forms under B^+ implantation (Table 2).

The fact of the given phases formation is clear from the viewpoint of the principle of structural compliance. Indeed, the hexagonal lattices of AlN and Al_4C_3 may be built from the initial cubic lattice of aluminum (FCC) by mutual pairwise shift (sliding) of the (111) planes in the ABCABC… package and occupation of a part of the tetrahedral interstitials by N and C atoms, respectively. The case of the AlB phase synthesis is most interesting from this point of view. There is no phase with a structure of NaCl-type in the equilibrium state diagram of Al-B. Metal sub-lattices of the known borides AlB_2, AlB_{10}, AlB_{12}, etc. differ greatly from the initial aluminum lattice, so, their formation, according to the principle of structural compliance, is complicated in conditions of the room-temperature implantation. On the contrary, formation of the NaCl-type lattice occurs much easier by the substitution of half of the aluminum atoms by the boron ones. This example serves as a demonstration of the fact that ion implantation allows to synthesize the materials that are difficult or even impossible to synthesize by the equilibrium or quasi-equilibrium techniques.

Table 2. Electron diffraction data for the Al films irradiated with B^+ ions

d (nm), experimental	0.293	0.252	0.179	0.153	0.146	0.125
d (nm), calculated for AlB	0.295	0.252	0.179	0.152	0.146	0126
hkl	(111)	(200)	(220)	(311)	(222)	(400)

The calculated values of *d* are indicated for AlB with a structure of NaCl type and a lattice parameter $a = 0.505$ nm.

4. CARBON AND CARBON-RICH NANOPHASES

As it is mentioned in Section 1, carbon and carbon-rich nanoclusters are interesting mainly due to a possibility to receive visible luminescence from the silicon-based materials. It is also pointed out that ion implantation is advantageous in the synthesis of thin layers of various chemical compounds, especially, owing to its natural compatibility with traditional silicon technology. At the same time, the strongly expressed non-equilibrium state of the ion-implanted substance requires accounting for the specific peculiarities of the method when considering phase composition and structure of the ion-synthesized layers.

Information on the relation between the phase composition and the luminescent properties of carbon-rich nanoclusters will be more useful if we consider the data obtained not only for the ion-synthesized nanostructures but also for similar nanostructures fabricated in a different way. It is of special importance, first, because of the existence of luxuriant literature on the non-implantation techniques of synthesis of the carbon-rich layers and, second, because of the possibility of more unambiguous interpretation of the luminescence bands.

There are various approaches to the formation of luminescent nanostructures of silicon carbide and carbon. On the analogy of silicon nanostructuring, the earliest approach was based on the fabrication of porous SiC layers by the electrochemical etching of bulk silicon carbide [18, 19]. Since the mid 1990's, several groups have attempted to demonstrate blue

Copyright © 2012. Nova Science Publishers, Incorporated. All rights reserved.

Diamond-Like Carbon Films, Nova Science Publishers, Incorporated, 2012. ProQuest Ebook Central,

and white light emission from the porous layers obtained by the etching of the ion-synthesized SiC layers [3, 4], and the layers obtained by the incorporation of carbon nanoparticles [20, 21] or SiC nanocrystals [22] into the pores of porous Si with subsequent thermal treatment. Light-emitting nanocrystals or amorphous nanoclusters of SiC form both in the vapor-phase deposited SiC films (see e.g. [23]), and the $Si_xC_yO_z$ oxide layers enriched with silicon and carbon [24, 25]. Carbon and silicon nanoclusters may serve as light emitters in addition to SiC. Formation of the optically active interface states related to small carbon clusters [26] is also possible when the SiC phase inclusions form in the SiO_2 matrix. The influence of carbon and silicon-carbon nanophases on the resulting properties of nanostructures depends strongly on the conditions of their formation and, correspondingly, on the prevailing type of the carbon bonding (sp^2 or sp^3).

Light-emitting properties of the porous silicon carbide have being discussed since the mid 1990's [18, 19] up to now [27, 28]. Without additional treatment, the porous layer formed by etching the original single-crystal SiC substrate does not contain an observable amount of elemental silicon or carbon phases, that makes the identification of photoluminescence (PL) spectra easier. In this case, the light emission in the wavelength region of 300-700 nm comes from crystallites of original SiC polytypes with the sizes from several unities to several hundreds of nm. A non-exponential character of the PL decay with the lifetimes from hundreds of picoseconds to several nanoseconds [19], as well as a comparison of the luminescence with the Raman scattering data [28, 29], has allowed making a conclusion that, in addition to the deexcitation of quantum-confined excitons, electrons and holes can recombine radiatively with the participation of surface states, which are sensitive to the chemical surrounding of the crystallites [27]. Another method of porous SiC layer formation is the ion synthesis of the surface β-SiC layer followed by its electrochemical etching [3, 4] (see below).

Observation of the stable visible luminescence in porous SiC has generated a number of alternative approaches with the use of chemical technologies. One of these approaches is based on the procedure when the layer of luminescent β-SiC precipitates forms during annealing of porous silicon embedded with the C_{60} fullerene molecules [20]. The phases of Si, graphite and SiO_2 coexist in the layer, and the diamond-like carbon is also observed after oxidation (although the authors of [20] do not comment on this fact). Carbonization of porous Si with subsequent oxidation reported in [21] also gives rise to the formation of SiO_2 layer containing the randomly oriented graphite-like carbon clusters displaying the yellow-white PL.

The technology of porous layers formation is based on the so called 'wet chemistry' and is not compatible with the traditional integrated circuits technology. During the last decade, special attention of researchers and technologists has been focused on the other, more compatible with the silicon planar technology, techniques such as chemical-vapor deposition [30, 31, 32, 33, 34] and magnetron sputtering [23, 35]. The as-deposited film generally represents a system of the crystalline silicon carbide inclusions with the sizes from several unities to tens of nm in the amorphous SiC matrix. The chemical and phase composition of the films strongly depends on the conditions of deposition and subsequent thermal treatment. At certain conditions of the chemical-vapor deposition, in addition to the SiC particles, the disordered phase of carbon with both sp^2 and sp^3 bonding types is revealed [31, 33], either in the form of isolated clusters or being located at the surfaces of SiC nanocrystals [31]. The controllable change of the deposited layer composition by the co-sputtering of separate Si and

Copyright © 2012. Nova Science Publishers, Incorporated. All rights reserved.

Diamond-Like Carbon Films, Nova Science Publishers, Incorporated, 2012. ProQuest Ebook Central,

C targets has allowed the authors of [23] to monitor the formation of various phases during the high-temperature annealing. It is found that, when the carbon concentration is low, Si nanocrystals predominantly form in the deposited layer, whereas, when the Si and C concentrations tend to be equal, SiC nanocrystals form and a fraction of carbon atoms are re-organized into the amorphous phase as well as into the fullerene-like clusters.

The PL data for the deposited SiC layers and the carbon phases existing in these films are not unambiguous. PL is often observed in a wide spectral region from ~ 400 to ~ 700 nm with the two PL bands being the most expressed: the 'longwave' band at around 600 nm and the 'shortwave' band centered in the range of 400-450 nm. The shortwave band is usually attributed to the luminescence of β-SiC with a maximum that is blueshifted in respect to the maximum of bulk β-SiC due to the quantum confinement effect (see [34] as an example, for which the cubic SiC structure is identified by the X-ray diffraction). There is no common opinion about the nature of the longwave PL band. In [34], this band is related to radiative recombination at the surface states of SiC clusters, whereas in [31], it is associated with the amorphous SiC phase (*a*-SiC) argued by the fact that a high-temperature annealing in an argon atmosphere leads to the PL reduction (when the *a*-SiC should be crystallized). The complicated structure of the deposited films and its strong dependence on the deposition conditions makes it difficult to interpret PL spectra, especially, because theoretical calculations of the electronic structure and radiative transitions are not so developed for SiC and C nanocrystals (nanoclusters) in contrast to those for Si nanocrystals. (The calculations performed in [18, 31, 36] for the clusters of cubic, hexagonal and amorphous SiC, as well as for amorphous C with the diameter of 1.5 nm, may be applied only with precaution to real systems for which the cluster size is more than 2 nm).

The greatest progress in understanding the properties of Si nanocrystals has been reached in the case of their incorporation into a silicon dioxide matrix. In this connection, it is of special interest to carry out an analogous investigation for the carbon-rich nanoclusters. The ensemble of SiC nanocrystals (or, more general, nanoclusters) embedded into the SiO_2 matrix has such advantages as chemical and mechanical stability together with the complete compatibility of their formation process with the current silicon planar technology. High barriers at the interface with the matrix provide the localization of the photo-excited carriers in nanoclusters and, correspondingly, the modification of optical properties of the nanostructures. Such systems include the abovementioned layers obtained by oxidation of the porous Si chemically treated with carbon [20, 21], and SiO_2 layers embedded with the β-SiC nanocrystals synthesized by C^+ ion implantation in silicon with subsequent annealing in the oxidizing atmosphere [5].

Another approach to the given system formation is based on the use of the sub-stoichiometric silicon oxide enriched with silicon and carbon as the initial material. Its annealing at the temperatures above 800 °C results in the phase separation – the recovery of stoichiometry of silicon dioxide matrix and the synthesis of carbon-rich nanoclusters. The deposited SiO_x:C:Si films [24, 37] represent an example of such a system that is characterized, after the high-temperature annealing, by the white luminescence peaked at around 500-550 nm. However, the investigations of optical properties and chemical composition of the films without direct correlation with their microstructure [24, 37] have added no clarity to the understanding of the nature of the visible luminescence. The main conclusion that can be derived from these reports is the relation of visible emission to the presence of carbon-rich phases, not defects in the oxide matrix. The presence of excess

Copyright © 2012. Nova Science Publishers, Incorporated. All rights reserved.

Diamond-Like Carbon Films, Nova Science Publishers, Incorporated, 2012. ProQuest Ebook Central,

(overstoichiometric) silicon in the films appears to be necessary for the synthesis of carbon-rich clusters. Moreover, its presence prevents carbon atoms from out-diffusion in the form of volatile CO and/or CO_2 compounds, owing to the stronger binding of carbon to excess silicon than to oxygen.

Let us now switch to the discussion of the ion-beam synthesis of silicon-carbon nanostructures. It should be emphasized again that ion implantation is perfectly compatible with the traditional silicon integrated circuits technology.

The methods which employ ion implantation for the synthesis of silicon- and carbon-containing nanostructures can be divided into three kinds. The first kind [3, 4] is a combination of the silicon carbide ion synthesis and the formation of porous layers. At the first stage, SiC is synthesized by the implantation of the 'stoichiometric' doses of carbon ions into silicon with subsequent thermal or laser annealing. Then, the nanopores are formed by anodic etching to separate the SiC layer into nanocrystals. A distinctive peculiarity of the method is the formation of only one silicon carbide polytype – β-SiC. The synthesis of cubic SiC polytype is explainable from the viewpoint of the principle of structural compliance (see section 3.2). Of course, the β-SiC phase is retained under etching. PL spectrum of such layers [3, 4] demonstrates a band in the range of 400-450 nm. Its shift to the shorter wavelengths with respect to the bulk β-SiC phase with a typical PL emission at 560 nm (2.2 eV) can be explained by the quantum confinement effect.

Due to the inhomogeneous profile of implanted ions, a situation is possible, when the stoichiometric concentration of carbon in silicon is reached only at some depths, whereas at the other depths, carbon concentration is either lower or higher than the stoichiometric one. In this situation, in addition to the PL emission from β-SiC, the PL bands that come from nanocrystals (or amorphous clusters) of elemental carbon and silicon can be observed. So, the PL of β-SiC at 400–450 nm is found in [3, 4] to be accompanied by the PL peaks at around 500–525 nm [3] and 600 nm [4]. Observation of the graphite-like carbon phase [4] (not the diamond-like as expected from the principle of structural compliance) probably originates from the very high C^+ dose that can cause ion-stimulated graphitization of the diamond-like carbon. Indeed, when the C^+ dose is lower [3], the graphite phase is not observed.

The methods of the given kind suffer from the same disadvantage as for the other techniques based on 'wet chemistry'. That is why this kind is mainly of scientific interest than of practical importance. The *second* and *third* kinds of the formation methods of carbon-based phases with the application of ion implantation use amorphous silicon dioxide instead of crystalline silicon as an original material. For the *second kind*, SiO_2 is only implanted with C^+ ions, whereas co-implantation of Si^+ and C^+ ions is performed for the *third kind* of methods. Unfortunately, only few reports [6 , 25, 38, 39, 40] are devoted to these kinds of methods. There are even less reports on the complex investigations combining a study of optical (luminescent) properties with a thorough analysis of structure and phase composition of the implanted oxide layers.

Let us consider the case of thermal SiO_2 films implanted with only carbon ions. According to the authors of [41], the data of Fourier-transform infrared (FTIR) spectroscopy supports the formation of amorphous SiC and crystalline β-SiC along with amorphous carbon, even in the as-implanted layer, however, there is no direct proof of that. The amorphous carbon phase transforms to the graphite nanocrystals upon annealing at 800 °C (according to the data of Raman spectroscopy). The PL spectra are similar before and after annealing and consists of the two bands – a relatively narrow band at 480 nm and a broader one at 520-620

Copyright © 2012. Nova Science Publishers, Incorporated. All rights reserved.

Diamond-Like Carbon Films, Nova Science Publishers, Incorporated, 2012. ProQuest Ebook Central,

nm, ascribed by the authors to emission from SiC and carbon, respectively. In the earlier report [38], the PL spectra are decomposed to several lines in the range of 380-450 nm that are also related to the SiC phase. The attribution of the 400-450 nm PL emission to the cubic SiC modification is supported by the observation of similar PL in other carbon-based nanostructures for which the presence of β-SiC phase has reliable confirmation (see e.g. [3, 22, 34]). Some differences in the positions of such PL bands may result from a variety of the nanocrystals mean sizes (taking into account the quantum confinement effect). The formation of SiC phase in the absence of excess silicon in the carbon-implanted oxide film probably could result from the reaction of carbon with those silicon atoms that are released during the SiO_2 dissociation under the ion beam. A degree of dissociation should depend on the implantation dose, so the presence of silicon carbide is not expected in the SiO_2 implanted with low carbon dose.

An important advantage of the *third kind* of methods (involving co-implantation of Si^+ and C^+ into SiO_2) is a possibility of precise control of the distribution profiles and concentrations of Si and C that allows to adjust the spectral composition and intensity of luminescence in a proper way.

One of the most informative reports on this approach is presented in [40]. The thermally grown SiO_2 film was first implanted with Si^+ at two energies and doses so that the rectangular-shaped Si excess profile was achieved at the depths between 100 nm and 300 nm. Then, C^+ ions were implanted with the concentration being approximately equal to the Si excess concentration at the distribution maximum. At the smaller and larger depths, the carbon concentration was lower than the silicon excess concentration. The peak concentrations of both species varied between 1 to 30 at.%. The implanted samples were annealed at 1100 °C in N_2 for 1-1000 min. The complex investigation by the methods of PL, scanning cross-section PL (XS-PL), Raman scattering, X-ray photoelectron spectroscopy (XPS), cross-section transmission electron microscopy (XS-TEM) allowed the authors to come to the following conclusions. In the depth region close to the maximum of carbon ion distribution, the layer is observed that contains amorphous carbon, C-rich and SiC nanoclusters responsible for the 'blue-green' PL band. The spectral position of this band shifts from ~ 3.1 eV to ~ 2.1 eV with raising the ion dose, i.e. the increase in Si excess and C concentrations at around the profile maximum. This shift is related by the authors to the change in composition and structure of the clusters. At the higher excess concentrations (20 and 30 at.% at the maximum), there is another 'blue' band at ~ 3 eV that is related to the emission of carbon-containing clusters (SiC) of another type. Silicon nanocrystals responsible for a typical 'red' emission at the photon energies of 1.4-1.7 eV along with carbon-rich clusters are synthesized at either sides of the C^+ distribution maximum. The presence of carbon in these depth regions leads to a limited Si nanocrystal growth and thus results in smaller nanocrystal mean size compared to the case when Si^+ implantation is performed into the carbon-free SiO_2 (see below for the more detailed discussion).

The carbon-rich phases have not been exactly identified by the authors of [40]. The C1s line position in the XPS spectrum depends on the ion dose, the implanted depth and varies between the binding energy typical of the C–Si_4 bond in stoichiometric SiC and the binding energy corresponding to the C–C bond in graphite. The highest proximity of the XPS line to a position of the C–C bond takes place at the depths of maximal C concentrations. It should be noted that the XPS data in [40] is analyzed only for those implantation conditions which provide the concentrations of excess Si and C (20-30 at.%) that are higher than the optimal

Copyright © 2012. Nova Science Publishers, Incorporated. All rights reserved.

Diamond-Like Carbon Films, Nova Science Publishers, Incorporated, 2012. ProQuest Ebook Central,

concentrations from the viewpoint of PL intensity. Nevertheless, the careful examination of XPS data and the coincided XS-TEM and XS-PL data [40] allows us to draw the following conclusions. First, in the case of the equal concentrations of implanted Si and C atoms, the composition of a carbon-containing phase is approaching to the SiC stoichiometry with raising the Si and C concentrations. Second, the carbon-rich phases are observed only at the depths, where the ratio $C_C/C_{Si} \geq 0.5$ (C_C and C_{Si} – concentrations of carbon and excess silicon, respectively). Thus, the presence of sufficiently high Si excess concentration stimulates the formation of silicon carbide and also the elemental carbon phase. The carbon clusters are graphitized at high doses, i.e. form the phase with the sp^2 bonds.

To study in more detail the peculiarities of ion synthesis for the range of lower concentrations of implanted atoms and to trace the evolution of phase transitions in dependence of the C_C/C_{Si} ratio, we have carried out the complex investigation for the case of Si^+ and C^+ co-implantation into thermal SiO_2 films, with the maximal Si excess concentration being fixed at ~ 10 at.% which is optimal for the PL intensity, and the implanted C concentration being varied between 0.1 and 20 at.%.

To minimize the interference effect on PL spectra, the thickness of SiO_2 films is chosen lower than in our previous work [42], namely, 300 nm instead of 800 nm. This, however, does not affect the interpretation and regularities of PL reported in [42]. There are two variants of annealing considered. The first variant provides for the two annealing procedures: the first annealing (1100 °C, 2 h., N_2) is performed after Si^+ implantation and forms Si nanocrystals in SiO_2 matrix (see typical XS-TEM data in [42]), then C^+ ions are implanted followed by the final annealing (1100 °C, 2 h., N_2) resulting in the formation of carbon-based phases. Another variant does not involve intermediate annealing, so that both silicon and carbon-based phases form under a single thermal treatment procedure (1000 or 1100 °C, 2 h., N_2). The energies of implanted Si^+ and C^+ ions provide satisfactory coincidence of their SRIM-simulated profiles [43]. A schematic representation of the cross-section of the implanted SiO_2:Si:C structure and the SRIM-simulated distributions of Si and C ions are shown in Figure 4.

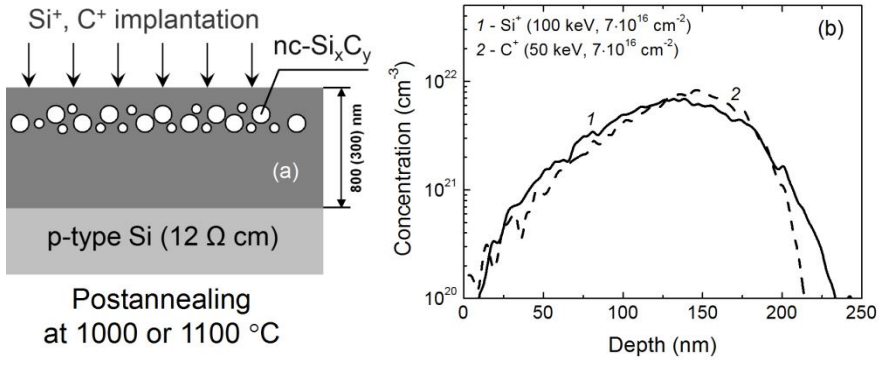

Figure 4. Schematic representation of the SiO_2:Si:C structure synthesized by Si^+, C^+ co-implantation with post-annealing (a), and the SRIM-simulated profiles of Si^+ and C^+ ions in SiO_2 (b).

Copyright © 2012. Nova Science Publishers, Incorporated. All rights reserved.

Diamond-Like Carbon Films, Nova Science Publishers, Incorporated, 2012. ProQuest Ebook Central,

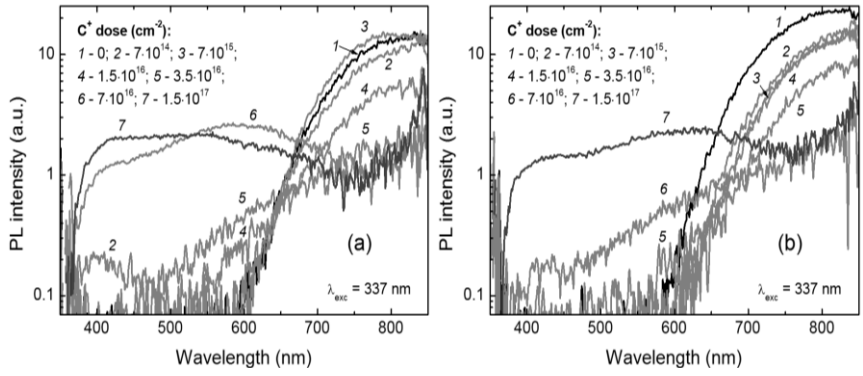

Figure 5. PL spectra of SiO_2 films (300 nm thick) implanted with Si^+ (100 keV, $7 \cdot 10^{16}$ cm^{-2}), C^+ (50 keV, various doses) and post-annealed at 1100 °C without (a) or with (b) intermediate annealing at 1100 °C.

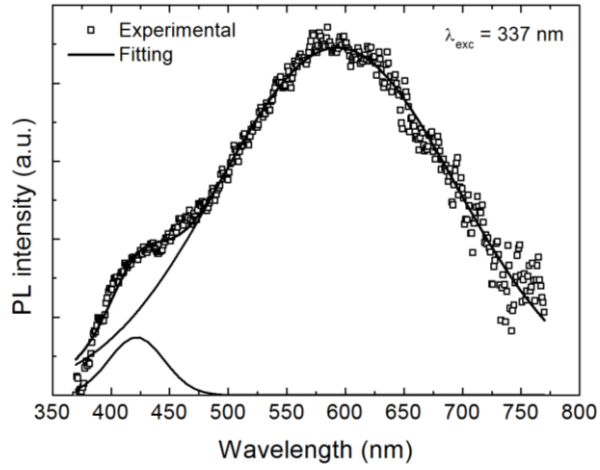

Figure 6. PL spectrum of SiO_2 film (300 nm) co-implanted with Si^+ (100 keV, $7 \cdot 10^{16}$ cm^{-2}), C^+ (50 keV, $7 \cdot 10^{16}$ cm^{-2}) and annealed at 1100 °C. The spectrum is deconvoluted in two Gaussian bands centered at 420 and 595 nm.

In such a way, the following combinations of the implantation and annealing conditions have been realized (the sequence of procedures is indicated by the arrows):

1) $SiO_2 \rightarrow Si^+$(100 keV, $7 \cdot 10^{16}$ cm^{-2}) $\rightarrow C^+$(50 keV, $7 \cdot 10^{13}$-$1.5 \cdot 10^{17}$ cm^{-2}) $\rightarrow$ 1000 °C;
2) $SiO_2 \rightarrow Si^+$(100 keV, $7 \cdot 10^{16}$ cm^{-2}) $\rightarrow C^+$(50 keV, $7 \cdot 10^{13}$-$1.5 \cdot 10^{17}$ cm^{-2}) $\rightarrow$ 1100 °C;
3) $SiO_2 \rightarrow Si^+$(100 keV, $7 \cdot 10^{16}$ cm^{-2}) $\rightarrow$ 1100 ºC $\rightarrow C^+$(50 keV, $7 \cdot 10^{13}$-$1.5 \cdot 10^{17}$ cm^{-2}) $\rightarrow$ 1100 °C.

In Figure 5, the evolution of PL spectra is demonstrated for the samples implanted with Si^+, C^+ and annealed at 1100 °C in different ways. PL intensity is given in the logarithmic scale in Figure 5. One of the spectra is plotted in the linear scale (Figure 6) to show how the spectrum is decomposed into the two PL bands – the 'blue' band at 420 nm and the 'green' band at 590 nm.

Copyright © 2012. Nova Science Publishers, Incorporated. All rights reserved.

Diamond-Like Carbon Films, Nova Science Publishers, Incorporated, 2012. ProQuest Ebook Central,

Let us discuss possible PL mechanisms of the ion-synthesized SiO_2:Si:C layers. Generally speaking, the green PL band may be caused by small Si nanocrystals (with a size less than 3 nm) [44, 45, 46], noncrystalline Si clusters [47, 48, 49], the phase precipitates of SiC and C [40] and by their combinations.

If we assume that the green PL comes from Si nanocrystals, this will lead to a conclusion that, at the high enough concentration of carbon, the latter hinders the formation of large Si nanocrystals emitting light at the longer wavelengths (700-1000 nm [44, 45, 46]). Such a situation is quite possible: indeed, as it is mentioned above, the carbon impurity causes the decrease in size of Si nanocrystals [40]. This may be explained by the much smaller atomic radius of C that induces elastic stress in a Si nanocrystal. The corresponding increase in the free energy makes the growth of large nanocrystals energetically unfavorable. Moreover, the carbon atoms dissolved in SiO_2 matrix or their complexes can act as the centers of silicon precipitation (like nitrogen atoms [50]). This should lead to an increase in the concentration of Si nanocrystals at the same volume fraction and to the corresponding decrease in their mean size. The carbon impurity can also hamper the crystallization process for amorphous Si nanoclusters (earlier, this effect was observed for the bulk silicon [51]), and those nanoclusters can also contribute to the green PL.

Recently, the described SiO_2:Si:C samples have been studied using a number of spectroscopic techniques at the Ural Federal University, Ekaterinburg, Russia [52]. The data kindly provided by our colleagues A.F. Zatsepin, E.A. Buntov, V.S. Kortov shows that the green PL band is characterized by the lifetimes of 1-20 ns and a complicated temperature dependence. The latter is represented by a superposition of the Street's temperature quenching curve [53] and non-monotonous temperature dependence characterized by the spectral-independent activation energies of ~ 15 and ~ 100 meV for radiative and non-radiative recombination processes, respectively. Such activation energies are typical of non-crystalline Si clusters in SiO_2 [54] and speak in favor of the presence of amorphous Si nanoclusters in the implanted layers. At the same time, the superposition of two temperature dependencies evidences that at least two sources of light emission contributes to the observed green PL band.

Another mentioned possibility consists in the relation of the green band to clusters of the carbon-based phases SiC and C. This interpretation agrees well with both the results of [40] and the results of electron spectroscopy given below.

As for the short-wavelength emission at 400-450 nm denoted as the blue PL band, one of possible candidates for its source is presented by defects in the oxide matrix [55], associated with the radiation damage or silicon excess. In the carbon-free SiO_2, these defect centers are completely annealed out even at the moderate temperatures than used here [56, 57]. However, generally speaking, a possibility that in the carbon-implanted films, there exist more complex defects involving the Si, C, and O atoms even after high-temperature annealing must not be ruled out. Such an interpretation of the 'white' PL in SiO_2 films implanted with silicon and carbon has been suggested previously [25, 39] but not supported by direct experimental evidence. The data reported in [25] allows us to infer that such an interpretation is valid for low (<10 at.%) concentrations of excess silicon (especially for carbon implantation into the stoichiometric SiO_2 films) and at relatively low annealing temperatures – 800 °C and lower. The formation of complexes of the Si, C, and O atoms is actually the initial stage of formation of the oxycarbide phase. But stability of the SiCO complexes is less probable in the conditions used here, i.e. at high and nearly equal concentrations of excess silicon and carbon,

Copyright © 2012. Nova Science Publishers, Incorporated. All rights reserved.

Diamond-Like Carbon Films, Nova Science Publishers, Incorporated, 2012. ProQuest Ebook Central,

since the binding energy of atoms in the oxycarbide phase is lower than that in the SiC and SiO_2 phases [37]. As an indirect confirmation of the above statement, we can refer to the electron spin resonance (ESR) spectroscopy data [57] demonstrating that annealing at 1100 °C heals to equal extent the known paramagnetic defects in both SiO_2:Si^+ and SiO_2:Si^+:C^+ films and does not induce any new carbon-related defect centers. The spectral position of the short-wavelength PL band is close to that observed for the other methods of SiC synthesis (see above). So, it can be concluded with a high degree of confidence that, in our case, this band is related to silicon carbide nanoclusters.

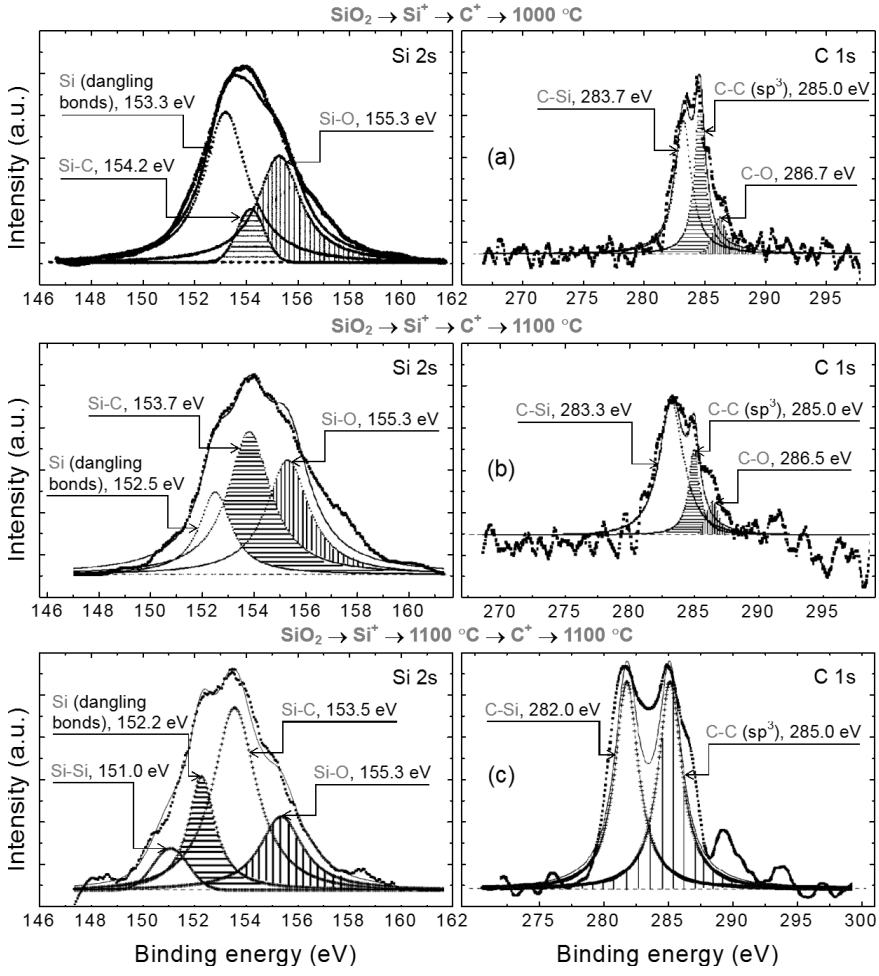

Figure 7. XPS spectra of SiO_2 films (800 nm thick) implanted with Si^+ (100 keV, $7 \cdot 10^{16}$ cm^{-2}), C^+ (50 keV, $7 \cdot 10^{16}$ cm^{-2}) and post-annealed at 1000 °C (a) and 1100 °C (b, c) without (a, b) and with (c) intermediate annealing. Ion etching to the depth of peak concentration of implanted ions was performed before the measurements. (The data is kindly provided by A.I. Kovalev and D.L. Wainstein, Surface Phenomena Research Group, Moscow, Russia, who have carried out the measurements and analysis).

To study the composition and the state of chemical species in layers, obtained by co-implantation of Si^+ and C^+ into SiO_2, the X-ray photoelectron spectroscopy (XPS) and analysis of the electron energy-loss fine structure (EELFS) [42] have been used. The used experimental conditions, in particular, the application of the monochromatized X-ray source,

Copyright © 2012. Nova Science Publishers, Incorporated. All rights reserved.

Diamond-Like Carbon Films, Nova Science Publishers, Incorporated, 2012. ProQuest Ebook Central,

provided the spectrometer resolution sufficient to distinguish various states and bonds of elements. XPS spectra of the SiO_2 films implanted with Si^+ and C^+ to the equal doses ($7 \cdot 10^{16}$ cm^{-2}) and annealed at 1000 and 1100 °C (with and without the intermediate annealing) are shown in Figure 7. By decomposing the XPS spectra into Gaussian components, the presence of Si-C and C-C bonds with binding energies ~ 283 eV and 285 eV, respectively, is revealed. The volume fraction of a carbon phase is found to be higher in the case of C^+ implantation into layers with the pre-synthesized Si nanocrystals (Figure 7c). This indicates that the process of transformation of Si nanocrystals into SiC clusters goes on less intensively than the direct formation of SiC clusters in the absence of intermediate annealing. In the latter case, the process of SiC formation does not require the diffusion of C atoms at long distances and subsequent incorporation of carbon into the Si lattice. Moreover, it proceeds on the background of a higher concentration of radiation defects, which is known to stimulate chemical reactions and phase formation [58]. It is established that Si-Si bonds (with the binding energy of 151 eV), which indicates the presence of silicon nanoclusters, are observed only for the case of intermediate annealing along with Si-C and C-C bonds (Figure 7c). For the other conditions of ion-beam synthesis presented in Figure 7, the existence of silicon nanocrystals is not revealed by XPS.

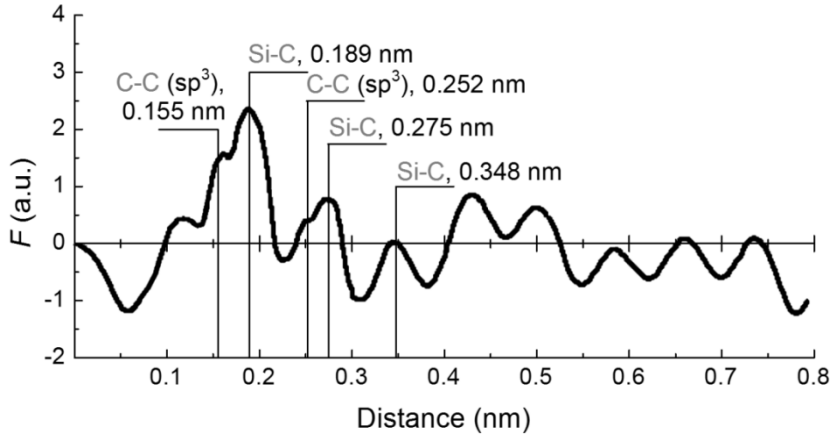

Figure 8. Fourier transform (*F*) of the EELFS spectrum for SiO_2 film (800 nm) co-implanted with Si^+ (100 keV, $7 \cdot 10^{16}$ cm^{-2}), C^+ (50 keV, $7 \cdot 10^{16}$ cm^{-2}) and post-annealed at 1100 °C. Ion etching to the depth of peak concentration of implanted ions was performed before the measurements. (The data is kindly provided by A.I. Kovalev and D.L. Wainstein, Surface Phenomena Research Group, Moscow, Russia, who have carried out the measurements and analysis).

The types of inter-atomic bonds in the SiO_2 layer successively implanted with Si^+ and C^+ and then annealed at 1100 °C have been investigated by the EELFS method near a peak of elastic scattered electrons (1000 eV) at the depth of maximal concentration of implanted impurities. The Fourier transform for the energy loss spectrum (an analog of the atomic radial distribution function) is shown in Figure 8. The presence of SiC nanoclusters and inclusions of diamond-like carbon with the sp^3 hybridization is revealed. The Si–C and C–C inter-atomic distances (0.189 and 0.155 nm) are equal to the reference values for the SiC and diamond phases, respectively [59, 60]. The C–C bonds with a length of 0.142 nm typical of the sp^2 hybridization (graphite) are not found. This evidences that the carbon nanoclusters in the film have mainly the diamond-like modification.

Copyright © 2012. Nova Science Publishers, Incorporated. All rights reserved.

Diamond-Like Carbon Films, Nova Science Publishers, Incorporated, 2012. ProQuest Ebook Central,

The XS-TEM analysis of the sample implanted to the equal doses with Si^+ and C^+ ions and annealed at 1000 °C [57] have revealed the disordered particles with an average size of ~ 5 nm in the implanted layer at the depths close to the projected ion range. The composition of these particles is not determined by the selected area diffraction. It may be supposed that there are C and SiC nanoclusters mentioned above.

So, there are two alternative processes possible, depending on the ratio of concentrations of excess Si and C atoms in the SiO_2 matrix during annealing – either the formation of Si nanocrystals with the dissolved carbon atoms or the precipitation of nanophases in the form of noncrystalline silicon, carbon, and SiC nanoclusters. Which of the two scenarios of phase formation is realized under Si^+ and C^+ co-implantation depends also on the presence or absence of intermediate annealing. In the presence of such annealing, Si nanocrystals exist in SiO_2 already before C^+ implantation. After the C^+ implantation and final annealing in the case of low carbon dose, the carbon atoms are incorporated into the Si nanocrystals during implantation and/or annealing in the form of a solid solution or in the form of small clusters, which yield no PL but serve as the non-radiative centers and thus, reduce the PL intensity from Si nanocrystals. For the higher C^+ doses (high carbon concentrations), a fraction of carbon atoms in SiO_2 matrix precipitates in the form of nanoclusters mainly with the diamond-like structure, another fraction reacting with Si nanocrystals to form SiC nanoclusters. Without the intermediate annealing, i.e. when the annealing is provided only after the successive implantation of Si^+ and C^+, there exists a supersaturated solid solution of Si and C in SiO_2 in the as-implanted samples. Then, in the case of small carbon doses, Si nanocrystals form and grow during annealing. The growing Si nanocrystals capture the carbon atoms from the SiO_2 matrix, but it is not sufficient for the formation of carbon-based phases. For the high carbon doses, a fraction of carbon forms the diamond-like clusters and another fraction forms the SiC phase nanoclusters as in the case of the intermediate annealing. These nanoclusters can form either via the reaction between the Si and C dissolved in SiO_2 or via the reaction of carbon with the pre-synthesized Si nanocrystals, or via both reactions, as well.

After this analysis of XPS and EELFS data, it is possible to identify the PL bands (Figure 5) with more confidence. The PL spectral range of 500-700 nm is related, at least partially, to the diamond-like carbon clusters, however, some contribution to this PL band can be made by the small crystalline or amorphous Si clusters. One can suppose, by analogy with the systems of amorphous Si nanoclusters [61], that the small size of a nanocluster provides spatial, not quantum, confinement of the excited carriers and the corresponding opening the optical bandgap so that the smaller the size, the wider the gap. If the PL from nanoclusters is size-dependent, the high width of a PL band can be explained by a broad size dispersion of nanoclusters. The width of the green-red PL band (Figure 5) is higher than that of the PL band from pure Si nanocrystals; this may be an evidence for the broad size dispersion of carbon nanoclusters. Such a broad size dispersion may result from the concurrent formation of SiC clusters due to a reaction of carbon with Si nanocrystals. Due to this reaction, there are regions of the reduced (inhomogeneous) carbon concentration around those SiC clusters. Because the final size of a cluster depends on the degree of impurity supersaturation in a matrix [62], the mentioned inhomogeneity leads to a fluctuation in the size of carbon nanoclusters.

As it is seen in Figure 5, the dependence of PL intensity in the spectral range below 700 nm on the carbon dose at the constant silicon dose has a sharp increase at the carbon

Copyright © 2012. Nova Science Publishers, Incorporated. All rights reserved.

Diamond-Like Carbon Films, Nova Science Publishers, Incorporated, 2012. ProQuest Ebook Central,

concentrations approaching to the silicon excess one (it should be noted that the ordinate axis has a logarithmic scale). The green and blue PL bands related to the carbon and β-SiC clusters, respectively, grow almost simultaneously with the C^+ dose. In this connection, two questions arise.

1) Why the carbon-based SiC and C phases practically do not form at the relatively low carbon doses, e.g. at the dose of $3.5 \cdot 10^{17}$ cm^{-2}, when the carbon concentration is about ~ 5 at.%, at which Si nanocrystals are certainly synthesized (see the curves 5 in Figure 5)?
2) Why, in the case of coincidence of Si and C ion profiles, the phases of carbon and silicon carbide form at the close doses of Si and C?

The answers to these questions can be found in the mechanisms of the formation of the phases.

Generally, the process of nanoclusters formation includes the stages of nucleation and growth, the latter being limited either by the diffusion or the rate of atom joining to the nucleus. Which of these factors is responsible for a delay in the formation of carbon-based clusters at progressive increasing Si and C concentrations? The critical nuclei for a Si nanocrystal in SiO_2 is the pair of Si-Si atoms [63, 64, 65] due to the low solubility of silicon in SiO_2. This is apparently correct for carbon, as well (the smaller atomic radius of carbon compared to that of Si should reduce the solubility of carbon atoms in the SiO_2 network). It is unlikely that the diffusion mobility of carbon is lower than that of silicon, as the implanted carbon is volatilized from the SiO_2 film in the absence of Si excess [38]. That is why the most probable factor that reduces the effectiveness of the carbon-based phase formation is the higher barrier for the joining of atoms to the clusters.

The approximately simultaneous synthesis of the SiC and C clusters is an evidence of the correlation between the processes of their formation. This can be explained by the principle of structural compliance at ion synthesis. As mentioned above, the C nanoclusters are synthesized predominantly in the diamond-like structure. If we assume that the SiC nanoclusters mainly have the cubic (β-SiC) allotropic form (likewise the β-SiC formed under C^+ implantation in Si [3, 4]), then the formation of nanocrystals in one of these phases will assist the formation of nanoparticles in another phase by the endotaxial growth mechanism, because the diamond and β-SiC lattices are similar.

Special attention should be paid to an interesting peculiarity of the dependence of PL spectra on the C^+ dose (Figure 5). Intensity of the 'red' PL band related to radiative recombination in the quantum-confined Si nanocrystals is significantly quenched for such C^+ doses, at which the SiC-related band is not yet expressed. Such a PL quenching cannot be explained by a consumption of Si excess on the formation of silicon carbide. This means that the incorporation of carbon atoms into silicon nanocrystals hampers the recovery of luminescence (quenched by irradiation) during annealing even at high temperature of 1100 °C. (In the case of the implantation of only Si^+ ions into SiO_2, the temperature of 1100 °C is quite sufficient for the observation of intense PL from Si [63]). This fact shows that the carbon impurity reduces the structural perfection of Si nanocrystals. Indeed, the dissolution of carbon in Si nanocrystal and incorporation of its atoms into the lattice sites, as mentioned before, should lead to a strong mechanical stress due to a size mismatch of Si and C atoms.

Copyright © 2012. Nova Science Publishers, Incorporated. All rights reserved.

Diamond-Like Carbon Films, Nova Science Publishers, Incorporated, 2012. ProQuest Ebook Central,

This causes breaking the bonds inside or at the interface of a nanocrystal, i.e. the formation of non-radiative recombination centers.

Thus, the peculiarities of the phase formation and the PL spectra related to them can be explained taking into account such a regularity of the ion synthesis as the principle of structural compliance and the effect of ratio of the implanted species radii to those of the target atoms on the resulting composition and/or structure of the ion-implanted layers.

CONCLUSION

Ion-beam synthesis of the carbon-based phases is interesting both in the fundamental and applied aspects. It is of scientific importance that this is a convenient example for the study of some peculiarities of ion implantation methods which are related to the non-equilibrium character of physical and chemical processes. One of those peculiarities is defined here as the principle of structural compliance. Other discussed peculiarities originate from the formation of radiation defects and influence of two kinds of thermal factors – macroscopic (the substrate temperature) and microscopic (thermal spikes).

The formation and accumulation of defects under ion irradiation are determined by two processes – generation of defects and their transformation, including annealing (annihilation). The rate of the defect generation depends on the masses of ions and substrate atoms. The transformation and annealing of defects take place either during the implantation or during the subsequent thermal treatment. The resulting state of the defect system depends strongly on the implantation conditions – the macroscopic temperature and ion flux, the role of these factors being especially great for light ions including $^{12}C^{+}$ and (to a lesser extent) $^{28}Si^{+}$. Therefore, in the case considered, the density and state of defects may vary significantly in different experiments. The role of these factors as well as the temperature in thermal spikes remains practically unstudied for the ion synthesis of nanocrystals or nanoinclusions. Furthermore, it is required to investigate the ion-beam synthesis of carbon-rich phases under variation of the macroscopic substrate temperature and ion flux. From the fundamental point of view, the results of these investigations would be especially interesting for the case of synthesis of such an exotic phase as carbon with the face-centered cubic lattice. Physical properties and thermal stability of this phase should be investigated, too.

Carbon is amazing with its polymorphism. There are at least seven crystalline and nanocrystalline forms of this element known (graphite, diamond, lonsdalite, carbyne, fullerenes, nanotubes, graphene), and now the additional face-centered cubic phase of carbon. The capabilities of ion synthesis and ion-beam modification of various carbon phases have not yet been exhausted and can present new surprises. For example, it would be of interest to investigate a possibility of ion synthesis of a nanocrystalline diamond in different matrices, as well as a possibility of the growth of a diamond crystalline layer (or islands) on a silicon surface with the application of ion-beam methods. Another important trend is the ion synthesis of carbon and silicon-carbon phases in flexible (e.g. polymer) substrates. Usually, the polymer films are graphitized under ion implantation [66]. At the same time, in principal, it may be possible to form by ion implantation silicon nanocrystals in this material [66]. It cannot be excluded that, at a double Si^{+} and C^{+} implantation, the SiC nanoclusters and/or the

Copyright © 2012. Nova Science Publishers, Incorporated. All rights reserved.

Diamond-Like Carbon Films, Nova Science Publishers, Incorporated, 2012. ProQuest Ebook Central,

diamond-like clusters isolated by a dielectric from each other will be synthesized by analogy with the implantation into SiO_2.

The use of other dielectrics such as high-k insulators Al_2O_3, TiO_2, HfO_2 as an initial material might be also interesting. Implantation of carbon into Al_2O_3 (sapphire) has already been reported [67]).

It is practically important to continue the study of light emission and other properties of the ion-synthesized layers of carbon-based phases and, first of all, to establish a possibility of fabrication of the efficient light-emitting diodes, lasers and other devices (memory elements, solar cells, non-linear optics devices etc.) on the basis of nanocrystals of such phases. Progress in these fields would allow to realize for nanoelectronic applications such valuable advantages of silicon carbide as high bandgap, thermal and chemical stability, high breakdown voltage. These investigations are still at the initial stage of development.

ACKNOWLEDGMENTS

Support through the Federal Targeted Program ‘Scientific and pedagogical cadres of innovative Russia’ and Analytical Departamental Targeted Program ‘Development of scientific potential of higher school’ is gratefully acknowledged.

REFERENCES

[1] Canham, L. T. *Appl. Phys. Lett.* 1990, *57*, 1046-1048.
[2] Fan, J. Y.; Wu, X. L.; Chu, P. K. *Progress in Materials Science.* 2006, *51*, 983-1031.
[3] Liao, L.-S., Bao, X.-M.; Yang, Z.-F.; Min, N.-B. *Appl. Phys. Lett.* 1995, *66*, 2382-2384.
[4] Bayazitov, R. M.; Khaibullin, I. B.; Batalov, R. I.; Nurutdinov, R. M.; Antonova, L. Kh.; Aksenov, V. P.; Mikhailova, G. N. *Nucl. Instr. Meth. Phys. Res. B.* 2003, *206*, 984-988.
[5] Chen, D.; Liao, Z. M.; Wang, L.; Wang, H. Z.; Zhao, F.; Cheung, W. Y.; Wong, S. P. *Opt. Mat.* 2003, *23*, 65-69.
[6] Gonzalez-Varona, O.; Perez-Rodriguez, A.; Garrido, B.; Bonafos, C.; Lopez, M.; Morante, J.R.; Montserrat, J.; Rodriguez, R. *Nucl. Instr. Meth. Phys. Res. B.* 2000, *161-163*, 904-908.
[7] Brinkman, J. A. *J. Appl.Phys.* 1954, *25*, 961-970.
[8] Seitz, F.; Koehler, J. S. *Prog. Solid State Phys.* 1957, *2*, 305-449.
[9] Pavlov, P. V. *Doklady Akademii Nauk SSSR* 1981, *vol.258*, 617-619.
[10] Pavlov, P. V. *Kristallografiya* 1979, *24*, 481-485.
[11] Pavlov, P. V. *Nucl. Instrum. Meth,* 1983, *209/210*, 791-798.
[12] Anisimov, S. I.; Sukhorukov, V. V.; Tetelbaum D. I.; Zorin, E. I. *Sov. Tech. Phys. Lett.* 1981, *7(1)*, 50-51.
[13] Palatnik, L. S.; Guseva, M. B.; Babaev, V. G.; Savchenko, N. F.; Fal'ko, I. I. *Sov. Phys. JETP.* 1984, *60*, 520-523.

Copyright © 2012. Nova Science Publishers, Incorporated. All rights reserved.

Diamond-Like Carbon Films, Nova Science Publishers, Incorporated, 2012. ProQuest Ebook Central,

[14] Pauling, L. *The Nature of the Chemical Bond and the Structure of Molecules and Crystals: An Introduction to Modern Structural Chemistry;* 3-rd edition; Cornell University Press: New York, 1960; 644 p.
[15] Spitzer, W. G.; Kleinman, D.; Walsh, D. *Phys. Rev.* 1959, *113*, 127-137.
[16] Kimura, T.; Kagiyama, Sh; Yugo, Sh. *Thin Solid Films.* 1981, *81*, 319-327.
[17] Pavlov, P. V.; Zorin, E. I.; Tetelbaum, D. I.; Lesnikov, V. P.; Ryzhkov, G. M.; Pavlov, A. V. *Phys. Status Solidi A.* 1973, *19*, 373-378.
[18] Shor, J. S.; Bemis, L.; Kuttz, A. D.; Grimberg I.; Weiss, B. Z.; MacMillian, M. F.; Choyke, W. J. *J. Appl. Phys.* 1994, *76*, 4045-4049.
[19] Matsumoto, T.; Takahashi, J.; Tamaki, T.; Futagi, T.; Mimura, H.; Kanemitsu, Y.; *Appl. Phys. Lett.* 1994, *64*, 226-228.
[20] Wu, X. L.; Siu, G. G.; Stokes, M. J.; Fan, D. L.; Gu, Y.; Bao, X. M. *Appl. Phys. Lett.* 2000, *77*, 1292-1294.
[21] Ishikawa, Y.; Vasin, A. V.; Salonen, J.; Muto, S.; Lysenko, V. S.; Nazarov, A. N.; Shibata, N.; Lehto, V.-P. *J. Appl. Phys.* 2008, *104*, 083522.
[22] Fan, J. Y.; Wu, X. L.; Li, H. X.; Liu, H. W.; Huang, G. S.; Siu, G. G.; Chu, P. K. *Appl. Phys. A.* 2006, *82*, 485-487.
[23] Song, D.; Cho, E.-Ch.; Cho, Y.-H.; Conibeer, G.; Huang, Y.; Huang, Sh.; Green, M. A. *Thin Solid Films* 2008, *516*, 3824-3830.
[24] Liu, X.; Zhang, J.; Yan, Z.; Ma, S.; Wang, Y. *Mater. Phys. Mech.* 2001, *4*, 85-88.
[25] Zhao, J.; Mao, D. S.; Lin, Z. X.; Jiang, B. Y.; Yu, Y. H.; Liu, X. H.; Wang, H. Z.; Yang, G. Q. *Appl. Phys. Lett.* 1998, *73*, 1838-1840.
[26] Afanas'ev, V. V.; Bassler, M.; Pensl, G.; Schulz, M. J.; Stein von Kamienski, E. *J. Appl. Phys.* 1996, *79*, 3108-3114.
[27] Zakharko, Yu.; Botsoa, J.; Alekseev, S.; Lysenko, V.; Bluet, J.-M.; Marty, O.; Skryshevsky, V. A.; Guillot, G. *J. Appl. Phys.* 2010, *107*, 013503.
[28] Polupan, G.; Torchynska, T. V. *Thin Solid Films.* 2010, *518*, S208-S211.
[29] Rittenhouse, T. L.; Bohn, P. W.; Hossain, T. K.; Adesida, I.; Lindesay, J.; Marcus, A. *J. Appl. Phys.* 2004, *95*, 490-496.
[30] Xu, S. J.; Yu, M. B.; Rusli; Yoon, S. F.; Che, C. M.; *Appl. Phys. Lett.* 2000, *76*, 2550-2552.
[31] Kassiba, A.; Makowska-Janusik, M.; Boucle, J.; Bardeau, J. F.; Bulou, A.; Herlin-Boime, N. *Phys. Rev. B.* 2002, *66*, 155317.
[32] Rajagopalan, T.; Wang, X.; Lahlouh, B.; Ramkumar, C.; Dutta, P.; Gangopadhyay, S. *J. Appl. Phys.* 2003, *94*, 5252-5260.
[33] Yu, W.; Lu, W.; Yang, Y.; Wang, C.; Zhang, L.; Fu, G. *Thin Solid Films.* 2007, *515*, 2949-2953.
[34] Yu, W.; Wang, X.; Lu, W.; Wang, S.; Bian, Y.; Fu, G. *Physica B.* 2010, *405*, 1624-1627.
[35] Kerdiles, S.; Berthelot, A.; Gourbilleau, F.; Rizk, R. *Appl. Phys. Lett.* 2000, *76*, 2373-2375.
[36] Feng, D. H.; Xu, Z. Z.; Jia, T. Q.; Li, X. X.; Gong, S. Q. *Phys. Rev. B.* 2003, *68*, 035334.
[37] Seo, S.-Y.; Cho, K.-S.; Shin, J. H. *Appl. Phys. Lett.* 2004, *84*, 717-719.
[38] Mitchell, L. J.; Naab, F.; Holland, O. W.; Duggan, J. L.; McDaniel, F. D. *J. Non-Crist. Solids.* 2006, *352*. 2562-2564.

Copyright © 2012. Nova Science Publishers, Incorporated. All rights reserved.

Diamond-Like Carbon Films, Nova Science Publishers, Incorporated, 2012. ProQuest Ebook Central,

[39] Rebohle, L.; Gebel, T.; Frob, H.; Reuther, H.; Skorupa, W. *Appl. Surf. Sci.* 2001, *184*, 156-160.
[40] Perez-Rodriguez, A.; Gonzalez-Varona, O.; Garrido, B.; Pellegrino, P.; Morante, J. R.; Bonafos, C.; Carrada, M.; Claverie, A. *J. Appl. Phys.* 2003, *94*, 254-262.
[41] Poudel, P. R.; Rout, B.; Hossain, K. M.; Dhoubhadel, M. S.; Kummari, V. C.; Neogi, A.; McDaniel, F.D. *Rev. Mex. Fis.* 2010, *56*, 297-301.
[42] Wainstein, D.; Kovalev, A.; Tetelbaum, D.; Mikhaylov, A.; Belov, A. *Surf. Interf. Anal.* 2008, *40*, 571-574.
[43] Ziegler, J.F. The Stopping and Range of Ions in Matter. http://www. srim.org
[44] Burdov, V.A. *Semiconductors* 2002, *36*, 1233-1236.
[45] Fauchet, P.M. *Materials Today.* 2005, *8*, 26-33.
[46] Sa'ar, A. *J. Nanophotonics.* 2009, *3*, 032501.
[47] Inokuma, T.; Wakayama, Y.; Muramoto, T.; Aoki, R.; Kurata, Y.; Hasegawa, S. *J. Appl. Phys.* 1998, *83*, 2228-2234.
[48] Rinnert, H.; Vergnat, M.; Burneau, A. *J. Appl. Phys.* 2001, *89*, 237-243.
[49] Yi, L. X.; Heitmann, J.; Scholz, R.; Zacharias, M. *Appl. Phys. Lett.* 2002, *81*, 661-663.
[50] Kachurin, G. A.; Yanovskaya, S. G.; Zhuravlev, K. S.; Ruault, M.-O. *Semiconductors* 2001, *35*, 1183-1186.
[51] Lau, S.S. *J. Vac. Sci. Technol.* 1978, *15*, 1656-1661.
[52] Zatsepin, A. F.; Buntov, E. A.; Kortov, V. S.; Mihailov, A. N.; Belov, A. I.; Tetelbaum, D. I. *Abstracts of 18th International Workshop on Inelastic Ion-Surface Collisions (IISC-18)*, Gatlinburg, Tennessee, USA, September 26 - October 1, 2010, P.61.
[53] Street, R. A. *Adv. Phys.* 1976, *25*, 397-453.
[54] Wang, J.; Righini, M.; Gnoli, A.; Foss, S.; Finstad, T.; Serincan, U.; Turan, R. *Solid State Communications*. 2008, *147*, 461-464.
[55] Zatsepin, A. F. *Phys. Solid State* 2010, *52*, 1176-1187.
[56] Valakh, M. Ya.; Yukhimchuk, V. A.; Bratus', V. Ya.; Konchits, A. A.; Hemment, P. L. F.; Komoda, T. *J. Appl. Phys.* 1999, *85*, 168-173.
[57] Tetelbaum, D. I.; Mikhaylov, A. N.; Vasiliev, V. K.; Belov, A. I.; Kovalev, A. I.; Wainstein, D. L.; Mendeleva, Yu. A.; Finstad, T. G.; Foss, S.; Golan, Y.; Osherov, A. *Surf. Coat. Tech.* 2009, *203*, 2658-2663.
[58] Hirvonen J.K. Ion implantation. Treatise on material science and technology. Academic Press: London, 1980; Vol. 18, 502 p.
[59] Muto, S.; Tanabe, T. *J. Appl. Phys.* 2003, *93*, 3765-3775.
[60] Robertson, J. *Adv. Phys.* 1986, *35*, 317-374.
[61] Estes, M. J.; Moddela, G. *Appl. Phys. Lett.* 1996, *68*, 1814-1816.
[62] Ross, G. G.; Smirani, R.; Levitcharsky, V.; Wang, Y. Q.; Veilleux, G.; Saint-Jacques, R. G. *Nucl. Instr. Meth. Phys. Res. B.* 2005, *230*, 198-202.
[63] Garrido Fernandez, B.; Lopez, M.; Garcia, C.; Perez-Rodriguez, A.; Morante, J. R.; Bonafos, C.; Carrada, M.; Claverie. A. *J. Appl. Phys.* 2002, *91*, 798-807.
[64] Leier, A. F.; Safronov L. N.; Kachurin, G. A. *Semiconductors* 1999, *33*, 380-384.
[65] Tetelbaum, D. I.; Gorshkov, O. N.; Kasatkin, A. P.; Mikhaylov, A. N.; Belov, A. I.; Gaponova, D. M.; Morozov, S. V. *Phys. Sol. State.* 2005, *47*, 13-17.
[66] Hadjichristov, G. B.; Ivanov, V.; Faulques, E. *Appl. Surf. Sci.* 2008, *254*, 4820-4827.
[67] Orwa, J. O.; Jamieson, D. N.; Prawer, S.; McCallum, J. C. *Nucl. Instr. Meth. Phys. Res. B.* 2001, *175-177*, 554-558.

Copyright © 2012. Nova Science Publishers, Incorporated. All rights reserved.

Diamond-Like Carbon Films, Nova Science Publishers, Incorporated, 2012. ProQuest Ebook Central,

In: Diamond-Like Carbon Films
Editor: Yuto S. Tanaka
ISBN: 978-1-61324-791-4
© 2012 Nova Science Publishers, Inc.

Chapter 3

ELECTRON FIELD EMISSION PROPERTIES OF NONMETAL AND METAL DOPED DIAMOND LIKE CARBON

Sk. Faruque Ahmed*
Department of Physics, Aliah University, Kolkata, India

1. ABSTRUCT

Diamond like carbon (DLC) can be defined as a metastable phase of amorphous carbon (a-C) or hydrogenated amorphous carbon (a-C:H) containing a significant fraction of sp^3 hybridization. DLC has some extreme properties like diamond, such as high mechanical hardness, chemical inertness, dielectric strength, low wear and friction, optical transparency in the visible and infrared region, high electrical resistivity, high thermal conductivity and low electron affinity.

Instead of these interesting properties, DLC films have several inherent problems, such as their high internal stress and low thermal stability. The high intrinsic stress generated in the film causes some serious problems in various applications of this material, like degradation of electrical and optical properties and leads to peel off the films from the substrate and poor adhesion.

The ratio of sp^2/sp^3 carbon atoms is one of the most important factors determining the quality of the DLC films, which can be changed by incorporating different metal or nonmetal into DLC matrix. Metal and nonmetal doped DLC films have been an interesting field since last few years because, they have a great potential for solving some of the major drawbacks of pure DLC films. Various attempts have been made to dope DLC films with different nonmetals and metals such as nitrogen, iodine, boron, phosphorous, fluorine, gold, silver, titanium, tin, cupper etc. and the doping effects of these elements have been extensively investigated in terms of the chemical, electrical, optical and mechanical properties of DLC films. Doping of different elements in the DLC films reduced residual internal stress without sacrificing the hardness, leads to good adhesion to metal alloys, steels and glasses, improved high temperature stability, reduced hydrogen loss, graphitization and resistance to oxidation. Due to these noble properties of

* Corresponding author: E-mail: faruquekist@gmail.com

Copyright © 2012. Nova Science Publishers, Incorporated. All rights reserved.

Diamond-Like Carbon Films, Nova Science Publishers, Incorporated, 2012. ProQuest Ebook Central,

doped DLC, it has been studied in the last few years and has potential applications in many areas, such as electronic applications, solar cells, photoluminescence cells, optoelectronic devices, field effect transistor and high-temperature engineering materials. In this chapter, work done on synthesis, characterizations and electron field emission properties of metal or nonmetal doped DLC and diamond like nanocomposite materials will be discussed.

2. INTRODUCTION

2.1. Diamond Like Carbon (DLC) as a Material

Amorphous hydrogenated carbon (a:C-H) or diamond-Like Carbon (DLC) is the generic name of a mixture of graphite and diamond-type bound carbon [1]. Also, it is well known that in DLC graphitic sp^2 clusters are embedded in the amorphous sp^3 bonded matrix, where the collective behavior of sp^2 sites is responsible for the optical and electrical properties, whereas the sp^3 regions govern mechanical properties [2,3].

DLC not only consists of amorphous carbon (a-C), but also the amorphous hydrogenated carbon (a-C:H). The composition of DLC is most conveniently displayed on a ternary phase diagram as in Figure 2.1, first used by Jacob and Moller [4].

If the fraction of sp^3 bonding reaches a high degree, McKenzie [5] suggested to denote the a-C as tetrahedral amorphous carbon (ta-C), to distinguish it from sp^2 a-C. Koidl et al [6] produced DLC by plasma enhanced chemical vapour deposition (PECVD) method; whose composition reached the interior of the triangle, this was named as a-C:H. A more sp^3 bonded material with less hydrogen content, was denoted as hydrogenated tetrahedral amorphous carbon (ta-C:H) by Weiler et al [7]. Typical properties of the various forms of a-C are compared to diamond and graphite in Table - 2.1.

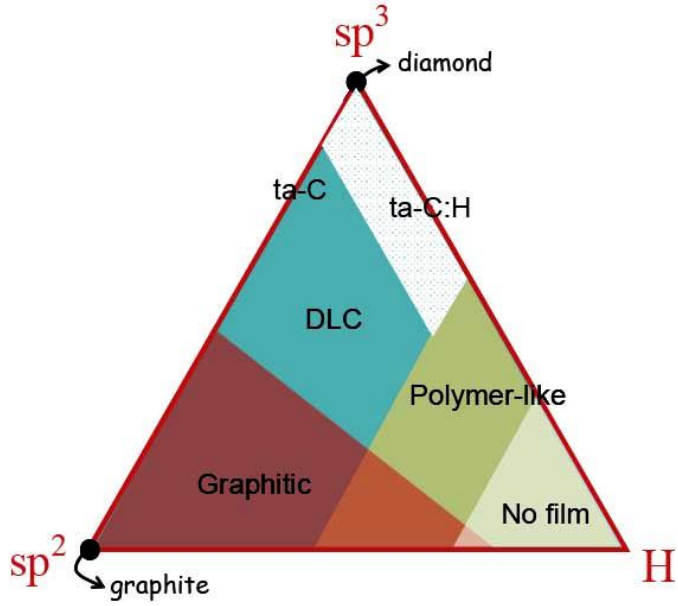

Figure 2.1. Ternary phase diagram of various forms of DLC [Ref. 1,4].

Copyright © 2012. Nova Science Publishers, Incorporated. All rights reserved.

Diamond-Like Carbon Films, Nova Science Publishers, Incorporated, 2012. ProQuest Ebook Central,

Table 2.1. Comparison of major properties of a-C with those of reference materials like diamond, graphite and C_{60}

Sample	sp^3 (%)	H (%)	Density (gm-cm^{-3})	Optical Gap (eV)	Hardness (Gpa)	Ref.
Diamond	100	0	3.515	5.5	100	8
Graphite	0	0	2.267	0	-	9
C_{60}	0	0	-	1.6	-	10
Glassy C	0	0	1.3-1.55	0.01	3	11
Evaporated C	0	0	1.9	0.4-0.7	3	11
Sputtered C	5	0	2.2	0.5	-	12
ta-C	80-88	0	3.1	2.5	80	10,13
a-C:H hard	40	30-40	1.6-2.2	1.1-1.7	10-20	14
a-C:H soft	60	40-50	1.2-1.6	1.7-4.0	<10	14
ta-C:H	70	30	2.4	2.0-2.5	50	15,16

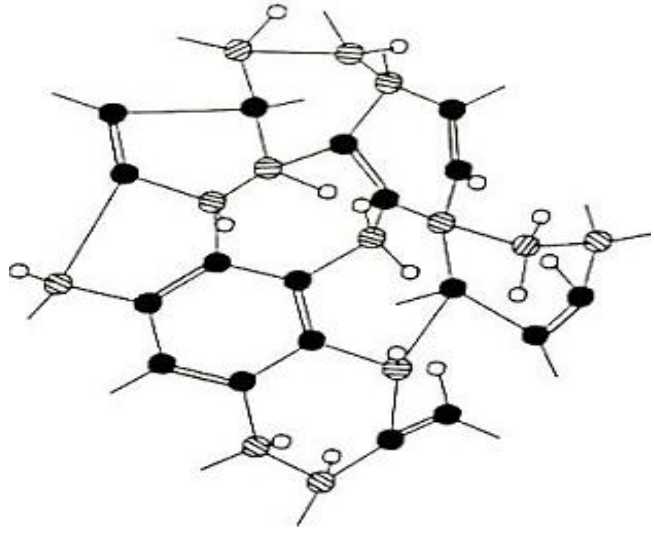

Figure 2.2. A two-dimensional representation of a proposed structure for diamond like hydrocarbon (a-C:H) [Ref. 1].

2.2. Structure of DLC

The structure of DLC is still a matter of research. However, some overall feature of this solid has become clear in the past several years. A proposed structure of DLC is shown in Figure 2.2. The shaded circles are sp^3 coordinated carbon, tetrahedrally bonded to four other atoms. The fully black circles represent sp^2 carbon atoms, trigonally bonded to three other atoms. The open circles are hydrogen atoms. One major feature of DLC is the type of clustering that the sp^2 carbon atoms undergo. It is proved, on the basis of optical spectroscopic evidences that, many of the sp^2 carbon atoms are present as large graphite-like

Copyright © 2012. Nova Science Publishers, Incorporated. All rights reserved.

Diamond-Like Carbon Films, Nova Science Publishers, Incorporated, 2012. ProQuest Ebook Central,

clusters within DLC. These clusters appear to be spatially isolated from one another, because the films have extremely low conductivity.

2.3. Why also there is Interest in DLC

Studies of DLC have been performed extensively since 1971, when Aisenberg and Chabot [17] first prepared such films, and there has been explosive attention in understanding the growth mechanisms, material properties and usage in industrial applications. Amorphous DLC has been extensively studied all over the world during the last few decades, as it possesses properties close to those of diamond, such as high mechanical hardness, chemical inertness, dielectric strength, low wear and friction, optical transparency in the visible and infrared region, high electrical resistivity, high thermal conductivity and low electron affinity which make them a powerful candidate for the next generation of high performance electronic devices and other vacuum micro-electronic devices [6,11,18-21]. At present, high quality diamond films can be produced at high temperatures (> 500 ^{o}C) that tend to develop preferential growth of individual grains, thus resulting in faceted and rough film surfaces. On the other hand, DLC films can be deposited at low temperature on a large area substrate with high deposition rates; hence the range of materials it can coat is greatly increased and low-cost, large area electronic devices can be easily realized. Also, there are some practical advantages of DLC over diamond. DLC can be smooth on nanometer scale, with its hardness approaching that of diamond. DLC films have widespread applications. The comparison of some major property of DLC over diamond and graphite are given in Table 2.2.

Table 2.2. Comparison of some major property of DLC over diamond and graphite

Property	Diamond	DLC	Graphite
Crystal structure	Cubic, a = 3.57 Å; Hexagonal, a = 2.52 Å, c = 4.12 Å	Amorphous with small crystal regions mixed with sp^2 and sp^3 bonds	Hexagonal a = 2.47 Å, c = 6.71 Å
Fraction of hybrid orbital	100 % sp^3	40-75 % sp^3 20-60 % sp^2; ~2 % sp^1	100 % sp^2
Density (g/cm^3)	3.51	1.6 – 2.0	2.26
Hardness (GPa)	70 - 100	20 – 80	< 5
Friction Coefficient	0.05	0.03 – 0.2	0.1
Refractive Index	2.42	1.8 – 2.6	2.15 – 1.8
Transparency	UV-VIS-IR	VIS-IR	Opaque
Optical gap (eV)	5.45	1.0 – 2.6	0
Resistivity (Ω-cm)	> 10^{16}	10^2 – 10^{14}	0.2 – 0.4

Copyright © 2012. Nova Science Publishers, Incorporated. All rights reserved.

Diamond-Like Carbon Films, Nova Science Publishers, Incorporated, 2012. ProQuest Ebook Central,

Nowadays, DLC films have attracted great interest due to their negative or low electron affinity. As electron affinity depends fundamentally on the type of bonding, not on crystallinity, so that amorphous DLC also has the low electron affinity. So, they have great potential in the application as electron emitters in vacuum microelectronics, such as field emission displays. Also incorporated metal particles along with the sp^2 regions can form conductive channels in the insulating sp^3 matrix through the whole thickness of the film. These channels lead to field enhancement and hence result in enhanced electron emission.

DLC films have widespread applications, as protective coatings in areas, such as optical windows, magnetic storage disks, car parts, biomedical applications, photovoltaic cell, field emission display and as micromechanical devices (MEMs) [22-28]. One of the most interesting properties of DLC is the ability to vary the optical band gap by simply varying the relative proportion of the sp^2/sp^3 bond hybridization. This allows for the formation of band gap modulated super-lattice structures based on a single homogeneous material system [29]. Typical properties of DLC and its different applications are shown in Table 2.3.

Table 2.3. Summary of properties and applications of DLC films

Property	Type of use	Applications
Transparency in Vis and IR; optical band gap = 1.0-4.0 eV	Optical coatings	Antireflective and wear-resistant coatings for IR optics
Chemical inertness to acids, alkalis and organic solvents	Chemically passivating coatings	Corrosion protection of magnetic media, biomedical
High hardness; 5-80 Gpa; low friction coefficient < 0.01- 0.7	Tribological, wear-resistant coatings	Magnetic hard drives, magnetic tapes, razor blades, bearings, gears
Nanosmooth	Very thin coatings < 5 nm	Magnetic media
Wide range of electrical resistivities = 10^2-10^{16} Ω–cm	Insulating coatings	Insulating films
Low dielectric constants < 4	Low-*k* dielectrics Field emission	Interconnect dielectrics, Field emission flat panel displays

2.4. Difficulties of Pure DLC Material and how to over Come the Problems

Although due to extensive research activities in the field of diamond and DLC during the last three decades, the materials and the technology are more or less well understood by the time, still there are numerous problems with these materials, which need motivated works. For example, the high intrinsic stress generated in the film causes some serious problems in various applications of this material, like degradation of electrical and optical properties and leads to peeling-off of the films from the substrate and poor adhesion.

Copyright © 2012. Nova Science Publishers, Incorporated. All rights reserved.

Diamond-Like Carbon Films, Nova Science Publishers, Incorporated, 2012. ProQuest Ebook Central,

By changing co-ordination number of the carbon atoms in the DLC, it is possible to reduce the generated stress. This can be achieved by introducing foreign atoms in the DLC matrix. Doping of DLC with n and p-type dopants such as nitrogen, phosphorous, boron, iodine, fluorine [30-34] etc. and their doping effects on the electrical, optical and mechanical properties of DLC films have been extensively investigated. Boron acts as a good acceptor and is well incorporated into the structure of DLC analogous with the case in diamond. In nitrogen doped DLC films, the optical band gap and the fraction of the sp^3 bonding were both found to remain constant, they only decreased at higher N contents. The optical and electrical properties of DLC films drastically change by boron and nitrogen doping [35]. Room temperature electrical conductivity increased by two orders of magnitude in N-DLC films and one order of magnitude in B-DLC films respectively. Incorporation of nitrogen and boron reduced the electrical activation energy of the films from 0.75 eV for pure DLC to 0.32 eV and 0.58 eV respectively for doped films. Optical measurements in UV-Visible-NIR region showed an increase in the optical band gap energy from 1.0 eV to 2.12 by N doping where as by B doping it increased up to 2.0 eV. The films showed high transparency in visible region [35]. However, the doping efficiency is very low. It has been claimed that the decrease of resistivity by incorporation of dopants may be related to a dopant induced graphitization [36]. The electronic transport mechanism was investigated in pulsed laser deposited ta-C by correlating the effect of annealing on electrical conductivity and stress relaxation and using the latter to estimate the changes in sp^2 carbon concentrations [37]. The results indicated that, in the specific films, the conductivity is an exponential function of the changes in the sp^2 concentration, indicating a tunneling or hopping transport mechanism. The electronic transport could be modeled as taking place by thermally activated conduction along linkages or chains of sp^2 carbon atoms with variable range and variable orientation hopping, resulting in heterogeneity of conduction pathways through the sample.

Metal incorporated DLC (Me-DLC) films have aroused immense interest among the workers due to their interesting tribological, electrical and optical properties. Nanometer-sized clusters incorporated into the DLC matrix can drastically change different properties for the application point of view. Various groups have tried to deposit Me-DLC using different metal elements such as Au, Ta, Ti, Li, Sn, Mo, Al etc. [38-42]. Czyzniewski et al [39] reported the deposition of tungsten incorporated DLC (W-DLC) nanocomposite coatings on steel substrates below 423 K temperature and discussed their mechanical properties. Rusli et al [40] have shown that resistivities of their tungsten incorporated a-C films (W-C:H) decreased drastically upon incorporation of several atomic percentage of tungsten. Schuler et al [41] have studied the optical properties in details of the Ti-C:H carbon films deposited by reactive magnetron sputtering. Huang et al [42] have studied in detail the dielectric properties of Mo-C:H films deposited by ECRCVD process. Due to incorporation of nanocrystalline tin (Sn) particles into the amorphous DLC matrix, the resistivity of the films decreased drastically compared to the undoped DLC film and the threshold field for electron emission decreased to 3.5 V/μm for an optimum Sn % from 15 V/μm for the undoped DLC film [43].

Copyright © 2012. Nova Science Publishers, Incorporated. All rights reserved.

Diamond-Like Carbon Films, Nova Science Publishers, Incorporated, 2012. ProQuest Ebook Central,

3. Basic Theory of Electron Field Emission

A schematic diagram, which reviews the various emission mechanisms associated with electron emission from solid surfaces, is shown in Figure 3.1. In the case of hot filaments, as found in tungsten light bulbs, thermionic emission takes place due to the heating up of the material, which allows electrons to gain enough energy via Ohmic heating to surmount the work function of the metal. Schottky emission is similar in nature but occurs as a result of electrons gaining enough energy to be emitted to vacuum with a slightly reduced defective work function. There is also the situation when the emission process is a combination of significant field-induced band lowering and thermal heating. Finally, there is the Fowler-Nordheim (F-N) process where there is no thermal energy dissipated but only field lowered electron emission, which is based on quantum mechanical tunneling phenomena.

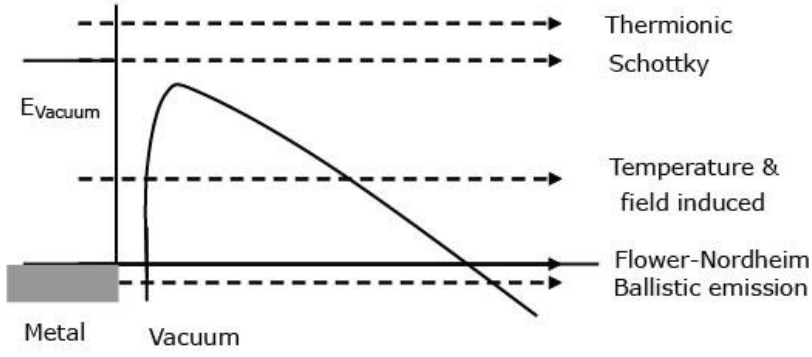

Figure 3.1. Schematic diagram of the electron emission process from solids into vacuum.

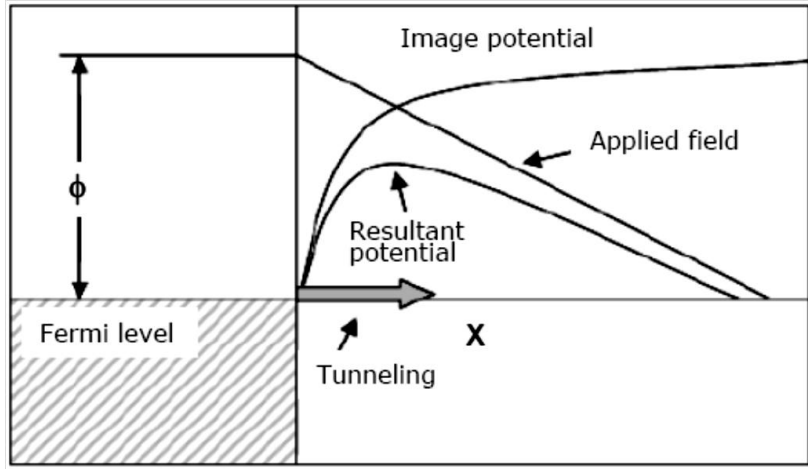

Figure 3.2. Potential-energy diagram for electrons at a metal surface under an applied electric field, where a strongly deformed potential results from the combination of the applied field and the image charges induced by the emitted electrons.

Field emission (FE) is based on the physical phenomenon of quantum tunneling, in which electrons are injected from the surface of materials into vacuum under the influence of a

Copyright © 2012. Nova Science Publishers, Incorporated. All rights reserved.

Diamond-Like Carbon Films, Nova Science Publishers, Incorporated, 2012. ProQuest Ebook Central,

strong external electric field [44]. The potential barrier is rectangular when no electric field is present, and becomes triangular when a negative potential is applied to the solid. The slope of the latter depends on the amplitude of the local electric field E just above the surface. This local electric field is drastically enhanced if the structure of the emitter is very sharp and protruding (high aspect ratio) as in the case of a carbon nanotubes Compared to thermionic electron emission and photo electron emission where electrons have sufficient energy to overcome the potential barrier (work function φ), field emitted electrons tunnel into the vacuum because of a strongly deformed barrier under an electrical field (shown in Figure 3.2).

In the presence of high electric field, flat thin films of some materials emit electrons at macroscopic fields of about 1 to 10 V/μm, although cold field emission of electrons normally occurs only at fields of about 2 V/μm or above.

a) This occurs because the thin film is an electrically nanostructured heterogeneous (ENH) material.
b) Internal nanostructure creates geometrical field enhancement at or near the film or vacuum interface, so local fields are much greater than macroscopic fields.
c) Electron emission at low macroscopic field strengths is a property of all ENH materials under appropriate conditions.
d) Field enhancement is the primary effect, but there also be the secondary effects that contribute to facilitating emission at low fields.

A simple mathematical expression for field emission can be obtained from the Heisenberg uncertainty principle:

$$\Delta p.\ \Delta x \cong \hbar/2 \tag{3.1}$$

where Δp is the uncertainty of the electron momentum and Δx is the corresponding uncertainty in position. Considering electrons near the Fermi level, the barrier height is the work function φ, so the uncertainty of the electron momentum $\Delta p = (2m\varphi)^{1/2}$ and Δx can be obtained from equation 3.1.

$$\Delta x = \hbar / 2\,(2m\,\varphi)^{1/2} \tag{3.2}$$

Thus when Δx is of the order of the barrier width, the probability that electrons would penetrate the barrier is high. The barrier width is

$$x = \varphi / E \tag{3.3}$$

where E is the electrical field. Combining equations 3.2 and 3.3, we can obtain an estimate of the electrical field required for electron field emission:

$$E = 2(2m/\hbar^2)^{\frac{1}{2}}\frac{\varphi^{\frac{3}{2}}}{e} \tag{3.4}$$

Copyright © 2012. Nova Science Publishers, Incorporated. All rights reserved.

Diamond-Like Carbon Films, Nova Science Publishers, Incorporated, 2012. ProQuest Ebook Central,

A more detailed mathematical description has been done with the Wentzel- Kramers-Brillouin (WKB) method. The emission current density (*J*) can be obtained as a function of the electrical field, *E*, and work function, φ, which is described by Fowler-Nordheim (F-N) equation [45]:

$$J = \frac{AE^2}{\varphi t^2(y)} \exp\left[-B\alpha(y) \frac{\varphi^{\frac{3}{2}}}{E} \right] A/cm^2 \tag{3.5}$$

where *A* and *B* are constants with values of 1.54 x 10^{-6} and 6.87 x 10^7, respectively, and $\alpha(y) = 0.95 - y^2$, where $y = 3.8x10^{-4} E^{1/2}/\phi$, Both $t^2(y)$ and $\alpha(y)$ are contributions arising from the image potential, which is due to positive image charges induced by the emitted electrons at the surface. Image charges can cause a further lowering of the barrier height by a factor of - $e^2/4x$ (Figure 3.2). Under typical conditions, $t^2(y)$ and $\alpha(y)$ are close to unity and normally omitted in practice. The standard physical assumptions of F-N theory are that the metal: (i) has a free-electron band structure; (ii) has electrons that are in thermodynamic equilibrium and obey Fermi-Dirac statistics; (iii) is at zero temperature; (iv) has a smooth flat surface; and (v) has a local work function that is uniform across the emitting surface and is independent of external field. It is also assumed that: (vi) there is a uniform electric field above the emitting surface; (vii) the exchange-and-correlation interaction between the emitted electron and the surface can be represented by a classical image potential; and (viii) barrier penetration coefficients may be evaluated using the JWKB approximation. In addition, the F-N equation is based on the assumption of a flat surface and only valid at 0 K, therefore, a modified F-N equation has to be used for an irregular surface and at different temperatures. In order to initiate field emission, an extremely large electrical field has to be employed, which is difficult to achieve from flat surface. However, with a tip structure, a high local electrical field can be obtained around high curvature regions. For instance, an electrical field *E* at a surface of a sphere, with a radius *r* and a potential *V*, is *E* = *V*/*r*. When *r* becomes smaller, *E* will become larger. Therefore, to account for the geometrical effects on the local electric field, a field enhancement factor β is introduced in the F-N equation as follows:

$$J = 1.54x10^{-6} \frac{(\beta E)^2}{\varphi} \exp\left[-6.87x10^7 \frac{\phi^{\frac{3}{2}}}{\beta E} \right] A/cm^2 \tag{3.6}$$

An experimental F-N plot is modeled by the tangent, which can be written in as [46-48]

$$\ln\left(I/V^2\right) = a - S/V \tag{3.7}$$

where *a* is a constant and

Copyright © 2012. Nova Science Publishers, Incorporated. All rights reserved.

Diamond-Like Carbon Films, Nova Science Publishers, Incorporated, 2012. ProQuest Ebook Central,

$$S = -\frac{6.83x10^{7}\varphi^{\frac{3}{2}}d}{\beta} \tag{3.8}$$

A linear relationship can be obtained when plotting $\ln(I/V^2)$ vs I / V, and if we know the work function (φ) of the material, specially for a-C it is ~ 4.7 eV, [49,50] the inter-electrode distance (d), and the slope (S) of the F-N plot, the field enhancement factor β can be obtained.

In geometrical configurations resembling a parallel plate capacitor, the macroscopic field E_M is defined by:

$$E_M = V/d, \tag{3.9}$$

where V is the voltage applied across a gap of thickness d. The local field E is the field, close to the emitting surface (within 1-2 nm of the surface atoms), that determines the barrier through which field emitted electrons tunnel. The field E is some times called the barrier field. E is typically a few V/nm, and is often significantly higher than E_M. Their ratio defines a field enhancement factor β

$$\beta = E/E_M \tag{3.10}$$

Considering the simple physical models of a 'floating sphere at the emitter plane potential' and a 'hemisphere on a post' the corresponding mathematical expressions have the form:

$$\beta = m + h/r \tag{3.11}$$

where r is the radius of the sphere or the hemisphere, h is its height above the emitter plane, and m is a constant generally taken as 0, 2 or 3 [51].

In addition to the geometric field enhancement factor (β), the emission can depend on various parameters such as negative electron affinity, band gap, surface termination, depletion layers and film thickness [52-55]. In these cases, the emission can be interpreted in terms of homogeneous films and a well-defined band structure.

In a-C, the sp^3 content controls the band gap and electron affinity. Nanostructured carbon, nanocrystalline diamond, and carbon nanotubes are the types of carbon that emit at lowest applied field. In microcrystalline diamond, emission is found to occur from grain boundaries, i.e., nm-scale sp^2 bonded regions of positive electron affinity. Similarly, emission from carbon nanotubes occurs from 1 nm curved regions.

4. FIELD EMISSION OF DLC THIN FILMS

The electron field emission (FE) properties from diamond or carbon-based materials have been studied to use these materials as the cold cathodes of field emission displays (FEDs) [56]. In order to manufacture the FEDs, development of electron emitters with low operating electric field and high emission current is necessary. The emission of electrons from the

Copyright © 2012. Nova Science Publishers, Incorporated. All rights reserved.

Diamond-Like Carbon Films, Nova Science Publishers, Incorporated, 2012. ProQuest Ebook Central,

surface of DLC films is an interesting field due to potential applications in cold cathode devices. The original work on emission from diamond was motivated by the discovery of its negative electron affinity [57]. The negative electron affinity of the hydrogenated diamond surface plays an important role [58]. The ability of large area growth of flat thin films coupled with the observation of electron emission at low threshold fields has made a-C based materials a leading candidate for FEDs [59,60]. These carbon-based films are attractive from a manufacturing view point, because they can be grown on glass substrates at low temperatures, resulting in a reduction of the manufacturing cost [61,62].

The first direct study of field emission from a-C:H was performed by Amaratunga and silva in 1996 [63]. There have been numerous studies of field emission DLC [62,64]. DLC is a semiconductor whose band gap varies from 1 - 4 eV according to its sp^2 content. Field emission from DLC is generally easier than for diamond and the typical threshold emission field for DLC is 20 - 40 V/μm [63], which can be lowered to about 10 V/μm for more optimized films, and to 5 V/μm for nitrogen doped films [62]. Toyama et al showed that the turn-on electric field depended on the film thickness and that the values ranged from 4 - 52 V μm^{-1} for undoped diamond films [65]. The effect of annealing on the field emission property of DLC films have been reported [66,67]. The field emission properties of DLC films are mainly dependent on the variation of chemical bonding structure other than surface roughness and the doping such as boron, phosphor and nitrogen into DLC films. Doping can improve the field emission properties of DLC or ta-C. Nitrogen decreases the emission barrier by increasing the bulk Fermi level and decreasing the work function, therefore generally improves the field emission from these films. Turn-on fields as low as 4 V/μm have been reported for N-DLC [63]. It has been observed that the incorporation of boron into the DLC films increased emission current density from 80 mA/cm^2 to 2500 mA/ cm^2 [68]. Cheng et al showed that the boron doping increases the electron field emission current density and also improved the stability of emission behavior [69]. The boron doped DLC films deposited on Au-coated Si substrate can emit a current density as large as 1400 μA/cm^2 for 720 min without significant degradation [69]. Enhancement in field emission properties was attributed to the alternation of the electronic structure by the incorporation of substitutional defect states and the donor activity of incorporated material. It can be seen that turn-on field was reduced from 24.33 V/μm for undoped DLC to 6.97 V/μm and 14.76 V/μm for nitrogen doped DLC and sulfur doped DLC respectively [35,43]. Also exponential increase in current density was observed, exhibiting strong effect of nitrogen and sulfur addition on field emission behavior. Nitrogen and sulfur act as weak donors in DLC and provide electrons close to the conduction band. Also incorporation of nitrogen and sulfur introduces structural defects. These defects lead to tailing of the valance band maxima and conduction band minima and creating sub-bands within the mid-gap states (band gap), thus contribute electrons for emission at low electric fields.

The case of emission from the large variety of carbon-based materials suggests that the NEA is not a prerequisite and more general emission models are desired for these systems. Many models have been proposed to discuss the origin of electron emission from ta-C films and other a-C films [70,71]. Robertson suggested that field emission at a low electric field is due to the low electron affinity of ta-C films [72]. Other models based on space-charge-induced band bending [63], surface dipole controlled emission [72], field enhancement due to film microstructure [73] and conductive paths caused by localized sp^2 sites [74] were also

Copyright © 2012. Nova Science Publishers, Incorporated. All rights reserved.

Diamond-Like Carbon Films, Nova Science Publishers, Incorporated, 2012. ProQuest Ebook Central,

proposed. Thermal annealing is an effective method to alter structure of DLC films. Groning et al [74] explained the emission mechanism from DLC films in a way that, like a freestanding conductive tip in the vacuum, sp^2 bonded carbon clusters are assumed to form a conductive channel in an insulating matrix, which leads to local field enhancement and hence to an enhanced electron emission. Since the sp^2 clusters are located at or near the Fermi level and high concentration sp^2 carbon clusters in the films play a more important role in determining the electron emission property of the films.

Field enhancement can occur at interfaces between sp^3 and sp^2 phases or at a triple junction between the sp^2 and sp^3 phases and vacuum because of high-aspect ratio geometries and the presence of space-charge distributions. Conductive filaments normal to the film surface, such as grain boundaries in microcrystalline diamond, can cause large local electric fields. The field lines will focus onto such filaments or grain boundaries as shown in Figure 4.1(a). The positive potential on the anode creates negative space charge in the film. sp^2 bonded filaments possess amphoteric gap states around the Fermi level, which become negatively charged as shown in Figure 4.1(b). The filaments are distributed inhomogeneously in the film so the field lines focus onto the filaments, creating a field enhancement. The local field is enhanced compared to the macroscopic field.

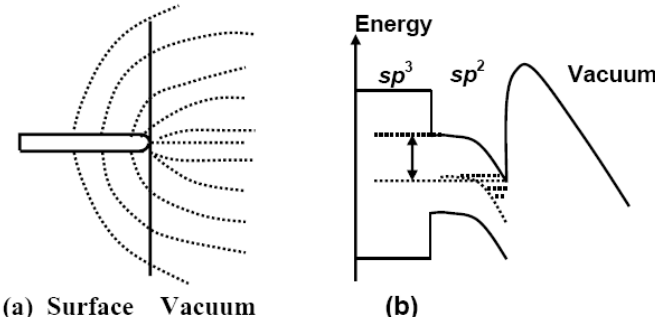

Figure 4.1. (a) Field focusing around a high-aspect ratio filament nanostructure and (b) band model for field emission from filament-type sp^2 clusters perpendicular to the film/vacuum interface.

5. Synthesis and Field Emission of Metal and Nonmetal Doped DLC Thin Films

5.1. Synthesis and Electron Field Emission Property of Silicon Incorporated DLC (Si-DLC) Thin Films

Silicon incorporated DLC (Si-DLC) films were deposited via DC plasma-enhanced chemical vapor deposition (PECVD) technique. The deposition apparatus for the DLC films is a conventional vacuum system equipped with rotary and diffusion pumps. Dow corning silicone oil (DC-704) is used as the diffusion pump fluid. Figure 5.1 shows the schematic diagram of the PECVD apparatus [75].

The vacuum chamber is designed with appropriate stainless steel (SS) vacuum couplings through which different feed-throughs like vacuum port, pressure gauge, gas mixture inlets, thermocouple etc. could be introduced. For the measurement of pressure of the vacuum

Copyright © 2012. Nova Science Publishers, Incorporated. All rights reserved.

Diamond-Like Carbon Films, Nova Science Publishers, Incorporated, 2012. ProQuest Ebook Central,

chamber, pirani and penning gauges are used. The plasma is produced between two parallel plate SS electrodes. The lower disc is grounded upon which the substrate is placed and the upper disc is used as the cathode electrode.

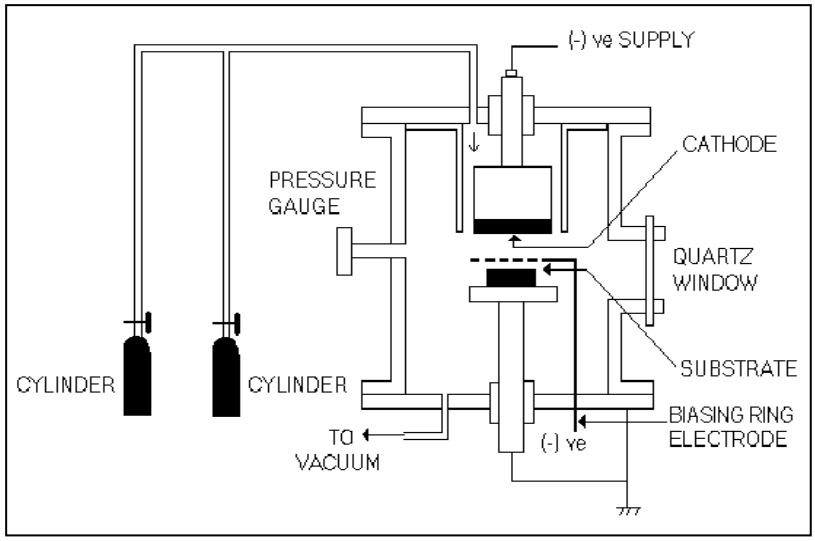

Figure 5.1. Schematic diagram of the DC-PECVD unit [Ref. 75].

A shutter is used just above the substrate and can be mechanically operated from outside. For substrate heating purpose low tension heating terminals have been connected to substrate heater. Previously calibrated cupper-constantan and chromel-alumel thermocouple were used for measuring the substrate temperature during film deposition. To measure the thickness of the deposited films and its deposition rate, a quartz crystal thickness monitor (HindHivac, Bangalore, Model DTM 101) is attached to the vacuum chamber through the base plate. A DC power supply (0 - 5 kV), is used to apply required voltage to the cathode. When the chamber pressure attained ~10^{-6} mbar, then C_2H_2 gas was introduced and DLC films were deposited at a pressure of 0.4 mbar. Glass, silicon and alumina were used as substrates. For silicon (Si) incorporation, tetraethyl orthosilicate (TEOS) dissolved in methanol solution was used. Ar gas was passed through the solution for bubble formation and then introduced into the chamber with appropriate needle valve arrangement. At. % of Si was varied in the deposited films by varying the concentration of TEOS in the methanol solution. The deposition parameters for the synthesis of Si-DLC thin films have been shown in Table - 5.1.

AFM imaging provides detailed information involving the surface morphology of the Si-DLC films as shown in Figure 5.2 [76]. The measured surface roughness shows the surfaces of the Si-DLC films are rougher than that of the undoped DLC film. The undoped DLC film generally exhibits a very smooth morphology, with the RMS roughness 1.8 nm within the surface area of 1 μm × 1 μm. However, the RMS roughness of the Si-DLC film is 3.7 nm within the same area of 1 μm × 1 μm, respectively. The increase of the RMS roughness is due to the changes of the microstructures of the DLC films due to Si incorporation. A change of the sp^2 clusters size due to Si incorporation is mainly responsible for the observed changes of surface roughness.

Copyright © 2012. Nova Science Publishers, Incorporated. All rights reserved.

Diamond-Like Carbon Films, Nova Science Publishers, Incorporated, 2012. ProQuest Ebook Central,

Table 5.1. Deposition parameters used for Si-DLC thin films synthesis

Deposition parameters	Corresponding values
1. Deposition time	30 min.
2. DC voltage	1.0 kV
3. Electrode distance	2.0 cm
4. Precursor material	C_2H_2, TEOS
5. Gas pressure	0.4 mbar
6. Substrates used	Glass, Silicon and Alumina
7. Substrate temperature	300 ^{0}C

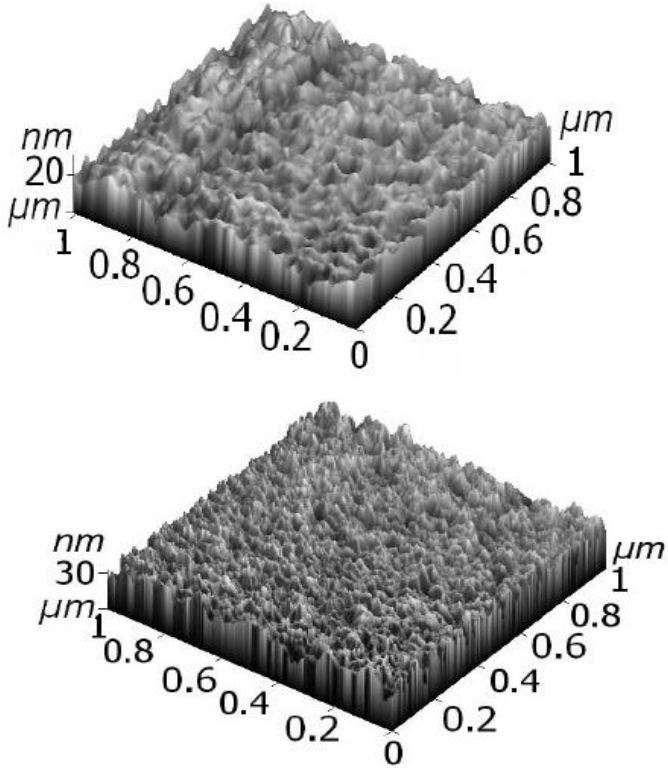

Figure 5.2. AFM 3D images of (a) undoped and (b) 19.31 at. % Si-DLC film [Ref. 76].

Field emission measurements were carried out by using a diode configuration consisting of a cathode (the film under test) and a stainless steel tip anode (conical shape with a 1 mm tip diameter) mounted in a liquid nitrogen trapped rotary-diffusion vacuum chamber with appropriate chamber baking arrangement. The schematic diagram of the field-emission apparatus is shown in Figure 5.3 [75]. The measurements were performed at a base pressure of ~ 10^{-7} mbar and the temperature was measured with the help of a PID control system. As the substrate glass was non-conducting, the negative terminal of the high voltage DC power supply was connected with the films by silver paint (Acheson Colloid Co. UK), at least 6 mm away from the position of the anode tip. The Ohmic nature of the contact was checked before field emission experiment. The tip-sample distance was continuously adjustable to a few hundred μm by spherometric arrangement with screw-pitch of 10 μm.

Copyright © 2012. Nova Science Publishers, Incorporated. All rights reserved.

Diamond-Like Carbon Films, Nova Science Publishers, Incorporated, 2012. ProQuest Ebook Central,

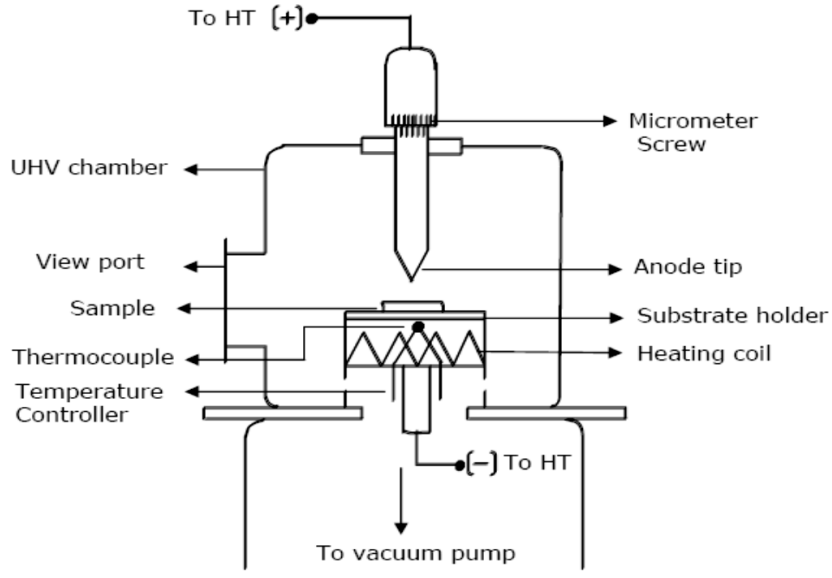

Figure 5.3. Schematic diagram of the field-emission apparatus [Ref. 75].

The position of just touching the anode with the sample was determined by an optical microscope and then various spacings were obtained by rotating the micrometer screw as its screw-pitch is known. Field emission current-voltage measurements were done with the help of an Agilent multimeter (model 3440-1A). The whole surface of the film was visible through the chamber view port, which enabled us to recognize the electron emission and discharge. For temperature dependent electron field emission study, the film under test is heated by substrate heater. Emission characteristics were registered and analyzed with the help of a personal computer.

Figure 5.4 shows the emission current (I) vs. macroscopic field (E) curves for undoped and Si-DLC films for a fixed anode-sample separation of 80 μm for different Si concentrations in the films. Field emission characteristics of the films were studied using the Fowler-Nordheim (F-N) theory [45]. The macroscopic field is calculated from the external voltage applied (V), divided by the anode-sample spacing (d). Theoretically, the emission current I is related to the macroscopic electric field E by

$$I = A a t_F^{-2} \phi^{-1} (\beta E)^2 \exp\{\frac{-b v_F \phi^{3/2}}{\beta E}\} \tag{5.1}$$

where, ϕ is the local work-function, β is the field enhancement factor, A is the effective emission area, a is the first Fowler-Nordheim Constant (1.541434×10^{-6} A eV V^{-2}), b is the second F-N Constant (6.830890×10^{9} $eV^{-3/2}$ V m^{-1}), and v_F and t_F are the values of the special field emission elliptic functions [46] v and t, evaluated for a barrier height ϕ. In so-called Fowler-Nordheim coordinates, this equation takes the form:

$$\ln\{\frac{I}{E^2}\} = \ln\{t_F^{-2} A a \phi^{-1} \beta^2\} - \frac{(v_F b \phi^{3/2} \beta^{-1})}{E} \tag{5.2}$$

Copyright © 2012. Nova Science Publishers, Incorporated. All rights reserved.

Diamond-Like Carbon Films, Nova Science Publishers, Incorporated, 2012. ProQuest Ebook Central,

An experimental F-N plot is modeled by the tangent, which can be written in the form [46-48]:

$$\ln\{\frac{I}{E^2}\} = \ln\{rAa\phi^{-1}\beta^2\} - \frac{(sb\phi^{3/2}\beta^{-1})}{E} \tag{5.3}$$

where *r* and *s* are appropriate values of the intercept and slope correction factors, respectively. Typically, *s* is of the order of unity, but *r* may be of order 100 or greater. Both *r* and *s* are relatively slowly varying functions of 1/*E*, so a F-N plot (plotted as a function of 1/*E*) is expected to be a good straight line.

The F-N plots of our sample are shown in Figure 5.4(b). The turn-on field (E_c), which we define as the macroscopic field needed to get an emission current I = 0.034μA, were lying in the range 3.61 - 16.19 V/μm. It has been observed that the turn-on field was greatly reduced for the Si-DLC films than that of the film grown without Si. The lowest turn-on field achieved was 3.61 V/μm for the sample with 19.31 at. % of Si, while for the intrinsic material it was 16.19 V/μm. The variation of turn on field with at. % of Si in the films shown in Figure 5.5.

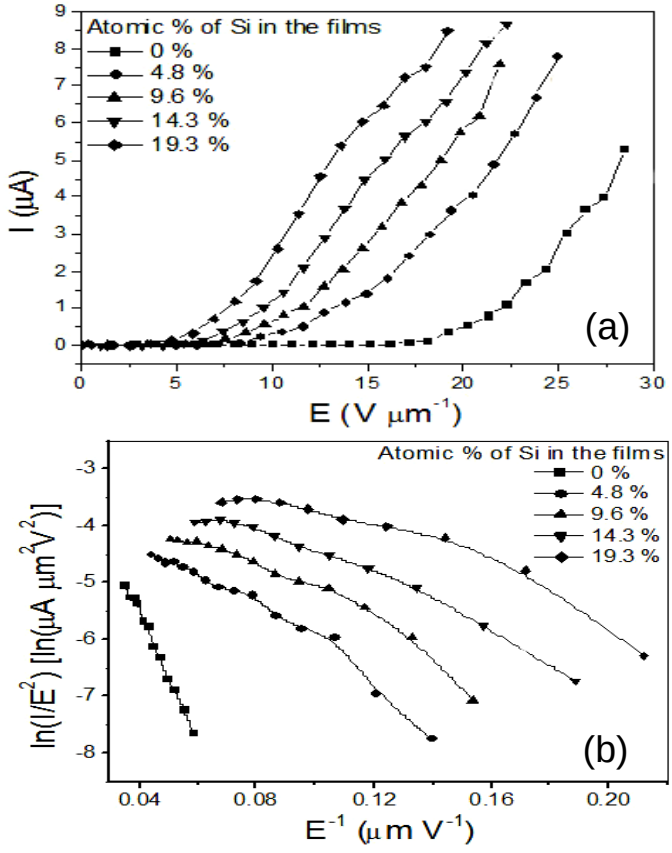

Figure 5.4 (a) Emission current (*I*) vs. macroscopic field (*E*) curves of Si-DLC films for different at. % of Si and (b) corresponding F-N plot [Ref. 77].

Copyright © 2012. Nova Science Publishers, Incorporated. All rights reserved.

Diamond-Like Carbon Films, Nova Science Publishers, Incorporated, 2012. ProQuest Ebook Central,

Emission barriers (ϕ) were calculated from the slopes of F-N plots. The value of ϕ was reduced from 0.065 eV to 0.016 eV for an optimum Si incorporation. But, true barrier must be larger than these values. Such low work function obtained may be due to an underestimation of the field enhancement factor β [77]. Previously Amaratunga et al [63] proposed a hot electron space charge induced band bending model to account for the emission from a-C films. Robertson [1] suggested that the Fermi level, from which emission occurs, does not vary much with sp^3 fraction. The effect of introducing any foreign species into the DLC matrix, like Si may be to allow an easier formation of sp^2 channels. In the case of Si-DLC films, the sp^2 regions within the insulating sp^3 matrix are assumed to form conductive channels extended through the whole thickness of the film to the vacuum. The electron traversing through the channels experiences a high electric field. The effective barrier height was reduced with the addition of Si impurity in the amorphous DLC matrix.

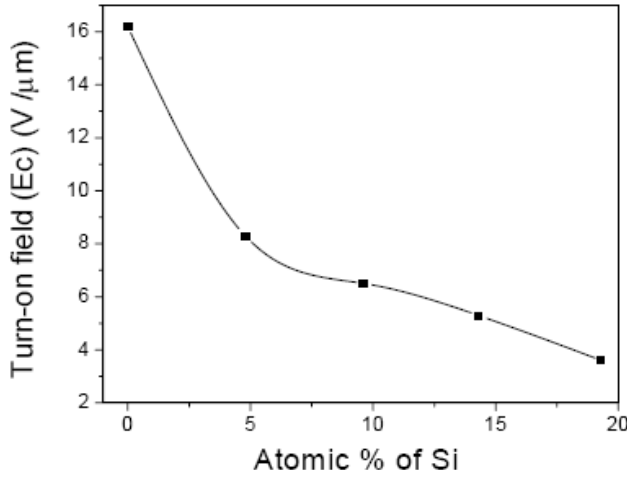

Figure 5.5. Variation of turn on field (Ec) with at. % of Si in the DLC films [Ref. 75].

Table 5.2. Deposition parameters used for Ag-DLC thin films synthesis.

Deposition parameters	Corresponding values
1. RF power	150-180 Watt
2. Gases used	CH_4, Ar
3. CH_4/Ar	80-20 %
4. Gas pressure	0.1 mbar
5. Substrates used	Glass, Si (400)
6. Substrate temperature	300 K

5.2. Synthesis and Field Emission Property of Ag-DLC Thin Films

The silver incorporated DLC (Ag-DLC) thin films were synthesized by the radio frequency reactive sputtering technique at room temperature (300 K). The silicon substrates were cleaned by standard cleaning procedure before they were placed in the deposition chamber. To deposit the Ag-DLC thin films, the deposition chamber was evacuated to a base

Copyright © 2012. Nova Science Publishers, Incorporated. All rights reserved.

Diamond-Like Carbon Films, Nova Science Publishers, Incorporated, 2012. ProQuest Ebook Central,

pressure 2 x 10^{-6} mbar and then methane (CH_4) and Argon (Ar) gases were introduced into the chamber for a fixed deposition pressure of 0.1 mbar. A RF power (13.56 MHz) supply was applied in the high purity (99.99 %) Ag sputter target. For the variation of Ag at % in the films, the ratio of CH_4 to Ar sputter gas and RF power has been changed from 80 - 40 % and from 150 to 180 Watt, corresponding Ag at. % ranging from 0 to 12.5 respectively. The deposition parameters for the synthesis of Ag-DLC thin films have been shown in Table - 5.2.

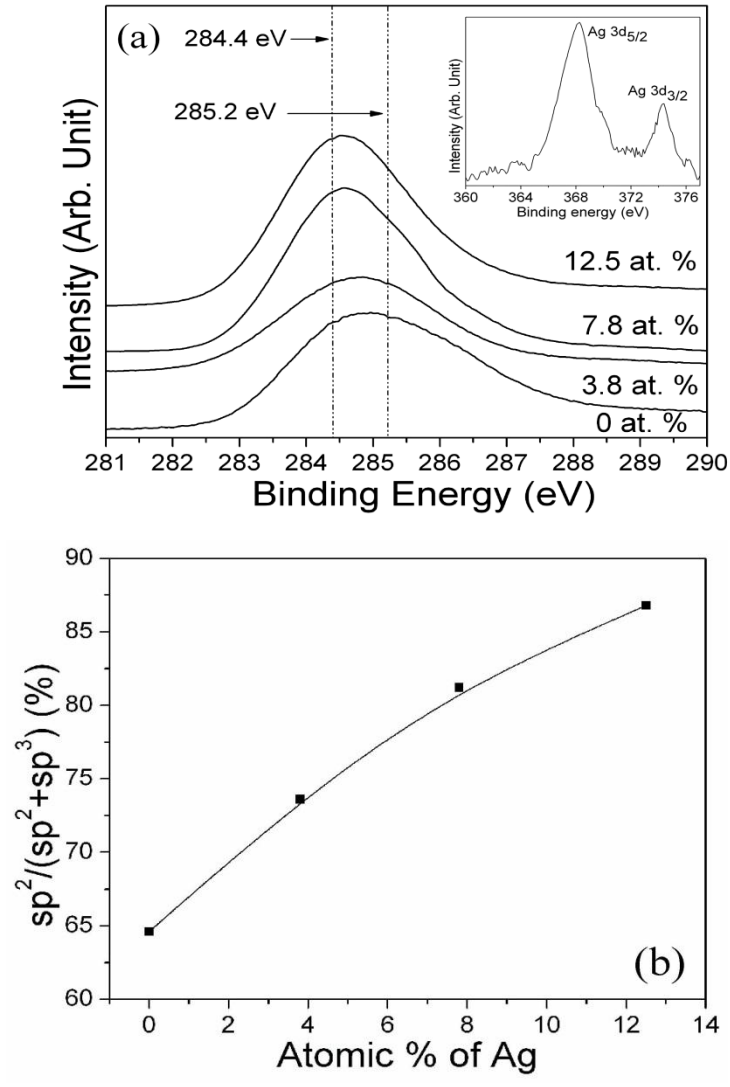

Figure 5.6. (a). XPS spectra of C 1s peak of DLC films for different at. % of Ag and the Ag core level spectra of 7.8 at. % Ag content DLC films in the inset and (b) variation of $sp^2/(sp^2+sp^3)$ ratio with Ag at. % in the DLC films [Ref. 80,81].

Copyright © 2012. Nova Science Publishers, Incorporated. All rights reserved.

Diamond-Like Carbon Films, Nova Science Publishers, Incorporated, 2012. ProQuest Ebook Central,

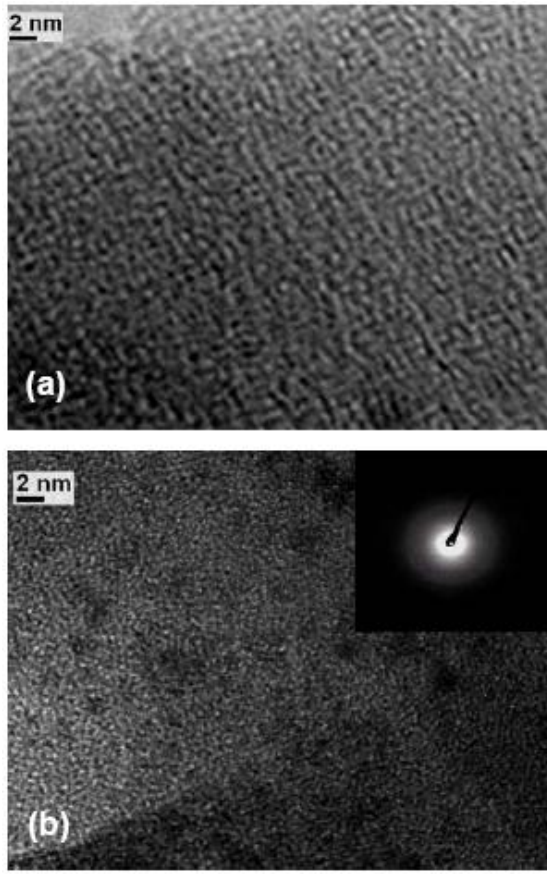

Figure 5.7(a). HRTEM images of undoped and (b) 12.5 at. % Ag doped DLC film [Ref. 81].

Figure 5.6(a) shows the XPS C 1s (~284 eV) peaks of Ag-DLC films deposited with different Ag at. %. The core level XPS spectrum (inset of Figure 5.6(a)) of Ag 3*d* region consists of two binding energy peaks corresponding to Ag $3d_{5/2}$ (368.2 eV) and $3d_{3/2}$ (374.2 eV) respectively, which suggests the Ag has been incorporated into the DLC matrix. Differences can be observed from the C 1s spectra (Figure 5.6(a)) acquired from the Ag-DLC films with different at. % of Ag. As the at. % of Ag increases the peak position shifted towards the lower energy (sp^2) value.

Deconvolution of the spectra showed that the broad C 1s peaks are composed of three peaks corresponding respectively to sp^2 carbon atoms (284.4 – 284.8 eV), sp^3 carbon atoms (285.3 – 285.7) and a third peak at about 286.2 – 286.6 eV was found, which was due to some C-O contamination formed at the surface of the samples with air exposure [78]. Figure 5.6(b) shows that the $sp^2/(sp^2+sp^3)$ ratio increases with increase of Ag at. % in the films. Increasing at. % of Ag, the film structure significantly changes, which is most evident from the increasing intensity of the sp^2 and the decreasing intensity of the sp^3, as well as the overall increase in the sp^2/sp^3 ratio. This means that with increasing Ag at. % the Ag-DLC film changes to graphite like film [79].

Copyright © 2012. Nova Science Publishers, Incorporated. All rights reserved.

Diamond-Like Carbon Films, Nova Science Publishers, Incorporated, 2012. ProQuest Ebook Central,

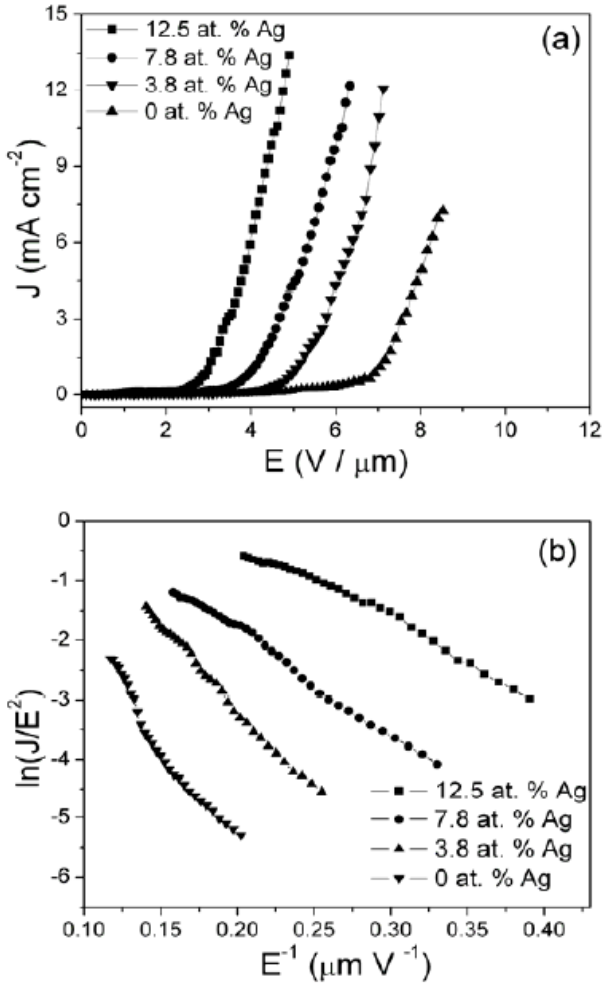

Figure 5.8(a) Emission current density (*J*) vs. macroscopic field (*E*) curves of Ag-DLC films for different at. % of Ag and (b) corresponding F-N plot [Ref. 81].

HRTEM images (Figure 5.7(a)) showed that for low Ag at. %, a uniform amorphous structure was observed i.e., the incorporated Ag atoms were dissolved in the DLC matrix. In the films of high concentration (12.5 at. %), the Ag atoms began to agglomerate and form an amorphous Ag phase with a diameter of ~ 2 nm as shown in Figure 5.7(b). The darker spots correspond to metallic Ag region, while the brighter region corresponds to the DLC matrix. Electron diffraction pattern in inset of Figure 5.7(b) reveals that the film is amorphous even when agglomeration of Ag atoms occurs. Low deposition temperature would limit the atomic rearrangement during deposition, suppressing the crystallization of Ag clusters.

Figure 5.8(a) shows the emission current density (*J*) vs. macroscopic field (*E*) curves for Ag-DLC films for different at. % of Ag at fixed anode-sample separation of 200 μm. Field emission characteristics of the films were analyzed using the simplified Fowler-Nordheim (F-N) equation [45-47]. It has been observed that all the *J-E* curves (Figure 5.8(b)) are fitted with the F-N equation, which suggests that the electrons are emitted by the cold field emission process. The threshold field (E_{th}) was laying in the range 6.8 - 2.6 V/μm for the variation of Ag at. % in the films. It has been observed that the threshold field was greatly reduced due to

Copyright © 2012. Nova Science Publishers, Incorporated. All rights reserved.

Diamond-Like Carbon Films, Nova Science Publishers, Incorporated, 2012. ProQuest Ebook Central,

Ag doping. This value is quite lower than that of nitrogen doped DLC (4 V/μm) [63], sulfur doped DLC (6.97 V/μm) [35], Sn doped DLC (3.5 V/μm) [43] and aligned carbon nanofiber arrays (~3 V/μm) [82].

According to the F-N plot, the slope m (given by equation (5.4)) would represent the combined effect of work function and enhancement of local electric field and is given by

$$m = -\frac{b\phi^{3/2}}{\beta} \tag{5.4}$$

using $\phi = 4.7$ eV for the work function of DLC [83,84]; the field enhancement factor was calculated from the slope of the F-N plot, varying in the range 2081 to 5876 for different Ag at. % in Ag:DLC films. The emission mechanism may involve a strong field enhancement at the front surface. To understand the F-N emission process in our Ag-DLC films, it is necessary to explain the origin of the large enhancement factor required to lower the barrier for easy electron emission. Carey et al. [85] and Gao et al [86] proposed that the presence of sp^2 clusters within the insulating sp^3 matrix could give rise to field enhancement in a-C films containing large defect densities ($>10^{19}$ cm^{-3}). Since sp^2 clusters will have different dielectric constants so the presence of dielectric inhomogeneity is responsible for field enhancement in DLC films [85,87,88]. Groning et al [75] explained the emission mechanism from DLC films in a way that, like a freestanding conductive tip in the vacuum, sp^2 bonded carbon clusters are assumed to form a conductive channel in an insulating matrix, which leads to local field enhancement and hence to an enhanced electron emission. Since the energy level of sp^2 clusters are located at or near the Fermi level and high concentration sp^2 carbon clusters in the films play a more important role in determining the electron field emission property of the films. The effect of introducing metal into the DLC matrix, allow an easier formation of sp^2 clusters [79]. From XPS analysis it was observed that with the increase of Ag at. % in the DLC films sp^2 bonded carbon content in the films increased (shown in Figure 5.6(b)). The DLC films deposited for different at. % of Ag will consist of sp^3 matrix with varying sp^2 cluster concentration and size. HRTEM microstructure (Figure 5.7(b)) shows that the Ag clusters are uniformly distributed in the film with the distance at most 5 nm. Therefore, if the formation of sp^2 region is closely related to the Ag incorporation as can be deduced from Figure 5.6(b), the sp^2 regions within the insulating sp^3 matrix would form conductive channels extended through the whole thickness of the film to the vacuum. The electron traversing through the channels experiences a high electric field. The effective barrier height was reduced with the addition of Ag impurity in the DLC matrix. The emission current density also strongly depends on the work function. Therefore, the decrease of threshold field with the increase of Ag at. % may be due to the decrease of the effective work function of Ag-DLC films. The reason is that the high concentration sp^2 carbon clusters in the DLC films created defect induced band. Urbach parameter calculation [80] showed that with increase of Ag at. % in the DLC films, the defect density increases. As the defect bands raises the Fermi level toward the conduction band so work function reduced and the electron field emission property enhanced.

Copyright © 2012. Nova Science Publishers, Incorporated. All rights reserved.

Diamond-Like Carbon Films, Nova Science Publishers, Incorporated, 2012. ProQuest Ebook Central,

5.3. Synthesis and Study the Field Emission of Fluorine Doped (F-DLC) Thin Films

Fluorine doped DLC (F-DLC) thin films have been synthesized by DC-PECVD technique. Ultrasonically cleaned glass and silicon substrates were used for deposition of F-DLC thin films. The chamber was evacuated to a base pressure 2 x 10^{-6} mbar before deposition and then acetylene (C_2H_2) gas was introduced with chamber pressure at 0.15 mbar during deposition. For F incorporation hydrofluoric acid (HF) dissolved in methanol solution was used. Ar gas was passed through the solution for bubble formation and then introduced into the chamber with appropriate needle valve arrangement. The deposition conditions for the synthesis of F-DLC thin films have been shown in Table - 5.3.

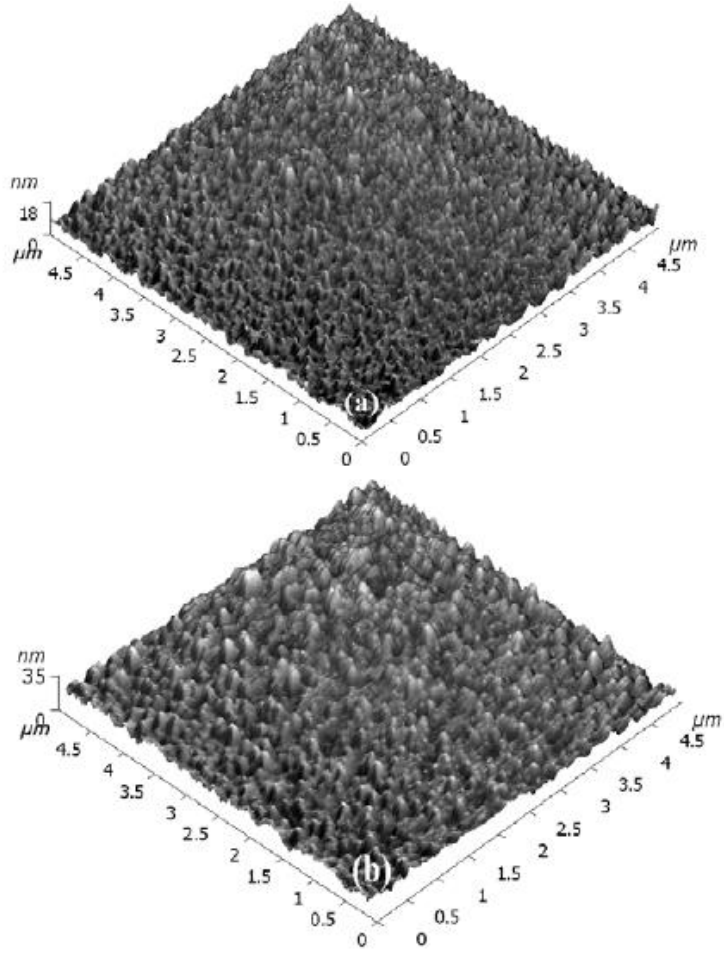

Figure 5.9. AFM 3D pictures of (a) without F and (b) 15.3 at. % of F doped DLC films [Ref. 89,90].

Figure 5.9 shows typical AFM image of the DLC films for (a) undoped and (b) 15.3 at. % F doped DLC films respectively [89,90]. The measured surface roughness shows the surfaces of the F-DLC films are rougher than that of the undoped DLC film. The undoped DLC film generally exhibits a very smooth morphology, with the RMS roughness 1.1 nm within the

Copyright © 2012. Nova Science Publishers, Incorporated. All rights reserved.

Diamond-Like Carbon Films, Nova Science Publishers, Incorporated, 2012. ProQuest Ebook Central,

surface area of 5 μm × 5 μm (shown in Figure 5.9(a)). However, the RMS roughness of the F doped DLC film is approximately 2.5 nm within the same area of 5 μm × 5 μm (shown in Figure 5.9(b)). Surface roughness increased with increased of at. % of F in the DLC films. Most likely the increased surface roughness is due to the etching effect of fluorine. Presence of F atoms in the plasma alters the growth condition and it is observed that percentages of sp^2 bonded carbon increased with increasing F concentration. Etching of the growing films by F atoms present in the plasma also takes place. Many other authors also have reported increase of sp^2/sp^3 ratio and increased surface roughness with F incorporation [91,92] in the DLC films.

Table 5.3. Deposition parameters used for F-DLC thin films synthesis

Deposition parameters	Corresponding values
1. Deposition time	20 min.
2. dc voltage	2.0 kV
3. Electrode distance	2.0 cm
4. Precursor material	C_2H_2, HF
5. Gas pressure	0.15 mbar
6. Substrates used	Glass, Silicon
7. Substrate temperature	200 ^{0}C

Figure 5.10 shows the emission current density (J) vs. macroscopic field (E) curves of for F-DLC films for different at. % of F at fixed anode-sample separation (d) of 100 μm. The threshold field (E_{th}), which we define as the macroscopic field needed to get an emission current density J = 10 μA/cm^2, were lying in the range 8.5 to 2.9 V/μm with a variation of F at. % in the films 0 % to 15.3 %. Since the sp^2 clusters are located at or near the Fermi level and high concentration sp^2 carbon clusters in the films play a more important role in determining the electron field emission property of the films. With increasing at. % of F, the DLC film changes to polymer-like film, optical gap decreases and sp^2 cluster size increases [89]. AFM analysis confirmed that the grain size as well as rms roughness of the F-DLC films increases with increase of F at. % in the films. The DLC films deposited for different at. % of F will consist of sp^3 matrix with varying sp^2 cluster concentration and size. Therefore, we assumed that lowering of the threshold field with incorporation of F to an increase in the sp^2 bonds and cluster size.

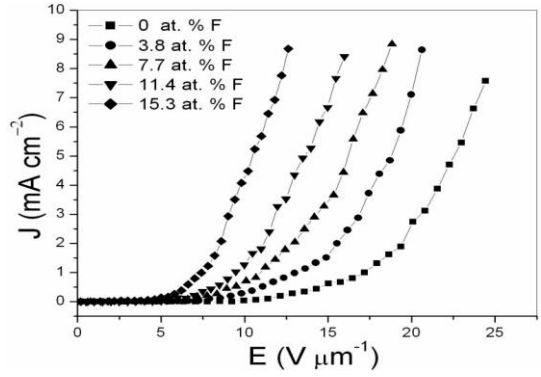

Figure 5.10. Emission current density (J) vs. macroscopic field (E) curves of F-DLC films [Ref. 93].

Copyright © 2012. Nova Science Publishers, Incorporated. All rights reserved.

Diamond-Like Carbon Films, Nova Science Publishers, Incorporated, 2012. ProQuest Ebook Central,

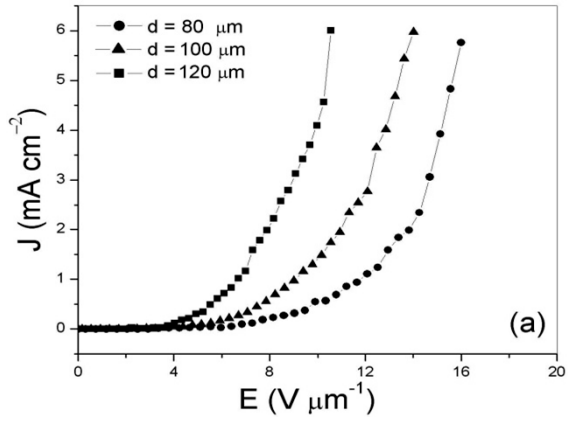

Figure 5.11. *J-E* curves of 15.3 at. % F doped DLC film for different *d* [Ref. 93].

The plots of emission current density (*J*) vs. electric field (*E*) are shown in Figure 5.11 for different anode-sample distance (*d*). The threshold field was found to vary in the range 2.6 - 4.3 V/μm for a variation of *d* 120 - 80 μm, for the 15.3 at. % F-DLC film. In the *J-E* graph (Figure 5.11), a parallel shift of curves with respect to *d* observed i.e., for a particular electric field the current density increases with increasing the anode-sample separation.

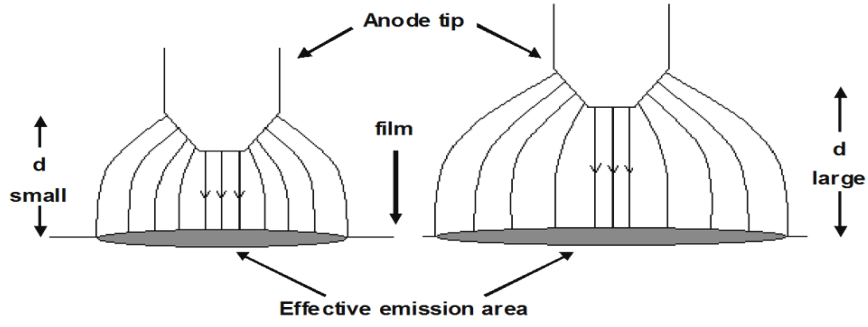

Figure 5.12. Schematic diagram for the dependence of effective emission area as an increasing function of anode-sample separation (*d*) [Ref. 95].

Zhou et al [94] reported similar type of observation for their β-SiC nanorods. This type of shift observed in our sample is due to the change in the effective emission area of the sample for different anode-sample separation. The change of effective emission area with respect to *d* may be related to the geometry of the anode. In our experiment we have used a conical shape anode with tip diameter 1 mm, therefore the lines of force immerging from the edge of the anode tip and terminating to the sample surface are diverging in nature, whereas the lines of force immerging from the flat surface of the tip are parallel in nature. Hence, the effective emission area of the sample increases with increasing *d* as shown in Figure 5.12.

Au et al [96] performed field emission of silicon nanowires using a spherical-shaped stainless steel probe with a tip diameter of 1 mm as an anode. They also found a parallel shift in their *I-V* curve. Okano et al [96] reported that their macroscopic current density for diamond films was independent of the anode-sample separation. Their field emission apparatus consisted of a parallel plate arrangement of the anode and sample, separated by

Copyright © 2012. Nova Science Publishers, Incorporated. All rights reserved.

Diamond-Like Carbon Films, Nova Science Publishers, Incorporated, 2012. ProQuest Ebook Central,

spacers. So the electric lines of force between the anode and the sample were parallel in nature, hence effective emission area remained independent of the anode-sample spacing.

For temperature dependent field emission total current density ($J = J_E + J_T$, where J_E and J_T are the field current and thermoionic current density respectively) given by simplified F-N equation and Richardson equation as [98,99]:

$$J = J_E + J_T \tag{5.5}$$

$$J = a\ \phi^{-1}(\beta E)^2 \exp\left(\frac{-sb\phi^{3/2}}{\beta E}\right)\left[\frac{\theta}{\sin(\theta)}\right] + ADT^2 e^{-\phi/KT} \tag{5.6}$$

where A is a constant about 120 A/ (cmK)^2, D is the average transmission coefficient of emitter surface, T is the temperature in Kelvin, ϕ is the work function of F-DLC, k is the Boltzmann constant and θ is the temperature correction factor, and is given by

$$\theta \approx \frac{2.2\pi(kT/q)\phi^{1/2}}{1.959E} \tag{5.7}$$

For F-DLC with a work function ~ 4.7 eV [100] and temperature below 1000 K, the value of [θ/(sin(θ))] in eqn. (5.6) is always 1.0 and in our studied temperature range, (< 350 ^{o}C), the highest contribution of thermionic emission is much smaller than the field emission current density i.e., the measured emission property is predominated by field emission current because below 1000 K, the thermoionic emission effect is less significant than the field emission emission effect [101]. Hence eqn. (5.6) reduced as:

$$\ln\left\{\frac{J}{E^2}\right\} = \ln\{r\,a\,\phi^{-1}\beta^2\} - \frac{(sb\phi^{3/2}\beta^{-1})}{E} \tag{5.8}$$

Figure 5.13(a) shows the emission current density (J) vs. macroscopic field (E) curves of for 15.3 at. % F doped DLC films for different temperature and corresponding F-N plot is shown in Figure 5.13(b). It has been observed that the *J-E* curve is closely fitted with straight line. This suggests that the electrons are emitted by cold field emission process. The threshold field were lying in the range 2.2 - 4.2 V/μm for the variation of temperature. From Figure 5.14 it is clear that with the increase of temperature, threshold field decreases and current density increases. The emission current density strongly depends on the work function. The work function of materials is temperature dependent. Therefore, the decrease of threshold field with the increase of temperature may be due to the decrease of work function of F-DLC films.

According to the F-N plot the slope m (given by equation (5.4) would represent the combined effect of work function and enhancement of local electric field and is given by,

Copyright © 2012. Nova Science Publishers, Incorporated. All rights reserved.

Diamond-Like Carbon Films, Nova Science Publishers, Incorporated, 2012. ProQuest Ebook Central,

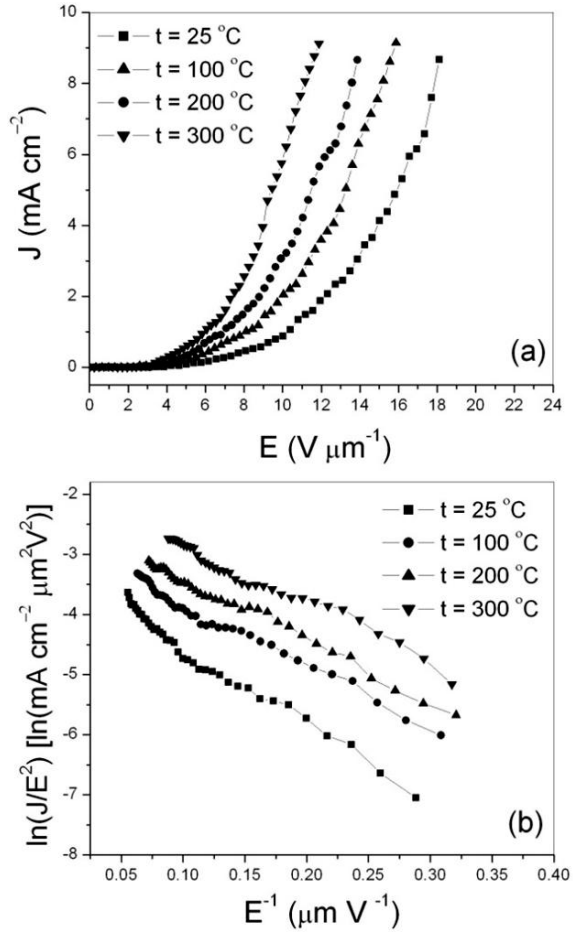

Figure 5.13. (a) *J-E* curves of 15.3 at. % F doped DLC films for different temperature and (b) corresponding F-N plot [Ref. 93].

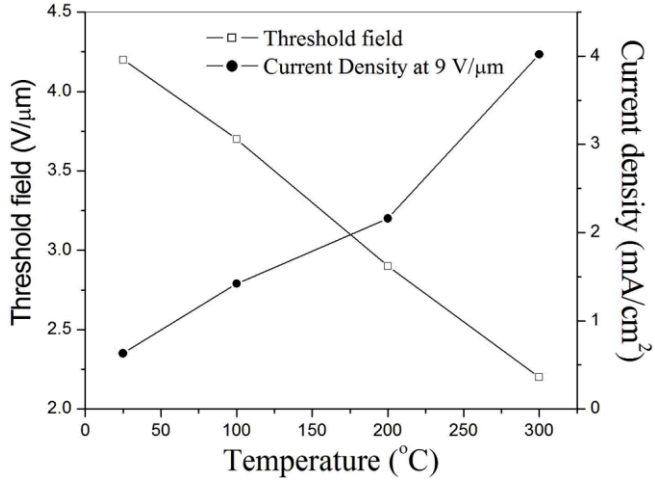

Figure 5.14. The variation of threshold field and emission current density with temperature for 15.3 at. % F doped DLC film [Ref. 93].

Copyright © 2012. Nova Science Publishers, Incorporated. All rights reserved.

Diamond-Like Carbon Films, Nova Science Publishers, Incorporated, 2012. ProQuest Ebook Central,

Using ϕ = 4.7 eV is the work function of F-DLC [84]; the field enhancement factor was calculated from the slope of the F-N plot, lies in the range 2784 to 7411 for the films with different ambient temperature. The field enhancement factor β increases monotonously with the temperature, which explains very well the increase in emission current density with measuring temperature (shown in Figure 5.14). A probable explanation for such a phenomenon is that the presence of a defect band raises the Fermi level toward the conduction band, and reduces the work function for enhancing field emission. Robertson et al [102] suggest that the width of the optical gap was dependent on the cluster size of sp^2 bonding. From defect bands within the band gap, electrons in the conduction band were significantly increased due to electrons transmitting from defect bands. As temperature increases, the sp^2 bonding, density of the defects, and the conductivity of the DLC film increase [103] so lower threshold field and higher current density at the same field (shown in Figure 5.14) obtained.

CONCLUSION

DLC is a metastable phase of a-C or a-C:H containing a significant fraction of sp^3 hybridization. In this article recent progress of DLC and metal and nonmetal DLC films are reviewed due to its tremendous importance in many applications. In spite of having tremendous potential for many applications DLC films possessed many difficulties like having large intrinsic stress and poor electrical conductivity etc. Recent progress in nonmetal and metal doped DLC nanocomposite films have shown that many of such limitations can be eliminated and new properties can be grafted in the DLC films.

REFERENCES

[1] J. Robertson, *Mater. Sci. Eng. R,* 37 (2002) 129.
[2] J. Robertson and E. P. Oreilly, *Phys. Rev. B,* 35 (1987) 2946.
[3] J. Robertson, *Phil. Mag. B,* 76 (1997) 335.
[4] W. Jacob and W. Moller, *Appl. Phys. Lett*., 63 (1993) 1771.
[5] D. R. Mckenzie, *Rep. Prog. Phys*., 59 (1996) 1611.
[6] P. Koidl, C. Wagner, B. Dischler, J. Wagner and M. Ramsteiner, *Mater. Sci. Forum*, 52 (1990) 41.
[7] M. Weiler, S. Sattel, K. Jung, H. Ehrhardt, V. S. Veerasamy and J. Robertson, *Appl. Phys. Lett*., 64 (1994) 2797.
[8] J. E. Field, Properties of Diamond, Academic Press, London, 1993.
[9] B. T. Kelly, Physics of Graphite, *Appl. Sci. Pub*., London, 1981.
[10] M. S. Dresselhaus, G. Dresselhaus and P. C. Eklund, Science of Fullerenes and Carbon Nanotubes, Academic Press, London, 1996.
[11] J. Robertson, *Adv. Phys*., 35 (1986) 317.
[12] G. M. Pharr, D. L. Callahan, S. D. Mcadams, T. Y. Tsui, S. Anders, A. Anders, I. G. Brown, C. S. Bhatia, S. R. P. Silva and J. Robertson, *Appl. Phys. Lett.*, 68 (1996) 779.

Copyright © 2012. Nova Science Publishers, Incorporated. All rights reserved.

Diamond-Like Carbon Films, Nova Science Publishers, Incorporated, 2012. ProQuest Ebook Central,

[13] P. J. Fallon, V. S. Veerasamy, C. A. Davis, J. Robertson, G. A. J. Amaratunga, W. I. Milne, and J. Koskinen, *Phys. Rev*. B, 48 (1993) 4777.
[14] P. C. K. Wagner, B. Dischler, J. Wagner and M. Ramsteiner, *Mater. Sci. Forum*, 52 (1990) 41.
[15] M. Weiler, S. Sattel, K. Jung, H. Ehrhardt, V. S. Veerasamy and J. Robertson, *Appl. Phys. Lett*., 64 (1994) 2797.
[16] M. F. Ashby and D. R. H. Jonesm, Eng. Mater. Pergamon Press, Oxford, 1980.
[17] S. Aisenberg and R. Chabot, *J. Appl. Phys*., 42 (1971) 2953.
[18] A. Ilie, N. M. J. Conway, B. Kleinsorge, J. Robertson and W. I. J. Milne, *Appl. Phys*., 10 (1998) 5575.
[19] H. Tsai and D. B. Bogy, *J. Vac. Sci. Technol*. A, 5 (1987) 3287.
[20] S. R. P. Silva and J. D. Carey, Amorphous Carbon Thin Films, Handbook of Thin Films, In: H. S. Nalwa (Eds.), Academic Press, New York, 2002.
[21] L. Y. Chen and F. C. Hong, *Appl. Phys. Lett*., 82 (2003) 3526.
[22] A. Lettington, P. Koidl and P. Oelhafen, Amorphous Hydrogenated Carbon Films, *Proc. Eur. Mater. Res. Soc. Symp*., Paris, 1987.
[23] D. S. Kim, T. E. Fischer and B. Gallois, *Surf. Coat. Technol*., 49 (1991) 531.
[24] S. Mitura, E. Mitura and A. Mitura, *Diam. Relat. Mater*., 302-303 (1995) 4.
[25] V. Elinson, V. V. Sleptsov, A. N. Laymin and A. D. Moussina, *Diam. Relat. Mater*., 8 (1999) 2103.
[26] T. Hasebe, Y. Matsuoka, H. Kodama, T. Saito, S. Yohena, A. Kamijo, N. Shiraga, M. Higuchi, S. Kuribayashi, K. Takahashi and T. Suzuki, *Diam. Relat. Mater.*, 15 (2006) 129.
[27] Z. Q. Ma and B. X. Liu, *Solar Energy Mater. Solar Cells*, 69 (2001) 339.
[28] A. C. Callegari, K. Babich, S. Purushothaman, S. Mansfield, R. Ferguson, A. Wong, W. Adair, D. Ogrady and V. Chao, *Microelectron. Eng.*, 107 (1998) 4142.
[29] S. R. P. Silva, J. D. Carey, X. Guo, W. M. Tsang and C. H. P. Poa, *Thin Solid Films*, 482 (2005) 79.
[30] S. Bhattacharya, K. Walzer, M. Hietschold, F. J. Richter, *Appl. Phys*., 89 (2001) 1184.
[31] H. Spicka, M. Griesser, H. Hutter, M. Grasserbauer, S. Bohr, R. Haubner and B. Lux, *Diam. Relat. Mater*., 5 (1996) 383.
[32] C. L. Tsai, C.F. Chen and C. L. Lin, *J. Appl. Phys*., 90 (2001) 4847.
[33] M. A. Alaluf and N. Croitoru, *Diam. Relat. Mater*., 6 (1997) 555.
[34] N. Biswas, H. R. Harris, X. Wang, G. Celebi, H. Temkin and S. Gangopadhyay, *J. Appl. Phys.*, 89 (2001) 4417.
[35] S. Kundoo, P. Saha and K. K. Chattopadhyay, *Mater. Lett*., 58 (2004) 3920.
[36] C. W. Chen and J. Robertson, *Mater. Res. Soc. Symp. Proc*., 498 (1998) 31.
[37] J. P. Sullivan, T. A. Friedmann, R. G. Dunn, P. A. Schultz, M. P. Siegal and N. Missert, *Mater. Res. Soc. Symp. Proc*., 498 (1998) 97.
[38] J. Robertson, *Prog. Solid State Chem*., 21 (1991) 317.
[39] A. Czyzniewski, *Thin Solid Films*, 433 (2003) 180.
[40] Rusli, S. F. Yoon, H. Yang, J. Ahn, Q. F. Huang, Q. Zhang, Y. P. Guo, C. Y. Yang, E. J. Teo, A. T. S. Wee and A. C. H. Huan, *Thin Solid Films*, 355-356 (1999) 174.
[41] A. Schuler, C. Ellenberger, P. Oelhafen, C. Haug and R. Brenn, *J. Appl. Phys.*, 87 (2000) 4285.
[42] Q. F. Huang, S. F. Yoon, Rusli, Q. Zhang and J. Ahn, *Thin Solid Films*, 409 (2002) 211.

Copyright © 2012. Nova Science Publishers, Incorporated. All rights reserved.

Diamond-Like Carbon Films, Nova Science Publishers, Incorporated, 2012. ProQuest Ebook Central,

[43] S. Kundoo, P. Saha and K. K. Chattopadhyay, *J. Vac. Sci. Technol. B*, 22(6) (2004) 2709.
[44] R. Gomer, Field Emission and Field Ionization, *American Ins. of Phys*., New York, 1993.
[45] R. H. Fowler and L. W. Nordheim, *Proc. R. Soc. London*, series A, 119 (1928) 173.
[46] E. L. Murphy and Jr. R. H. Good, *Phys. Rev*., 102 (1956) 1464.
[47] R. G. Forbes, *Ultramicroscopy*, 79 (1999)11.
[48] R. G. Forbes, Proceedings of 4th Moscow International ITEP School of Physics (Eds: A. L. Suvorov, Y. G. Abov, V. G. Firsov) Moscow, 2001.
[49] L. Nilsson, O. Groening, P. Groening, O. Kuettel and L. Schlapbach, *J. Appl. Phys*., 90 (2001) 768.
[50] R. Gao, Z. Pan and Z. L. Wang, *Appl. Phys. Lett*., 78 (2001) 1757.
[51] R. G. Forbes, C. J. Edgcombe and U. Valdre, *Ultramicroscopy*, 95 (2003) 57.
[52] M. W. Geis, J. C. Twichell, J. Macaulay and K. Okano, *Appl. Phys. Lett.*, 67 (1995) 1328.
[53] B. S. Satyanarayana, A. Hart, W. I. Milne and J. Robertson, *Appl. Phys. Lett.*, 71 (1997) 1430.
[54] A. Hart, B. S. Satyanarayana, J. Robertson and W. I. Milne, *Appl. Phys. Lett.*, 74 (1999) 1594.
[55] R. D. Forrest, A. P. Burden, S. R. P. Silva, L. K. Cheah and X. Shi, *Appl. Phys. Lett*., 73 (1998) 3784.
[56] J. C. Angus and A. T. Collins, *Nature*, 370 (1994) 601.
[57] F. J. Himpsel, J. S. Knapp, J. A. VanVechten and D. E. Eastman, *Phys. Rev*. B, 20 (1979) 624.
[58] C. Bandis and B. B. Pate, *Appl. Phys. Lett*., 69 (1996) 366.
[59] W. B. Choi, D. S. Chung, J. H. Kang, H. Y. Kim, Y. W. Jin, I. T. Han, Y. H. Lee, J. E. Jung, N. S. Lee, G. S. Park and J. M. Kim, *Appl. Phys. Lett.*, 75 (1999) 3129.
[60] J. E. Jaskie, *MRS Bull*., 21 (1996) 59.
[61] R. Wachter, S. Cordery and J. S. Foord, *Diam. Relat. Mater*., 7 (1998) 687.
[62] B. S. Satyanarayana, A. Hart, W. I. Milne and J. Robertson, *Appl. Phys. Lett*., 71 (1997) 1430.
[63] G. A. J. Amaratunga and S. R. P. Silva, *Appl. Phys. Lett.*, 68 (1996) 2529.
[64] A. A. Talin, L. S. Pan, K. F. McCarty, T. E. Felter, H. E. Doerr and R. F. Bunshah, *Appl. Phys. Lett.*, 69 (1996) 3842.
[65] T. Toyama, Y. Koide and M. Murakami, *Diam. Films Technol.*, 8 (1998) 407.
[66] Z. Y. Chen, J. P. Zhao, X. Wang, Y. H. Yu and T. S. Shi, *J. Phys. D: Appl. Phys.*, 33 (2000) 1018.
[67] J. J. Li, C. Z. Gu, H. Y. Peng, H. H. Wu, W. T. Zheng and Z. S. Jin, *Appl. Surf. Sci*., 251 (2005) 236.
[68] F. Y. Chuang, W. C. Wang, J. T. Lai, J. H. Tsai, C. M. Huang, C. M. Lin, M. Yokoyama, I. N. Lin, 10th Int. *Vacuum Microelectronics Conf. Tech. Dig.* (1997) 541.
[69] H. F. Cheng, F. Y. Chuang, C. H. Tsai, W. C. Wang, C. M. Huang and I. N. Lin, *Appl. Surf. Sci*., 142 (1999) 504.
[70] J. Robertson, *Thin solid Films*, 296 (1997) 61
[71] O. M. Kuttel, O. Groning, E. Schaller, L. Diederich, P. Groning and L. Schlapbach, *Diam. Relat. Matter*., 5 (1996) 807.

Copyright © 2012. Nova Science Publishers, Incorporated. All rights reserved.

Diamond-Like Carbon Films, Nova Science Publishers, Incorporated, 2012. ProQuest Ebook Central,

[72] J. Robertson and M. J. Rutter, *Diam. Relat. Mater*., 7 (1998) 620.
[73] F. Y. Chuang, F. Y. Sun, C. Y. Cheng, H. F. Wang, W. C. and I. N. Lin, *Appl. Surf. Sci.*, 113-114 (1997) 259.
[74] O. Groning, O. M. Kuttel, P. Groning and L. Schlapbach, *Appl. Surf. Sci*., 111 (1997) 135.
[75] S. F. Ahmed, Ph.D. Thesis (2008), Jadavpur University, Kolkata, India,
[76] S. F. Ahmed, M. K. Mitra and K. K. Chattopadhyay, *Appl. Surf. Sci*., 253 (2007) 5480.
[77] S. R. P. Silva and J. D. Carey, *Diam. Relat. Mater*., 12 (2003) 151.
[78] C. P. Lungu, *Surf. Coat. Technol*., 200 (2005) 198.
[79] H. W. Choi, J. H. Choi, K. R. Lee, J. P. Ahn and K. H. Oh, *Thin Solid Films*, 516 (2007) 248.
[80] S. F. Ahmed, M. W. Moon and K. R. Lee, *Thin Solid Films*, 517 (2009) 4035.
[81] S. F. Ahmed, M. W. Moon and K. R. Lee, *Appl. Phys. Lett*., 92 (2008) 193502.
[82] A. Y. Cao, X. F. Zhang, X. Xiao, M. Q. Ding, D. M. Zhuang, C. L. Xu, B. Q. Wei, J. Liang, and D. H. Wu, *Mater. Lett.*, 51 (2001) 37.
[83] O. M. Kuttel, O. Groning, C. Emmenegger, L. Nilsson, E. Maillard, L. Diederich and L. Schlapbach, Carbon, 37 (1999) 745.
[84] S. H. Lai, K. L. Chang, H. C. Shih, K. P. Huang and P. Lin, *Appl. Phys. Lett.*, 85 (2004) 6248.
[85] J. D. Carey, R. D. Forrest, R. U. A. Khan and S. R. P. Silva, *Appl. Phys. Lett.*, 77 (2000) 2006.
[86] P. S. Gao, Z. Sun, S. M. Huang and Y. Sun, *J. Appl. Phys.*, 98 (2005) 74906.
[87] J. D. Carey, R. D. Forrest and S. R. P. Silva, *Appl. Phys. Lett.*, 78 (2001) 2339.
[88] A. Ilie, A. C. Ferrari, T. Yagi and J. Robertson, *Appl. Phys. Lett.*, 76 (2000) 2627.
[89] S. F. Ahmed, D. Banerjee and K. K. Chattopadhyay, *Vacuum*, 84 (2010) 837.
[90] S. F. Ahmed, M. K. Mitra and K. K. Chattopadhyay, *J. of Nanosci. Nanotechnol.*, 9 (2009) 5545.
[91] C. Ronning, M. Buttner, U. Vetter, H. Feldermann, O. Wondratschek, H. Hofsass, W. Brunner, F. C. K. Au, Q. Li and S. T. Lee, *J. Appl. Phys.*, 90 (2001) 4237.
[92] G. Q. Yu, B. K. Tay, Z. Sun and L. K. Pan, *Appl. Surf. Sci.*, 219 (2003) 228.
[93] S. F. Ahmed, M. K. Mitra and K. K. Chattopadhyay, *J. of Phys. Conden. Matt.*, 19 (2007) 346233.
[94] X. T. Zhou, H. L. Lai, H. Y. Peng, F. C. K. Au, L. S. Liao, N. Wang, I. Bello, C. S. Lee and S. T. Lee, *Chem. Phys. Lett.*, 318 (2000) 58.
[95] S. F. Ahmed and K. K. Chattopadhyay, In: W. N. Chang (Eds.), "Nanofibers: Fabrication, Performance, and Applications", Nova Science Publishers, NY, USA, (2009) pp. 1-60.
[96] F. C. K. Au, K. W. Wong, Y. H. Tang, Y. F. Zhang, I. Bello and S. T. Lee, *Appl. Phys. Lett*., 75 (1999) 1700.
[97] K. Okano, S. Koizumi, S. R. P. Silva and G. A. J. Amartunga, *Nature*, 381 (1996) 140.
[98] W. Zhu, Vacuum Microelectronics, Wiley, New York, 2001.
[99] A. Modinos, Field, Thermionic and Secondary Electron Emission Spectroscopy, New York, 1984.
[100] C. M. Tan, J. Jia and W. Yu, *Appl. Phys. Lett.*, 86 (2005) 263104.
[101] M. C. Kan, J. L. Huang, J. C. Sung, K. H. Chen and B. S. Yau, *Carbon*, 41 (2003) 2839.

Copyright © 2012. Nova Science Publishers, Incorporated. All rights reserved.

Diamond-Like Carbon Films, Nova Science Publishers, Incorporated, 2012. ProQuest Ebook Central,

[102] J. Robertson and E. P. Oreilly, *Phys. Rev. B,* 35(6) (1987) 2946.
[103] P. S. Guo, Z. Sun, S. M. Huang and Y. Sun, *J. Appl. Phys.*, 98 (2005) 74906.

Copyright © 2012. Nova Science Publishers, Incorporated. All rights reserved.

Diamond-Like Carbon Films, Nova Science Publishers, Incorporated, 2012. ProQuest Ebook Central,

Copyright © 2012. Nova Science Publishers, Incorporated. All rights reserved.

Diamond-Like Carbon Films, Nova Science Publishers, Incorporated, 2012. ProQuest Ebook Central,

In: Diamond-Like Carbon Films
Editor: Yuto S. Tanaka
ISBN: 978-1-61324-791-4
© 2012 Nova Science Publishers, Inc.

Chapter 4

INTERNAL STRESS OF HYDROGENATED DIAMOND-LIKE CARBON FILMS

Masahito Ban
Nippon Institute of Technology, Miyashiro, Saitama, Japan

ABSTRACT

This paper reviews recent studies on an internal stress and its reduction of hydrogenated diamond-like carbon (DLC) thin films deposited by plasma CVD methods. Especially, focused on the DLC thin films prepared using CH_4 or C_6H_6 with varying deposition parameters by an electron-beam-excited plasma (EBEP) CVD system, the correlations between the internal stress and the structural properties such as the film density, total, bonded and unbound hydrogen contents, sp^3 ratio and graphite crystallite are discussed. As the result, it is found that the fraction of unbound hydrogen to total hydrogen content is the most influential factor for the compressive stress. The result implies that the insertion of unbound hydrogen, suggested to be into the disordered microstructure of graphite crystallites, can contribute to an increase in volume, and the strains by the expansion induce the compressive stress. Moreover, the internal stress reduction by incorporation of silicon into the DLC thin film is described. The Si-containing DLC thin films are deposited using CH_4 + SiH_4 by the EBEP-CVD system. From the relationships between the internal stress and the structural properties, it is found that Si-H bonds formed by silicon incorporation can play the role of reducing the compressive stress. It can be explained that the formation of Si-H bonds causes the relaxation of a three-dimensional rigid network of DLC thin film and the reduction in unbound hydrogen.

Copyright © 2012. Nova Science Publishers, Incorporated. All rights reserved.

Diamond-Like Carbon Films, Nova Science Publishers, Incorporated, 2012. ProQuest Ebook Central,

1. INTERNAL STRESS OF DIAMOND-LIKE CARBON (DLC) THIN FILM

1.1. Origin of the Internal Stress

So-called DLC thin film was produced by Aisenberg and Chabot in 1971 for the first time using an ion beam deposition technique [1], and now have been known for exhibiting a variety of the excellent properties such as high hardness, low friction, chemical inertness, biocompatibility, gas barrier property and wide optical transparency. The application fields of the DLC thin films have widely spread in recent two decades, and the uses in mass-produced mechanical lubricating components have become a leading objective. To rise the potential for use in mechanical components under severe conditions, however, the durability of DLC thin films must be further improved. That is, it is essential for the DLC thin films to perform the high toughness and high adhesion to steel-based materials, and to increase the film thickness. The principal cause of deteriorating the durability of the DLC thin films is their high compressive stress reported to reach values of several gigapascals [2,3]. Techniques to deposit the DLC thin films with low compressive stresses have been developed by means of containing additional elements, like nitrogen and silicon, into the film [4,5]. However, in spite of such successes in the deposition methods, little is known about the origins of compressive stress in DLC. In addition,

In the case of hydrogen-free amorphous carbon films, the compressive stress increases almost linearly with increasing the fraction of sp^3 bonded carbon [6,7]. The mechanism of generating the compressive stress can be explained by a subplantation model proposed by Robertson [8] and Davis [9], where medium-energy ions cause a quenched-in strain and density increment by directly entering into a interlayer region or displacing a surface atom into an interstitial site in the interlayer region. The increased stress and density result in the transformation of the stable sp^2 bonding into the metastable sp^3 bonding. On the other hand, an internal stress of (hydrogenated) DLC thin films must be discussed considering the effects of not only C-C bonds but also C-H bonds and unbound hydrogen in the films. Moreover, Raman spectra of DLC thin films predict the existence of graphite crystallites embedded into the network of carbon and hydrogen [10], which can be taken into consideration for discussing the internal stress. The previous studies have pointed out that DLC thin films with lower total hydrogen content and higher density were apt to indicate higher compressive stress and hardness [11,12]. While, Grill and Patel investigated the stress of DLC thin films deposited using various source gases and reported that the compressive stresses were directly correlated to the relative fraction of unbound hydrogen and increased with increasing the fraction of unbound hydrogen independently of the source gases [13]. In these previous studies, the internal stress and hardness were investigated for the correlations with few structural properties, and it is not clear how other structural properties can affect the internal stress.

Copyright © 2012. Nova Science Publishers, Incorporated. All rights reserved.

Diamond-Like Carbon Films, Nova Science Publishers, Incorporated, 2012. ProQuest Ebook Central,

1.2. Reduction in the Internal Stress

In general, DLC thin films containing additional elements exhibit markedly lower internal compressive stresses than conventional DLC thin films. Nitrogen is a well-studied element to reduce the compressive stress. Wood et al. reported a study of nitrogen-doped DLC thin films deposited by rf plasma decomposition of mixtures of a hydrocarbon vapor and N_2, in which both the compressive stress and the hardness were reduced by a similar factor with nitrogen addition [14]. Franceschini et al. reported that nitrogen-doped DLC thin films were deposited by rf glow discharge from CH_4 and N_2, and the compressive stress decreased with increasing the nitrogen content, while the hardness, structure and hydrogen concentration remained unchanged [15]. They explained that a reduction in average coordination number by nitrogen incorporation in the DLC thin films could be responsible for the stress reduction [15]. Moreover, it was reported that DLC thin films grown using C_2H_2 and N_2 by saddle-field fast atom beam source showed lower compressive stress per unit hardness compared to DLC thin films from only C_2H_2 [16].

It is well known that DLC thin films containing metals (e.g., W, Cr, Ti) indicate low internal stresses and high toughnesses, and have been recently used as alternatives to DLC thin films. It was reported that for W-containing DLC films prepared by dc magnetron sputtering the compressive stresses below 1 GPa were obtained [17]. Doping of Ti into DLC thin film was reported to indicate a drastic reduction in the compressive stress when deposited on steel substrate [18]. It is to be noted that metal-containing DLC thin films commonly show lower hardnesses compared with DLC thin films. Concerning the effects of silicon addition on the properties of DLC thin films, Vassell et al. indicated that the compressive stress largely decreased while the hardness was almost unchanged [19]. Meneve et al. reported that Si-containing DLC thin films prepared by RF plasma-assisted CVD using CH_4 and SiH_4 showed 30 % lower internal compressive stresses than DLC thin films [20]. In this manner, DLC thin films with low internal stresses were studied by means of additional elements incorporation. However, little is known about correlations between internal stress and structural properties of the DLC thin films containing additional elements.

2. INTERNAL STRESS OF DLC THIN FILMS DEPOSITED BY EBEP-CVD

2.1. EBEP-CVD System

Electron-beam-excited plasma (EBEP) is a high-density plasma efficiently generated by a high-current low-energy electron beam [21,22], and has been applied to the various processes such as dry etching [23], film deposition [24-29] and surface modification [30,31]. By setting the electron beam near the energy corresponding to the maximum electron collisional ionization cross-section of gas atoms, highly ionized and dissociated plasmas can be produced even at low pressures by the EBEP generation system. These plasmas have the following features. First, the electron energy and the electron current can be independently controlled with ease by changing the accelerating voltage and discharge current, respectively. Second,

Copyright © 2012. Nova Science Publishers, Incorporated. All rights reserved.

Diamond-Like Carbon Films, Nova Science Publishers, Incorporated, 2012. ProQuest Ebook Central,

since the substrate is not used to produce the plasma, the plasma parameters can be varied independently of the substrate bias voltage.

The plasma chemical vapor deposition using EBEP, named EBEP-CVD, is characteristic of the following features:

(1) high deposition rate due to high decomposition of gases,
(2) high crystallinity due to excellent controllability of plasma parameters, and
(3) ease of producing compound films, for example, nitrogen containing compounds.

To date the EBEP-CVD systems have been mainly applied for the depositions of DLC, microcrystalline silicon, carbon nitride and BCN films.

2.2. Correlation between Deposition Parameters and Film Properties [32]

The properties of DLC films prepared by the EBEP-CVD system were investigated with the intention of improving the durability of DLC thin film and using in protective coatings of mechanical lubricating components. In this section, for the DLC thin films deposited by EBEP-CVD system from CH_4 or C_6H_6 under the several deposition conditions, internal stress, dynamic hardness, and the structural properties such as the film density, total, bonded and unbound hydrogen contents, sp^3 ratio and graphite crystallite are described.

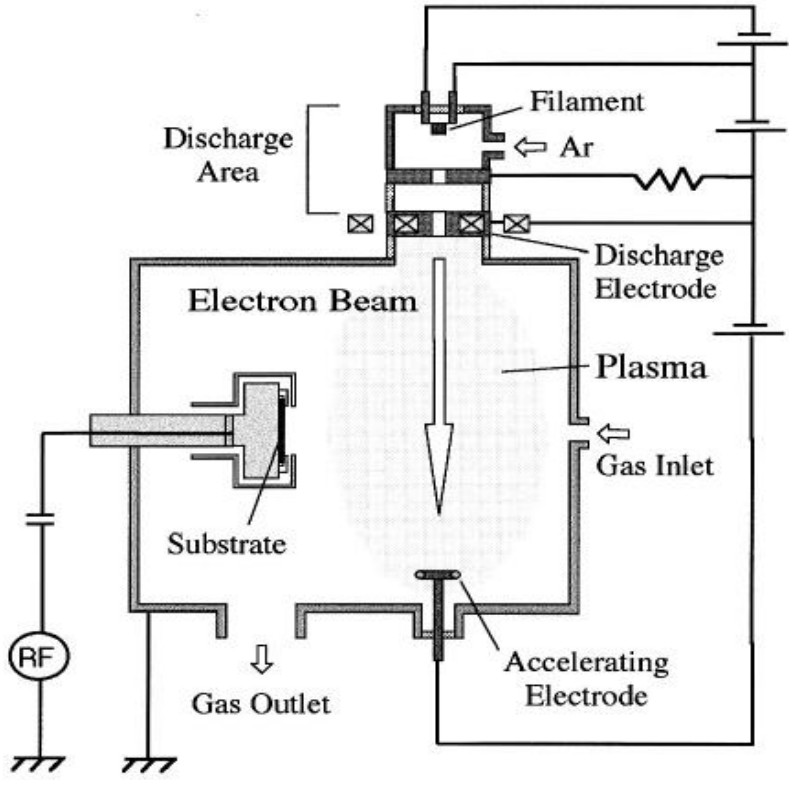

Figure 1. Schematic diagrams of the used electron-beam-excited plasma (EBEP) CVD systems.

Copyright © 2012. Nova Science Publishers, Incorporated. All rights reserved.

Diamond-Like Carbon Films, Nova Science Publishers, Incorporated, 2012. ProQuest Ebook Central,

Table 1. Deposition conditions

No.	Gas	Negative Bias Voltage (V)	Distance (mm)	Pressure (mTorr)
1	CH_4	0	395	6
2		150	395	6
3		200	395	6
4		300	395	6
5*		400	395	6
6		400	195	6
7		400	295	6
8		400	345	6
9*		400	395	6
10		400	395	4.5
11*		400	395	6
12		400	395	8
13		400	395	10
14	C_6H_6	150	295	4.5
15		300	295	4.5
16		400	295	4.5
17**		700	295	4.5
18		700	245	4.5
19**		700	295	4.5
20		700	345	4.5
21		700	395	4.5
22		700	295	3
23**		700	295	4.5
24		700	295	6
25		700	295	8

The symbol * or ** represents the same sample.

The DLC thin films were deposited by the EBEP-CVD system as shown in Figure 1[33]. A Si (100) substrate with 2 inch in diameter was fixed on the holder without water-cooling and placed parallel to the direction of an electron beam. A negative bias was applied to the substrate using a 2 MHz radio frequency generator. Table 1 summarizes the deposition conditions. CH_4 or C_6H_6 was used as the source gas. The negative bias voltage to the substrate, distance of the substrate from an electron beam and pressure during deposition were taken as the deposition parameters, and varied for each gas as shown in Table 1. The DLC thin films with the thicknesses of 0.3 to 0.8 μm were deposited on the substrates. The film thickness was determined from profilometric measurements of a step formed during deposition. Before deposition, the substrate was cleaned by accelerated ions in an argon plasma for 10 min.

The internal stresses of the films were calculated from the curvature of Si substrate and the DLC thin film thickness using the well-known Stoney's formula defined by

$$S = \delta Es\, ds^2 / 3\, r^2\, (1-\nu)\, df, \quad (1)$$

Copyright © 2012. Nova Science Publishers, Incorporated. All rights reserved.

Diamond-Like Carbon Films, Nova Science Publishers, Incorporated, 2012. ProQuest Ebook Central,

where S is the internal stress, δ the bending of the substrate, ν the Poisson's ratio of the substrate, r the radius of the substrate, Es the Young's modulus of the substrate, and ds and df the thicknesses of the substrate and the film, respectively. The values of 1.13×10^5 MPa and 0.42 were adopted for Es and ν, respectively [34]. The measured curvature of the substrate arises from both the intrinsic stress of DLC thin film and the stress generated by a mismatch in thermal expansion between the DLC and the substrate material. However, the thermal expansion coefficient of DLC was reported to be 2.3 ppm/℃, which was the same range as that of Si (100) substrate [35]. This can be confirmed from the experimental results that when the stresses of DLC thin films on Si substrates were measured at the range of room temperature to 200 ℃, little change in the measured stresses was observed [36,37]. Therefore, the stress by the difference in thermal expansion can be ignored, and the measured stresses are assumed to be the intrinsic stresses of DLC thin films.

Figure 2 shows the variations in the measured internal stresses as functions of (a) negative bias voltage, (b) distance from an electron beam and (c) pressure during deposition, respectively. The results are plotted for the DLC thin films deposited using CH_4 or C_6H_6. All films indicated the compressive stresses and the obtained values were in the same range as the previous studies [2-5,11].

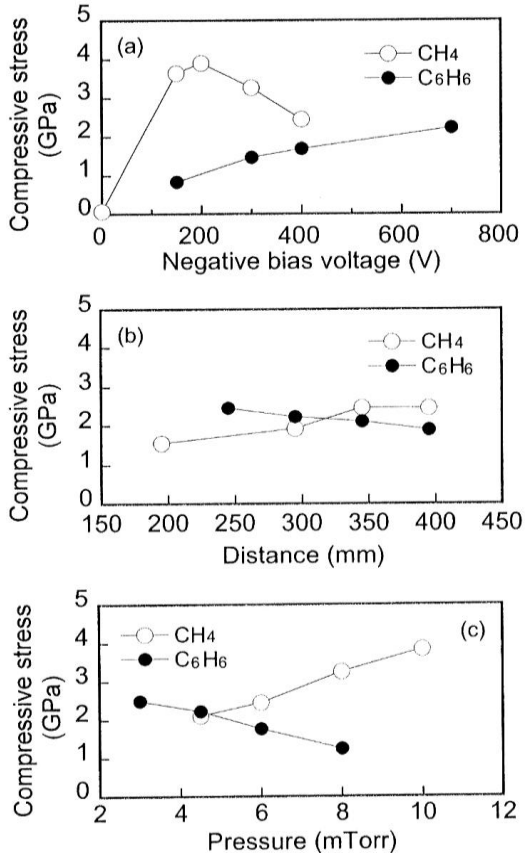

Figure 2. Variations in the compressive stress as functions of (a) negative bias voltage, (b) distance from an electron beam and (c) pressure during deposition. The open and solid circles represent the films from CH_4 and C_6H_6, respectively.

Copyright © 2012. Nova Science Publishers, Incorporated. All rights reserved.

Diamond-Like Carbon Films, Nova Science Publishers, Incorporated, 2012. ProQuest Ebook Central,

Regarding the DLC thin films from CH_4, the compressive stress had a peak value of 3.9 GPa at the negative bias voltage of 200 V (Figure 2 (a)), while it increased with both the distance (Figure 2 (b)) and the pressure (Figure 2 (c)). On the other hand, the DLC thin films from C_6H_6 showed a monotonous increase in compressive stress with increasing the negative bias voltage (Figure 2 (a)) and decreasing both the distance (Figure 2 (b)) and the pressure (Figure 2 (c)). In this matter, it is noticed that the dependences of compressive stress on deposition parameters differ strongly by the precursor. As an overall trend, using CH_4, the DLC thin films having lower compressive stress were obtained, when deposited under a higher degree of decomposition of the precursor in the plasma and on the substrate surface. In contrast, when C_6H_6 was used, the higher degree of decomposition of the precursor made the compressive stress higher. This seems to arise from the difference in the bonding structure of two precursors, that is, CH_4 molecule consists of sp^3 bonded carbon and hydrogen atoms while C_6H_6 molecule sp^2 bonded carbon and hydrogen atoms.

Dynamic hardness measurements were carried out using a nano indentation tester (Elionix ENT-1100) with a load of 40 mgf. Loading and unloading curves versus the depth of indentation were obtained. Five separate measurements were performed on different locations, and the results represent an average of these measurements.

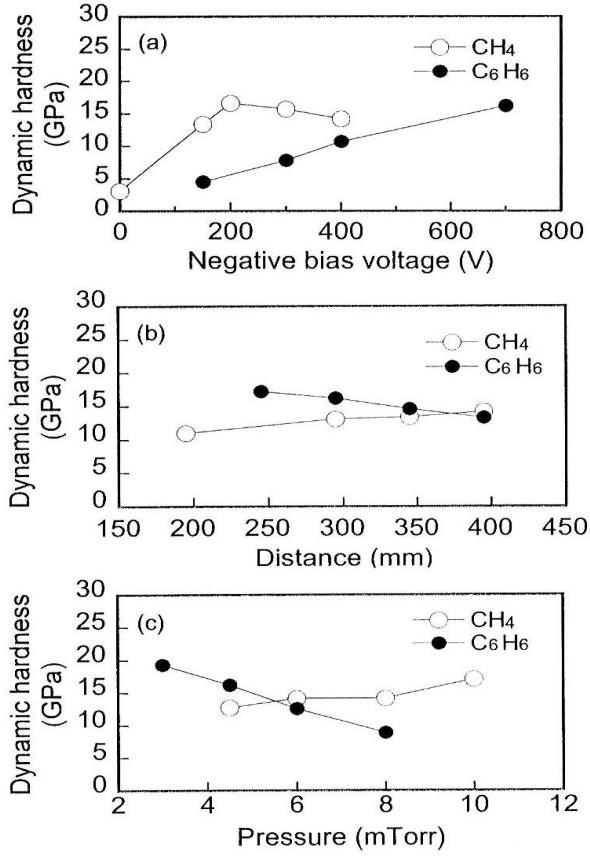

Figure 3. Variations in the dynamic hardness as functions of (a) negative bias voltage, (b) distance from an electron beam and (c) pressure during deposition. The open and solid circles represent the films from CH_4 and C_6H_6, respectively.

Copyright © 2012. Nova Science Publishers, Incorporated. All rights reserved.

Diamond-Like Carbon Films, Nova Science Publishers, Incorporated, 2012. ProQuest Ebook Central,

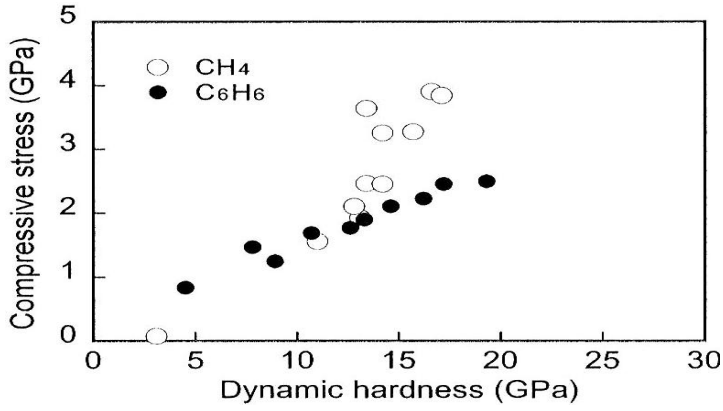

Figure 4. Correlations between dynamic hardness and compressive stress. The open and solid circles represent the films from CH_4 and C_6H_6, respectively.

Figures 3 (a)-(c) show the dynamic hardnesses of the DLC thin films from CH_4 or C_6H_6 as functions of the deposition parameters similar to Figures 2. Comparing Figures 3 with Figures 2, the variations of the dynamic hardness demonstrated the same tendency as those of the compressive stress. The correlations between dynamic hardness and compressive stress are shown in Figure 4 for the DLC thin films deposited from CH_4 or C_6H_6. It is observed from the figure that both of the compressive stresses increased linearly when the dynamic hardnesses increased, but each slope considerably differed by the source gas. This result implies that the deposited DLC thin films in the present work had the different microstructure in accordance with the difference in precursor.

Fourier transform infra red (FT-IR) analysis was carried out using a Perkin Elmer Spectrum GX system in the 400 to 4000 cm^{-1} range to investigate the chemical bonding and the hydrogen bonded to carbon atom. An average of 100 scans was taken for each sample. Raman spectroscopy was carried out using an argon ion laser with a wavelength of 514.5 nm in the 900 to 1800 cm^{-1} range. Hydrogen forward scattering spectrometry / elastic recoil detection (HFS / ERDA) was performed using a He^+ ion beam with an energy of 2.275 MeV to estimate the total hydrogen content in the DLC thin film and the film density. For the calculation of the DLC thin film density, the bulk densities of 1.12×10^{23} and 1.30×10^{23} atoms / cm^3 were used for carbon and hydrogen, respectively. By electron energy loss spectroscopy (EELS), the fraction of sp^3 bonded carbon in the DLC film was calculated from the 280 - 360 eV region of carbon K edge electron-energy-loss spectra for 4 samples of No. 2, 5, 14 and 17 shown in Table 1. The carbon K edge contains information on both the σ (sp^3) and the π (sp^2) bonding in the films. The EELS analysis was performed on a H-9000UHR (Hitachi) scanning transmission electron microscope with an EELS spectrometer (Gatan, PEELS Model 676).

The variations in the film density, total hydrogen content in film, $[H]_{total}$, content of hydrogen bonded to carbon atom, $[H]_{bond}$, sp^3 ratio in C-H bonds and I(D) / I(G) with the negative bias voltage, distance from an electron beam and pressure during deposition are shown in Figures 5 (a)-(e), Figures 6 (a)-(e) and Figures 7 (a)-(e), respectively. The film density and $[H]_{total}$ were the values obtained from HSF analysis. $[H]_{bond}$ was estimated from the total areas of the infrared absorption in C-H bonds centered at 2900 cm^{-1} in the FT-IR spectra using the following formula [11],

Copyright © 2012. Nova Science Publishers, Incorporated. All rights reserved.

Diamond-Like Carbon Films, Nova Science Publishers, Incorporated, 2012. ProQuest Ebook Central,

$$[H]_{bond} = A / ((1.68\times10^{5})\sigma + 0.916A), \quad (2)$$

where A is the area of the absorption band in square centimeter and σ is the film density in grams per cubic centimeter, which is the value obtained from the HFS analysis. The infrared absorption band at 2900 cm^{-1} corresponding to the C-H stretching vibration was also used to estimate the sp^3 ratio in C-H bonds. Deconvolution of the spectra was performed using the individual C-H vibrations, CH_2 sp^2 (olefinic) at 3020 cm^{-1}, CH sp^2 (olefinic) at 3000 cm^{-1}, CH_3 sp^3 (asymmetrical) at 2965 cm^{-1}, CH sp^3 at 2920 cm^{-1}, CH_2 sp^3 (asymmetrical) at 2920 cm^{-1}, CH_3 sp^3 (symmetrical) at 2870 cm^{-1} and CH_2 sp^3 (symmetrical) at 2850 cm^{-1} [11]. The areas of absorption coefficients were calculated for both C-H bonds with sp^3 carbon and C-H bonds with sp^2 carbon. The sp^3 ratio in C-H bonds was defined as the ratio of the areas of C-H bonds with sp^3 carbon to the total areas of C-H bonds. I(D)/I(G) means the intensity ratio of D-peak to G-peak in broad bands observed from 1200 to 1600 cm^{-1} in Raman spectra. It is well known that G-peak and D-peak correspond to spectra of sp^2 bonded carbon in graphite crystals and defect-induced disorders in the microcrystalline graphite, respectively.

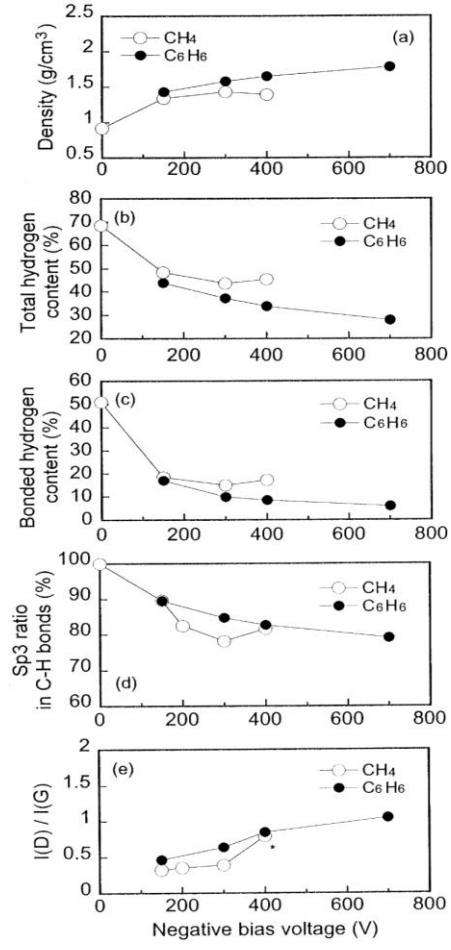

Figure 5. Variations in (a) film density, (b) $[H]_{total}$, (c) $[H]_{bond}$, (d) sp^3 ratio in C-H bonds and (e) I(D) / I(G) as a function of the negative bias voltage. The open and solid circles represent the films from CH_4 and C_6H_6, respectively. The sample * indicated relatively high value, but the cause has been unclear.

Copyright © 2012. Nova Science Publishers, Incorporated. All rights reserved.

Diamond-Like Carbon Films, Nova Science Publishers, Incorporated, 2012. ProQuest Ebook Central,

From Figures 5-7 (a), it is found that the film density was especially affected by both the negative bias voltage and the difference in source gas. The film deposited with the bias voltage of 0 V indicated the density of 0.9 g/cm^3 (Figure 5 (a)), while other films prepared under applying a negative bias voltage had the density of more than 1.3 g/cm^3. The increase in film density with applying a negative bias voltage can be explained from the replacement of hydrogen atoms and the condensation of carbon atoms due to ion bombardment. The films obtained from C_6H_6 had the density of 1.4 to 1.8 g/cm^3, which were larger than those from CH_4; 0.9 to 1.5 g/cm^3. Concerning $[H]_{total}$ and $[H]_{bond}$, as well as the film density, the negative bias voltage and the source gas were the most influential parameters as shown in Figures 5-7 (b) and Figures 5-7 (c). For the films from CH_4, increasing the negative bias voltage from 0 to 150 V, $[H]_{total}$ and $[H]_{bond}$ rapidly decreased from 69 % and 51 % to less than 50 % and 20 %, respectively. The films from C_6H_6 showed reductions by 36 % and 65 % in $[H]_{total}$ and $[H]_{bond}$ while the negative bias voltage increased from 150 V to 700 V. In the case of depositions with applying the negative bias voltage, the DLC thin films from CH_4 showed $[H]_{total}$ of 36 to 48 % and $[H]_{bond}$ of 15 to 20 %, and when C_6H_6 was used, $[H]_{total}$ and $[H]_{bond}$ were in the range of 25 to 40 % and 4 % to 18 %, respectively. A value subtracted bonded hydrogen content from total hydrogen content, $[H]_{total}$ - $[H]_{bond}$, means the content of unbound hydrogen, $[H]_{unbound}$, which is considered to be not directly bonded to carbon atom. This unbound hydrogen is not infrared active so that it can not be detected by FT-IR analysis. The comparisons between Figures 5-7 (b) and Figures 5-7 (c) imply that the deposited DLC thin films contained a large amount of the unbound hydrogen. The DLC thin films from CH_4 or C_6H_6 contained $[H]_{unbound}$ of 17 - 30 % or 21 - 27 %, respectively. These results are in agreement with the previous studies [13]. The film prepared from CH_4 with 0 V bias included a considerable amount of the total hydrogen, 68 %, and its majority was the bonded hydrogen.

It is seen in Figures 5-7 (d) that the obtained values of sp^3 ratio in C-H bonds were more than 70 %, and carbon atoms connected to hydrogen atoms in the films were mainly hybridized in sp^3 bonding. Comparing Figures 5-7 (d) with Figures 5-7 (c), the variations of sp^3 ratio in C-H bonds revealed similar tendencies to those of $[H]_{bond}$ as functions of the deposition parameters. That is, an increase in the sp^3 ratio in C-H bonds was accompanied with an increase in the content of hydrogen connected to carbon atom. The result can be explained that when an sp^2 bonded carbon is transformed into an sp^3 bonded carbon, the remained dangling bond is terminated with hydrogen atom. In the case of the film with the sp^3 ratio in C-H bonds of 100 % (Figure 5 (d)), it is considered that the majority of carbon atom is connected with hydrogen atom. Taking the value of density, 0.92 g/cm^3, into account, the film seems to have a structure near polyethylene. The values of sp^3 ratio obtained from FT-IR analysis do not include any useful information of carbon without protonation. On the other hand, EELS analysis can provide some information of not only carbon with protonation but also carbon without protonation. From EELS, the sp^3 ratio of 67 %, 71 %, 61 % and 54 % were obtained for No. 2, 5, 14 and 17 as shown in Table 1, respectively, and those were less than the values obtained from FT-IR analysis. Therefore, it can be noticed that the sp^3 ratio of carbon without protonation is much smaller than that of carbon with protonation (sp^3 ratio in C-H bonds), which implies that a large number of sp^2 bonded carbon sites exist in the DLC film. Robertson proposed the cluster model and its modification, and predicted that sp^2 sites form clusters embedded in an sp^3 bonded matrix and the sp^2 clusters are limited to single sixfold rings and short chains of sp^2 sites [37,38].

Copyright © 2012. Nova Science Publishers, Incorporated. All rights reserved.

Diamond-Like Carbon Films, Nova Science Publishers, Incorporated, 2012. ProQuest Ebook Central,

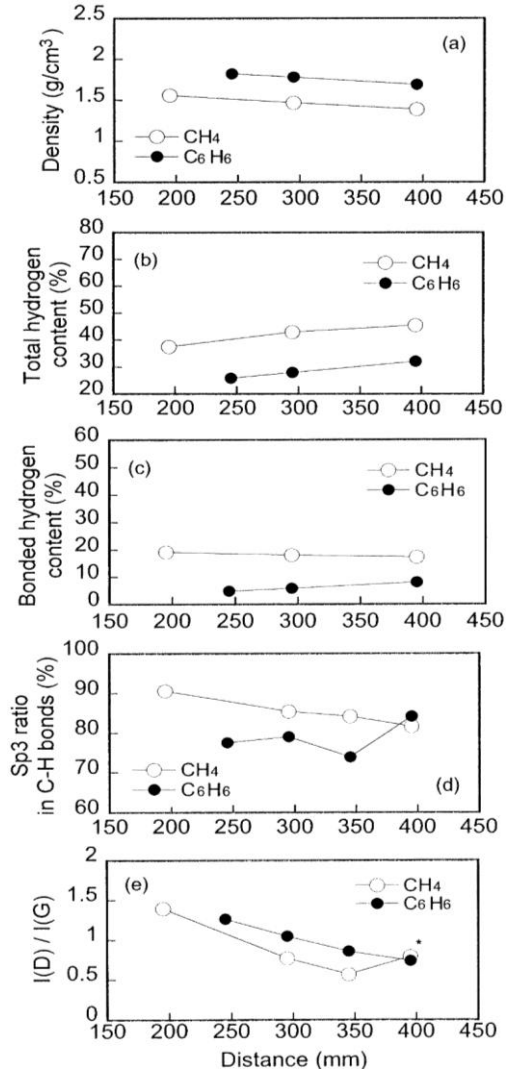

Figure 6. Variations in (a) film density, (b) $[H]_{total}$, (c) $[H]_{bond}$, (d) sp^3 ratio in C-H bonds and (e) I(D) / I(G) as a function of the distance from an electron beam. The open and solid circles represent the films from CH_4 and C_6H_6, respectively. The sample * indicated relatively high value, but the cause has been unclear.

The presence of sp^2 clusters may be supported by the observation of D-peak corresponding to spectra of disordered microcrystalline graphite. Tuinstra and Koenig reported that I(D)/I(G) calculated from Raman spectra was inversely proportional to the size of graphite crystallite [39]. Figures 5-7 (e) show that the DLC thin films from CH_4 and C_6H_6 had almost the same range of I(D) / I(G) and the similar tendency as functions of the investigated deposition parameters. Namely, the size of graphite crystallites decreased with increasing the negative bias voltage, and decreasing the distance from an electron beam. These trends imply that graphite crystallites become finer, when ions with higher energy are bombarded at the surface of growing film, and also a film is deposited under a higher degree of gas decomposition.

Copyright © 2012. Nova Science Publishers, Incorporated. All rights reserved.

Diamond-Like Carbon Films, Nova Science Publishers, Incorporated, 2012. ProQuest Ebook Central,

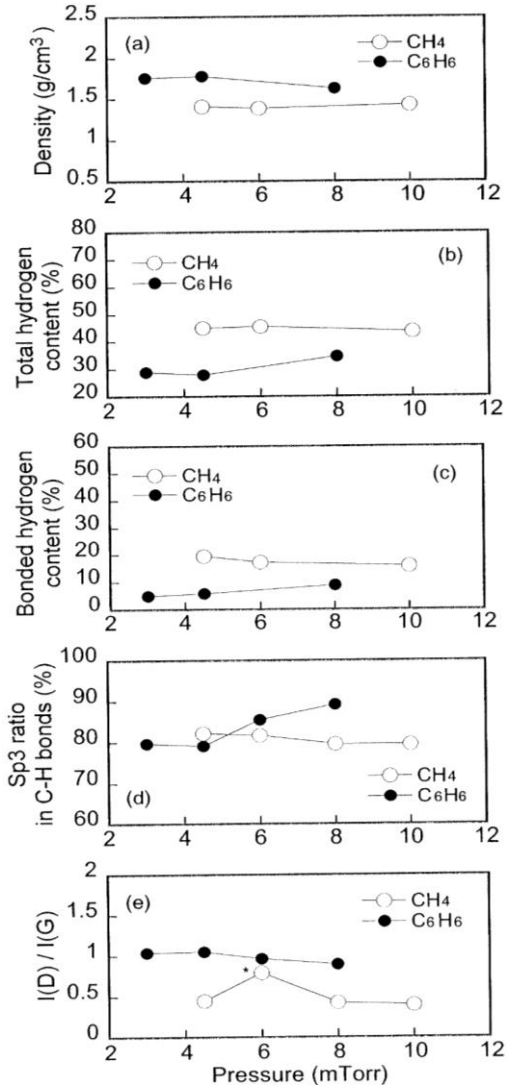

Figure 7. Variations in (a) film density, (b) $[H]_{total}$, (c) $[H]_{bond}$, (d) sp^3 ratio in C-H bonds and (e) I(D) / I(G) as a function of the pressure during deposition. The open and solid circles represent the films from CH_4 and C_6H_6, respectively. The sample * indicated relatively high value, but the cause has been unclear.

The ratios of sp^3 to sp^2 bonded carbon, sp^3/sp^2, obtained from EELS analysis are plotted as a function of $[H]_{total}$ for the samples of No. 2, 5, 14 and 17, as given in Figure 8. The solid line in the figure presents the following equation,

$$sp^3/sp^2 = (6[H]_{total} - 1) / (8 - 13[H]_{total}), \quad (3)$$

and represents the ideal relationship between sp^3/sp^2 and hydrogen content predicted by the fully constrained network (FCN) model proposed by Angus and Jansen [40]. It was reported that this equation was obtained based on the theories of random covalent networks, assuming that DLC had a completely constrained random amorphous network. It is notable from Figure

Copyright © 2012. Nova Science Publishers, Incorporated. All rights reserved.

Diamond-Like Carbon Films, Nova Science Publishers, Incorporated, 2012. ProQuest Ebook Central,

8 that the values of sp^3/sp^2 obtained from the films were higher than those predicted by the theory.

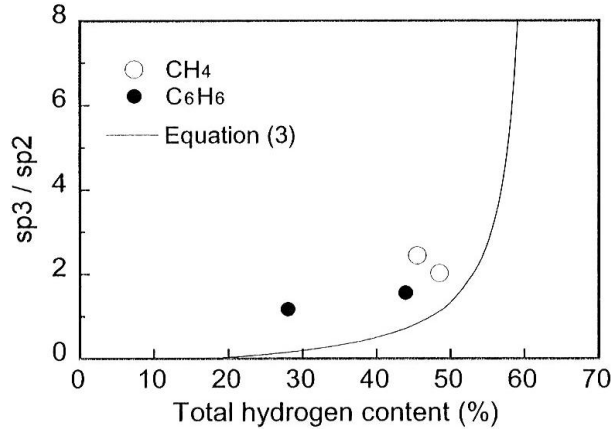

Figure 8. Variations in the sp^3 / sp^2 ratio as a function of the total hydrogen content. The line is Eq. (3).

This means that the DLC thin films in the present work have the overconstrained structure, which can be commonly characterized in most DLC thin films reported [41,42]. It is explained in the paper [40] that one of the reasons why the random covalent network of DLC is overconstrained is that the medium range order such as graphite crystallites is formed in the network. As mentioned above, the idea is considered to be consistent with the results obtained from our DLC thin films, and will be adopted for the following discussion.

2.3. Correlations between Internal Stresses and Structural Properties [32]

In this section, the origins of internal stress generated in the DLC thin films deposited by the EBEP-CVD system are discussed based on the correlations between internal stress and structural properties. All data shown in Table 1 are used for the following discussion to investigate the correlations between internal stresses and structural properties.

Figure 9 shows the variations in compressive stresses as a function of the film density. It is observed that the compressive stress of DLC thin films from C_6H_6 increased linearly from 0.8 to 2.5 GPa for the increase in the film density from 1.4 to 1.8 g/cm^3. On the other hand, the DLC thin films from CH_4 had almost the same range of density, but demonstrated a wide range of compressive stresses from 1.6 to 3.9 GPa (not mentioned for the film with the density of 0.9 g/cm^3 because of not having the structure of DLC). Figure 10 shows the variations in compressive stresses as a function of $[H]_{total}$. As described above, an increase in $[H]_{total}$ was accompanied by a decrease in the film density. Accordingly, the compressive stress of DLC thin films from C_6H_6 decreased monotonously with increasing $[H]_{total}$, while concerning the DLC thin films from CH_4, the compressive stress was independent of $[H]_{total}$. From Figure 9 and Figure 10, it is found that for the DLC thin films deposited using C_6H_6, the films with higher density and lower total hydrogen content had higher compressive stress (and hardness, see Figure 3), which is consistent with the results reported in the previous studies [11,12]. However, in regard to the DLC thin films from CH_4, the compressive stress

Copyright © 2012. Nova Science Publishers, Incorporated. All rights reserved.

Diamond-Like Carbon Films, Nova Science Publishers, Incorporated, 2012. ProQuest Ebook Central,

varied largely in spite of little variations of both the film density and total hydrogen content, and it seems to be attributed to other structural properties.

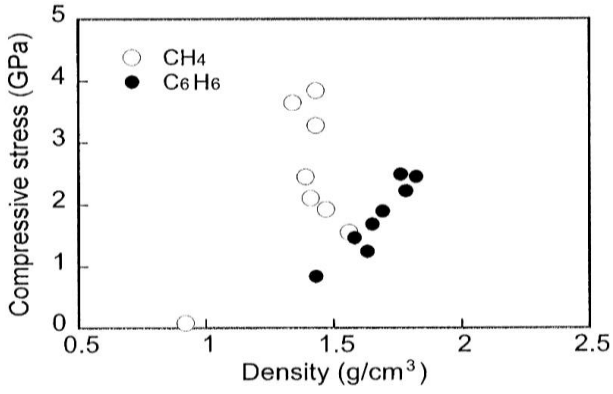

Figure 9. Variations in the compressive stress as a function of the film density. The open and solid circles represent the films from CH_4 and C_6H_6, respectively.

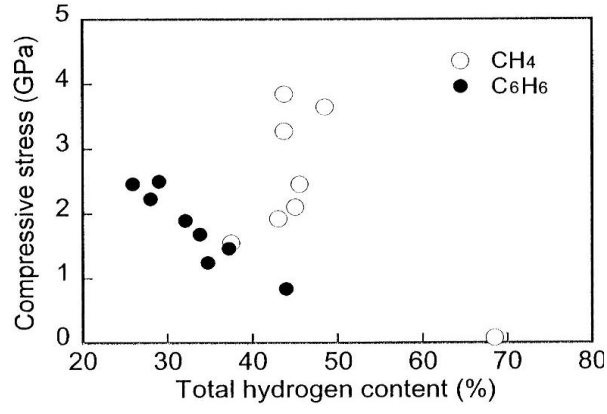

Figure 10. Variations in the compressive stress as a function of the total hydrogen content. The open and solid circles represent the films from CH_4 and C_6H_6, respectively.

The compressive stresses are plotted as a function of the fraction of $[H]_{unbound}$ to $[H]_{total}$ in Figure 11. The figure shows the obvious relationship and the compressive stresses increased almost linearly with increasing the fraction of $[H]_{unbound}$ to $[H]_{total}$ for the DLC thin films from CH_4 or C_6H_6. Gllil and Patel reported that the values of compressive stress were 0.84 and 1.4 GPa in the case of the fractions of unbound hydrogen of 0.44 and 0.58 for DLC thin films deposited from CH_4, respectively [13], which is in good agreement with our results. Also, the paper [13] described that the compressive stresses of DLC thin films prepared from various precursors such as CH_4, C_2H_2, C_6H_{12} and C_6H_{12}+H_2 increased almost linearly as a function of the fraction of unbound hydrogen. However, the results in the present work displayed that the absolute values of compressive stress at the same fraction of $[H]_{unbound}$ to $[H]_{total}$ indicated the discrepancies by the difference in precursor. Hence, it means that a fraction of $[H]_{unbound}$ to $[H]_{total}$ is not the only factor to determine the internal stress of any DLC thin films deposited from several precursors.

Copyright © 2012. Nova Science Publishers, Incorporated. All rights reserved.

Diamond-Like Carbon Films, Nova Science Publishers, Incorporated, 2012. ProQuest Ebook Central,

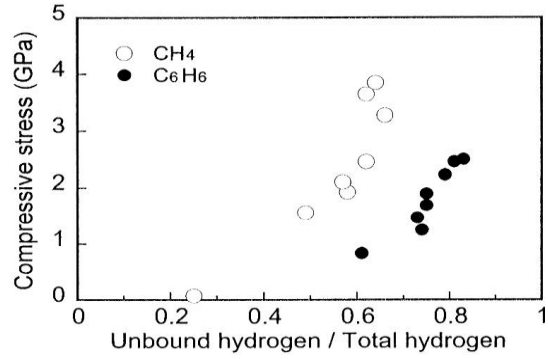

Figure 11. Variations in the compressive stress as a function of the fraction of unbound hydrogen content to total hydrogen content. The open and solid circles represent the films from CH_4 and C_6H_6, respectively.

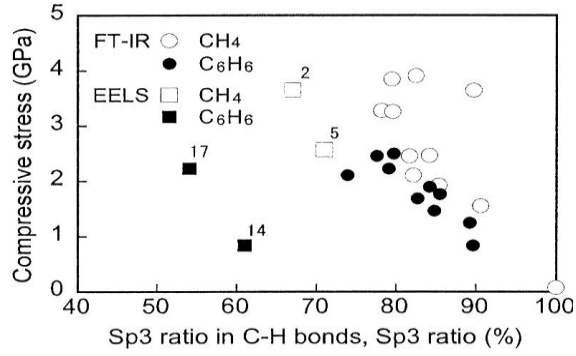

Figure 12. Variations in the compressive stress as functions of the sp^3 ratio in C-H bonds by FT-IR and the sp^3 ratio by EELS. The open and solid circles represent the films from CH_4 and C_6H_6, respectively. The numbers represent the sample Nos. shown in Table 1.

The compressive stresses in the films prepared from CH_4 or C_6H_6 are presented in Figure 12 as a function of the sp^3 ratio in C-H bonds obtained from FT-IR. In addition, the results are plotted as a function of the sp^3 ratio obtained from EELS in this figure. The numbers in the figure represent the sample No. shown in Table 1. As can be seen in Figure 12, the compressive stresses were apt to decrease with increasing the sp^3 ratio in C-H bonds. The present tendency is contrary to that for hydrogen-free amorphous carbon, where the compressive stress increased with increasing the sp^3 ratio [6,7]. This fact is related to the existence of C-H bonds. That is, for the DLC thin films (hydrogenated amorphous carbon films), an increase in the sp^3 ratio in C-H bonds was accompanied with an increase in hydrogen atom connected to carbon atom (see Figures 5-7 (c) and (d)), and it is considered that the network in film is segmented by the termination with hydrogen atoms so that the compressive stress is released. This can be supported by FCN model. On the other hand, a hydrogen-free amorphous carbon film has a more rigid structure by forming a larger number of C-C single bonds than C-C double bonds. It should be noticed that in the case of the films from CH_4, the scatter was considerably large and for example, the obtained compressive stresses were in the range from 2 to 4 GPa at the sp^3 ratio in C-H bonds of about 80 %. Therefore, it can not be considered that the sp^3 ratio in C-H bonds has a direct effect on the compressive stress of the films from CH_4. From the results of EELS, it is difficult to estimate

Copyright © 2012. Nova Science Publishers, Incorporated. All rights reserved.

Diamond-Like Carbon Films, Nova Science Publishers, Incorporated, 2012. ProQuest Ebook Central,

the trend of compressive stress in case the films deposited from each source gas are separately evaluated. However, observing the trend using all samples, it is found that the films from CH_4 indicated the higher compressive stress with the higher sp^3 ratio than those from C_6H_6. Considering that the sp^3 ratio by EELS includes information of carbon without protonation, the trend may show that C-C single bonds give some contribution to the compressive stress, as reported for a hydrogen-free amorphous carbon film.

Figure 13 displays the correlations of the compressive stresses with I(D)/I(G) calculated by Raman analysis. It is observed from the figure that the compressive stress decreased for the DLC thin films from CH_4 and increased for the DLC thin films from C_6H_6 as I(D)/I(G) increased. Taking into consideration that I(D)/I(G) is inversely proportional to the size of graphite crystallite in the network of film, when CH_4 was used for the deposition of DLC thin films, the films including the larger graphite crystallites showed higher compressive stresses. On the contrary, in the case of the DLC thin films deposited from C_6H_6, when the finer graphite crystallites were included, the compressive stresses were higher. The previous studies have suggested both cases that the compressive stress (or hardness) decreased or increased with increasing I(D)/I(G) [10,43]. Figure 14 shows the variations of the fraction of $[H]_{unbound}$ to $[H]_{total}$ as a function of I(D)/I(G). From the figure, as for the films from CH_4, the fraction of $[H]_{unbound}$ to $[H]_{total}$ increased with decreasing I(D)/I(G). In other words, an increase in the size of graphite crystallites was accompanied with an increase in the fraction of unbound hydrogen content, which means the compressive stress increment as already mentioned in Figure 11. In the case of the DLC films from C_6H_6, it can be explained in the same fashion as the films from CH_4 that the compressive stress increased with the fraction of $[H]_{unbound}$ to $[H]_{total}$ (see both Figure 13 and Figure 14 or Figure 11), but it is notable from Figure 14 that the fraction of $[H]_{unbound}$ to $[H]_{total}$ decreased with decreasing I(D)/I(G), that is, increasing the size of graphite crystallites. This indicates that an increase in the size of graphite crystallites coincides with an increase in the fraction of bonded hydrogen content. That is to say, it is suggested that when the size of graphite crystallites increases, the termination with hydrogen may proceed in the boundaries of graphite crystallites and the bonding between graphite crystallites and surrounding networks reduces. The presence of disconnected graphite crystallites results in a decrease in the compressive stress. When the segmentation of network occurs, the unbound hydrogen can give little effect on an increase in compressive stress.

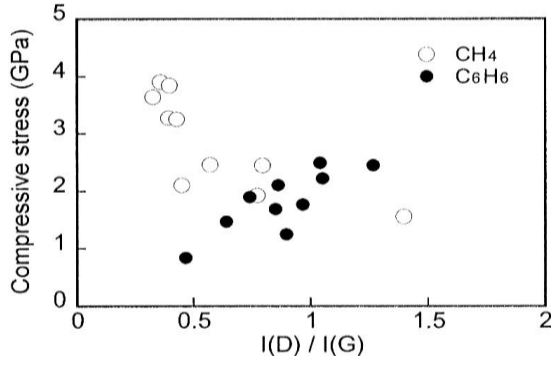

Figure 13. Variations in the compressive stress as a function of I(D) / I(G). The open and solid circles represent the films from CH_4 and C_6H_6, respectively.

Copyright © 2012. Nova Science Publishers, Incorporated. All rights reserved.

Diamond-Like Carbon Films, Nova Science Publishers, Incorporated, 2012. ProQuest Ebook Central,

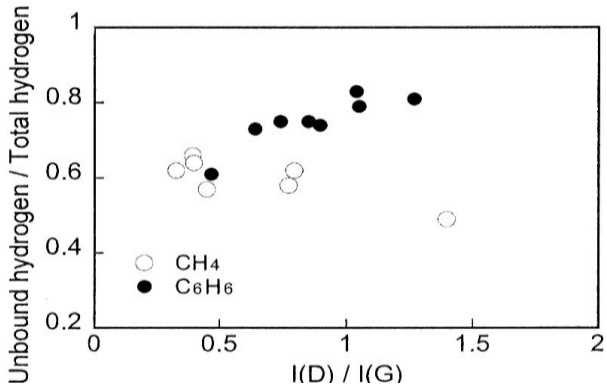

Figure 14. Variations in the fraction of unbound hydrogen content to total hydrogen content as a function of I(D) / I(G). The open and solid circles represent the films from CH_4 and C_6H_6, respectively.

Finally, we will discuss where and how the unbound hydrogen exists in the DLC thin film. From I(D)/I(G) values, the effective sizes of graphite crystallite, L_a (Å), can be estimated using the equation,

$$I(D)/I(G) = 44 / L_a, \quad (4)$$

Obtained from the experimental results of Tuinstra and Koenig [39]. L_a was found to be in the range of 30 to 140 Å for the present DLC thin films. These L_a values are much larger than the cluster size predicted by the modified cluster model [38]. This may be comprehended that the internal microstructure of effective cluster is in disorder and the minimum size of sp^2 sites is much smaller than L_a. The presence of a broad D-peak in the Raman spectra of DLC films can support the existence of disordered microstructure in graphite crystallites. Here, the unbound hydrogen contents are plotted as a function of I(D)/I(G) in Figure 15. The figure obviously shows that an increase in the unbound hydrogen content was directly correlated with an increase in the size of graphite crystallites independently of the investigated precursor. These facts imply that the location where the unbound hydrogen is incorporated is related to the disordered microstructure in graphite crystallites. Moreover, in Figure 8, if the sp^3/sp^2 values are plotted using not the total hydrogen content including the unbound and bonded hydrogen content but the bonded hydrogen content, the experimental and theoretical values display larger discrepancies. This might indicate that the unbound hydrogen is not completely independent of a skeleton formed in the DLC thin film. It follows from the above discussion that the unbound hydrogen may be trapped into the disordered microstructure of graphite crystallites, and "chemisorbed" to carbon (not enough to absorb infra-red light) rather than "perfectly unbound". To make sure of the location and the condition of unbound hydrogen, the further studies such as the direct measurements of unbound hydrogen need to be carried out.

Summing up the correlations between compressive stress and structural properties from the above discussions, the following can be derived. First, as for the DLC thin films deposited from CH_4, the fraction of unbound hydrogen to total hydrogen content was the most influential factor for the compressive stress. The film density and total hydrogen content had little effect on the compressive stress. The DLC thin films including a larger size of graphite

Copyright © 2012. Nova Science Publishers, Incorporated. All rights reserved.

Diamond-Like Carbon Films, Nova Science Publishers, Incorporated, 2012. ProQuest Ebook Central,

crystallites, involving a decrease in the sp^3 ratio in C-H bonds, demonstrated higher compressive stresses. It is highly probable that the unbound hydrogen is trapped into the disordered microstructure of graphite crystallites, and the insertion of unbound hydrogen can contribute to an increase in volume and the strains by the expansion induce a compressive stress. Second, concerning the DLC thin films deposited from C_6H_6, the several factors were correlated with the compressive stress. As well as the DLC thin films deposited from CH_4, the insertion of unbound hydrogen is suggested to give a contribution to the compressive stress.

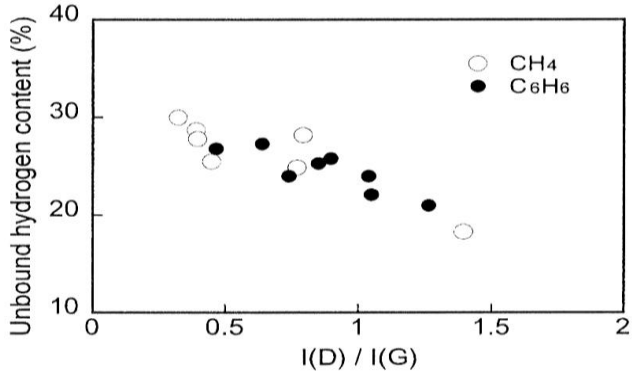

Figure 15. Variations in the unbound hydrogen content, $[H]_{unbound}$, as a function of I(D) / I(G). The open and solid circles represent the films from CH_4 and C_6H_6, respectively.

Moreover, it is found that the compressive stress increased with increasing the film density, and decreasing the total and bonded hydrogen contents, accompanied with a decrease in the size of graphite crystallites and sp^3 ratio in C-H bonds. This means that the compressive stress increment arises from the promotion of cross-linking between graphite crystallites embedded into the three-dimensional network. Namely, it is considered that the change of sp^2 sites into sp^3 C-C bonds by the cross-linking induces the expansion in film in accordance with an increase in bond length, which results in an increase in the compressive stress.

2.4. Internal Stress Reduction by Silicon Incorporation [44]

In section 2.2 and 2.3, the internal stresses of DLC thin films deposited by the EBEP-CVD system are discussed based on their correlations with the structural properties, and it is mentioned that the DLC thin films with the higher fraction of unbound hydrogen to total hydrogen content showed higher compressive stresses (and dynamic hardnesses). In this section, for the Si-containing DLC thin films deposited by the EBEP-CVD system using CH_4 and SiH_4, the internal stress, dynamic hardness and structural properties are investigated, and the correlations between the internal stress and the structural properties are discussed.

The depositions of DLC and Si-containing DLC thin films were performed using the EBEP-CVD system shown in Figure 1. The procedure to generate the EBEP is described in section 2.2. The substrate Si (100) was fixed on the holder without water-cooling and placed parallel to the direction of an electron beam. The distance between the substrate and the electron beam was 395 mm. A negative bias of 400 V was induced to the substrate by a 2 MHz radio frequency generator. CH_4 and CH_4 + SiH_4 were used for depositing DLC thin

Copyright © 2012. Nova Science Publishers, Incorporated. All rights reserved.

Diamond-Like Carbon Films, Nova Science Publishers, Incorporated, 2012. ProQuest Ebook Central,

films and Si-containing DLC thin films as the source gases, respectively. SiH_4 flow ratio, that is, the SiH_4 flow rate / (SiH_4 flow rate + CH_4 flow rate) was varied from 0 to 36.4 % as a deposition parameter. The pressure during deposition was controlled at 6 mTorr. Before deposition, the substrate was cleaned by an argon plasma for 10 min. The film thickness was determined from profilometric measurements of a step formed during deposition and was 440 to 1000 nm.

Internal stress was calculated by the Stoney's formula (see Eq. 1) using the curvature of Si substrate and the film thickness. The variation in the internal stress as a function of the SiH_4 flow ratio is shown in Figure 16. All deposited films indicated the compressive stresses. This figure clearly demonstrates a compressive stress reduction from 2.5 to 1.0 GPa when the SiH_4 flow ratio during deposition is varied from 0 to 36.4 %. For the Si-containing DLC thin films deposited by the EBEP-CVD system, the effect of silicon incorporation on the reduction in compressive stress was confirmed as well as the previous studies [19,20].

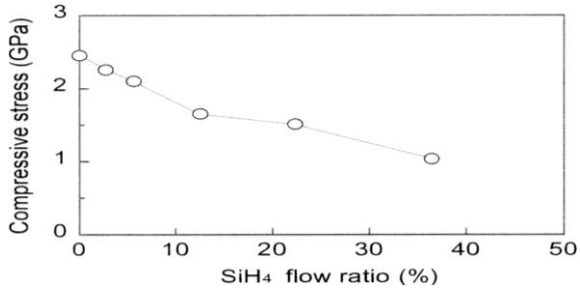

Figure 16. Variation in the compressive stress as a function of the SiH_4 flow ratio.

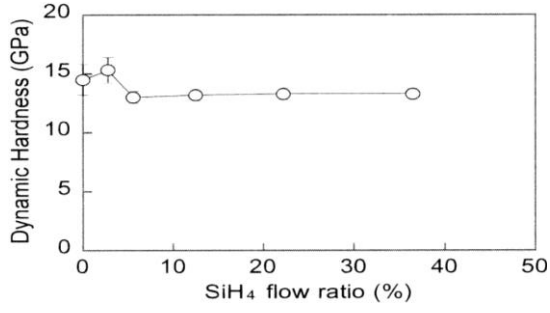

Figure 17. Variation in the dynamic hardness as a function of the SiH_4 flow ratio.

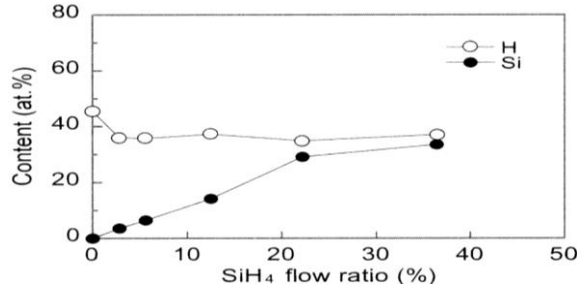

Figure 18. Variations in the silicon and hydrogen contents as a function of the SiH_4 flow ratio.

Copyright © 2012. Nova Science Publishers, Incorporated. All rights reserved.

Diamond-Like Carbon Films, Nova Science Publishers, Incorporated, 2012. ProQuest Ebook Central,

Dynamic hardness measurements were carried out using a nano indentation tester (Elionix ENT-1100) with a load of 40 mgf. Five separate measurements were performed on different locations, and the results represent an average of these measurements with the standard deviations. Figure 17 shows the variation in the dynamic hardness as a function of the SiH_4 flow ratio. The dynamic hardness indicated nearly constant behavior with a variation from 13 to 15 GPa in the investigated range. That is, the Si-containing DLC thin films were found to indicate a trend that the compressive stress decreased while the dynamic hardness was maintained. This trend is different from the DLC thin films showing that a decrease in compressive stress is accompanied by a decrease in dynamic hardness (See Figure 3). As mentioned above, the nitrogen-containing DLC thin films were reported to show the similar properties to the Si-containing DLC thin films in the present work [4].

Hydrogen forward scattering spectrometry / elastic recoil detection (HFS / ERDA) was performed using a He^+ ion beam with an energy of 2.275 MeV to estimate silicon and hydrogen contents in the deposited films. Figure 18 shows the variations of silicon and hydrogen contents obtained by the HFS analysis as a function of the SiH_4 flow ratio. The silicon content increased almost linearly with increasing the SiH_4 flow ratio, and the Si-containing DLC thin films deposited at the SiH_4 flow ratio of 36.4 % indicated a silicon-to-carbon ratio of about 1. The hydrogen content was measured at 46 at.% for the DLC thin film (SiH_4 flow ratio: 0 %), and rapidly reduced to 36 at.% with silicon addition. When the SiH_4 flow ratio was varied from 2.8 to 36.4 %, the hydrogen content remained constant (35 to 37 at.%) even if the silicon content ranged from 3 to 32 at.%, suggesting that carbon was replaced by silicon.

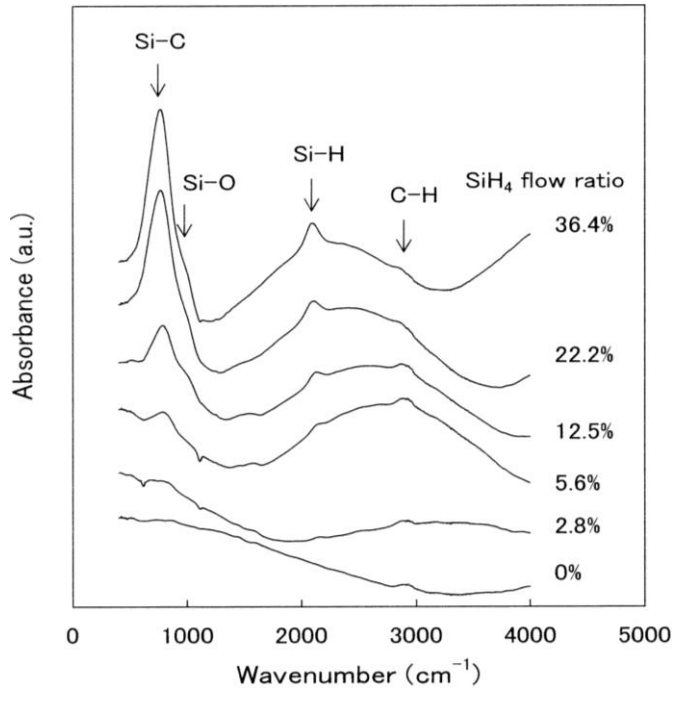

Figure 19. FT-IR spectra in the range 400 to 4000 cm^{-1} for the films deposited at the SiH_4 flow ratio of 0 to 36.4 %.

Copyright © 2012. Nova Science Publishers, Incorporated. All rights reserved.

Diamond-Like Carbon Films, Nova Science Publishers, Incorporated, 2012. ProQuest Ebook Central,

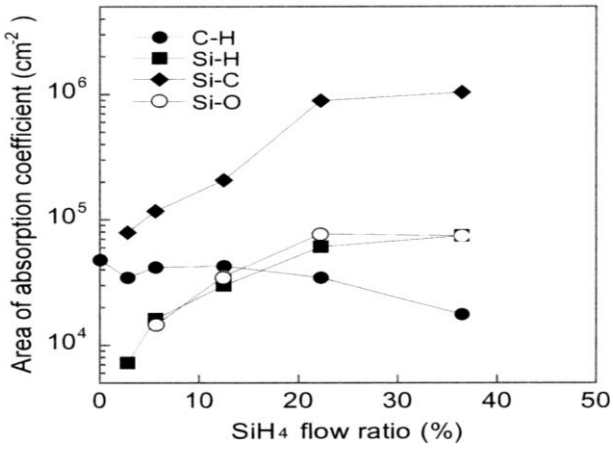

Figure 20. Areas of absorption coefficients of C-H, Si-H, Si-C and Si-O bonds calculated from the results shown in Figure 4.4 as a function of the SiH_4 flow ratio.

Fourier transform infrared (FT-IR) analysis was carried out using a Perkin Elmer Spectrum GX in the 400 to 4000 cm^{-1} range to investigate the chemical bonding. An average of 100 scans was taken per sample. FT-IR spectra in the range 400 to 4000 cm^{-1} are shown in Figure 19 for the films deposited at the SiH_4 flow ratio of 0 to 36.4 %. For the DLC thin film (SiH_4 flow ratio: 0 %), an absorption peak at 2900 cm^{-1} corresponding to C-H bonds was observed. From the spectra of Si-containing DLC thin films, not only C-H bonds but also Si-H (2140 cm^{-1}), Si-C (800 cm^{-1}) and Si-O (1100 cm^{-1}) bonds were observed [45,46]. It is considered that the formation of Si-O bonds arises from oxidation of silicon present on the film surface. To clarify the variation of each peak, the areas of absorption coefficients for C-H, Si-H, Si-C and Si-O bonds are calculated and shown in Figure 20 as a function of the SiH_4 flow ratio. It can be seen from the figure that the contributions of Si-H, Si-C and Si-O bonds increase when the SiH_4 flow ratio increases, and their increasing behaviors are very similar to that of silicon content shown in Figure 18. While, the contribution of C-H bonds decreases with silicon addition as a whole, and range from 3×10^4 to 4×10^4 cm^{-2} at the SiH_4 flow ratio of 2.8 to 22.2 %. The reduction in the contribution of C-H bonds at the SiH_4 flow ratio of 2.8 % is consistent with the rapid drop of hydrogen content with silicon addition observed in Figure 18.

Figure 21 shows absorption spectra of the C-H bonds in the range 2700 to 3200 cm^{-1} for the films prepared at the SiH_4 flow ratio of 0, 2.8, 5.6 and 12.5 %. The individual C-H vibrations are represented in the figure: CH_2 sp^2 (olefinic) at 3020 cm^{-1}, CH_3 sp^3 (asymmetrical) at 2965 cm^{-1}, CH sp^3 at 2920 cm^{-1}, CH_2 sp^3 (asymmetrical) at 2920 cm^{-1} and CH_3 sp^3 (symmetrical) at 2870 cm^{-1} [11]. The C-H vibrations of the DLC thin film (SiH_4 flow ratio: 0 %) imply the existence of both CH_x sp^3 (x = 1-3) and CH_2 sp^2 configurations. For the Si-containing DLC thin films, however, it can be noted that the contribution of CH_2 sp^2 configuration is suppressed compared with the DLC thin film. Considering that silicon forms only sp^3 bonding, it is suggested that the decrease in CH_2 sp^2 configuration with silicon addition is caused by formation of Si-C bonds. The existence of Si-C bonds, which increased with the SiH_4 flow ratio, may be related to maintaining the dynamic hardness of Si-containing DLC thin films as shown in Figure 17, while the DLC films indicate that the internal stress reduction is accompanied by the dynamic hardness reduction (see Figure 3).

Copyright © 2012. Nova Science Publishers, Incorporated. All rights reserved.

Diamond-Like Carbon Films, Nova Science Publishers, Incorporated, 2012. ProQuest Ebook Central,

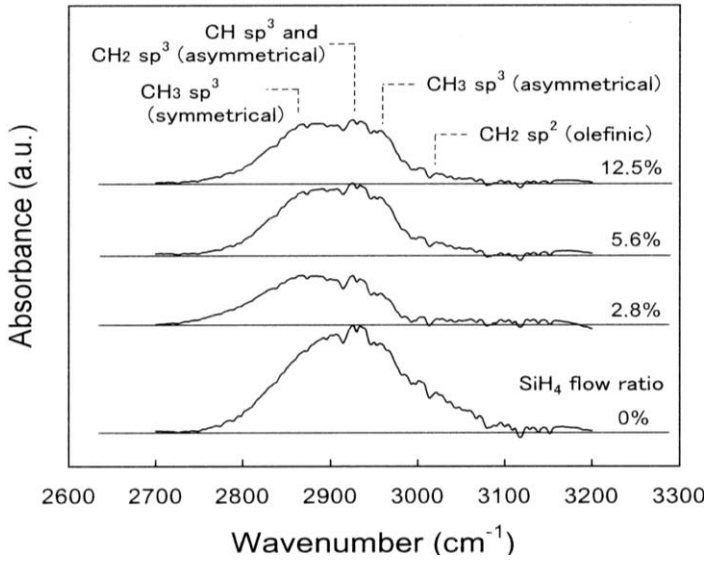

Figure 21. Absorption spectra of the C-H bonds in the range 2700 to 3200 cm^{-1} for the films prepared at the SiH_4 flow ratio of 0, 2.8, 5.6 and 12.5 %.

Correlations between the internal compressive stress and structural properties of the obtained films are discussed below. Amorphous hydrogenated silicon (a-Si:H) films generally include the dangling bonds saturated with hydrogen and are relaxed so that the films indicate low internal stresses below 1 GPa [46]. As explained in Figure 20, for the Si-containing DLC thin films in the present work, the Si-H bonds were found to increase with an increase in the SiH_4 flow ratio, that is, silicon content (see Figure 18). From this, the reason why the silicon incorporation is responsible for the compressive stress reduction is suggested that the Si-H bonds increment causes the relaxation of a three-dimensional rigid network of DLC thin film. As another significant aspect of the structural properties, it should be noted from Figures 18 and 20 that the hydrogen content of the Si-containing DLC thin films indicated a constant behavior despite the fact that the contribution of Si-H bonds increased with silicon content. This means that hydrogen in C-H bonds and unbound hydrogen are consumed for forming the Si-H bonds. Particularly, in the range 2.8 to 22.2 % of the SiH_4 flow ratio, the contribution of C-H bonds shows no significant change while the Si-H bonds increase as can be seen in Figure 20, suggesting that the unbound hydrogen is primarily used for the Si-H bonds. Considering that the compressive stress increased almost linearly with increasing the fraction of unbound hydrogen content for the DLC thin films deposited by the EBEP-CVD system, which is described in section 2.3, a transformation of the unbound hydrogen into the bonded hydrogen in Si-H bonds may be correlated with the compressive stress reduction.

REFERENCES

[1] S. Aisenberg and R. Chabot, *J. Appl. Phys.* 42 (1971) 2953.
[2] K. J. Clay, S. P. Speakman, N. A. Morrison, N. Tomozeiu, W. I. Milne and A. Kapoor, *Diamond Relat. Mater.*, 7 (1998) 1100.
[3] R. G. Lacerda and F. C. Marques, Appl. Phys. Lett., 73 (1998) 617.

Copyright © 2012. Nova Science Publishers, Incorporated. All rights reserved.

Diamond-Like Carbon Films, Nova Science Publishers, Incorporated, 2012. ProQuest Ebook Central,

[4] D. F. Franceschini, C. A. Achete and F. L. Freire Jr, *Appl. Phys. Lett*., 60 (1992) 3229.
[5] W. C. Vassell, A. K. Gangopadhyay, T. J. Potter, M. A. Tamor and M. J. Rokosz, *JMEPEG*, 6 (1997) 426.
[6] S. Xu, D. Flynn, B. K. Tay, S. Prawer, K. W. Nugent, S. R. P. Silva, Y. Lifshitz and W. I. Milne, *Philosophical Magazine* B, 76 (1997) 351.
[7] P. J. Fallon, V. S. Veerasamy, C. A. Davis, J. Robertson, G. A. J. Amaratunga, W. I. Milne, J. Koskinen, *Phys. Rev.* B, 48 (1993) 4777.
[8] J. Robertson, *Diamond Relat. Mater*., 2 (1993) 984.
[9] C. A. Davis, *Thin Solid Films*, 226 (1993) 30.
[10] B. Marchon, N. Heiman, M. R. Khan, A. Lautie, J. W. Ager III and D. K. Veirs, *J. Appl. Phys*., 69 (1991) 5748.
[11] P. Couderc and Y. Catherine, *Thin Solid Films*, 146 (1987) 93.
[12] P. Koidl, C. Wild, B. Dischler, S. Wagner and M. Ramsteiner, *Materials Science Forum*, 52and53 (1989) 41.
[13] A. Grill and V. V. Patel, *Diamond Films and Techno*., 1 (1992) 219.
[14] P. Wood, T. Wydeven and O. Tsuji, *Thin Solid Films*, 258 (1995) 151.
[15] D. F. Franceschini, C. A. Achete and F. L. Freire Jr, *Appl. Phys. Lett*., 60 (1992) 3229.
[16] D. Sarangi, S. Kumar, R. Bhattacharyya, *Diamond Relat. Mater*., 13 (2004) 1844.
[17] M. Grischke, K. Bewilogua and H. Dimigen, *Material and Manufacturing Processes* 8, (1993) 407.
[18] P. Wang, X. Wang, T. Xu, W. Liu and J. Zhang, *Thin Solid Films*, 515 (2007) 6899.
[19] W. C. Vassell, A. K. Gangopadhyay, T. J. Potter, M. A. Tamor and M. J. Rokosz, *JMEPEG*, 6 (1997) 426.
[20] J. Meneve, E. Dekempeneer and J. Smeets, *Diamond Films and Technology*, 4 (1994) 23.
[21] For example, T. Hara, M. Hamagaki, A. Sanda, Y. Aoyagi and S. Namba: *J. Vac. Sci. and Technol*. B5 (1987) 366.
[22] M. Hamagaki, doctoral thesis, Saitama University, 1996.
[23] M. Ryoji, T. Hara, K. Ohnishi, M. Hamagaki, Y. Dake, M. Tohkai and Y. Aoyagi: *Jpn. J. Appl. Phys.* 31 (1992) 4357.
[24] T. Sasaki, M. Ryoji, Y. Ichikawa and M. Tohkai: Technical Digest of the International PVSEC-9, *Miyazaki* (1996) P-II-D-34.
[25] M. Imaizumi, K. Okitsu, M. Yamaguchi, T. Hara, T. Ito, I. Konomi, M. Ban, M. Tokai and K. Kawamura, *J. of Vacuum Science and Technology* A, 16 (1998) 3134.
[26] T. Ito, M. Imaizumi, K. Yamaguchi, K. Okitsu, I. Konomi, M. Yamaguchi, T. Hara, M. Ban, M. Tokai and K. Kawamura, *Jpn. J. Appl. Phys*., 39 (2000) 6035.
[27] K. Okitsu, M. Imaizumi, K. Yamaguchi, A. Khan, M. Yamaguchi, M. Ban, M. Tokai and K. Kawamura, *Solar Energy Materials and Solar Cells*, 65 (2001) 185.
[28] T. Hasegawa, K. Yamamoto, Y. Kakudate and M. Ban, Proc. Plasma Science Symposium 2001 / The 18th Symposium on Plasma Processing, Kyoto, January, 2001, p. 581.
[29] T. Hasegawa, K. Yamamoto, Y. Kakudate and M. Ban, Proc. Frontiers of Surface Engineering 2001, Nagoya, October, 2001, p. 56.
[30] K. Taniguchi, H. Sato, M. Hamagaki, P. Abraha, Y. Tsunekawa and T. Hara, Proc. vol. 1 Int. Conf. on Phenomena in Ionized Gases, Nagoya, July, 2001, p. 169.

Copyright © 2012. Nova Science Publishers, Incorporated. All rights reserved.

Diamond-Like Carbon Films, Nova Science Publishers, Incorporated, 2012. ProQuest Ebook Central,

[31] R. Ichiki, Y. Kubota, M. Yoshida, Y. Fukuda, Y. Mizukamo and T. Hara, *J. Plasma Fusion Res*., 8 (2009) 1408.
[32] M. Ban, M. Ryoji, T. Hasegawa, Y. Mori, S. Fujii and J. Fujioka, Dia. *Relat. Mater*., 12 (2003) 47.
[33] M. Ban, M. Ryoji, T.Hasegawa, Y Mori, S Fujii and J. Fujioka, Dia. *Relat. Mater*., 11 (2002) 1353.
[34] J. W. Zou, K. Schmidt, K. Reichelt and B. Stritzker, *J. Vac. Sci. Technol*., A 6 (1988) 3103.
[35] I. A. Blech and P. Wood, *J. Vac. Sci. Technol*. A, 11 (1993) 728.
[36] H. Yamada, O. Tsuji and P. *Wood, Thin Solid Films, 270 (1995) 220.*
[37] *J. Robertson, Phys*. Rev. Lett., 68 (1992) 220.
[38] J. Robertson, *J. Non-Cryst. Solids*, 198-200 (1996) 614.
[39] F. Tuinstra and J. L. Koenig, *J. Chem. Phys*., 53 (1970) 1126.
[40] J. C. Angus and F. Jansen, *J. Vac. Sci. Technol.* A, 6 (1988) 1778.
[41] S. Kaplan, F. Jansen and M. Machonkin, *Appl. Phys. Lett*., 47 (1985) 750.
[42] Y. Wang, H. Chen, R. W. Hoffman and J. C. Angus, *J. Mater. Res*., 5 (1990) 2378.
[43] R. G. Lacerda and F. C. Marques, *Appl. Phys. Lett*., 73 (1998) 617.
[44] M. Ban, T. Hasegawa, *Surf. Coat. Technol*., 154 (2003) 1.
[45] B. Goranchev, K. Reichelt, J. Chevallier, P. Hornshoj, H. Dimigen and H. Hubsch, *Thin Solid Films*, 139 (1986) 275.
[46] P. Paduschek, C. Hopel and H. Mitlehner, *Thin Solid Films*, 110 (1983) 291.

Copyright © 2012. Nova Science Publishers, Incorporated. All rights reserved.

Diamond-Like Carbon Films, Nova Science Publishers, Incorporated, 2012. ProQuest Ebook Central,

In: Diamond-Like Carbon Films
Editor: Yuto S. Tanaka
ISBN: 978-1-61324-791-4
© 2012 Nova Science Publishers, Inc.

Chapter 5

DIAMOND-LIKE CARBON FILMS IMPROVE THEIR PROPERTIES WITH THE INCORPORATION OF CRYSTALLINE DIAMOND PARTICLES

F. R. Marciano,[1,2,3] E. C. Almeida,[4] R. P. C. Costa,[2] D. A. Lima-Oliveira,[2] A. O. Lobo,[1,2,3] E. J. Corat[2,3] and V. J. Trava-Airoldi[2,3]

[1]Universidade do Vale do Paraíba (Univap),
São José dos Campos/SP, Brazil
[2]Instituto Nacional de Pesquisas Espaciais (INPE),
São José dos Campos/SP, Brazil
[3]Instituto Tecnológico de Aeronáutica (ITA),
São José dos Campos/SP, Brazil
[4]Universidade Estadual de Santa Cruz (UESC), Ilhéus/BA, Brazil

Copyright © 2012. Nova Science Publishers, Incorporated. All rights reserved.

ABSTRACT

Diamond-like carbon (DLC) has been widely studied due to its mechanical properties such as low friction coefficient, high hardness, and high adherence on different substrate materials. The unique combination of chemical and mechanical properties of DLC films has opened the possibilities for the electrochemical applications of these film materials. In this chapter, a review of DLC films with extremally high hardness and very resistant to corrosion by incoporating crystalline diamond (CD) particles during the deposition process will be presented. These films were for the first time developed in our laboratories and the characterization performed will be also showed.

The studies carried out in our laboratories show CD-DLC films improving DLC and stainless steel electrochemical corrosion resistance. CD-DLC prevented aggressive ions from attacking metallic surfaces, becoming a potential candidate for an anti-corrosion material in industrial applications, like pipelines in petroleum industry. It was also investigated the influence of the diamond particle sizes on the electrochemical corrosion resistance of these films. The electrochemical parameters obtained from the potentiodynamic polarization curves and the impedance were correlationated with the

Diamond-Like Carbon Films, Nova Science Publishers, Incorporated, 2012. ProQuest Ebook Central,

qualitative sp^3/sp^2 ratio of the CD-DLC films obtained from Raman scattering spectroscopy. The results show that both protection efficiency and impedance increase with the decrease of I_D/I_G ratio. It means the increase of sp^3 bonds in DLC films reduce its electrochemical corrosion, improving the electrochemical protection efficiency and the impedance. In addition, diamond crystallites bigger than the DLC grain size reduced the pitting corrosion, which is an indication of the chemical inertness of the CD-DLC coatings to the Cl^- ions. The tribological behavior of these films under aggressive solution was also investigated. The presence of bigger CD particles increased the film roughness. In addition, these CD particles demonstrated to reduce DLC friction and wear. CD-DLC(500nm) films presented the lowest friction coefficient and wear rate under 5% NaCl saline solution. This result suggests the potential use of these films in aggressive environment even when suffer friction.

INTRODUCTION

The recent interest of the petroleum companies on improving the efficiency and viability of oil duct flow have been increased in the several last years [1-2]. However, the commercial extraction viability has some obstacles, such as drilling of the salt layer that can block and hold the drill pipes. Drill and flow pipes are made with seamless steel coated with resin to decrease the wear and corrosion. However, this resin wears very quickly due to the contact sliding between steel cables and inner wall of the drill pipes. In addition, corrosion of the steel components due to the great pressure and the sulfur dioxide presence decreases its efficiency and viability. The water from the oil extraction generally contains high salinity, oil particles in suspension and chemicals added as demulsifying and defoaming [3]. The corrosive environment can result deposition/precipitation of corrosion products in the metal surface and increase wear inside of the drill and flow pipes.

Technologies based on the flow of oil through ducts coated with diamond-like carbon (DLC) films represent an alternative way [1]. DLC coatings can potentially increase the efficiency by reducing the friction, wear and corrosion on the drill pipes. Such improvement will reduce the operating costs by reducing the equipment downtime for maintenance and extend the life of the existing machinery. The most common way to control corrosion in oil ducts is by chemical inhibition, but it is not fully understood. The mechanism can be dominated by inhibitor adsorption on the surface of film and/or metal; the inhibitor provokes a small extent of corrosion on the film surface and/or metal and is also adsorbed forming a compact protective thin layer. The inhibitor forms a precipitate on the surface metal in such a way to protect it. The protective combination of corrosion product/inhibitor layer is dynamic [4]. Inhibitors have also been shown to be effective in reducing erosion [5].

Tribocorrosion

Tribocorrosion is a term which describes the degradation of materials that result from the combined action of wear and corrosion [6-7]. Tribocorrosion includes the solid particle erosion, sliding wear and oxidation as surface degradation process [8]. Examples include degradation of articulation prosthesis and dental fillers, accelerated corrosion of steel conveyors exposed to ambient air of high relative humidity, erosion-corrosion of slurry pipes,

Copyright © 2012. Nova Science Publishers, Incorporated. All rights reserved.

Diamond-Like Carbon Films, Nova Science Publishers, Incorporated, 2012. ProQuest Ebook Central,

and numerous others. When corrosion and wear are simultaneously involved, their synergistic action significantly deteriorates the performance of the materials in contact with them [9].

Over the past years, a number of authors investigated the tribocorrosion behavior of engineering substrates. DLC coatings have been deposited in order to take advantage of its high wear resistance associated to its very low friction coefficient [10]. However, another important factor that influences the protective character of DLC films is their adhesion to the substrate [9]. Many authors pointed out the importance of the bond layers for enhanced adhesion of the DLC films. Azzi et al [9], for example, investigated the tribocorrosion behavior of DLC films on 316L stainless steel substrates in the context of biomedical applications. They pointed that a nitrided bond layer shows significant improvement of the dry wear resistance of DLC coatings [9,11], however, this bond layer was insufficient when sliding wear takes place in simulated body fluid condition, even at lower contact pressure. This was explained mainly due to the infiltration of the liquid through the pores and the weakening of the interface due to corrosion processes.

Diamond-Like Carbon (DLC)

DLC is a metastable form of amorphous carbon containing a significant fraction of sp^3 bonds [12]. Carbon forms a great variety of crystalline and disordered structures because it is able to exist in three hybridizations, sp^3, sp^2 and sp^1. According to Robertson [12], in sp^3 configuration, as in diamond, a carbon atoms four valence electrons are each assigned to a tetrahedrally directed sp^3 orbital, which makes a strong σ bond to an adjacent atom; and in the three-fold coordinated sp^2 configuration, as in graphite, three of the four valence electrons enter trigonally directed sp^2 orbitals, which form σ bonds in a plane. The fourth electron of the sp^2 atom lies in a π orbital, which lies normal to the σ bonding plane [12]. The π orbital forms a weaker π bond with a π orbital on one or more neighbouring atoms [12].

The extreme physical properties of diamond derive from its strong, directional σ bonds [12-13]. The sp^3 bonding of DLC confers on it many of the beneficial properties of diamond itself, such as hardness, chemical and electrochemical inertness, and wide band gap [12]. DLC films also present low-friction coefficient, low wear rate and excellent tribological properties [14-16]. Due to the mechanical, electrical, optical and chemical properties of these films, the use of DLC coatings in mechanical and electrical fields has increased with recent applications in food, beverage and medical application [14].

Nanoparticle-Incorporated DLC Films

Nanoparticle doping in DLC films prepared by chemical/physical vapor deposition techniques had been the issue of obtaining a new class of materials [17-18] but dispersing the naparticles homogeneously in DLC matrix by the techniques used by the researches until now was found to be difficult [18]. The main reported problem in producing these films is the difficulty of dispersing particles homogeneously in the DLC matrix [18-19].

Some authors have reported the improvement of DLC electrochemical corrosion resistance by addition of silicon [20], nitrogen [21], fluorine [22], and so on. However, crystalline diamond (CD) particles have never been used. In 1997, Zarrabian et al [23]

Copyright © 2012. Nova Science Publishers, Incorporated. All rights reserved.

Diamond-Like Carbon Films, Nova Science Publishers, Incorporated, 2012. ProQuest Ebook Central,

observed for the first time the formation of cubic crystalline diamond grains in an amorphous matrix using electron cyclotron resonance plasma at low pressure with radio frequency power applied to the substrate. According to Lian et al [24], the properties of DLC films can be significantly enhanced by the presence of nanocrystalline diamond. They also reported the characterization of nanocrystalline diamond in pure and Ru-doped DLC films. Later, Zhou et al [25] prepared composite films consisting of nanocrystalline diamond embedded in an amorphous carbon (a-C) matrix using a prolonged bias assisted hot filament chemical vapor deposition conventionally used for diamond nucleation only for a short time. The nanocomposite with the highest nanodiamond density and average crystalline size of ~6 nm was obtained for 1% CH_4, while increase of the CH_4 concentration resulted in an increase of the nanocrystalline diamond size, but a reduction of the nanodiamond particle density and the diamond volume fraction in the composite. Hsieh et al [26] deposited nanocrystalline diamond embedded in a-C/N films at a substrate temperature of 25°C in a nitrogen atmosphere using filtered cathodic arc plasma. According to them, nanocrystalline diamond clusters can be nucleated to a size of 2–5 nm at 25°C of substrate temperature to enhance the mechanical properties of the a-C/N film. Sakudo et al [27] developed a method to deposit a DLC layer embedded with nanodiamond particles. In order to make both DLC and diamond coexist on a same substrate, they developed a method to form diamond at lower temperature than 500 K, since at a higher temperature DLC is easily crystallized and changed to graphite. Their coating had higher hardness than DLC and very low friction comparable to DLC. In the present chapter, it was shown the production and characterization of crystalline diamond (CD) particles incorporated in DLC films produced by plasma enhanced chemical vapor deposition (PECVD). It was used a new technique developed in our laboratory that permits the deposit of DLC films from hexane [28] containing different kind of nanoparticles in order to create films for different applications.

The Synthesis Procedure of Crystalline Diamond-Incorporated DLC Films

The crystalline diamond-incorporated DLC (CD-DLC) films were deposited on 316L stainless steel disks that were previous polished to a mirror-like finish surface. The substrates were previous cleaned ultrasonically in acetone bath for 15 min. In the chamber (vacuum base pressure of 1.3 mPa) the substrates were additionally cleaned by argon discharge with 20 sccm gas flow at 10.7 Pa working pressure and a discharge voltage of -500 V for 20 min prior to deposition.

In order to enhance the adhesion of the film to the substrate, carbonitriding was performed before DLC deposition. The carbonitriding was carried out mixing nitrogen, hydrogen and methane gases in the proportion 12:3:1 respectively. The total flow was kept in 100 sccm at 10.7 Pa for 2 h and a discharge voltage of -560 V.

The DLC films started to be deposited using methane as the powered gas to a thickness of around 1.0 μm (20 sccm gas flow at 10.7 Pa for 2 h and a discharge voltage of -700 V). After, the DLC deposition continues using hexane as the powered gas to a thickness of around 1.5 μm (at 10.7 Pa for 1 h and a discharge voltage of -700 V). To produce CD-DLC films, CD particles from different average sizes (4 nm, 250 nm and 500 nm) dispersed in hexane (0.5 g/L) replaced the pure hexane during the DLC deposition.

Copyright © 2012. Nova Science Publishers, Incorporated. All rights reserved.

Diamond-Like Carbon Films, Nova Science Publishers, Incorporated, 2012. ProQuest Ebook Central,

CD-DLC Film Characterization

The film morphology and roughness value were characterized by a Wyko NT1100 optical profiler. Figure 1 shows macroscale images from the as-deposited DLC (Figure 1a) and CD-DLC films (Figure 1b-d) containing CD particles of different average sizes. The grains seen in the images are from the carbonitriding process of stainless steel substrates. It is possible to see that in macroscale, the incorporation of CD particles does not affect the surface appearance. The surface roughness (R_a) was measured over an area of 229 μm x 301 μm and can be seen on Table 1. The as-deposited DLC films presented roughness values around 115 nm. With the presence of bigger CD particles (average sizes of 250 and 500 nm), the films became rougher. However, with CD particles of 4 nm, the roughness value slightly decreased. In this case, minor nanoparticles occupying the nanospaces between DLC grains smooth the film surface, reducing its roughness value.

Raman scattering spectroscopy was used to evaluate the chemical structure of the DLC and CD-DLC films. The atomic arrangement of the films was analyzed using a Renishaw 2000 system with an Ar^+-ion laser (λ = 514 nm) in backscattering geometry. The laser power on the sample was ~0.6 mW and the laser spot had 2.5 μm diameter. The Raman shift was calibrated in relation to the diamond peak at 1332 cm^{-1}. All measurements were carried out in air at room temperature.

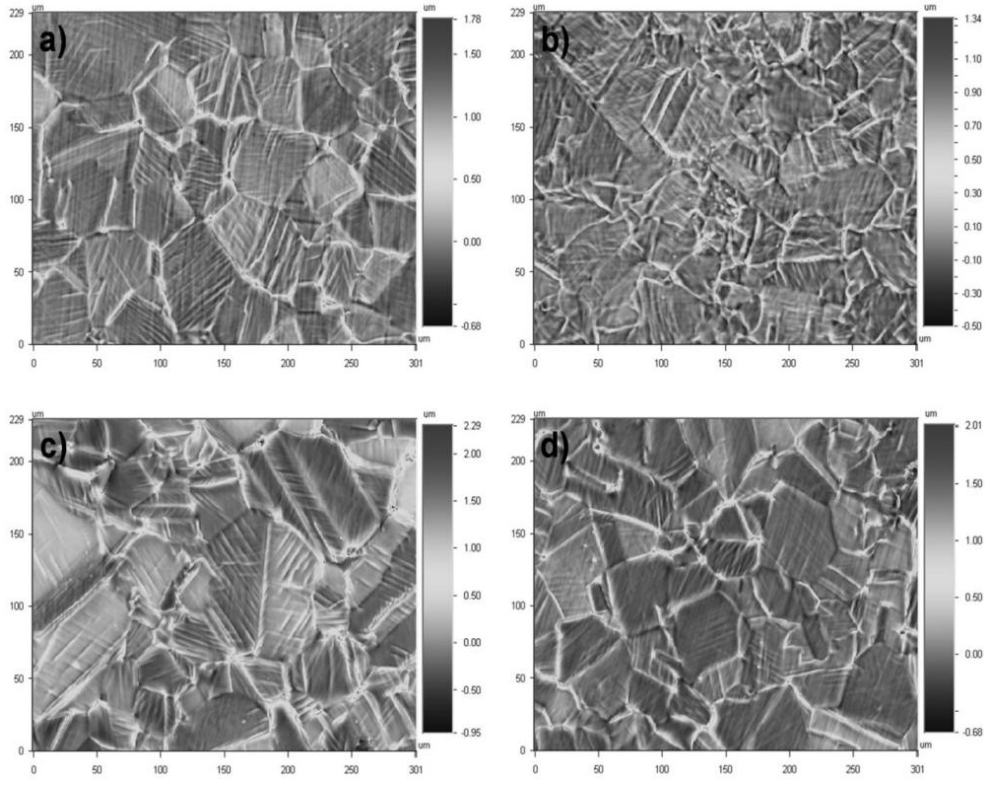

Figure 1. Surface images of (a) DLC and CD-DLC films containing particles of (b) 4 nm, (c) 250 nm and (d) 500 nm average size. All images acquired from optical profiler are in the amplification of 50x.

Copyright © 2012. Nova Science Publishers, Incorporated. All rights reserved.

Diamond-Like Carbon Films, Nova Science Publishers, Incorporated, 2012. ProQuest Ebook Central,

Table 1. Surface roughness (R_a) of DLC and CD-DLC films according to the CD average sizes. The error represents the standard deviation of 3 different samples

Samples	Roughness (nm)
DLC	115 ± 8
CD-DLC (4 nm)	92 ± 7
CD-DLC (250 nm)	216 ± 9
CD-DLC (500 nm)	145 ± 5

Table 2. Summarized Raman spectrum results of DLC and CD-DLC films according to the CD average sizes. The error represents the standard deviation of 5 different samples

Sample	*D* Band Position (cm^{-1})	*G* Band Position (cm^{-1})	FWHM (*D*)	FWHM (*G*)	I_D/I_G	[H] (%)	Tauc gap (eV)	Density (g/cm^3)
DLC	1301.3 ± 1.1	1522.8 ± 1.4	185.2 ± 2.8	153.6 ± 0.4	0.65 ± 0.01	34.1 ± 0.3	2.17 ± 0.03	1.95 ± 0.01
CD-DLC (4 nm)	1317.0 ± 2.2	1527.9 ± 0.4	243.0 ± 4.4	160.9 ± 1.6	0.50 ± 0.01	36.3 ± 0.4	2.37 ± 0.04	2.03 ± 0.02
CD-DLC (250 nm)	1314.9 ± 5.1	1527.1 ± 0.8	233.8 ± 7.0	159.7 ± 4.0	0.50 ± 0.01	36.6 ± 0.5	2.35 ± 0.04	2.00 ± 0.04
CD-DLC (500 nm)	1304.2 ± 0.5	1524.6 ± 1.0	222.9 ± 2.3	156.1 ± 1.7	0.57 ± 0.01	34.1 ± 0.7	2.17 ± 0.07	1.97 ± 0.02

Copyright © 2012. Nova Science Publishers, Incorporated. All rights reserved.

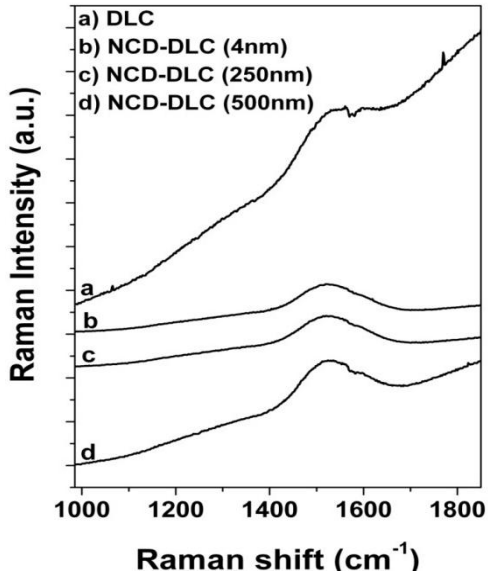

Figure 2. Raman scattering spectra from (a) pure DLC and CD-DLC films containing particles of (b) 4 nm, (c) 250 nm and (d) 500 nm average size. The spectra are vertically shifted for easy of comparison.

The Raman spectra are composed of two broad bands, centered approximately ~1300 cm^{-1} (*D* band) and ~1520 cm^{-1} (*G* band). The *D* and *G* band peak positions were determined by subtracting a linear background and fitting a Gaussian function to the peak of Raman spectrum. The peak position, width and ratio of integrated areas under *D* and *G* peaks were used to determine I_D/I_G. Figure 2 shows the spectra from DLC and CD-DLC films with different CD average sizes, which are vertically shifted for easy of comparison. The main parameters obtained through the spectra (Figure 2) are summarized in Tab. 2. The decrease of I_D/I_G ratio, together with the shift of *D* band's peak position towards higher frequencies, accompanied by an increase of the bandwidth is usually interpreted in terms of an increase of diamond-like domains [29-30].29 Some authors reported the incorporation of metallic particles in DLC films in order to increase DLC corrosion resistance, but metallic particles promote the graphitization of amorphous carbon around them due to their catalytic activity at high kinetic energy of the sputtered C species [31-32]. In the case of CD-DLC films, it can be deduced sp^3/sp^2 ratio slightly increased with the presence of CD particles. According to Robertson [12], the sp^3 bonding confers on DLC many of the beneficial properties of diamond itself, such as its mechanical hardness, chemical and electrochemical inertness and wide band gap. The results presented here also demonstrated an increase in the film density. Note that all the characteristics obtained through Raman for CD-DLC films are more evident in those containing particles of 4 nm of average size. This (4 nm) was the minor studied size and the only size minor than DLC average grain (~10 nm) [33]. It suggests that minor grains could occupy more nanospaces between DLC grains, increasing its density, disorder and diamond-like characteristics.

The structural analysis of CD-DLC films was performed by X-ray diffraction (XRD, Philips X'Pert) with Cu Ka radiation generated at 40 kV and 50 mA. Figure 3 shows the glancing incident X-ray diffraction pattern of a CD-DLC film containing particles of 250 nm.

Copyright © 2012. Nova Science Publishers, Incorporated. All rights reserved.

Diamond-Like Carbon Films, Nova Science Publishers, Incorporated, 2012. ProQuest Ebook Central,

The three diamond peaks, (111), (220) and (311) and the graphite peak (102) proves CD-DLC films are composing by diamond crystals in an amorphous carbon graphitic film.

The contact angle of DLC and CD-DLC films was measured by using the sessile drop method with a Kruss EasyDrop contact angle instrument (EasyDrop DSA 100). The liquid was dropped automatically by a computer-controlled system. The contact angle measurements were carried out by an image analysis system, which calculated both the left and the right contact angles from the shape of the droplet. Two different test liquids (distilled water and diiodomethane) were used for surface energy calculations. All measurements were carried out at room temperature.

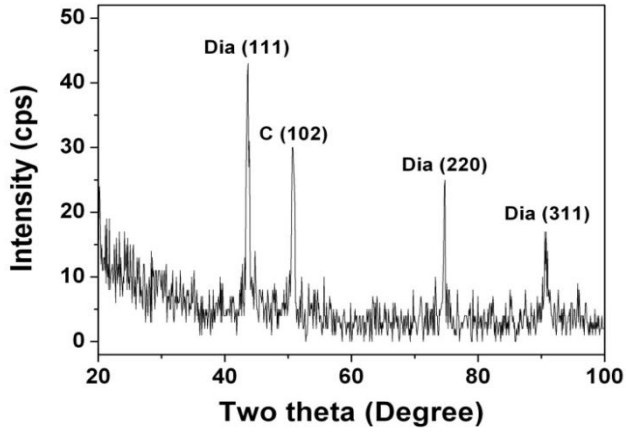

Figure 3. X-ray diffraction spectra of a CD-DLC film containing particles of 250 nm.

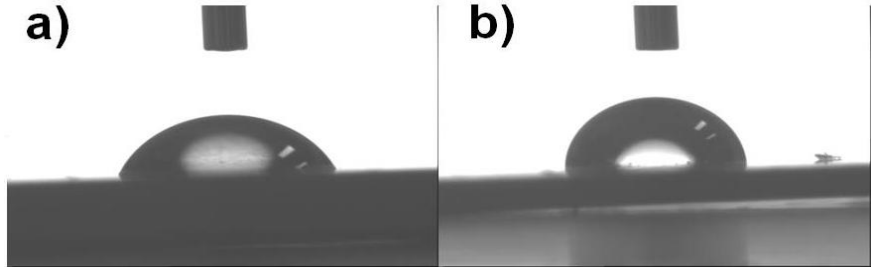

Figure 4. Water contact angle of (a) pure DLC film and (b) a CD-DLC film containing particles of 250 nm.

The water contact angle of DLC was 65.9º and ranged from 80.5º to 87.8° for CD-DLC films (Figure 4). It was not possible to observe any difference in the water contact angle of CD-DLC films according to the CD average size. Usually, a hydrophobic surface has a contact angle higher than 70°, while a hydrophilic surface has a contact angle lower than 70° [34]. The hydrophobic property of CD-DLC films could be explained by the presence of CD particles also on the surface. For the characterization of the surface energy additionally the contact angle on a disperse liquid (diiodomethane) was measured and analysed according to Fowkes [35]. A reduction in the total surface energy of the CD-DLC films was observed and attributed to the reduction in the polar component that is controlled by different intermolecular forces, permanent and induced dipoles and hydrogen bonds [36-38]. The

Copyright © 2012. Nova Science Publishers, Incorporated. All rights reserved.

Diamond-Like Carbon Films, Nova Science Publishers, Incorporated, 2012. ProQuest Ebook Central,

interfacial free energy determines the wetting characteristics and hence the wall shear stress generated when the liquid comes into contact with the surface [39].

Electrochemical Tests

Potentiodynamic polarization test was carried out in order to investigate the protective abilities of the coating. The electrochemical tests were performed using a conventional three-electrode electrochemical cell. In this cell, the reference electrode was a saturated Ag/AgCl electrode, the counter electrode was a platinum wire and the working electrodes were the stainless steel, DLC and CD-DLC films. The working electrode exposed area was 3.14 cm^2. The electrolyte solution was a 0.5 mol/L sodium chloride (NaCl) aqueous solution, pH 5.8, which was not stirred and was naturally aerated. Potentiodynamic tests were carried out by polarization of samples in the anodic direction, from -2.0 to +2.0 V, just after exposition to the electrolyte solution. The potential sweep rate was 1 mV/s.

The electrochemical stability of the systems in the test solution was investigated by the open-circuit potentials (OCP). The greatest E_{corr} value of -0.086 mV was observed for CD-DLC films with 2-3 µm diameter particles. The negative OCP values for the CD-DLC films may be caused by the penetration of the test solution [40-41]. The electrochemical parameters obtained from the potentiodynamic polarization curves (Figure 5) are given in Table 3. The corrosion current density (i_{corr}) of CD-DLC samples was reduced by more than one order of magnitude with comparison to the pure DLC films. The protection efficiency [42] also indicates that CD-DLC films offer the best protection among the uncoated samples up to 99.9%. The improvement in the breakdown potential values means the extension of the passive region in the coated system and a higher polarization is necessary to trigger the onset of anodic dissolution of the system [41,43]. In general, samples in the corrosion behavior with lower current density and higher potential indicate better corrosion resistance [44]. An improvement in the corrosion resistance of DLC films due to the presence of CD particles is evidenced by a shift of the polarization curve towards the region of lower current density and higher potential.

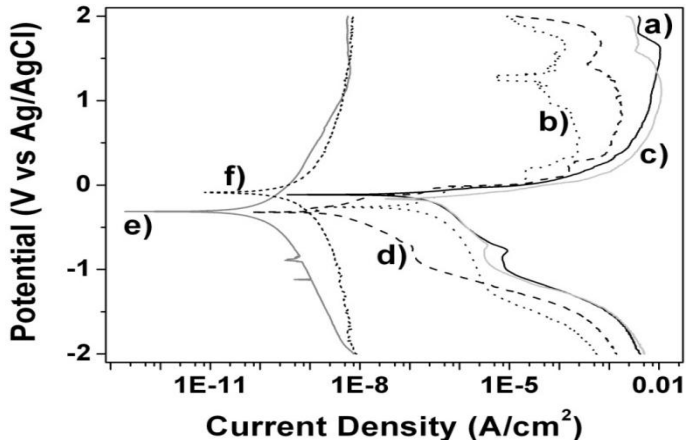

Figure 5. Potentiodynamic polarization curves of (a) stainless steel, (b) DLC, and CD-DLC films with (c) 4 nm, (d) 250 nm, (e) 500 nm and (f) 2-3 µm diameter particles.

Copyright © 2012. Nova Science Publishers, Incorporated. All rights reserved.

Diamond-Like Carbon Films, Nova Science Publishers, Incorporated, 2012. ProQuest Ebook Central,

Table 3. Electrochemical parameters obtained from potentiodynamic polarization curves

Samples	E_{corr} (mV)	i_{corr} (nA/cm^2)	Protection efficiency (%)
Stainless steel	-0.123	0.3589	-
DLC	-0.256	3.0450	-
CD-DLC (4 nm)	-0.169	30.715	-
CD-DLC (250 nm)	-0.321	0.0703	80.4
CD-DLC (500 nm)	-0.309	0.0002	99.9
CD-DLC (2-3 μm)	-0.086	0.0086	97.6

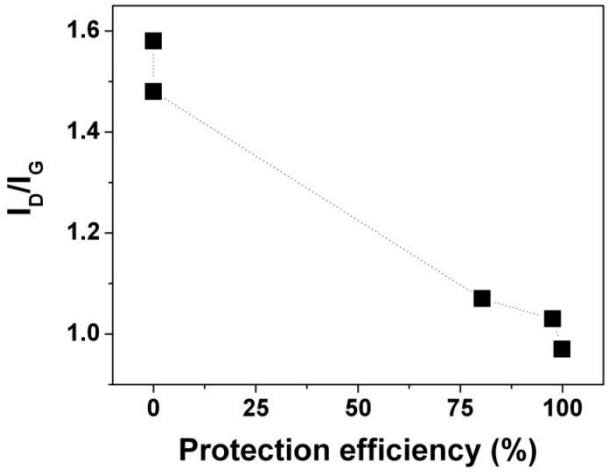

Figure 6. I_D/I_G ratio as function of the CD-DLC electrochemical protection efficiency.

The difference in corrosion behavior of DLC films is assigned to the difference in microstructure of these films [45]. Generally, the higher sp^3/sp^2 ratio, the higher electrochemical corrosion resistance [44,46]. The qualitative sp^3/sp^2 ratio of the CD-DLC films obtained from Raman scattering spectroscopy was compared to the protection efficiency (Table 3). Figure 6 shows the results of I_D/I_G ratio as function of the CD-DLC electrochemical protection efficiency. The results show protection efficiency increases with the decrease of I_D/I_G ratio. It means the increase of sp^3 bonds in DLC films reduce their electrochemical corrosion, increasing the electrochemical protection efficiency.

The impedance measurements were also carried out in 0.5 mol/L NaCl aqueous solution, pH 5.8. The electrochemical impedance spectra (EIS) were obtained over the frequency range 100 kHz–10 mHz, at open circuit potential, with an AC excitation of 10 mV. All experiments were performed at room temperature.

The Nyquist plots determined by the EIS technique (Figure 7) show the different corrosion behavior of the samples after immersion in NaCl. CD-DLC films present superior impedance in comparison to the pure DLC and the substrate. The mechanism for improving the corrosion resistance is related to the reduced electron conductivity of CD-DLC films in comparison to stainless steel and the pure DLC [47]. The low electrical conductivity of the

Copyright © 2012. Nova Science Publishers, Incorporated. All rights reserved.

Diamond-Like Carbon Films, Nova Science Publishers, Incorporated, 2012. ProQuest Ebook Central,

CD-DLC films reduces the electron transport and the exchange of electrical charges at the sample surface, which is necessary for electrochemical corrosion [47-48].

The increase of sp^3 bonds in DLC films also influences the film impedance. Figure 8 shows the results of I_D/I_G ratio as function of the CD-DLC impedance. The results pointed out the increase of sp^3 bonds in DLC films increase its impedance, improving DLC electrochemical corrosion resistance.

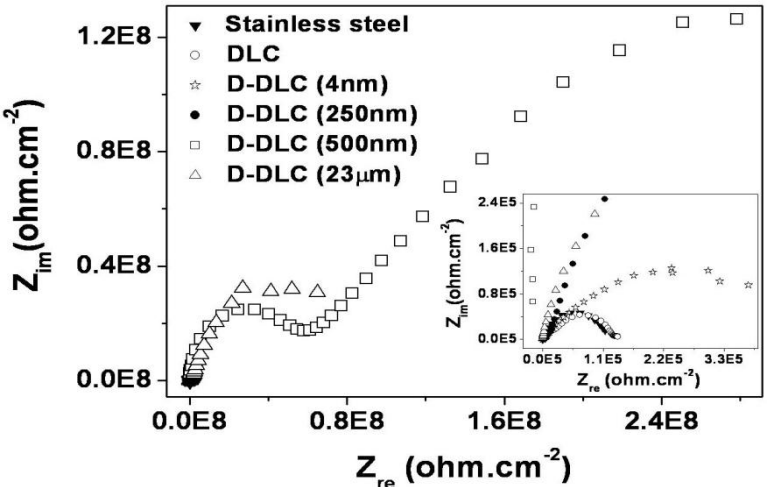

Figure 7. Nyquist plot of stainless steel, DLC and CD-DLC films.

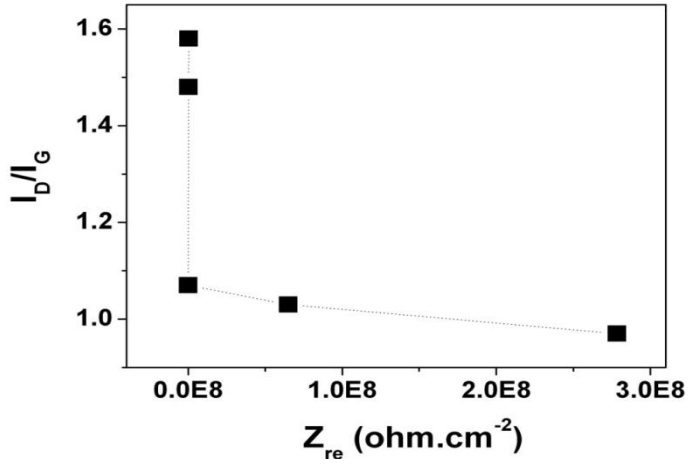

Figure 8. I_D/I_G ratio as function of the CD-DLC electrochemical impedance.

Figure 9 shows SEM images of the CD-DLC films before and after the electrochemical corrosion tests. The images of the films after the electrochemical corrosion tests show minor CD particles that did not belong to the film surface. These CD particles probably block the attacking of Cl^- ions, forming a barrier against the corrosion. The observed pits on DLC surface (Figure 10) indicate that the corrosion resistance of the film in the NaCl solution is attributed to pitting corrosion. Normally, the initiation of pits on the film surface occurs when small local sites on the film are exposed to the electrolyte and the pits always initiate at

Copyright © 2012. Nova Science Publishers, Incorporated. All rights reserved.

Diamond-Like Carbon Films, Nova Science Publishers, Incorporated, 2012. ProQuest Ebook Central,

defects such as surface compositional heterogeneities and porosities [49]. CD-DLC films can act as a passive film to prevent aggressive ions from attacking the substrate and thereby improve the corrosion resistance of 304 stainless steel. The chloride (Cl^-) ions of the NaCl solution attack the protective oxide layer on 304 stainless steel surface, penetrating to the austenite matrix and resulting in pitting corrosion [50]. Some of the researchers [51-52] have also reported similar pit initiation for austenitic stainless steels. SEM images show CD particles reduce the typical DLC pitting corrosion (Figure 10). The CD-DLC samples show very little pitting corrosion, which is an indication of the chemical inertness of CD-DLC coatings to the Cl^- ions. NaCl probably corrodes DLC film, and CD particles form a barrier against the corrosion.

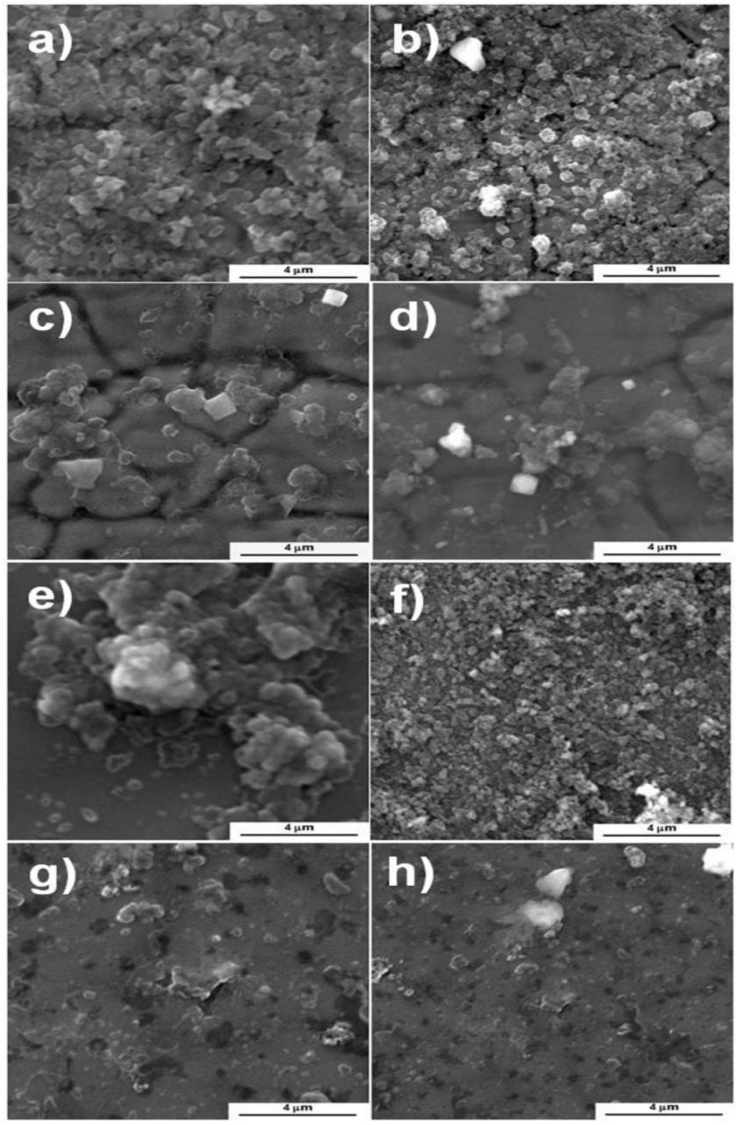

Figure 9. SEM images before the electrochemical corrosion tests of the DLC films containing CD particles of (a) 4 nm, (c) 250 nm, (e) 500 nm, and (g) 2-3 µm diameter. At the right side are the images of the same films after the tests.

Copyright © 2012. Nova Science Publishers, Incorporated. All rights reserved.

Diamond-Like Carbon Films, Nova Science Publishers, Incorporated, 2012. ProQuest Ebook Central,

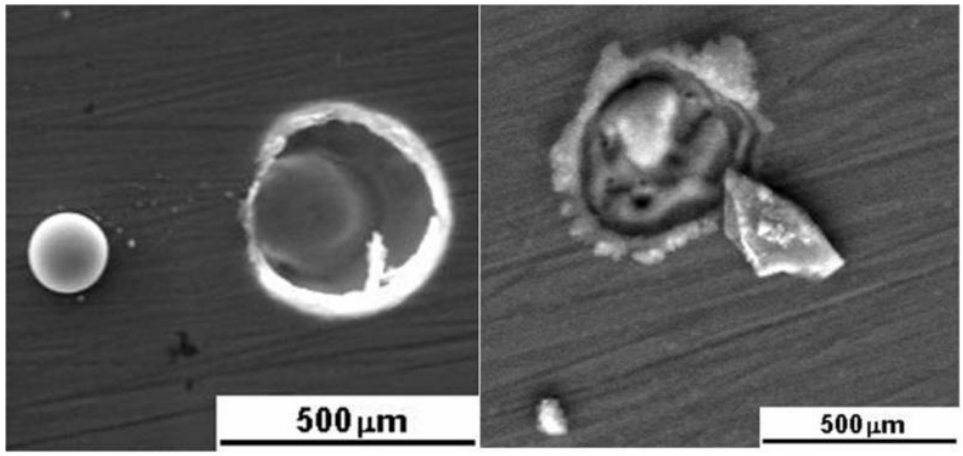

Figure 10. Examples of the pitting corrosion observed with SEM on DLC surfaces after the potentiodynamic tests.

Comparing the four sizes of diamond crystallites, the worst electrochemical corrosion result was for CD-DLC films produced with 4 nm diamond particle diameter. This diamond particle size (4 nm) was the only size minor than the DLC grain size (~10 nm) [33]. In this case, the CD particles could not act as a passive film to prevent aggressive ions from attacking the 304 stainless steel substrate.

Stainless steel is used in many industries e.g. the food industry for processing of products potentially aggressive due to low pH, high salt content or high processing temperatures [53]. Due to its high chromium content, the stainless steel itself has a good corrosion protection compared to other kinds of steel. Coated with CD-DLC films with 500 nm of average diameter, the stainless steel shows an improvement up to 99.9% in the electrochemical corrosion resistance and an increase in impedance more than three orders of magnitude. A typical example of potential application of these films in industry is in pipelines for petroleum and chemical products.

Tribocorrosion

Tribological tests were performed on 4 mm diameter 316L steel ball and 50 mm diameter 316L steel flat pairs with and without DLC and NCD-DLC films. The tribological tests were carried out in dry air (42% RH) and in saline solution with 5 mass% NaCl in distilled water, with 5.6 pH at room temperature. The saline solution was prepared according to DIN 50905 norm. The substrate was embedded in saline solutions using Aluminum vessel, as shown in the schematic diagram of tribotest system (Figure 11).

The friction and wear tests were carried out by using a UMT-CETR ball-on-disk tribometer in the rotational mode with constant linear sliding speed under 10 N normal load during 1000 cycles. The tests were performed three times for each pair combination. A new position on the ball/disk was used for each test, and the friction coefficients were collected from the steady-state region [54].

Copyright © 2012. Nova Science Publishers, Incorporated. All rights reserved.

Diamond-Like Carbon Films, Nova Science Publishers, Incorporated, 2012. ProQuest Ebook Central,

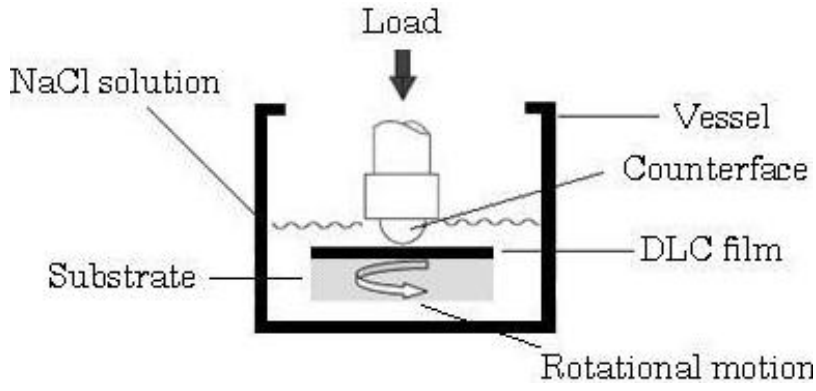

Figure 11. Schematic diagram of a friction in saline solution.

Figure 12 shows friction coefficient behavior of CD-DLC films with different diamond average sizes (4 nm, 250 nm and 500 nm). These friction coefficient measurements were plotted as function of cycle numbers for 316L stainless steel ball (a) coated and (b) uncoated with DLC, sliding against samples in dry air (42% RH) for load of 10 N and sliding speed of 120 mm.s^{-1}. In the curves from DLC/DLC and DLC/CD-DLC(250nm) pairs (Figure 12a), it is possible to see that the steady state starts after 500 cycles. However, DLC/CD-DLC(4nm) and DLC/CD-DLC(500nm) pairs did not show this behavior, with running-in process during almost 1000 cycles. Some authors [55-56] point that an interfacial transfer layer is formed during the running-in stage of tribological tests. This layer may oppose a very low resistance to shear strength sliding mechanism during the steady stage [55-56]. The lowest friction in this case was around 0.07 for DLC/DLC pair. For 316L/DLC pairs, including those with CD particles (Figure 12b), the friction coefficient remains between 0.18 and 0.21, which is similar than DLC/DLC pairs. The lowest friction coefficient was around 0.18 for 316L/CD-DLC(500nm) pair.

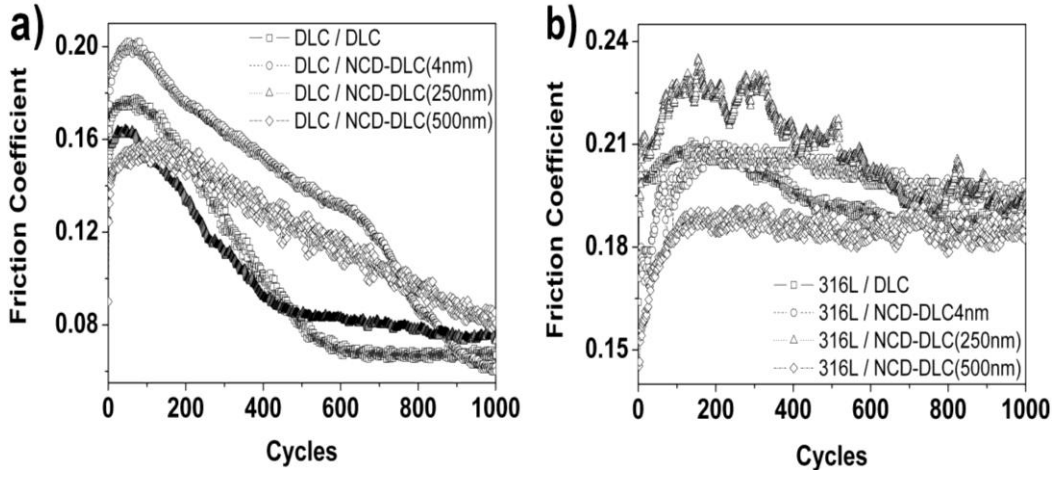

Figure 12. Friction behavior of DLC and NCD-DLC films containing particles of 4, 250 and 500 nm average size, sliding against 316L stainless steel ball (a) coated and (b) uncoated with DLC film, in dry air (42% RH).

Copyright © 2012. Nova Science Publishers, Incorporated. All rights reserved.

Diamond-Like Carbon Films, Nova Science Publishers, Incorporated, 2012. ProQuest Ebook Central,

Figure 13 shows friction coefficient behavior of CD-DLC films using the same parameters as described below, under 5% saline solution. In Figure 13a, the friction coefficient reached steady state after 200 cycles for all pairs. DLC/DLC and DLC/CD-DLC(500nm) pairs presented the lowest friction coefficient around 0.07. However, when the counter body changed to 316L stainless steel, 316L/DLC pair showed running-in process until 400 cycles and after this period, friction coefficient stabilized in 0.08, as seen in Figure 13b. The other pairs with CD particles showed similar behavior, without running-in period and friction coefficient between 0.07 and 0.09.

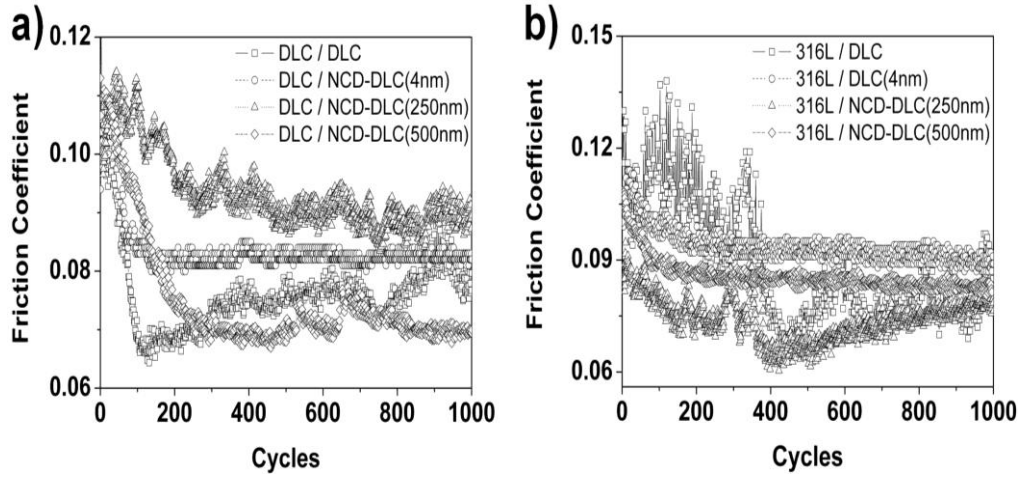

Figure 13. Friction behavior of DLC and CD-DLC films containing particles of 4, 250 and 500 nm average size, sliding against 316L stainless steel ball (a) coated and (b) uncoated with DLC film, in 5% saline solution.

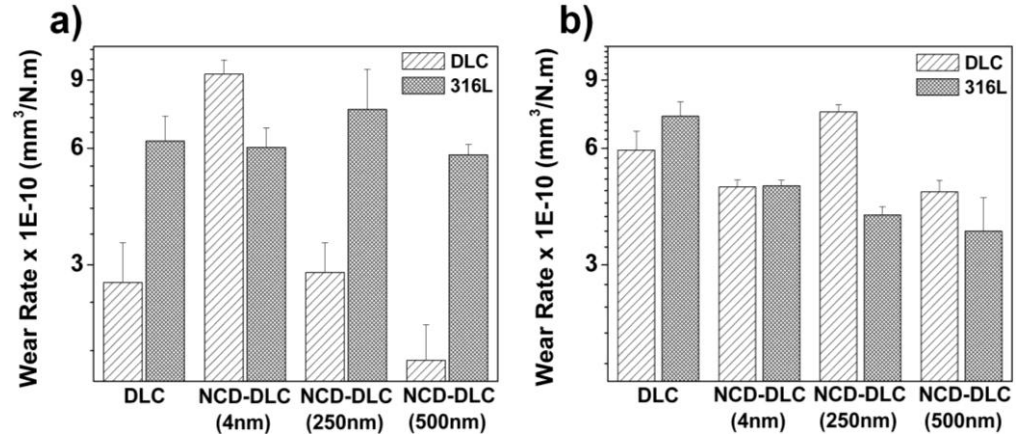

Figure 14. Wear rate from DLC and CD-DLC films in (a) dry air and (b) under saline solution. All the tests were performed varying the counter-body (316L stainless steel or DLC film). The error represents the standard deviation of 3 different measurements.

Copyright © 2012. Nova Science Publishers, Incorporated. All rights reserved.

Diamond-Like Carbon Films, Nova Science Publishers, Incorporated, 2012. ProQuest Ebook Central,

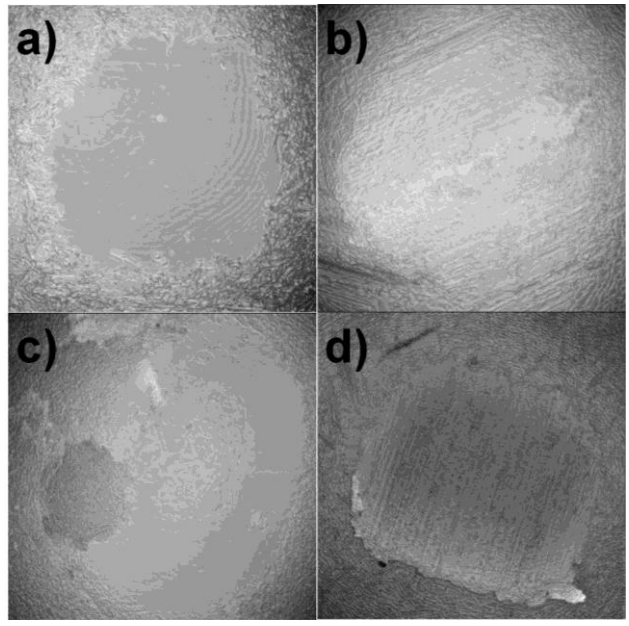

Figure 15. Surface images of the 316L stainless steel ball coated and uncoated with DLC films after tribological tests in air: (a) DLC/CD-DLC(500nm), (b) 316L/CD-DLC(500nm), (c) DLC/CD-DLC(4nm) and (d) 316L/CD-DLC(250nm) pairs. These images represent the best (a-b) and the worst (c-d) results in air. All images acquired from the optical profiler are in the amplification of 50x and represents an area of 0.069 mm^2.

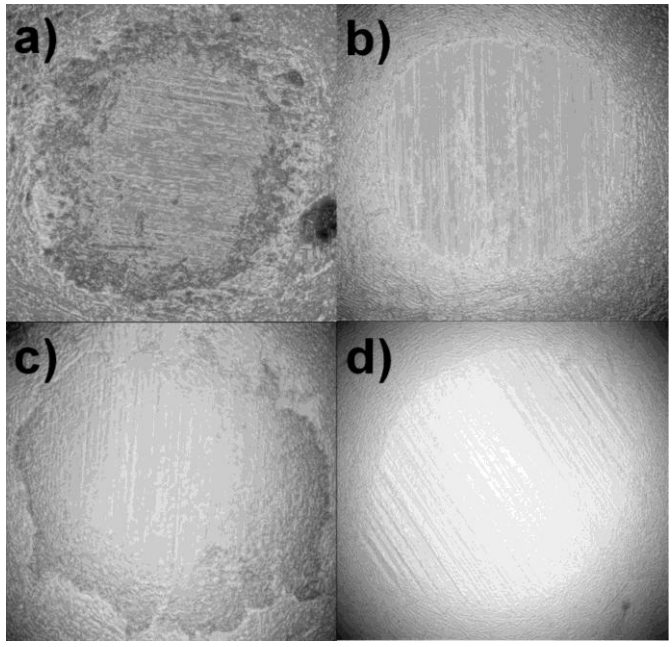

Figure 16. Surface images of the 316L stainless steel ball coated and uncoated with DLC films after tribological tests under saline solution: (a) DLC/CD-DLC(500nm), (b) 316L/CD-DLC(500nm), (c) DLC/CD-DLC(250nm) and (d) 316L/DLC pairs. These images represent the best (a-b) and the worst (c-d) results under saline solution. All images acquired from the optical profiler are in the amplification of 50x and represents an area of 0.069 mm^2.

Copyright © 2012. Nova Science Publishers, Incorporated. All rights reserved.

Diamond-Like Carbon Films, Nova Science Publishers, Incorporated, 2012. ProQuest Ebook Central,

CD particles are known to have low friction coefficient [57]. Despite these hard CD particles that are incorporated in a smoothness film (DLC), the average friction coefficient decreases in all samples under 5% NaCl saline solution, independently of the CD average size and the coated or uncoated counter-body. Hard coatings on a softer substrate can decrease friction and wear by preventing ploughing both on a macro and on a micro scale [58-59]. These coatings typically exhibit residual compressive stresses, which can prevent the likelihood of tensile forces occurring [60]. The reduction of friction coefficients can be explained by the formation of low-shear microfilms on the coating or perhaps only on the asperity tips of the coating [60].

Regarding the wear rate (Figure 14), it is possible to see in Figure 14a (dry air) that the lowest wear rate was obtained from DLC/CD-DLC(500nm) pair, with 37% less wear than DLC/DLC pair. This result suggests bigger particles incorporated in DLC structure helps to sliding the counter-body (in this case, DLC film). However, it is interesting to note that, when the counter-body is uncoated, the wear rate present similar behavior. Under 5% saline solution (Figure 14b) the 316L/CD-DLC(500nm) pair showed 50% less wear rate compared to 316L/DLC pair. When DLC film was used as the counter-body, the CD-DLC(500nm) also present the best result. Bigger CD particles (500 nm) reduced contact pressure (due to increased contact area). In addition, dangling σ-bonds of surface carbon atoms by CD particles can be mainly responsible for reduced friction and wear. These bonds can reduce the extent of adhesive interactions and hence lower friction [61]. Another factor that could explain reducing wear rates in CD-DLC(500nm) films is the formation of third-body from DLC wear that could fill nanospaces between bigger CD particles (500 nm).

Table 4. Summarized Raman spectrum results of DLC and CD-DLC films after tribological tests using 316L stainless steel ball coated with DLC film as counter-body. The error represents the standard deviation of 5 different samples

Pair of samples	Tribological environment	*D* Band Position (cm^{-1})	*G* Band Position (cm^{-1})	FWHM (*D*)	FWHM (*G*)	I_D/I_G
DLC / DLC	Air	1313.6 ± 4.2	1528.1 ± 1.4	244.8 ± 8.3	158.3 ± 1.3	0.50 ± 0.01
	NaCl Solution	1314.4 ± 0.4	1528.4 ± 0.2	253.0 ± 2.0	158.9 ± 1.3	0.50 ± 0.01
DLC / CD-DLC (4 nm)	Air	1328.1 ± 3.3	1532.4 ± 0.4	279.5 ± 2.6	160.0 ± 2.2	0.58 ± 0.02
	NaCl Solution	1328.6 ± 2.8	1532.8 ± 0.8	277.0 ± 2.9	161.4 ± 0.7	0.55 ± 0.02
DLC / CD-DLC (250 nm)	Air	1308.1 ± 1.8	1527.2 ± 0.8	234.9 ± 2.1	159.1 ± 1.8	0.50 ± 0.01
	NaCl Solution	1311.1 ± 1.0	1527.0 ± 1.0	240.4 ± 10.9	158.0 ± 1.4	0.48 ± 0.05
DLC / CD-DLC (500 nm)	Air	1319.0 ± 1.1	1529.3 ± 0.7	263.5 ± 8.6	160.5 ± 0.9	0.50 ± 0.05
	NaCl Solution	1320.8 ± 2.0	1530.1 ± 0.4	263.2 ± 1.8	160.0 ± 1.6	0.48 ± 0.02

Copyright © 2012. Nova Science Publishers, Incorporated. All rights reserved.

Diamond-Like Carbon Films, Nova Science Publishers, Incorporated, 2012. ProQuest Ebook Central,

Table 5. Summarized Raman spectrum results of DLC and CD-DLC films after tribological tests using 316L stainless steel ball uncoated as counter-body. The error represents the standard deviation of 5 different samples

Pair of samples	Tribological environment	*D* Band Position (cm^{-1})	*G* Band Position (cm^{-1})	FWHM (*D*)	FWHM (*G*)	I_D/I_G
316L / DLC	Air	1311.6 ± 4.8	1528.1 ± 1.5	242.8 ± 5.1	158.9 ± 1.6	0.49 ± 0.01
	NaCl Solution	1317.1 ± 0.4	1528.7 ± 0.4	257.7 ± 1.3	157.4 ± 0.4	0.52 ± 0.01
316L / CD-DLC (4 nm)	Air	1326.7 ± 2.2	1532.3 ± 0.2	276.1 ± 7.3	161.2 ± 2.2	0.56 ± 0.03
	NaCl Solution	1330.5 ± 1.4	1532.9 ± 0.4	280.4 ± 6.2	161.9 ± 1.6	0.56 ± 0.03
316L / CD-DLC (250 nm)	Air	1312.3 ± 2.2	1527.3 ± 0.9	233.9 ± 8.4	155.6 ± 2.0	0.49 ± 0.02
	NaCl Solution	1311.1 ± 3.8	1527.6 ± 1.4	247.4 ± 8.9	158.2 ± 1.1	0.51 ± 0.03
316L / CD-DLC (500 nm)	Air	1319.0 ± 0.6	1529.4 ± 0.5	265.0 ± 17.2	160.1 ± 0.8	0.51 ± 0.08
	NaCl Solution	1325.0 ± 3.5	1531.3 ± 0.9	280.7 ± 5.8	161.0 ± 1.0	0.56 ± 0.02

As a comparative, Figure 15-16 show the best and the worst results of wear tests performed in air and under saline solution, respectively. CD-DLC(500nm) films presented the lower wear rate independently of the counter-body, DLC (Figure 15a and 16a) or 316L stainless steel (Figure 15b and 16b), and also in both environments (air and saline solution). This result is in agreement with the electrochemical corrosion tests (Figure 7) in which a superior improvement in corrosion resistance and impedance was observed due to the presence of CD particles of 500 nm average size.

Raman spectroscopy was also performed in the track of tribological tests. Tables' 4-5 show summarized Raman spectrum results of DLC and CD-DLC films after tests in both environment according to the counter-body (DLC (Table 4) or 316L stainless steel (Table 5)). The main factor affecting peaks position, width and intensity is the clustering of sp^2 phase [62]. The full width at half maximum of *G* peak, FWHM(*G*), and *G* peak position both measure disorder, however, FWHM(*G*) is mainly sensitive to structural disorder, while *G* position is mainly sensitive to topological disorder [63]. Structural disorder arises from bond angle and bond length distortions, and topological disorder arises from the size and shape distribution of sp^2 clusters [63]. These results show both *G* band central position and FWHM(*G*) shifted to higher frequencies, indicating an increase of topological and structural disorder. This increase was more evident in the pure DLC films. The wear track spectrum shows the same behavior of the film surface, indicating that the film in the track did not change its structure.

Copyright © 2012. Nova Science Publishers, Incorporated. All rights reserved.

Diamond-Like Carbon Films, Nova Science Publishers, Incorporated, 2012. ProQuest Ebook Central,

CONCLUSION

This chapter shows the production and characterization of the first DLC films containing incorporated crystalline diamond particles. Raman scattering spectroscopy shows CD particles slightly increased sp^3/sp^2 ratio. The presence of bigger CD particles increased the film roughness. CD-DLC films improved DLC and stainless steel electrochemical corrosion resistance. CD particles reduced the pitting corrosion, which is an indication of the chemical inertness of the CD-DLC coatings to the Cl^- ions.

It was investigated the influence of the diamond particle sizes on the electrochemical corrosion resistance of these films. The electrochemical parameters obtained from the potentiodynamic polarization curves and the impedance were correlationated with the qualitative sp^3/sp^2 ratio of the CD-DLC films obtained from Raman scattering spectroscopy. The results show that both protection efficiency and impedance increase with the decrease of I_D/I_G ratio. It means the increase of sp^3 bonds in DLC films reduce its electrochemical corrosion, improving the electrochemical protection efficiency and the impedance.

Also, it was investigated the tribological behavior of DLC and CD-DLC films under environment air and aggressive solution. The CD particles demonstrated to reduce DLC friction and wear. CD-DLC(500nm) films presented the lowest friction coefficient and wear rate under 5% NaCl saline solution. This chapter is part of initial studies but, from the results obtained until now, CD-DLC films can be considered a potential candidate for an anticorrosion material under aggressive environment in industrial applications even when suffer friction.

ACKNOWLEDGMENTS

The authors are very thankful to CNPq and FAPESP for the financial support.

REFERENCES

[1] Loh, W.; Mohamed, R.S.; Ramos, A.C.S. *Energy Fuels* 13, 1999, 323-327.
[2] Loh, W.; Ramos, A.C.S.; Delgado, C.C.; Mohamed, R.S.; Almeida, V.R. *Petrol. Sci. Technol.* 17, 1999, 877-896.
[3] Allen, R.; Robinson, K. *Soc. Pet. Eng.* 1993, 25549.
[4] French, E.C.; Martin, R.L.; Dougherty, J.A. *Mater. Perform.* 28, 1989, 46-49.
[5] Wang, C.; Neville, A. *5th Int. Sym. Oilfield Corrosion*, 2008.
[6] Mischler, S.; Spiegel, A.; Stemp M.; Landolt, D. *Wear* **251,** 2001, 1295-1307.
[7] Jemmely, P.; Mischler S.; Landolt, D. *Tribol. Int.* **32,** 1999, 295-303.
[8] Srdjan, N. *Corrosion Sci.* 49, 2007, 4308-4338.
[9] Azzi, M.; Paquette, M.; Szpunar, J.A.; Klemberg-Sapieha, J.E.; Martinu, L. *Wear* 267, 2009, 860-866.
[10] Pech, D.; Schupp, N.; Steyer, P.; Hack, T.; Gachon, Y.; Héau, C.; Loir, A.S.; Sánchez-López, J.C. *Wear* 266, 2009, 832-838.

Copyright © 2012. Nova Science Publishers, Incorporated. All rights reserved.

Diamond-Like Carbon Films, Nova Science Publishers, Incorporated, 2012. ProQuest Ebook Central,

[11] Snyders, R.; Bousser, E.; Amireault, P.; Klemberg-Sapieha, J.E.; Park, E.; Taylor, K.; Casey, K.; Martinu, L. *Plasma Process Polym.* **4,** 2007, 51-57.
[12] Robertson, J. *Mater. Sci. Eng. R* 2002, 37, 129-281.
[13] Angus, J.C.; Hayman, C.C. *Science* 1988, 241, 913-921.
[14] Shirakura, A.; Nakaya, M.; Koga, Y.; Kodama, H.; Hasebe, T.; Suzuki, T. *Thin Solid Films* 2006, 494, 84-91.
[15] Dearnaley, G. *Clin. Mater.* 1993, 12, 237-244.
[16] Thomson, L.A.; Law, F.C.; Rushton, N.; Franks, J. *Biomaterials* 1991, 12, 37-40.
[17] Lau, S.P.; Li, Y.J.; Tay, B.K.; Sun, Z.; Chen, G.Y.; Ding, X.Z. *Diamond Relat. Mater.* 2001, 10, 1727-1731.
[18] Hussain, S.; Roy, P.K.; Pal, A.K. *Mater. Chem. Phys.* 2006, 99, 375-381.
[19] Schiffmann, K.I.; Fryda, M.; Goerigk, G.; Lauer, R.; Hinze, P.; Bulack, A. *Thin Solid Films* 347 (1999) 60-71.
[20] Nam, N.D.; Lee, S.H.; Kim, J.G.; Yi, J.W.; Lee, K.R. *Diamond Relat. Mater.* 18, 2009, 1145-1151.
[21] Marciano, F.R.; Almeida, E.C.; Lima-Oliveira, D.A.; Corat, E.J.; Trava-Airoldi, V.J. *Diamond Relat. Mater.* 19, 2010, 537-540.
[22] Marciano, F.R.; Almeida, E.C.; Bonetti, L.F.; Corat, E.J.; Trava-Airoldi, V.J. *J. Col. Inter. Sci.* 342, 2010, 636-637.
[23] Zarrabian, M.; Fourches-Coulon, N.; Turban, G.; Marhic, C.; Lancin, M. *Appl. Phys. Lett.* 70, 1997, 2535-2537.
[24] Lian, G.D.; Dickey, E.C.; Ueno, M.; Sunkara, M.K. *Microsc. Microanal.* 8, 2002, 1146-1147.
[25] Zhou, X.T.; Meng, X.M.; Meng, F.Y.; Li, Q.; Bello, I.; Zhang, W.J.; Lee, C.S.; Lee, S.T.; Lifshitz, Y. *Diamond Relat. Mater.* 12, 2003, 1640-1646.
[26] Hsieh, W.J.; Shih, P.S.; Lin, J.H.; Lin, C.C.; Chen, U.S.; Huang, S.C.; Chang, Y.S.; Shih, H.C. *Thin Solid Films* 469-470, 2004, 120-126.
[27] Sakudo, N.; Ikenaga, N.; Yasui, H.; Awazu, K. *Thin Solid Films* 516, 2008, 4483-4486.
[28] Marciano, F.R.; Bonetti, L.F.; Pessoa, R.S.; Massi, M.; Santos, L.V.; Trava-Airoldi, V.J. *Thin Solid Films*, 517, 2009, 5739-5742.
[29] Trava-Airoldi, V.J.; Bonetti, L.F.; Capote, G.; Fernandes, J.A.; Blando, E.; Hübler, R.; Radi, P.A.; Santos, L.V.; Corat, E.J. *Thin Solid Films* 516, 2007, 272-276.
[30] Capote, G.; Bonetti, L.F.; Santos, L.V.; Trava-Airoldi, V.J.; Corat, E.J. *Thin Solid Films* 516, 2008, 4011-4017.
[31] Hayashi, Y.; Krishna, K.M.; Ebisu, H.; Soga, T.; Umeno, M.; Jimbo, T. *Diamond Relat. Mater.* 10, 2001, 1002-1006.
[32] Lee, C.S.; Kim, T.Y.; Lee, K.R.; Yoon, K.H. *Thin Solid Films* 447-448, 2004, 169-173.
[33] Bonetti, L.F.; Capote, G.; Santos, L.V.; Corat, E.J.; Trava-Airoldi, V.J. *Thin Solid Films* 515 (2006) 375-379.
[34] Choi, H.W.; Dauskardt, R.H.; Lee, S.C.; Lee, K.R.; Oh, K.H. Diamond *Relat. Mater.* 17 (2008) 252-257.
[35] G 99 - Standard Test Method for Wear Testing with a Pin-on-Disk Apparatus in ASTM Standards, 2000.
[36] Van Oss, C.J.; Good, R.J.; Chaundhury, M.K. *J. Colloid Interf. Sci.* 111, 1986, 378-390.

Copyright © 2012. Nova Science Publishers, Incorporated. All rights reserved.

Diamond-Like Carbon Films, Nova Science Publishers, Incorporated, 2012. ProQuest Ebook Central,

[37] Roy, P.K.; Choi, H.W.; Yi, J.W.; Moon, M.W.; Lee, K.R.; Han, D.K.; Shin, J.H.; Kamijo, A.; Hasebe, T. *Acta Biomaterialia* 5, 2009, 249-256.
[38] Bendavid, A.; Martin, P.J.; Randeniya, L.; Amin, M.S. *Diamond Relat. Mater.* 18, 2009, 66-71.
[39] Saito, T.; Hasebe, T.; Yohena, S.; Matsuoka, T.; Kamijo, A.; Takahashi, K.; Suzuki, T. *Diamond Relat. Mater.* 14, 2005, 1116-1119.
[40] Zeng, A.; Liu, E.; Annergren, I.F.; Tan, S.N.; Zhang, S.; Gao, J. *Diamond Relat. Mater.* 11, 2002, 160-168.
[41] Liu, C.; Xu, M.; Zhang, W.; Pu, S.; Chu, P.K. *Diamond Relat. Mater.* 17, 2008, 1738-1742.
[42] Kim, H.G.; Ahn, S.H.; Kim, J.G.; Park, S.J.; Lee, K.R. *Diamond Relat. Mater.* 14 (2005) 35-41.
[43] Dorner-Reisel, A.; Schurer, C.; Irmer, G.; Muller, E. *Surf. Coat. Technol.* 177-178, 2004, 830-837.
[44] Sui, J.H.; Zhang, Z.G.; Cai, W. *Nucl. Instr. and Meth. B* 267, 2009, 2475-2479.
[45] Liu, E.; Kwek, H.W. *Thin Solid Films* 516, 2008, 5201-5205.
[46] Ferrari, A.C.; Robertson, *J. Phys. Rev. B* 61, 2000, 95-107.
[47] Sui, J.H.; Gao, Z.Y.; Cai, W.; Zhang, Z.G. *Mater. Sci. Eng. A* 452-453, 2007, 518-523.
[48] Annett, D.R.; Schurer, C.; Irmer G.; Muller, E. *Surf. Coat. Technol.* **177-178,** 2004, 830-837.
[49] Khun, N.W.; Liu, E.; Zeng, X.T. *Corrosion Sci.* 51, 2009, 2158-2164.
[50] Feng, H.P.; Hsu, C.H.; Lu, J.K.; Shy, Y.H. *Mater. Sci. Eng. A* 347, 2003, 123-129.
[51] Zhang, S.; Shibata, T.; Haruna, T. *Corrosion* **54,** 1998, 428-434.
[52] Hashizume, S.; Minami, Y.; Ishizawa, Y. *Corrosion* **54,** 1998, 1003-1011.
[53] Jellesen, M.S.; Christiansen, T.L.; Hilbert, L.R.; Møller, P. *Wear* 267, 2009, 1709-1714.
[54] Eryilmaz, O.L.; Erdemir, A. *Tribol. Lett.* 28, 2007, 241-249.
[55] Liu, Y.; Erdemir, A.; Meletis, E.I. *Surf. Coat. Technol.* **86-87,** 1996, 564-568.
[56] Bremond, F.; Fournier, P.; Platon, F. *Wear* 254, 2003, 774-783.
[57] Casiraghi, C.; Piazza, F.; Ferrari, A.C.; Grambole, D.; Robertson, J. *Diamond Relat. Mater.* 14, 2005, 1098-1102.
[58] Casiraghi, C.; Ferrari, A.C.; Robertson, *J. Phys. Rev. B* 72, 2005, 085401-14.

Copyright © 2012. Nova Science Publishers, Incorporated. All rights reserved.

Diamond-Like Carbon Films, Nova Science Publishers, Incorporated, 2012. ProQuest Ebook Central,

Copyright © 2012. Nova Science Publishers, Incorporated. All rights reserved.

Diamond-Like Carbon Films, Nova Science Publishers, Incorporated, 2012. ProQuest Ebook Central,

In: Diamond-Like Carbon Films
Editor: Yuto S. Tanaka
ISBN: 978-1-61324-791-4
© 2012 Nova Science Publishers, Inc.

Chapter 6

DLC THIN FILMS GROWTH IN THERMIONIC VACUUM ARC TECHNOLOGIES: TVA AND GTVA

***Rodica Vladoiu*[*], *Victor Ciupina*[‡], *Mirela Contulov*[≠], *Virginia Dinca*[£], *Aurelia Mandes*[¥] *and Madalina Prodan*[±]**
Ovidius University, Constanta, Romania

ABSTRACT

This work presents the comparative results concerning the surface free energy information processing, the reflective index, the hardness, and the morphology to provide a coherent description of the Diamond like Carbon films synthesized by Thermionic Vacuum Arc (TVA) and Gaseous Thermionic Vacuum Arc (GTVA). While in the TVA method the anode is solid, being suitable for deposition of the practically any solid material, the GTVA method enables the growth of DLC coatings using CH4 as gas precursor, in vacuum conditions. The main operational differences as well as the similarities between the two technologies are pointed out in this chapter, underlying the advantages in the development of advanced materials.

INTRODUCTION

The aim of this paper is to highlight what is known about the characteristics of an original method of deposition used for solid materials - Thermionic Vacuum Arc (TVA) - in order to extend it for a new class of materials used as precursors (gases) which lead to another technique namely Gaseous Thermionic Vacuum Arc (GTVA). We will present a comparative

[*] E-mail address: rvladoiu@univ-ovidius.ro
[‡] E-mail address: vciupina@univ-ovidius.ro
[≠] E-mail address: mcontulov@univ-ovidius.ro
[£] E-mail address: vdinca @univ-ovidius.ro
[¥] E-mail address: amandes @univ-ovidius.ro
[±] E-mail address: mprodan @univ-ovidius.ro

Copyright © 2012. Nova Science Publishers, Incorporated. All rights reserved.

Diamond-Like Carbon Films, Nova Science Publishers, Incorporated, 2012. ProQuest Ebook Central,

discussion of the many DLC' properties that have been reported and in particular those that are very important for some applications. Although TVA has been already investigated in order to control over the sp^2/sp^3 ratio by tuning plasma parameters [1] and to have an overview of structure, surface free energy evaluation, tribological properties [2-3], GTVA proved to be another versatile method of carbon deposition, with an interesting mechanism. The results presented here could have a great impact on the development of advanced materials and many manufacturing industries, as well as expanding the technologically important field of interface science where the control of the film – substrate interface would be critical. Also the main operational differences between the two technologies will be also pointed out in this chapter.

EXPERIMENTAL DETAILS

TVA technology is based on the localized ignition of the arc plasma in vacuum conditions, between the anode and the heated cathode. The plasma arc discharge is obtained by bombardment of the electrons emitted by the filament from inside of a Wehnelt cylinder directed towards the anode. On application of a positive DC high voltage on the anode, the electrons are accelerated, heating of the anode material until to the first vapors. By increasing the applied voltage the accelerated electrons are producing more vapors of the anode material and by fast electron – neutrals collisions, the first ions also appear. At a certain value of the applied voltage, ignition of arc plasma is obtained in the vapors of the anode material.

The extension of Thermionic Vacuum Arc technology to coatings using gases or evaporable liquids as in the case of GTVA instead of solid materials is of great interest especially for DLC's growth.

Electrodes Configuration

The schematical diagram of the TVA and GTVA technologies used for carbon deposition is presented in Fig 1. The **cathode** consists of a heated tungsten filament surrounded by a molybdenum Whenelt cylinder, which focuses the electrons on the anode surface. The refractory metal cathodes are used to provide an adequate thermo-electronic emission, which ensures enough density of evaporated atoms in the interelectrodic space to ignite the discharge. The symmetry of the cathode – anode arrangement allows a perpendicular bombardment of the electron beam on the anode surface. The cathode and the vacuum chamber are grounded, so that the potential difference between the interelectrodic plasma and the enclosure is equal to the cathodic fall. Therefore, the ions produced into the plasma will reach the wall of the metallic chamber with an energy direct proportional with the cathodic fall.

A hydrogen-free carbon rod was used as **anode** in the case of TVA while for G-TVA the anode consists from a stainless-steel piece provided with a tubing necessary to connect the anode to an out vacuum chamber gas source. Inside of the hole of the stainless steel piece is mounted a disk of sintered metal powder. A peculiarity of the G-TVA discharge is the critical value of the interelectrodic distance. For distances lower than 3 mm a cold cathode discharge

Copyright © 2012. Nova Science Publishers, Incorporated. All rights reserved.

Diamond-Like Carbon Films, Nova Science Publishers, Incorporated, 2012. ProQuest Ebook Central,

can be ignited. For distances higher than this critical distance we will have a true G-TVA discharge due to the heating of the cathode. In this case, the G-TVA discharge is sustained by the thermo-electron emission current from the cathode.

It has to be mentioned that in the TVA technology, as well as in the GTVA method plasma is localized, so it does not fill the whole chamber. In this way the substrate can be protected against the thermal heat of the plasma by placing it away from the core of plasma.

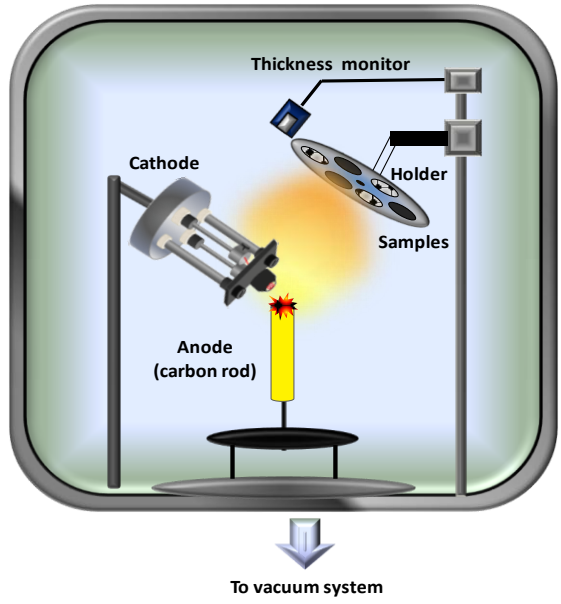

Figure 1.a. Schematic view of the TVA experimental setup.

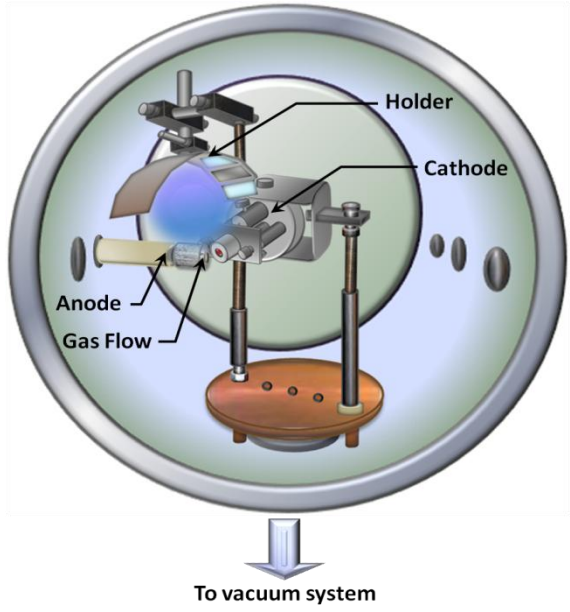

Figure1.b. Schematic view of the GTVA experimental setup.

Copyright © 2012. Nova Science Publishers, Incorporated. All rights reserved.

Diamond-Like Carbon Films, Nova Science Publishers, Incorporated, 2012. ProQuest Ebook Central,

The main experimental parameters involved in this comparative study are presented in Table I. There are several identical parameters to be taken into account, like electrical and geometrical parameters, but we should pay attention to other specific parameters. For instance, in the case of GTVA technology, the size and porosity of the sintered filter play an important role on the properties of the film. Nevertheless, the type of the gas – in our case methane- and the value of the gas flow are also crucial in order to maintain a stable discharge, taking into account that the pumping system is on.

Table 1. The main parameters for DLC thin films synthesis by TVA and GTVA methods

Method	TVA	GTVA
Electrical parameters	I_f – the intensity of the current of the heating filament I_{arc} – the intensity of the vacuum arc discharge current U_{arc} – the discharge voltage	
Geometrical parameters	φ – the angle between the cathode's axis and the anode d_{A-C} – the anode – cathode distance d_{A-S} –the anode – sample distance	
Specific parameters	Nature of the material The melting point of the material The crucible used as anode	Type of the used gas Size and porosity of the sintered filter Gas flow

RESULTS AND DISCUSSION

The stable G-TVA regime, with localized plasma, is obtained just for a certain threshold value of the current filament for a given interelectrodic distance, regardless of the applied voltage arc type discharge takes place. In the case of G – TVA, the ignition yields faster, because the power supply voltage has not to produce also the gas necessary to sustain the discharge (as in the case of solid anode – TVA), the state of gas being already achieved. The fresh methane is fed to vacuum chamber through this tubular anode, which is connected to gas sources outside of vacuum chamber.

Both type of discharges offer following advantages for thin carbon layer depositions:

- high rate of deposition up to 100 nm/s;
- no buffer gas is necessary;
- very low thermal energy transfer;
- deposited thin film layers are smooth, compact and of very fine structures;
- very stable discharge conditions;
- no cathode' impurities can be found in deposited thin films;
- low mechanical stress of the deposited layer;
- good adherence.

The deposited thin films have been investigated in terms of free surface energy, thickness, refractive index, hardness and morphology.

The free surface energy was determined by the measurement of the contact angle performed with a contact angle measuring device Surface Energy Evaluation System (See

Copyright © 2012. Nova Science Publishers, Incorporated. All rights reserved.

Diamond-Like Carbon Films, Nova Science Publishers, Incorporated, 2012. ProQuest Ebook Central,

System) using sessile drop contact angle measurements. This method represents a sensitive tool for assessing hydrophobicity or hydrophilicity of a surface by determination of the tangent angle between the liquid – solid interface and solid – vapour interface. [4]

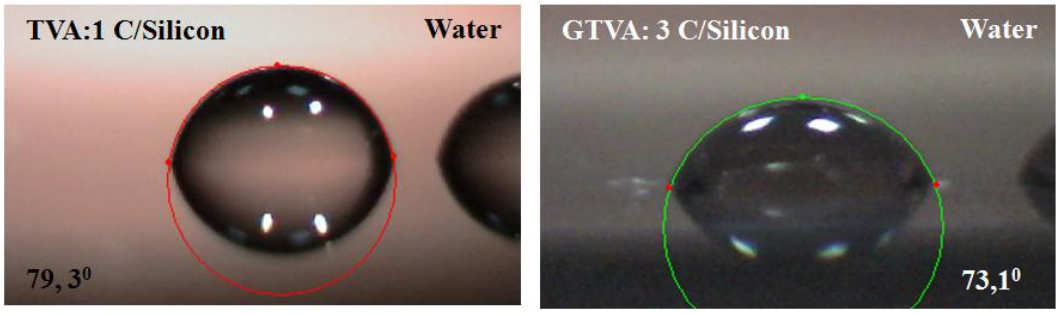

Figure 2. Pictures of the drops shape taken during the analysis.

Fig. 2 presents two pictures taken during the measurement of the contact angle on different samples (By TVA method C/Silicon and GTVA method 3C/Glass) for the most polar liquid, i.e. water.

Table 2. Measured contact angles Θ for samples obtained by TVA and G-TVA methods

Method	Sample no.	Θ_{Water} [⁰]	$\Theta_{Formamide}$ [⁰]	$\Theta_{Ethylene\ glycol}$ [⁰]
TVA	1 C/Silicon	79,6±0.3	59,3±0.6	52,5±0.5
	2 C/Glass	69,4±0.9	50,6±0.8	50,3±0.9
G-TVA	3C/Silicon	73.5±0.4	58.7±0.7	55.6±0.3
	4 C/Glass	88.3±0.4	78.4±0.4	65.7±0.6

Table 3. Surface free energy components obtained by Owens-Wendt Regression model

Method	Sample no.	γ_{total} [mJ/m^2]	γ^d [mJ/m^2]	γ^p [mJ/m^2]
TVA	1 C/Silicon	32,9	25,5	7,4
	2 C/Glass	30,7	24,2	7,8
G-TVA	3C/Silicon	31,8	17,4	14,4
	4 C/Glass	22,4	14,8	7,6

Table 4. Measured thickness and refractive index of the films

Method	Sample no.	Thickness (nm)	Refractive index
TVA	1 C/Silicon	48	1,7
	2 C/Glass	63,2	2,2
G-TVA	3 C/Silicon	48,8	1,8
	4 C/Glass	62,4	2,3

The refractive index of the films was performed by Filmetrics Model F20 Thin Film Analyzer based on spectral reflectance method. This device uses the spectral reflectance

Copyright © 2012. Nova Science Publishers, Incorporated. All rights reserved.

Diamond-Like Carbon Films, Nova Science Publishers, Incorporated, 2012. ProQuest Ebook Central,

measurements as optical technique. Spectral reflectance measures the amount of light reflected from the film over a range of wavelengths with the incident light perpendicular to the sample surface. The measured films must be optically smooth and within the thickness range set by the system configuration requirements.

Mechanical properties of the thin films were investigating using the Fischerscope H100 tester and the Ultrananoindenter (UNHT) equipment with two types of indenter: Vickers and Berkovich. Moreover, the influence of substrate material on the results of the indentation tests was performed.

The indentation tests were provided in a wide load range in order to study the indentation response of the film/substrate system from near surface up to the film/substrate interface. In Figure 3 is an example of the dependence of the sample hardness and elastic modulus on the indentation load for sample 3C prepared by means of the GTVA deposition technology using methane as the hydrocarbon source is shown. The substrate material was single crystal silicon.

The results presented in Figure 3 were obtained by means of depth sensing indentation technique from analysis of loading and unloading curves. At least 15 indents were carried out for each testing load in the rage from 2 to 40mN. The indentation hardness and elastic modulus values were calculated on the basis of the Oliver-Pharr (O&P) method [5]. The resulted values were averaged and the 95% confidence level was determined. The measured hardness values decreased with the increasing indentation load due to substrate influence (hardness of the silicon substrate was 13 GPa).

The maximum value of the sample hardness H = 23,5 GPa was obtained in indentation depths, which were approximately equal to 20% of the film thickness (d = 80 nm). The elastic modulus was almost constant in the range from 2 to 40 mN (see Figure 2). The substrate elastic modulus was 157 GPa, that means that the film modulus (162 GPa) differed only slightly from the substrate elastic modulus, therefore it did not influence the results of depth sensing indentation test. In Figure 4 the dependence of the differential hardness on the indentation depth is shown. The differential hardness H_{dif} is given by the relation: $H_{dif} = k\partial L/\partial(h^2)$, where L is the load, k is geometric constant and h is the indentation depth and represents the ratio of the small load increase and the corresponding change in contact area of the indenter and the tested material.

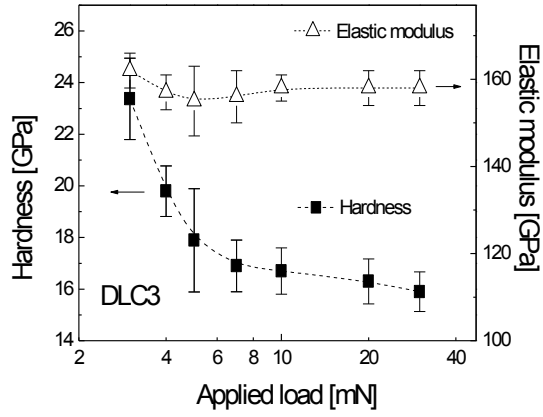

Figure 4a. The dependence of film hardness and elastic modulus on the indentation load for 3C sample.

Copyright © 2012. Nova Science Publishers, Incorporated. All rights reserved.

Diamond-Like Carbon Films, Nova Science Publishers, Incorporated, 2012. ProQuest Ebook Central,

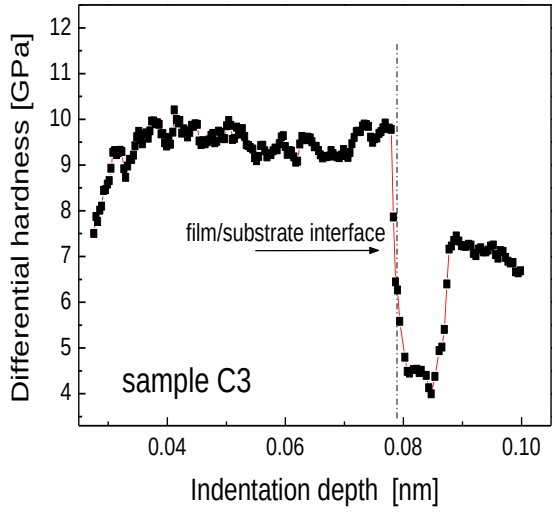

Figure 4b. The dependence of differential hardness on the indentation depth obtained for 3C sample

The differential hardness H_{dif} on the indentation depth is very sensitive to any changes in the material during the indentation test. In Figure 3 H_{dif} shows an abrupt change (jump in differential hardness values) achieving the indentation depth of 80 nm. This change was caused by abrupt change in hardness at the film/substrate interface. On the basis of the differential hardness dependence we can conclude, that the film fracture toughness was very high, because the film could withstand indentations with depths approaching the film thickness without cracking and delamination.

In Figure 5 the results of mechanical properties obtained for sample C3 by DMA method are shown. The dynamic measurement system applies a load to the indenter tip to force the tip into the surface while simultaneously superimposing an oscillating (sinus) force with the force amplitude generally several orders of magnitude smaller than the nominal load.

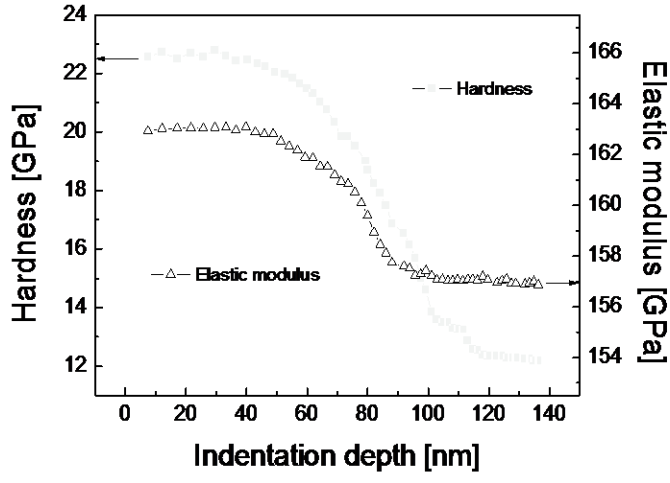

Figure 5. Hardness and elastic modulus dependences on the indentation depth obtained for 3C sample using DMA method (UNHT).

Copyright © 2012. Nova Science Publishers, Incorporated. All rights reserved.

Diamond-Like Carbon Films, Nova Science Publishers, Incorporated, 2012. ProQuest Ebook Central,

The tester analyses the dynamic response of the material, therefore it is possible to record continuously the depth dependence of the indentation hardness H and the indentation modulus E during the whole indentation period.

In case of dynamic measurement the maximum load was 10 mN, the load and the depth sensitivity were 0.001 μN and 0,001 nm, respectively. The amplitude of oscillating force was 50 μN and the oscillating frequency was 10 Hz. The studied samples did not exhibit time-dependent plasticity, so the storage modulus was found to be zero in the frame of the experimental errors.

The morphology of the films have been performed using Transmission Electron Microscopy (TEM) performed on a Phillips CM 120 ST (acceleration voltage of 120 kV) TEM with a resolution point of 1.4 Å and a magnification of 1.2 million times.

The intrinsic nonhomogeneity of the carbon nanostructured materials requires the use of characterization methods with a very high resolution. One of the best characterization device available is transmission electron microscopy (TEM), preferably high-resolution TEM (HRTEM). Other techniques were SAED (Selected Area electron Diffraction) and FFT (Fast Fourier Transform).

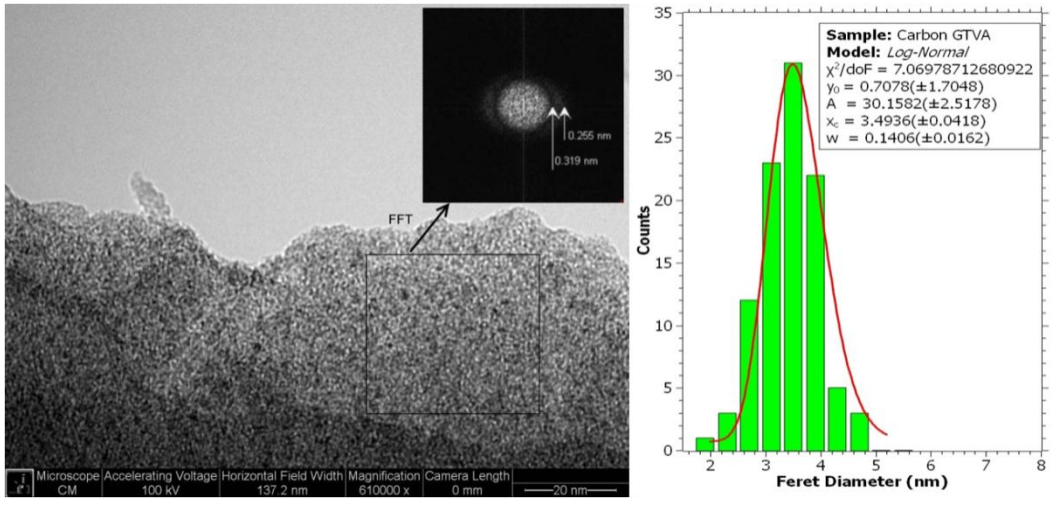

Figure 6. HR-TEM images of a Carbon film obtained by GTVA at 20 nm scale (left) and Grain size distribution (right).

A large number of crystallite inclusions inside the amorphous Carbon film *with diamond spherical grain* were observed by BF-TEM (Bright Field Transmission Electron Microscopy) (145kx working magnification) shaded correction and median filtered (Fig.7). Amorphous character of film are exibit by large background noise. Some crystalline intensities can be observed in diffraction pattern and can be indexed using graphite structure. (Spacial grup P63mc, a=0.254 nm, c=0.696nm).

Copyright © 2012. Nova Science Publishers, Incorporated. All rights reserved.

Diamond-Like Carbon Films, Nova Science Publishers, Incorporated, 2012. ProQuest Ebook Central,

CONCLUSIONS

The G – TVA method was introduced as a very powerful technique for thin carbon film deposition. In this way, the wettability of a:C-H films deposited by G-TVA technology can be controlled by the plasma parameters. The hydrogenated carbon films synthesized by G-TVA method have a strong hydrophobic character, with good adhesion due to the diffused interface dominated SFE.

From HRTEM image associated with grain size distribution by Log Normal function, the structure of the film reveals nanocrystallites of 3.5 nm embedded in amorphous carbon film. The prepared carbon films were smooth and pinhole-free and have appropriated index of refraction and similar values for contact angle if the intensity of the filament current is the same.

They exhibited good fracture toughness, wear resistance and adhesion to the silicon and carbon substrates. Potential applications might be in the fields of bio-medicine, material science, microelectronic technology and could have a great impact on the development of advanced nanostructured materials

ACKNOWLEDGMENTS

This work was supported by the strategic grant POSDRU/89/1.5/S/58852, Project „Postdoctoral programme for training scientific researchers" cofinanced by the European Social Found within the Sectorial Operational Program Human Resources Development 2007 – 2013

REFERENCES

[1] C. Surdu Bob, R. Vladoiu, M. Badulescu, G. Musa, *Diamond and Related Mater.*17, 1625 (2008).
[2] R. Vladoiu, V. Dinca, G. Musa, *Eur. Phys. J. D* 54, 433 (2009).
[3] R.Vladoiu, V. Ciupina, M. Contulov, A Mandes, V. Dinca, G. Prodan, C. P. Lungu,
[4] *J. Optoelectron Adv. M.* 12, 553 (2010).
[5] Bursikova V, St'ahel P, Navratil Z, Bursik J and Janca J 2004 *Surface energy evaluation of plasma treated materials by contact angle measurement*, Vyd. 1 st. Brno: Masaryk University Brno
[6] G.M. Pharr, W.C. Oliver, F.R. Brotzen, *J. Mater. Res.* 7 (1992) 613.

Copyright © 2012. Nova Science Publishers, Incorporated. All rights reserved.

Diamond-Like Carbon Films, Nova Science Publishers, Incorporated, 2012. ProQuest Ebook Central,

Copyright © 2012. Nova Science Publishers, Incorporated. All rights reserved.

Diamond-Like Carbon Films, Nova Science Publishers, Incorporated, 2012. ProQuest Ebook Central,

In: Diamond-Like Carbon Films
Editor: Yuto S. Tanaka
ISBN: 978-1-61324-791-4
© 2012 Nova Science Publishers, Inc.

Chapter 7

HARD CR-CONTAINING DIAMOND-LIKE CARBON FILMS IN MID-FREQUENCY DUAL-MAGNETRON SPUTTERING

Yu Xiang[1], Wang Cheng-biao[1], Liu Yang[2] and Yu De-yang[2]
[1] School of Engineering and Technology,
China University of Geosciences, Beijing, China
[2] Beijing Powertech Co. Ltd., Beijing, China

ABSTRACT

Diamond-like carbon (DLC) films have been extensively studied over the last two decades and applied as a good candidate for various sliding machine compnents and cutting tools, etc, due to their unique combined properties of high hardness, smooth surface and chemical inertness. Their inherent high compressive stresses induced during synthesis of their diamondlike content (sp^3 carbon bonding), resulting in a low adhesion strength (especailly with ferrous substrates) and a thickness limit of 1μm, and their thermal stability, thermally unstable beyond 350 ^{o}C, are two major drawbacks of DLC films.

Thereby, many scientific researches in the past decade have been concentrated on synthesizing metal-containing DLC (Me-DLC) films to overcome the two major drawbacks and, in turn, to improve the mechanical and sliding tribological behavior of DLC films. A number of studies on synthesis and characterization of Me-DLC films have been conducted, and their studies mainly emphasized on Ti, W, Ta, and Cr containing DLC, especially on Ti and W. Although chromium has been used as carbide former and possesses attractive properties of combined hardness and ductility, available work in this area is still rather lacking and it is even rarer in mid-frequency dual-magnetron sputtering deposition.

The purpose of this chapter is to intiate a systematic study of the processing-structure-property relationship in hard Cr-DLC films by a mid-frequency dual-magnetron sputtering system. The overall objective is to illustrate how to use methods of multilayer, gradient transitional layer, and doping to alleviate the two drawbacks, and then to synthesize an adherent thick Cr-DLC films of hard-and-lubricated property (micorhardness > 20 GPa, coefficient of friction < 0.2).

Copyright © 2012. Nova Science Publishers, Incorporated. All rights reserved.

Diamond-Like Carbon Films, Nova Science Publishers, Incorporated, 2012. ProQuest Ebook Central,

This chapter is divided into four sections. Section 1 deals with using the system to prepare the Cr-DLC films that exhibited some combined superior properties: high hardness of 30~46 GPa, good adhesion of critical load of 50~65 N, and friction coefficient about 0.1 in air condition. Section 2 deals with comparing the mechanical and tribological propertis of some Cr-DLC films whose puttering sources had three optional power modes of continuous DC, pulsed DC and AC (40 kHz). Section 3 deals with a Cr-DLC film whose thickness up to 6 μm. Section 4 deals with the infulence of synthesizing method, Cr content, C/Cr nanocrystalline size, on the micorstructure and properties of hard Cr-DLC nanocompoiste films. In some cases, the presentation of experimental results is accopanied by a brief intorduction of the technique, so that non-experts will also be able to understand the main message of the proposed case.

SECTION 1: HARD AND SUPERHARD CR-CONTAINING DIAMOND-LIKE CARBON FILMS

1. Introduction

Due to having some prominent tribological properties such as high hardness, low friction coefficient and high wear resistance, diamond-like carbon (DLC) films are of great interest for usages of wear-resistant films on cutting tool, forming die etc. Accordingly, numerous studies on quality improvement of such film have been made in various techniques, e.g. arc evaporation, HF-plasma or microwave-plasma CVD and unbalance magnetron sputtering [1]. Hydrogenated DLC film has limited microhardness due to inclusion of H atoms. A main limitation in hydrogen-free DLC film applications is its poor adhesion to steel substrates due to high residual stress in the DLC films and/or the large discrepancy of mechanical properties between the DLC films and steel substrates [2]. Some studies have attempted to improve the adhesion between DLC film and its substrates by applying adherent layer such as B and Ti to the film interface [3]. Methods enhancing the mechanical properties were also reported, such as doping TiN, TiCN and TiC layers in DLC matrix [4]. A graded composition and microstructure may be used to improve adhesion and microhardness of the graded film. In this section, several multilayered and graded DLC films with a single-phase homogeneous carbon layer were synthesized by selectively using C and Cr targets in a mid-frequency dual-magnetron sputtering.

The pulsed plasma technique was applied to both magnetron drives and substrate bias in this experiment. Resent studies demonstrated that mid-frequency (20-100 kHz) magnetron sputtering offered some advantages over traditional DC magnetron sputtering for deposition of metastable films like DLC and CNx [5]. Pulsing the discharge can significantly modify the characteristics of magnetron plasma, pulsing the substrate bias voltage can increase the ion current drawn at the substrate, which have some important effects on properties of the metastable films [6].

Focusing on improving properties of the hydrogen-free DLC film by controlling process parameters like target current, substrate bias voltage and etc. during the mid-frequency dual-magnetron sputtering. Structure, deposition process and resulting properties of the DLC film are investigated.

Copyright © 2012. Nova Science Publishers, Incorporated. All rights reserved.

Diamond-Like Carbon Films, Nova Science Publishers, Incorporated, 2012. ProQuest Ebook Central,

2. Experimental Details

Cr-doped hydrogen-free DLC films were deposited by unbalanced dual-magnetron sputtering in a coating rig SP8050 (Beijing Powertech Co. Ltd.), whose cross-sectional view is schematically shown in Figure 1. As can be seen, four pairs of dual-magnetron targets including two chromium (Cr) and six graphite (C) ones were set in the cylindrical coating rig. Two planar magnetrons of each pair of dual-magnetron targets were placed in vacuum chamber in face-to-face configuration approximately 70 cm apart, respectively. The substrate holder was placed in center area. A unipolar-pulse DC power supply on the substrates and four pulsed AC power supplies of 40 kHz, on each pair of dual-magnetrons, were used to control the substrate bias voltage, substrate bias current and target power. The duty ratio of the pulsed substrate bias voltage was 80 % in Ar ion cleaning and then was kept at 60 % in the following deposition processes. The mid-frequency power supplies used a current-constant mode to control the magnetron targets at constant values like 2, 4 and 6 A, respectively, corresponding to target power increased from 2 to 8 kW and target voltage from 200 to 800 V. The C and Cr targets had a uniform size of 420×80×8 mm^3 and a purity of 99 %. Argon gas was introduced through each target to enhance sputtering of the targets. Process parameters in each procedure could be automatically controlled by PLC (Programmable Logical Controller) through presetting.

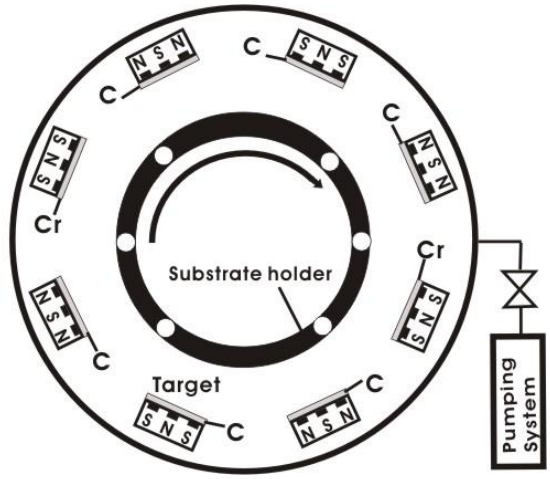

Figure 1. Schematic diagram of cross-sectional coating rig SP8050.

Sheets of M2 high-speed steel (HSS) in an uniform size of 20×20×3 mm were used as coupons for mechanical and tribological tests, and some coupons of Si(100) wafers in an uniform size of 8×8×0.2 mm^3 were used for cross-sectional SEM and Raman tests. Surfaces of the steel sheets were mirror polished to surface roughness of Ra 0.05 μm. All coupons were ultrasonically cleaned in acetone bath for 20 min, and the cleaned coupons were then blown by dry nitrogen.

After pumping down by a turbo-molecular pump to a base pressure of 2.0×10^{-3} Pa and before depositing, surfaces of the coupons were further cleaned by Ar ion bombardment under the bias voltage of - 800 V at pressure of 3.0 Pa for 15 min, in order to remove some adhering impurities on substrates.

Copyright © 2012. Nova Science Publishers, Incorporated. All rights reserved.

Diamond-Like Carbon Films, Nova Science Publishers, Incorporated, 2012. ProQuest Ebook Central,

After the substrate was heated to 100 °C, deposition process was started in condition that the depositing pressure was maintained at 0.3 Pa in argon atmosphere. The deposition procedures included three optional steps: firstly, Cr interlayer about 0.2 μm on the substrate was sputtered from two Cr targets; secondly, transitional layer of Cr_xC_y about 1 μm on Cr interlayer was co-sputtered from two Cr and six C targets, where Cr target current was decreased from 10 A to 1 A and C target current increased from 2 A to 6 A, continuously; thirdly, top DLC layer about 1 μm was sputtered from six C targets.

Scanning electron microscope (SEM) combined with energy-dispersive X-ray (EDX) analyzer, Quant 200, was used to investigate the morphologies and elemental compositions. Raman spectroscope, PHI-6100/SAM, was used to investigate the microstructure. Nanoindenter (MML[·] Nanotester 600) and scratch tester (LICP-CAS SW-97) were used to investigate the microhardness and adhesion, respectively. Ball-on-disk tester (LICP-CAS DD-92) was used to investigate the friction and wear property under conditions: DLC film was deposited on the disc, and counterpart ball used is a Φ6 mm Al_2O_3 ball; ambient air atmosphere; applied loads of 1 N, 2 N and 5 N; rotated speed constant at 1000 r/min, equal to 0.6 m/s of linear speed; tested time about 15 min. Optical microscope attached with a camera was used for analysis of wear traces.

3. Results

Properties of the graded DLC film in unbalanced magnetron sputtering show a strong dependence on flux and energy of ion bombardment during growth of the film [7]. According to our experimental results of mid-frequency dual-magnetron sputtering, the substrate bias current, an index of ion flux, had some close correlations with process parameters, such as: target power, substrate bias voltage, substrate temperature and gas pressure. For example, in condition that target power was 6 kW or substrate bias voltage was –250 V at substrate temperature less than 150 °C and argon pressure of 0.3 Pa, the substrate bias current had a high value of 5 A for the carbon deposition. This value could be even higher with increasing argon pressure from 0.3 Pa to 1 Pa and substrate temperature from 150 °C to 450 °C. The energy of ion bombardment was increased with the increasing bias voltage. For a convenient operation, the properties of DLC films were controlled by adjusting the target current and substrate bias voltage, under condition that the substrate temperature and sputtering pressure were fixed in this experiment.

Surface and cross-section SEM images of DLC films deposited at –100 V of the pulsed bias voltage are shown in Figure 2. As shown in Figure 2a, the film showed a very smooth morphology with no visible loose particles from the targets, whose average surface roughness, Ra, is about 4 nm. This is attributed to high ion current density of the mid-frequency dual-magnetron sputtering. During unbalance magnetron sputtering on precise forming die, substrate arcing is somewhat inevitable [8]. If the localized surface arcing persists, some droplets and holes from the running arcs may make the die unusable. The mid-frequency magnetron sputtering may be an effective method to reduce the defects induced by substrate arcing. In Figure 2b, the multilayered and graded structure, containing layers of Cr, C_xCr_y and DLC, can be observed.

[·]MML: Micro Materials Limited. LICP-CAS: Lanzhou Institute of Chemical Physics, Chinese Academy of Science

Copyright © 2012. Nova Science Publishers, Incorporated. All rights reserved.

Diamond-Like Carbon Films, Nova Science Publishers, Incorporated, 2012. ProQuest Ebook Central,

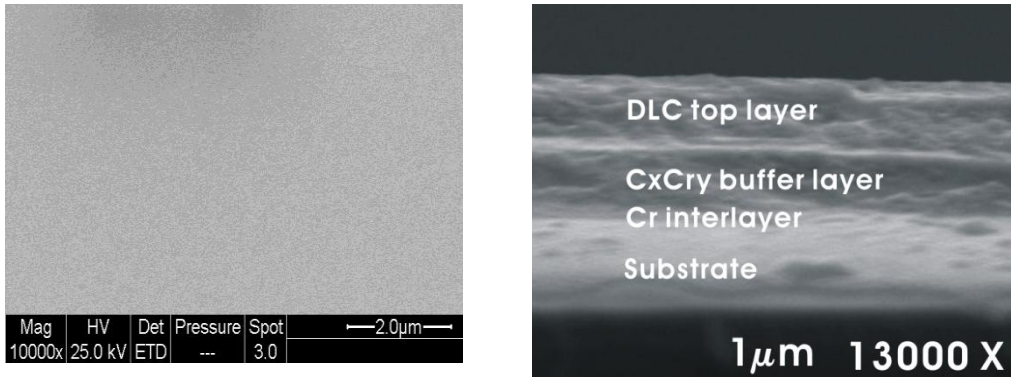

(a) Surface image (b) Cross-sectional image

Figure 2. Surface and cross-section SEM images showing structure of Cr-doped DLC film on Si wafer.

Apart from the imperfect smoothness of cross-section surface due to sampling difficulty, interfaces between each layer of the graded DLC film were well bonded without any visible flaw, of which C_xCr_y layer were embedded in DLC matrix. Such graded structure may be used to cope with the residual stress in DLC film and the large discrepancy of physical properties between DLC film and the substrate. The integral structure of graded DLC film is dense and compact, which is vital in achieving high hardness for wear resistance. As shown in Figure 3, the characteristic D and G bands of DLC film were investigated by Raman spectroscopy, and D-to-G bond ratio of I_D/I_G is 1.74, which coincides with the result of microhardness measurement. DLC layer was supported by a hard transitional layer of C_xCr_y. Similar to report by S. Yang [9], the metal Cr and Cr-C doping layers bolstered the stress management in hard a-C films. In this way, the stress state of metal-doped DLC film could be stepwise adjusted in graded structure from outer boundary through multilayer to inner boundary and substrate by specified process control.

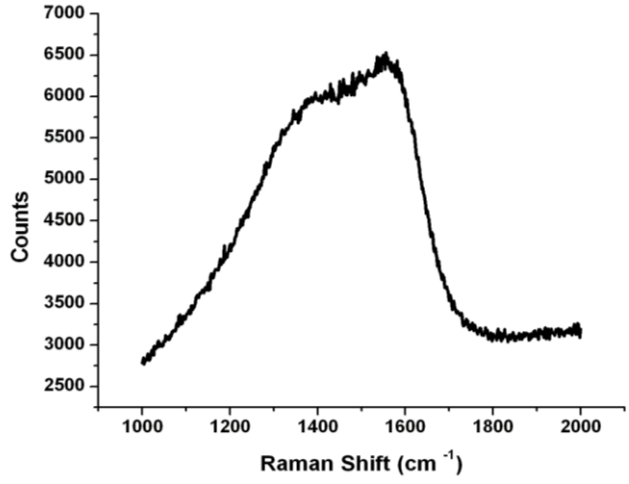

Figure 3. A typical Raman spectrum of DLC film deposited at –100 V of pulsed bias voltage.

Copyright © 2012. Nova Science Publishers, Incorporated. All rights reserved.

Diamond-Like Carbon Films, Nova Science Publishers, Incorporated, 2012. ProQuest Ebook Central,

Deposition rate of the DLC film was high, more than 0.8 μm/h, which was about twice of reported one using traditional sputtering [10]. The deposition rate was closely related with target power in this current-constant mode and thus could be controlled. When the biasing voltages was at –100, -150, and –200 V, meanwhile carbon target current kept constantly at 2 A corresponding to about 2 kW of target power, the deposition rates were measured at 0.96, 0.94 and 0.87 μm/h, respectively. When the C target currents was at 2, 4 and 6 A, meanwhile the bias voltage kept at –100 V, the deposition rates were measured at 0.96, 1.06, 1.14 μm/h, respectively. Above results were obtained in such condition: compared with chromium, carbon deposition rate was relatively low owing to the low sputtering yield of graphite. However, if the biasing voltage exceeded –200 V or the target current exceeded 6 A in above condition, the deposition rate was not increased and may be decreased little due to too intense ion bombardment, similar results can be seen in literature [11].

To accurately measure microhardness of DLC film in micron-scale thickness, a two-step penetration method in nanoindenter tests was used, i.e., after obtaining the test results of large-load, a penetration load range could be determined to ensure that range of deformation under the indenter was within DLC layer and did not extend into the transitional layer or substrate. As shown in Figure 4, microhardness of the hydrogen-free DLC films is between 34 GPa and 46 GPa. The microhardness value is higher than that of hydrogen carbon films (a-C:H) and a-C films, as reported in literatures [12]. The compactness of DLC film may contribute to such improved microhardness. The microhardness value increases with the increasing bias voltages, a typical result of increased residual stress by ion bombardment [13-14]. Target current also shows a clear effect on microhardness of the film.

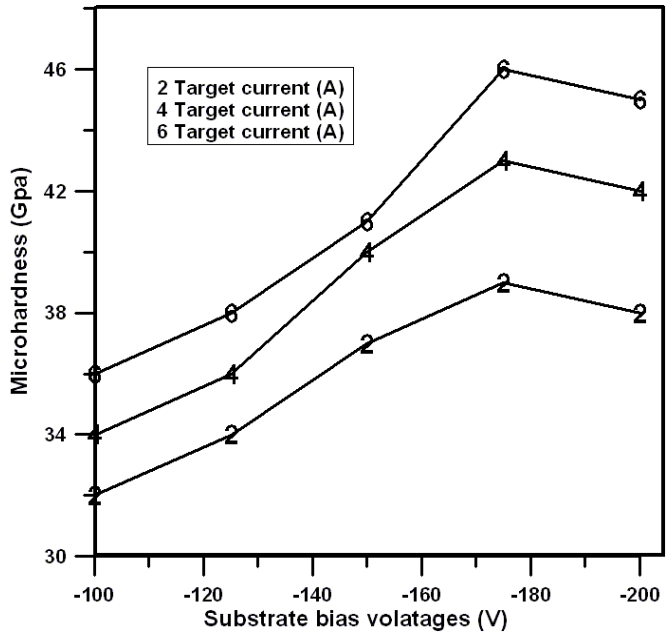

Figure 4. Influence of target current and substrate bias voltages on mirohardness of DLC films.

In case of using the graded structure, influences of interlayer design and substrate bias on film adhesion were evaluated by scratch test, whose results are shown in Figure 5.

Copyright © 2012. Nova Science Publishers, Incorporated. All rights reserved.

Diamond-Like Carbon Films, Nova Science Publishers, Incorporated, 2012. ProQuest Ebook Central,

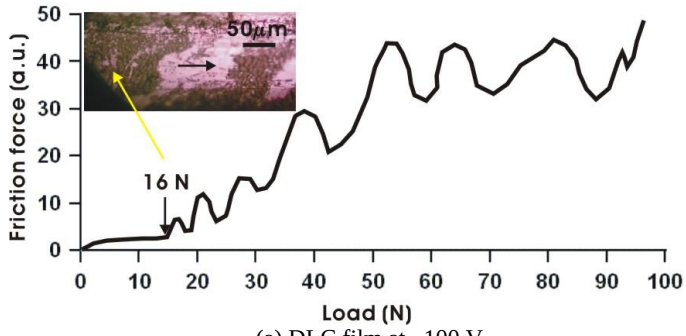

(a) DLC film at –100 V

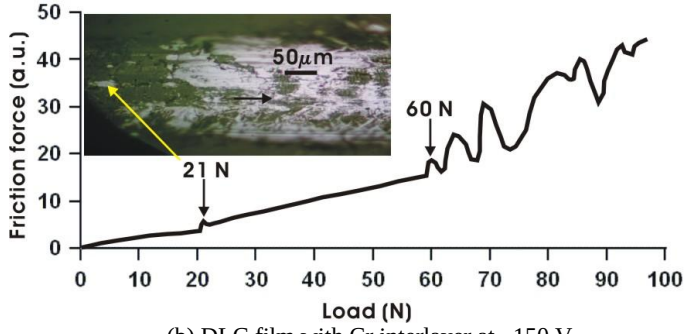

(b) DLC film with Cr interlayer at –150 V

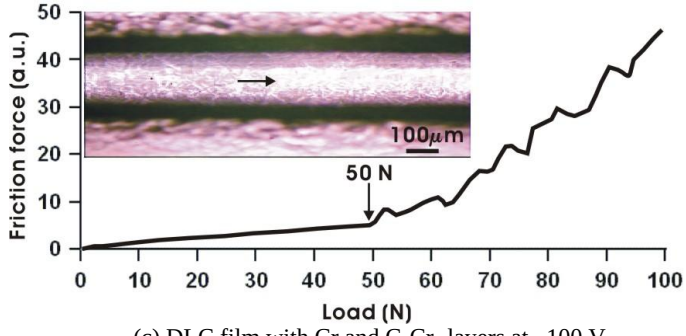

(c) DLC film with Cr and C_xCr_y layers at –100 V

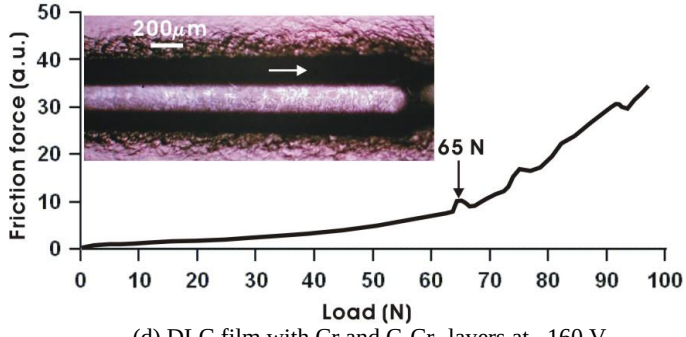

(d) DLC film with Cr and C_xCr_y layers at –160 V

Figure 5. Influence of transitional layer and substrate bias voltages on adhesion of DLC films (target current 6 A).

Copyright © 2012. Nova Science Publishers, Incorporated. All rights reserved.

Diamond-Like Carbon Films, Nova Science Publishers, Incorporated, 2012. ProQuest Ebook Central,

Being as index of adhesion force between film and substrate, the critical load *Lc*, was determined by onset of abrupt variations in friction forces, as a diamond stylus scratched with continuous loading on DLC films. Three types of DLC films were tested for evaluating their adhesions. In Figure 5a, a pure DLC film showed a poor adhesion, peeled off the substrate surface at 16 N of *Lc*, due to the poor interface compatibility. In Figure 5b, a DLC film with Cr interlayer was used to improve the adhesion. For a convenient analysis, *Lc* is divided into Lc_1 (critical load for cohesion) and Lc_2 (critical load for adhesion), determined by the first and secondary onsets of abrupt variations of the friction forces. DLC film was peeled off the substrate surface at 21 N of Lc_1, but Lc_2 was lasted to 60 N. Cr interlayer seemed to play an important role on adhesion improvement. In Figure 5c-d, the graded DLC films with Cr interlayer and C_xCr_y transitional layer at different substrate bias voltages of –100 V and –160 V were tested. Scratch results demonstrated a significant improvement in the adhesion, and the best one was 65 N of *Lc* from graded DLC film at substrate bias voltage of –160 V.

Friction and wear property of DLC films of hard one with 34 GPa and superhard one with 45 GPa was investigated in the ball-on-disc tester, whose results are shown in Figure 6. As can be seen, the average friction coefficient of the super-hard one is about 0.08, and that of the hard one is about 0.1. All DLC films show some low and constant friction coefficients between 0.15 and 0.08, and these fiction coefficients do not show a significant dependence on the low loads of 1N, 2N and 5N. In the test range of 500 m, no failure of DLC films was observed. After collecting the wear debris from the ball and disc and filtering the debris in acetone bath, it was found in the EDX analysis that the main element content of the debris was graphite, so abrasion was supposed as the wear mechanism. Under the same test condition, the superhard DLC film, microhardness more than 40 GPa, showed the lower volumetric wear rate (omitted) and friction coefficient than that of the hard one, microhardness between 30 GPa and 40 GPa. In this case, the wear resistance of DLC film might be correlated with the hardness of DLC film [15-16].

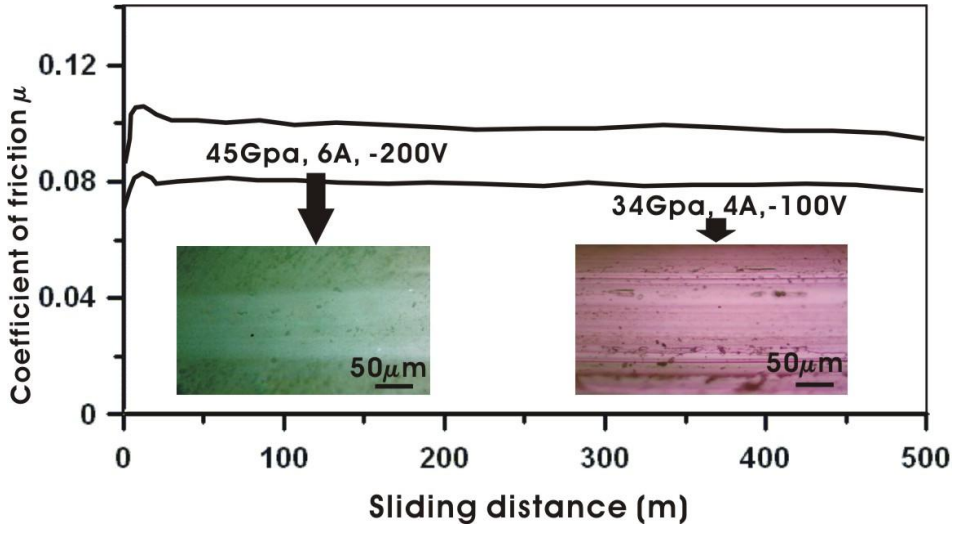

Figure 6. Two comparative curves of friction coefficients of DLC films with different hardness of 34 GPa and 45 GPa. Optical micrographs of wear tracks were from the discs at the end of 500 m of sliding distance.

Copyright © 2012. Nova Science Publishers, Incorporated. All rights reserved.

Diamond-Like Carbon Films, Nova Science Publishers, Incorporated, 2012. ProQuest Ebook Central,

4. Conclusion

A series of hydrogen-free DLC films were successfully synthesized using the mid-frequency dual-magnetron sputtering. The process parameters, structure and properties of Cr-doped graded DLC film, and their relationships have been investigated in trial for the films to be used as the protective films. The properties of these DLC films showed a clear dependence on the flux and energy of ion bombardment during growth of the film.

The DLC film possessed a graded and multilayered structure. The Cr interlayer played a role of adhesion improvement, and the transitional C_xCr_y layer played a role of hard support. The structural integrity was beneficial for the both high microhardness and good adhesion of the DLC films. The effect of target current and bias voltage on the properties of the DLC film was also examined. It was found that the DLC film possessed some combined advisable properties: a very smooth morphology, microhardness in range of 32~46 GPa, adhesion of *Lc* up to 65 N and reliable friction coefficient about 0.1. The super-hard DLC film has the behavior of both good adhesion and lower friction coefficient, and thus it is predicted that the one may be used as a high-quality wear-resistant film in the industrial applications.

SECTION 2: CR-DOPED DLC FILMS IN THREE MID-FREQUENCY MAGNETRON POWER MODES

1. Introduction

Pulsed magnetron sputtering, an enabling technology for the deposition of dielectric films, has attracted considerable interest in the recent years [17]. Pulsing the magnetron discharge in mid-frequency (20~250 kHz) could strongly affect the intrinsic parameters of plasma, inducing much greater energy fluxes to be delivered to the substrate than the DC magnetron discharge [18]. At present, many researchers concentrate their efforts on eliminating arcing and target poisoning through introducing the pulsed process in reactive sputtering [19,20]. The waveforms determine the characteristics of the plasma formed, but the influence of the features within the sputtering source waveforms of the bipolar modes on the structure and properties of the films are seldom found in the literature.

Due to exhibiting some attractive properties e.g. smooth surface, high hardness and low frictional coefficient, Cr-doped hydrogen-free sputtered DLC films display a significant technological potential in the tribological applications as wear-resistant films [21]. The properties of the DLC films depend on the deposition processes and conditions used, and a variety of hardness, densities and conductivities from conducting to insulating have been reported [22,23].

Since exploring the influence of driving voltage waveforms on DLC films might be beneficial to both improving quality of the DLC films and understanding the possible influence of the waveform on other films, the influence of the waveform on the properties of DLC films was studied. A series of Cr-doped DLC films were deposited using a mid-frequency dual-magnetron sputtering system with a new power supply of three modes, i.e. continuous DC, pulsed DC and AC. The variations in the properties of the films under different modes were investigated.

Copyright © 2012. Nova Science Publishers, Incorporated. All rights reserved.

Diamond-Like Carbon Films, Nova Science Publishers, Incorporated, 2012. ProQuest Ebook Central,

2. Experimental Details

Cr-doped hydrogen-free DLC films were deposited using unbalanced dual-magnetron sputtering in a coating rig (SP8050, Beijing Powertech Co., Ltd.). Four pairs of dual-magnetron targets were set in the cylindrical coating system. Two planar magnetrons constituted a pair of dual-magnetrons. The magnetrons were inserted into their pre-molded holes for the installations, and their magnetic fields were arranged.The dual-magnetron targets were installed in the vacuum chamber in the vertically opposed configuration approximately 70 cm apart, respectively. Six C and two Cr targets of a size of 420×80×8 mm^3 and a purity of 99.9 % were used. A unipolar pulse DC bias power supply was used to control the bias voltage and the bias current to the substrate. The duty ratio of the pulsed bias voltage was 50% in Ar ion cleaning and was 60 % during the deposition processes. Four 40 kHz AC power supplies (SP20MB, Beijing Powertech Co., Ltd.) were used in a current-constant mode to control the magnetron targets at constant values of 2, 4 and 6 A, respectively, with corresponding target voltage increases from 300 to 800 V. The substrate holder was placed at the centre of the chamber. Argon gas was fed through the magnetrons and targets by several intermittent holes of 3 mm diameter at the target surfaces, so as to enhance the ionization efficiency of the sputtering. Process parameters in each procedure could be controlled by a PLC (Programmable Logical Controller) system.

Each SP20MB power supply was connected to a pair of dual-magnetron targets, whose configuration and waveforms in the three optional modes are shown schematically in Figure 7. The waveforms are rectified from an AC sinewave signal. As shown in Figure 7a, the power supply has three optional modes of continuous DC, pulsed DC and AC. At each half cycle of the pulsed DC and AC modes, one of dual magnetrons is at a negative potential and acts as a sputter cathode, whilst the other magnetron acts as the anode. The magnetron voltage is inversed in the next supplied half cycle. Secondary electrons generated by the momentary cathode are accelerated towards the anode, neutralizing the positive surface charges that have been built up in the insulated areas of the target surfaces during the negative half cycle. The waveform of asymmetric bipolar pulsed DC mode is shown in Figure 7b. In this case, the target is sputtered at the nominal operating voltage (typically, -400 to –600 V) for a fixed "pulse-on" period of time. The pulse-on time is limited, so that charging of the poisoned regions does not reach the point where breakdown and arcing occurs. The charge is then dissipated through the plasma during the "pulse-off" period by switching the negative target voltage to a positive potential. Due to much higher mobility of electrons than that of ions in the plasma, the target voltage is reversed to about 10 % of nominal pulse-on voltage during pulse-off period, and the pulse-off time is 12.5 μs (i.e., 50 % of the full pulse cycle). The waveform of bipolar AC mode is shown in Figure 7c. Targets A and B have the same bipolar sinusoidal voltage waveform, and the phase difference between the waveforms of targets A and B is a half cycle. The waveform of the continuous DC mode is shown in Figure 7d. The targets A and B have the same negative half-sine waveform.

Sheets of M2 tool steel of a uniform size of 20×30×3 mm^3 were coated and used as the samples for mechanical and frictional tests, and some Si(100) wafers of small uniform size were used for SEM analysis. The surfaces of the steel sheets were polished to a surface roughness of Ra=0.1 μm. All samples were ultrasonically cleaned in an acetone bath for 15 min, and were then blown dry with nitrogen. After pumping down by a turbo-molecular pump

Copyright © 2012. Nova Science Publishers, Incorporated. All rights reserved.

Diamond-Like Carbon Films, Nova Science Publishers, Incorporated, 2012. ProQuest Ebook Central,

to a base pressure of 4.0×10^{-3} Pa, the surfaces of the samples were further cleaned by Ar ion bombardment under a bias voltage of -1000 V at a pressure of 4.0 Pa for 15 min.

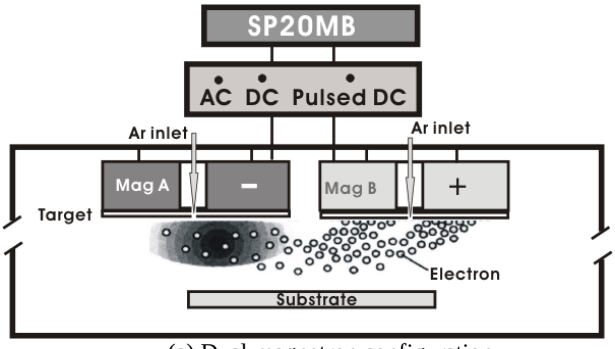

(a) Dual-magnetron configuration

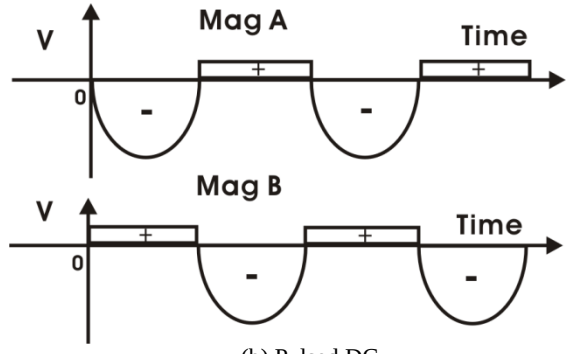

(b) Pulsed DC

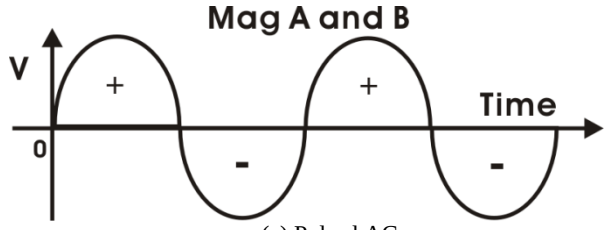

(c) Pulsed AC

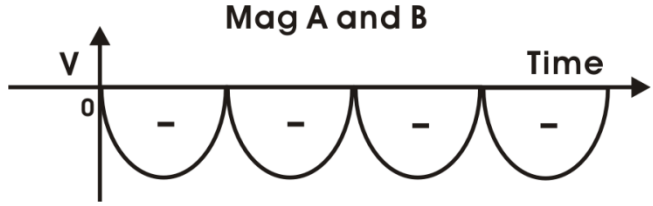

(d) Continuous DC

Figure 7. Schematic diagrams of dual-magnetron configuration and waveforms of V (target voltage V) vs. microsecond (Time) of three optional modes of SP20MB power supply.

To investigate the influence of three driving voltage modes on the properties of Cr-doped DLC films, the deposition parameters were kept constant for comparison. The chamber was heated by two heater groups of 8 KW and was monitored by a SR 93 (SHIMADEN)

Copyright © 2012. Nova Science Publishers, Incorporated. All rights reserved.

Diamond-Like Carbon Films, Nova Science Publishers, Incorporated, 2012. ProQuest Ebook Central,

temperature panel. After heating to a pre-set temperature of 120 °C, the deposition process was started at an argon pressure of 0.3 Pa and at substrate bias of –80 V. The main deposition process contained three steps. Firstly, a Cr interlayer on the substrate was sputtered from two Cr targets. Subsequently, a transitional layer of Cr_xC_y on the Cr interlayer was co-sputtered from two Cr and six C targets. The co-sputtering was conducted through the gradual decrease of the Cr target currents and the gradual increase of the C target currents. Finally, a top DLC layer was sputtered from six C targets.

Scanning electron microscopy (SEM) was used to investigate the morphology of the films. Nanoindentation with a NHT type nano-indenter was used to investigate the microhardness, and the continuous measurement was carried out by operating the indenter at a constant displacement penetration depth of 50 nm. Scratch testing was used to investigate the adhesion using the conditions: initial load 3 N, loading rate 100 N/min and transverse speed 10 mm/min. Ball-on-disk testing was used to investigate the frictional property, where DLC films were deposited on the disc, and the counterpart used was a Φ8 mm Al_2O_3 ball. The ball-on-disc test was in air at a load of 5 N, and a constant rotation speed of 1000 r/min, equivalent to a linear speed of 0.6 m/s. Optical microscopy attached with a video camera was used for analysis of the wear traces.

3. Results

Figure 8 shows surface SEM images of Cr-doped DLC films deposited in three different modes. In Figure 3, a significant difference can be seen in the morphologies of DLC films in the three modes. The films deposited in the pulsed DC and AC modes appear to have obviously smoother surfaces than the continuous DC film, and the one in pulsed DC mode is the smoothest. Values of average roughness *Ra* of these films conform to the observed result: the values are about 25 nm (*Ra*) for the film in continuous DC mode, 10 nm for the one in AC mode, and 4.5 nm for the one in pulsed DC mode.

Arcing events encountered in the sputtering process may result in surface defects on DLC films, giving a rough surface. The rough surface of the DLC film in continuous DC mode may be due to the arcing persistence. Pulsing the magnetron discharge can suppress the arcing and thus the film surfaces become smoother. At the frequency of 40 kHz, arcing during the sputtering could be efficiently suppressed when the reverse time was increased to a point at which pulse-off time was equal to the pulse-on time.

Using the mathematical mean of ten results as the measurement value, Figure 9 shows a comparison of microhardness of Cr-doped DLC films in the three modes. As can be seen, the average microhardness of the films are 25.62 GPa for the film in AC mode, 26.66 GPa for the film in pulsed DC mode and 13.13 GPa for the film in continuous mode. Thus, the microhardness of Cr-doped DLC films in pulsed modes is about twofold that in continuous DC mode, and the microhardness in the two different pulsed modes only have a slight difference.

Scratch test results indicated that adhesion between the M2 substrates and the DLC films in pulsed DC and AC modes were better than that in continuous DC mode. The average critical loads, *Lc*, of DLC films were 55 N for the film in pulsed DC mode and 40 N for the film in AC mode, compared to 25 N of the one in continuous DC mode. Optical micrographs of failure regions on scratch tracks of the DLC films in three modes are shown in Figure 10.

Copyright © 2012. Nova Science Publishers, Incorporated. All rights reserved.

Diamond-Like Carbon Films, Nova Science Publishers, Incorporated, 2012. ProQuest Ebook Central,

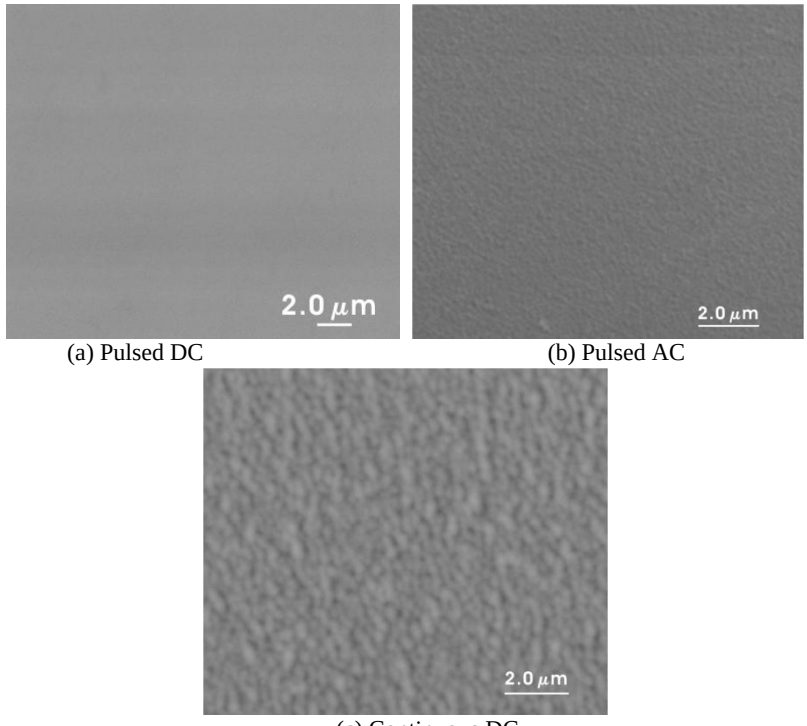

(a) Pulsed DC (b) Pulsed AC

(c) Continuous DC

Figure 8. Surface SEM images of Cr-doped DLC films in three modes.

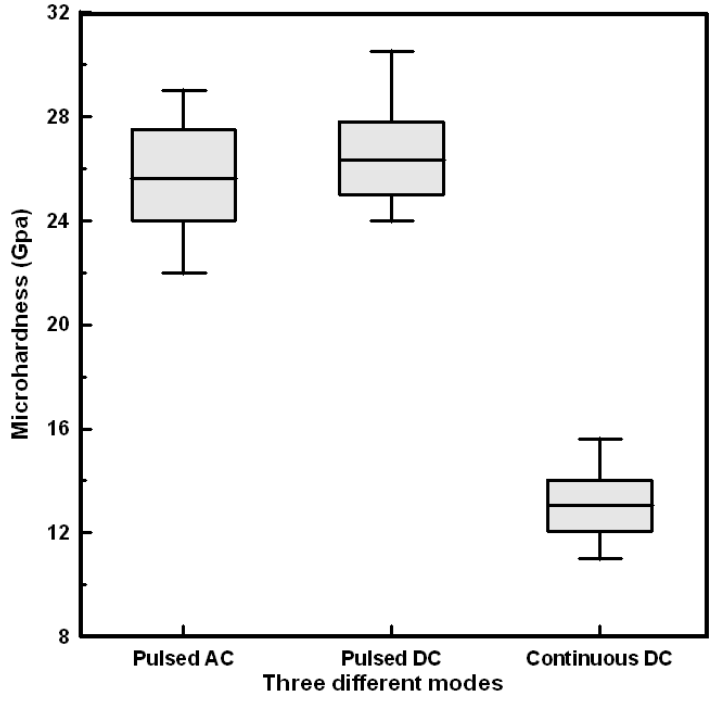

Figure 9. Contrast with microhardness of Cr- DLC films in three modes.

Copyright © 2012. Nova Science Publishers, Incorporated. All rights reserved.

Diamond-Like Carbon Films, Nova Science Publishers, Incorporated, 2012. ProQuest Ebook Central,

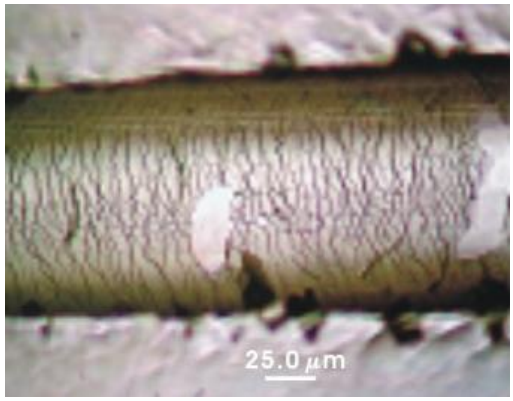

(a) Pulsed DC

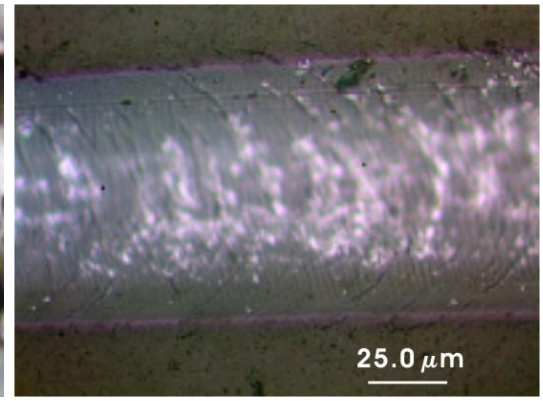

(b) Pulsed AC

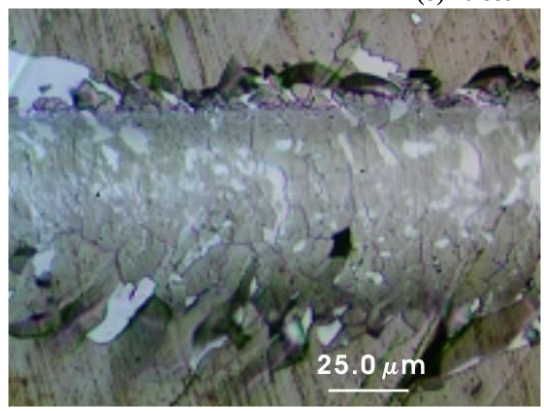

(c) Continuous DC

Figure 10. Optical micrographs of failure regions on scratch tracks of DLC films in three modes.

The pulsed DC film shown in Figure 5a and the continuous DC film in Figure 5c failed in peeling, whereas the pulsed DC film only showed a few traces of peeling; compared with the pulsed AC film in Figure 5b, the pulsed DC film remained more integral film matrix.The variation in the mechanical properties of DLC films at the different modes is related to the changes in ion currents and energies of the plasma. Compared with continuous DC mode, pulsing the magnetron can significantly increase the ion current and energy in the plasma [24,25]; and the reverse time and the pulse frequency affect the energies of ions arriving at the substrate [26]. An alternating voltage was applied to the substrate and the magnetrons, and thus the values of substrate bias current were measured as the time-average readings by the bias power supply. At a target current of 4 A and in a bias voltage range of –50 V to –200 V, the bias current, an index of ion current, in continuous DC mode saturated at 1.2 A with the increasing bias voltage; whereas the bias currents in AC mode and in pulsed DC mode were stable at 3 A and 4 A, respectively; after a sudden increase at the bias voltage of about –60 V, the bias currents in the pulsed modes still showed a small gradual increase. Bombarding the films by more particles with a suitable energy induces a more dense structure of the films and an improved interfacial layer, which improves the hardness and adhesion of the DLC films.

Figure 11 shows the results from the ball-on-disc tests, conducted on the DLC films in three modes for comparison. As can be seen, for a constant sliding distance of 500 m, the DLC films in pulsed modes showed lower friction coefficients than that in continuous DC

Copyright © 2012. Nova Science Publishers, Incorporated. All rights reserved.

Diamond-Like Carbon Films, Nova Science Publishers, Incorporated, 2012. ProQuest Ebook Central,

mode. The average friction coefficients of DLC films are 0.12 for the one in AC mode and 0.08 for the one in pulsed DC mode, whereas that in continuous DC mode is 0.19. The lowest friction coefficient for the DLC film in pulsed DC mode may be attributed to the smoothest surface and the best mechanical properties of the films.

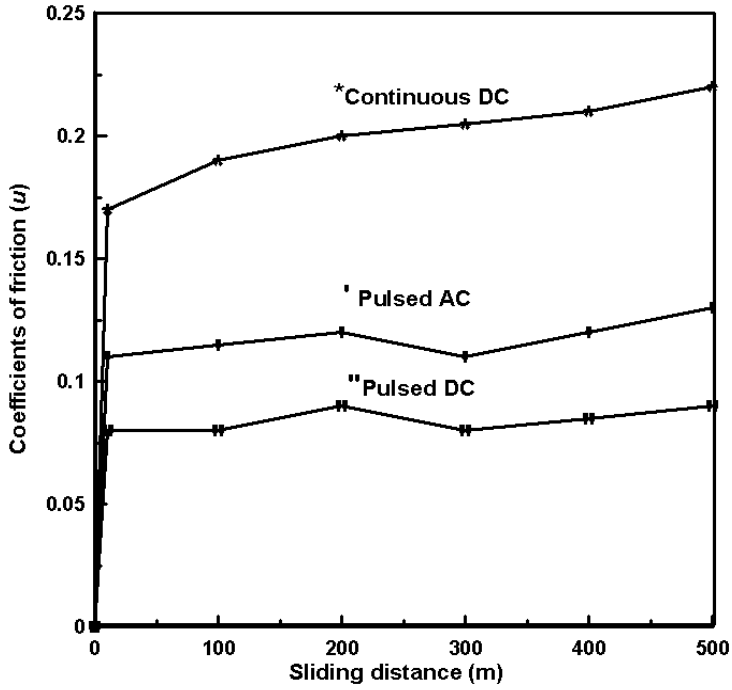

Figure 11. Comparison of frictional properties of Cr-doped DLC films in three modes.

The waveform modes of the driving voltage have an obvious influence on the properties of the DLC films, as shown in above contrasting figures. The reason for this may be attributed to the difference of the magnitude of reverse voltage in the three modes since the others parameters in the three modes are same. The magnitude of reverse voltage may affect the properties of the DLC films in the three modes, as shown in above contrasting figures. Poor integral properties of the DLC film in continuous DC mode may be due to the absence of a reserve voltage. The properties in AC mode are not superior to those in pulsed DC mode, which may be due to the greater magnitude of the reverse voltage. The best properties exhibited in pulsed DC mode may be due to the reserve voltage kept at 10% of normal magnetron voltage. It is predicted that asymmetric bipolar magnetron sputtering with the proper reverse time and reverse voltage magnitude may be an effective tool for improving the properties of DLC films.

4. Conclusion

Several Cr-doped DLC films were deposited using unbalanced dual-magnetron sputtering in the three driving voltage waveform modes. In contrast with the film in continuous DC mode, the films in AC and pulsed DC modes, especially in pulsed DC mode, showed

Copyright © 2012. Nova Science Publishers, Incorporated. All rights reserved.

Diamond-Like Carbon Films, Nova Science Publishers, Incorporated, 2012. ProQuest Ebook Central,

improved properties. In pulsed DC mode, the DLC film showed some admirable properties, i.e., very smooth surface, high microhardness of 26.66 GPa, good adhesion of *Lc* 55 N and low average friction coefficient of 0.08. It is hypothesized that the magnitude of the reverse voltages in the three voltage waveform modes influences the properties of the DLC films.

SECTION 3: PREPARATION AND PROPERTIES OF THICK DLC FILM

1. Introduction

Diamond-like carbon (DLC) films achieve some prominent tribological properties such as high hardness and low frictional coefficient. It is rarely reported to produce thick DLC films, thickness more than 3 μm, with excellent adhesive properties sufficient for an industrial use in a wear coating of steel system. This is due to the high internal stress in the DLC films and/or the large discrepancy of mechanical properties between the DLC films and steel substrates [27,28]. The protective applications against wear include applications in machine construction field for components with surfaces moving against one another, such as gears, pump and cup plungers, bearing sets or their individual parts, as well as, applications in material processing field for protection of cutting tools and moldings etc [29].

Process of magnetron sputtering has been known for some time. In recent years, applications of the process have grown dramatically and have been subject to refinement and development [30]. Resent studies demonstrated that medium-frequency (20-100 kHz) magnetron sputtering offered some advantages over traditional DC magnetron sputtering for deposition of metastable films like DLC and CN_x [5]. Pulsing the discharge can significantly modify the characteristics of magnetron plasma, pulsing the substrate bias voltage can increase the ion current drawn at the substrate, and thus have an important effect on properties of the metastable films [31,32].

This section focuses on preparing a new thick Cr-doped graded DLC film in our medium-frequency dual-magnetron system in trial. It was found that the graded and multilayered structure of the DLC film was closely related to its properties and process parameters. The structure, deposition process and resulting properties of the film are thus investigated.

2. Experimental Details

Cr-doped hydrogen-free DLC films were deposited using unbalanced dual-magnetron sputtering in a coating rig SP8050. Experimental conditions are listed in Table1.Two planar magnetrons of each pair were placed in vacuum chamber in face-to-face configuration approximately 70 cm apart, respectively. The substrate holder was placed in center area. A pulsed DC supply on substrates and four pulsed AC power supplies of 40 kHz, on each pair of dual-magnetrons, were used to control substrate bias voltage, substrate bias current and target power. Schematic diagrams of waveforms of the target power supplies and substrate bias power supply are shown in Figure 12. As shown in Figure 12a, one of two dual targets had the same bipolar-pulsed sine waveform as another, and the phase difference was a half

Copyright © 2012. Nova Science Publishers, Incorporated. All rights reserved.

Diamond-Like Carbon Films, Nova Science Publishers, Incorporated, 2012. ProQuest Ebook Central,

cycle. During one pulse cycle, pulse-on time was the same as pulse-off time, i.e., 12.5 μs, 50 % of the full pulse cycle.

Table 1. Experimental conditions

Sputtering system	Multi-target mid-freq. pulsed dual magnetron	
Sputtering targets	Cr×2 and C×6	420×80×8 mm^3 (99.9%)
Substrates	Steel (M2HSS)	20×20×3 mm^3
	Si (100)	8×8×0.2 mm^3
Growth temp.	150 ^oC	
Background pressure	3.0×10^{-3} Pa	
Sputtering pressure	0.3 Pa (Ar/N_2, Ar 60 sccm, N_2 0~120 sccm)	
Target pulsed power	0~25 kW, 200~800 V, 40 kHz	
Substrate bias power	0~1000 V (unipolar pulse), 5~95% (duty ratio), 0~20 A (bias current)	

The substrate bias power supply in unipolar pulse mode can be seen in Figure 12b, the duty timing of duty-on to duty-off could be adjusted according to process requirement. The duty ratio of the pulsed substrate bias voltage was 80% in Ar ion cleaning and uniformly was 60 % in the following deposition processes. The medium-frequency power supplies used power-constant mode to control the magnetron targets, at 2, 3 and 5 kW, respectively, corresponding to target voltage increased from 200 to 800 V. Argon gas was introduced through each target to enhance sputtering of the targets. Process parameters in each procedure could be automatically controlled by PLC (Programmable Logical Controller) through presetting.

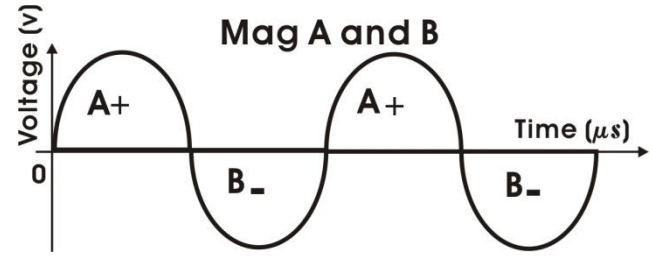

(a) Target power supply (pulsed AC of 40 kHz)

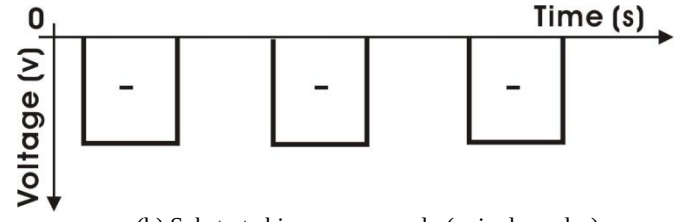

(b) Substrate bias power supply (unipolar pulse)

Figure 12. Schematic diagrams of waveforms of target power supplies and substrate bias power supply.

Coupons of M2 high-speed steel (HSS), microhardness about 7 GPa, were used as samples for the microhardness, scratch and ball-on-disc tests, and some coupons of Si(100)

Copyright © 2012. Nova Science Publishers, Incorporated. All rights reserved.

Diamond-Like Carbon Films, Nova Science Publishers, Incorporated, 2012. ProQuest Ebook Central,

wafers were used for AFM, SEM, AES and Raman tests. Surfaces of the steel sheets were mirror polished to a surface roughness of Ra=0.1 μm. All samples were ultrasonically cleaned in acetone bath for 20 min, and the cleaned coupons were then blown by dry nitrogen.

After pumping down by a turbo-molecular pump to a background pressure of 3.0×10^{-3} Pa and before depositing, surfaces of the coupons were further cleaned by Ar ion bombardment under bias voltage -700 V at pressure 3.0 Pa for 20 min, to remove some adhering impurities on substrates.

After heating the substrate to 150 °C, deposition process was started in condition that the depositing pressure was maintained at 0.3 Pa of argon pressure. Main deposition procedures comprised four steps. Firstly, Cr interfacial layer on substrate was sputtered from two Cr targets. Secondly, transitional layer of the CrN_z films was reactively sputtered from the two Cr target in the N_2 gas atmosphere onto the Cr interfacial-layer. Thirdly, the C_xCr_y graded layer was deposited by the co-sputtering of the two Cr targets and six carbon targets. The co-sputtering was done under the following conditions: gradual decrease of Cr target power from 5kW to 2kW and the gradual increase of carbon target power from 2kW to 5kW. Finally, the cover layer was deposited on the transitional layer by the alternating sputtering of six carbon targets and the two Cr targets. The Cr-doped graded films of DLC were synthesized by these deposition processes. The resultant film thickness was 3-6μm. The DLC films of about 6μm in thickness were used for the following analyses.

Morphology and microstructure of the Cr-doped DLC film on Si wafer were investigated using atomic force microscopy (AFM), scanning electron microscopy (SEM), Auger electron spectrometer (AES) and Raman spectroscopy. Microhardness was measured using MH-6 hardometer. Adhesion between substrate and DLC film was investigated using SW-97 scratch tester under condition: initial load 2 N, loading rate 100 N/min and transverse speed 4 mm/min. Friction and wear property was investigated using DD-92 ball-on-disc tester under conditions: DLC film deposited on the disc, and counterpart ball used Al_2O_3 ball; in ambient air and at loads of 10 N, 20 N and 50 N, respectively; rotated speed kept at 1000 r/min, equal to 0.6 m/s of linear speed. Wear traces were analyzed using an optical microscope attached with a camera.

3. Results

AFM and cross-section SEM images of the DLC film deposited at –100 V of pulsed bias voltage are shown in Figure 13. According to AFM measurement data shown in Figure 13a, Ra is 8.6 nm and average size of the projections is about 90 nm in diameter and 20 nm in height. The film has a smooth morphology with no visible loose particles from the targets, which is advantageous for molding applications when high surface finish is required [33]. Such smooth morphology is attributed to high ion current flux of the medium-frequency dual-magnetron sputtering. The substrate bias current, an index of ion current flux, was between 1.0 A and 2.5 A in this experiment. During DC unbalance magnetron sputtering on substrate of precise forming die, the substrate arcing is somewhat inevitable [34]. If the localized surface arcing persists, some droplets and holes from the running arcs may make the die unusable. The medium-frequency magnetron sputtering may be an effective method for reducing the defects induced by substrate arcing.

Copyright © 2012. Nova Science Publishers, Incorporated. All rights reserved.

Diamond-Like Carbon Films, Nova Science Publishers, Incorporated, 2012. ProQuest Ebook Central,

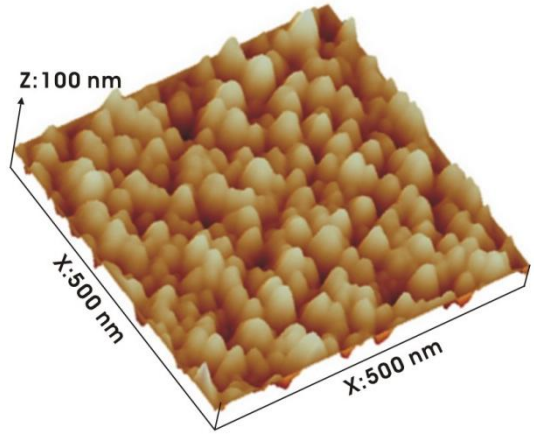

(a) Surface image

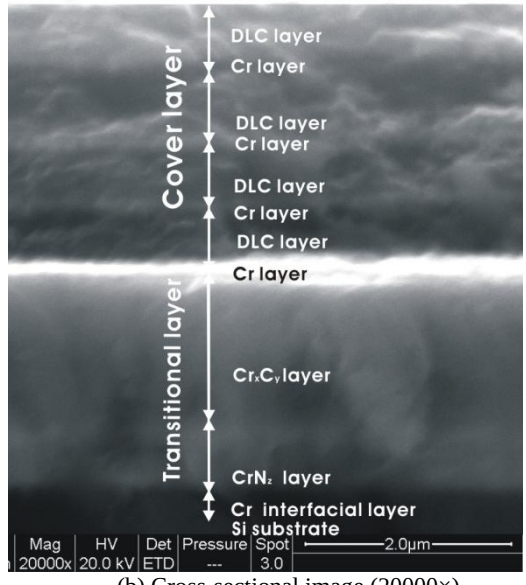

(b) Cross-sectional image (20000×)

Figure 13. Surface AFM and cross-section SEM images showing morphology and structure of Cr-doped DLC film on Si wafer.

Graded and multilayered structure of the DLC film can be seen in Figure 13b. The graded film is composed of three sections of Cr interfacial-layer, transitional layer and cover layer. The transitional layer consists of two support layers of CrN_z and Cr_xC_y, and the cover layer is lapped by four similar bilayers of Cr and DLC. Apart from imperfect smoothness of cross-section surface due to sampling difficulty, the integral film seems dense and compact, which is vital in achieving advisable hardness for wear resistance. Raman test result coincides with character of DLC film. The characteristic D and G bands of DLC layer were investigated by Raman spectroscopy, and D-to-G bond ratio of I_D/I_G was 1.48. Interfaces between each layer of the graded DLC film are well bonded without visible flaw. Such graded structure can be used to release the residual stress and to cope with large discrepancy of physical properties between DLC layer and substrate, and the transitional layer including C_xCr_y and CrN_z layers may also has an important role of hard support on steel substrate [35]. Similar to report by S.

Copyright © 2012. Nova Science Publishers, Incorporated. All rights reserved.

Diamond-Like Carbon Films, Nova Science Publishers, Incorporated, 2012. ProQuest Ebook Central,

Yang [36], the metal Cr and Cr-containing layers bolstered stress management in hard a-C films. In this way, the stress state of DLC layer at outer boundary may be stepwise adjusted to a totally different stress state at inner boundary to substrate by specified process control.

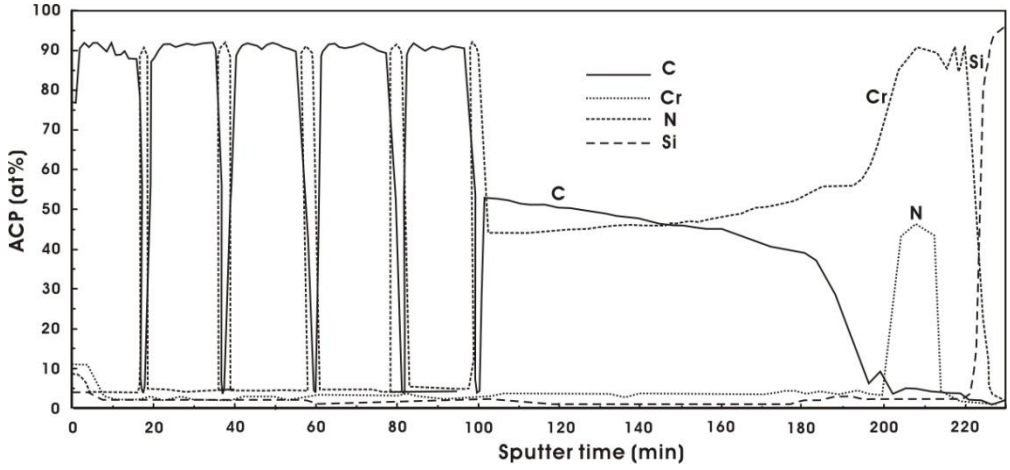

Figure 14. AES spectrum showing layer element depth changes of Cr-doped graded DLC film through ACP (at %) vs. sputter time (min).

The AES measurements show another evidence of the graded and multilayered structure in the graded films and reveal some deposition characters of present medium-frequency dual-magnetron sputtering. Typical AES spectra is shown in Figure 14. The AES spectra showed the depth profile of compositional elements in the graded films. The AES spectra suggested the graded films on Si substrates comprised DLC/Cr/ DLC/Cr/ DLC/Cr/ DLC/Cr/C_xCr_y/CrN_z structure. The DLC layer in the cover layer shown in Figure 4 is identified by the element C. The DLC layer shows a periodical pattern. The C_xCr_y and CrN_z in the transition layer shown in Figure 4 are identified by the element C, Cr, and N. It is seen the intensity of these elements gradually changes in the depth as expected. The abrupt increase of Si was observed at the interface of the graded films and the Si substrates. The multilayered and graded structure clearly observed in Figure 4 matches the cross sectional SEM image shown in Figure 3. The AES spectra show the thickness of each layer; thickness of the DLC layer and Cr layer in the cover layer is 0.7μm and 0.12μm, respectively; thickness of C_xCr_y layer, CrN_z layer, and Cr interfacial layer is 2.16μm, 0.7μm, and 0.14μm, respectively. The total thickness of the graded DLC films is 6.18μm.

According to the scheduled time of each procedure in the sputtering deposition, during the deposition of the graded DLC films, the deposition rate of the DLC layer is found to be 1.1 μm/h by the sputtering of six carbon targets and the deposition rate of Cr layer is 0.8 μm/h by the sputtering of two Cr targets. The deposition rate of C_xCr_y layer during the deposition of the graded layer is 1.8μm/h by the sputtering of six carbon and two Cr targets. These deposition rates are higher than those of reported values using conventional sputtering system [37]. Based on present experimental data, it is found the deposition rate was governed by the target power and substrate bias voltage. Under the constant target power of 3kW, when the deposition was done at the bias voltage of -100, -150, and -200V, the deposition rates of DLC layer were 0.94, 0.96, and 0.98 μm/h, respectively. Under the constant bias voltage of -100V,

Copyright © 2012. Nova Science Publishers, Incorporated. All rights reserved.

Diamond-Like Carbon Films, Nova Science Publishers, Incorporated, 2012. ProQuest Ebook Central,

when the deposition was done at the target power of 2, 3, and 5kW, the deposition rates of the DLC layers were 0.92, 1.06, and 1.28μm/h, respectively. These experimental results show the increase of substrate bias voltage and/or the increase of the target power increase the deposition rate of the DLC films. These substrate biases and/or target powers dependence of the deposition rate could be not observed when the substrate bias exceeded -200V and/or the target power exceeded 5kW, probably due to the re-sputtering arising from the heavy ion bombardment [38].

The variations of Vikers microhardness with the applied loads on the graded DLC film are shown in Figure 15. At low loads of 10 g and 20 g, Vickers microhardness of the film is 1050 and 1205, respectively. The Vickers microhardness increases with the increasing loads and tends to be stabile at high loads of 200 g and 300 g. After similar measurement in three times, an average microhardness value of 1560 kg/mm^2 was obtained at a load of 250 g. The reason may be like this: DLC layer in this graded film may not be as hard as predicted; Cr layer is soft as known [39]. The fact the relatively lower microhardness at low loads and relatively high one at high loads my result from the graded structure comprised multilayer and the graded layers of different mechanical strengths. The present relatively high microhardness may be owing to the presence of the hard transition layer.

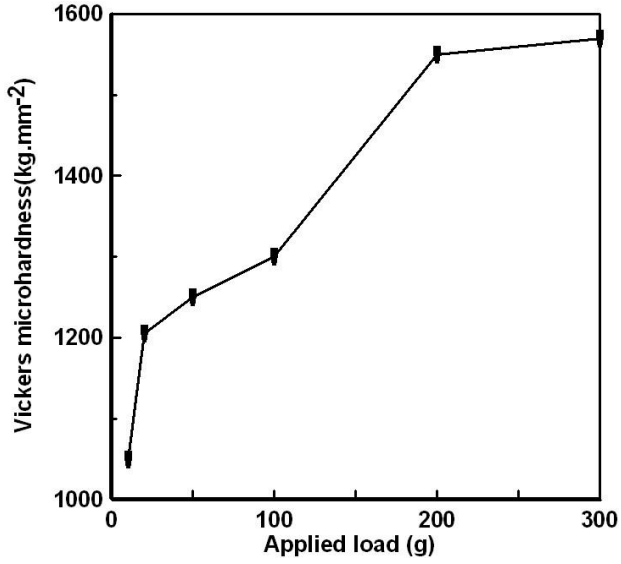

Figure 15. Influence of applied loads on Vickers microhardness of DLC film on steel substrate.

During the scratch test, a diamond stylus was drawn across the film surface at an ever-increasing normal load in ambient air. Friction force was monitored during the loading process, and micrographs of typical scratch trace were used to determine the critical load (*Lc*) and evaluate the scratch history. As shown in Figure 16, in initial contacting stage, reflected in picture 1, the scratch trace is flat and gentle and the friction force is low, no visible evidence of the film cracking. As the loading increases, reflected in picture 2, little wear cracks that tend to occur along the scratch trace become visible, these cracks do not bring the film breaking in thickness range of top DLC layer.

Copyright © 2012. Nova Science Publishers, Incorporated. All rights reserved.

Diamond-Like Carbon Films, Nova Science Publishers, Incorporated, 2012. ProQuest Ebook Central,

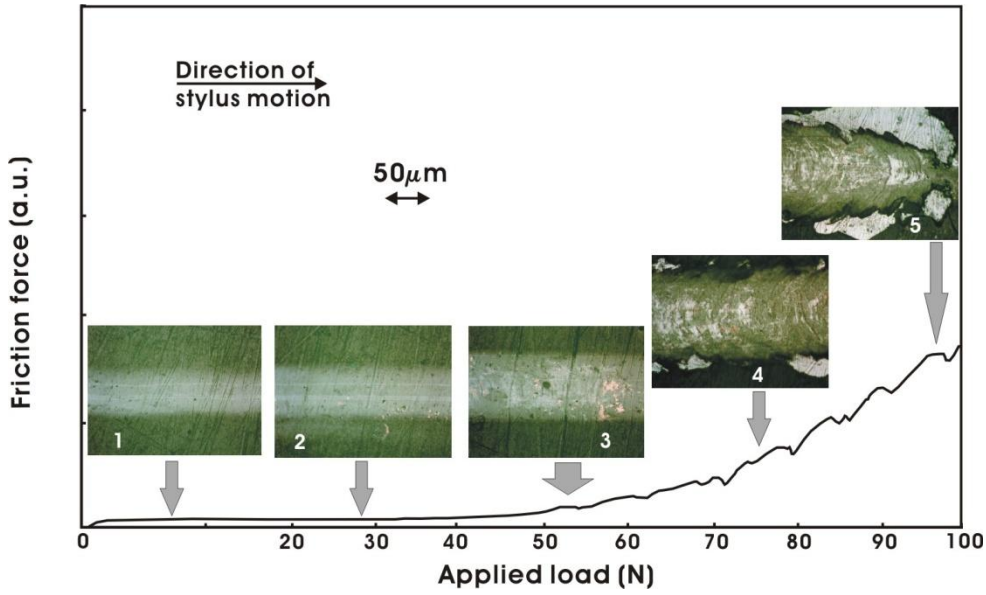

Figure 16. Curve of friction force change and typical morphology pictures of DLC film on steel substrate.

As the loading increases further, reflected in picture 3, the film begins to chip when the applied load was increased to point where the film was broken, i.e., approaching to the critical load, *Lc*, at 52 N. It is surprising to see, although the following increased load brought some enlarged cracks and chips along scratch trace of the film, a catastrophic failure was not encountered as predicted, as shown in picture 4. Even in last stage of scratch history, as reflected in picture 5, it can be seen that a majority of black film still remains at the end of test, compared with bright region of worn trace. This interesting phenomenon may be attributed to the thick DLC film with graded and multilayered structure and adhesion role of Cr layer and Cr-containing layer.

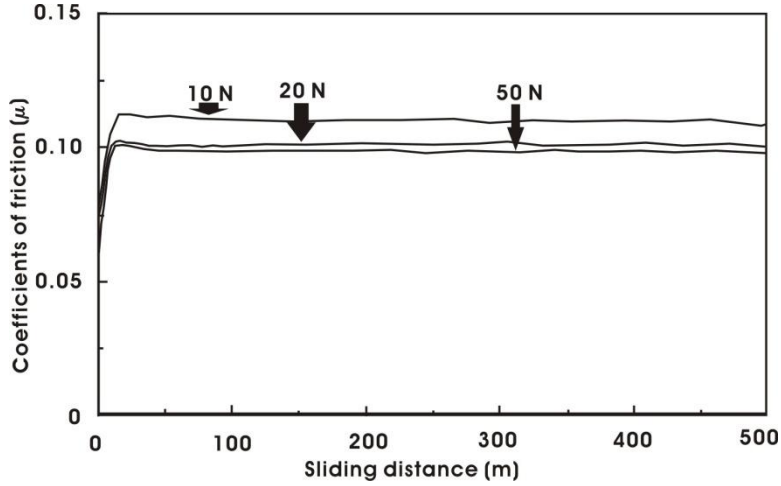

Figure 17. Friction coefficient as a function of applied loads of 10 N, 20 N and 50 N at a constant sliding distance of 500 m.

Copyright © 2012. Nova Science Publishers, Incorporated. All rights reserved.

Diamond-Like Carbon Films, Nova Science Publishers, Incorporated, 2012. ProQuest Ebook Central,

Friction and wear property of the film was investigated in the ball-on-disc tester, and curve of friction coefficient changed as a function of different applied loads is shown in Figure 17. As can be observed, the initial value of friction coefficients at different loads is approximately 0.1, and the friction coefficients in steady state are related to the applied loads, i.e., the greater the load the lower friction coefficient. The friction coefficients in steady-state range from 0.12 at 10 N to 0.09 at 50 N. Optical microscopic analysis of countersurface of the ball after testing showed a transfer layer in the contact area. It is estimated: a transferred graphite layer due to graphitization transformation of DLC film was contributed to the low friction coefficient, and high load capability of the film may be due to its structure.

4. Conclusion

The Cr-doped graded DLC film of 6.18 μm in thickness was successfully synthesized using the medium-frequency dual-magnetron sputtering. The thick DLC film contained a graded and multilayered structure to release the residual stress and to cope with the large discrepancy of physical properties between the DLC film and steel substrate. Cr layers played an important role of adhesion improvement, and the transitional layer including CrN_z and C_xCr_y layers played a role of hard support. The film possessed combined favorable properties: smooth surface morphology, Vickers hardness of 1560 kg/mm^2 at 250 g, good adhesion of *Lc* at 52 N and a majority of film maintained at the end stage of scratch test, low friction coefficient of 0.09 kept in a long sliding endurance distance. Due to having these advisable properties, it is predicted that such thick Cr-doped DLC film may have the potential to be used as a high-quality protective film on various steel substrates, such as cutting tools and moldings.

SECTION 4: INFLUENCE OF CR CONTENT AND NANOGRAIN SIZE ON MICROSTRUCTURE, MECHANICAL AND SLIDING TRIBOLOGICAL BEHAVIOR OF HARD CR-DLC FILMS

1. Introduction

Due to their unique combined properties of high hardness, smooth surface and chemical inertness, diamond-like carbon (DLC) films have been extensively studied and applied in various sliding machine components and cutting tools over the last two decades [40,41]. One major drawback of DLC films is their high compressive stresses inhered and induced during the synthesis of diamondlike content like sp^3 carbon bonding [42,43], which results in a poor adhesion.

Many scientific researches in the past decade have therefore been concentrating on the syntheses of metal-containing DLC (Me-DLC) films so as to alleviate the drawback and, in turn, to develop the mechanical and sliding tribological behavior of the DLC films. A number of studies on synthesis and characterization of Me-DLC films are available in literature, and they are focusing on Ti [44,45], W [46,47], Ta [48], and Cr [49] containing DLC, especially on Ti and W. Cr (Chromium) has been used as carbide former and chromium compounds

Copyright © 2012. Nova Science Publishers, Incorporated. All rights reserved.

Diamond-Like Carbon Films, Nova Science Publishers, Incorporated, 2012. ProQuest Ebook Central,

possess attractive properties of combined hardness and ductility. However, available work in this area is still rather lacking. We have synthesized some Cr-DLC films in mid-frequency dual-magnetron sputtering, whose microhardness varied from the hard to the superhard [50,51], and the Cr content and C/Cr nanograin size is supposed to induce the variety of the mechanical and and sliding tribological behavior, but its actual influence is still unkown. Y. Pauleau and F. Thiery [52] propounded that Me-DLC composite films with metal content in range of 10~20 at% could be produced using plasma-assisted deposition techniques and would possess excellent tribological properties. Unfortunately, they did not report any relevant microstructural and tribological information of Cr-DLC film. V. Singh et al [53] reported an initial reduction in hardness followed by stabilizing approximately at a value of 13.5 GPa when Cr was incorporated into the DLC film by a hybrid PVD/PECVD process.

This section has been initiated to investigate the technique for fabricating hard Cr-DLC nanocomposite films with variation of Cr content and Cr-containing nanocrystalline size. A systematic study is conducted so as to better understand the infulence of synthesizing method, Cr content, Cr-containing nanocrystalline size, on the micorstructure and properties of hard Cr-DLC nanocompoiste films. It then goes on to correlate adequately such synthesizing effect to the achievable mechanical and sliding tribological performances so that the microstructures and compositional ranges of the films can be suitably optimized.

2. Experimental Details

Silicon (100) wafers of diameter 70 mm were used as the substrate material. The substrate was first ultrasonically cleaned in acetone bath for 15 min. It then was mounted on a stainless steel holder in the depositing chamber after being blown dry with nitrogen. A mid-frequency dual-magnetron sputtering system was used to synthesize the Cr-DLC films. The configuration and deposition process of the mid-frequency dual-magnetron sputtering system were as described in references [50,51,54]. There were four pairs of dual-magnetron targets, which include two Cr and six C being set in the cylindrical coating rig of the system. In filming the necessary deposition, the substrate was connected to a pulsed DC supply while each pair of dual-magnetrons was connected to a 40 kHz pulsed AC power supply. Suitably adjusting the current of Cr magnetron targets and controlling the combination of pressure, substrate bias voltage and substrate temperature allow varying the Cr content and nonograin size in the films. Two layers of Cr-DLC films consisting of (i) an approximately 0.5 μm thick Cr interlayer and (ii) a 1 μm thick Cr-DLC cover layer were achievable by this filming technique.

A energy dispersive spectrometer (EDS) attached to a scanning electron microscope (SEM) was used to determine the Cr content in the films. A X-ray diffractometer (XRD) and a X-ray photoelectron spectroscopy (XPS) was respectively used to analyze Cr grain size and chemical state of C and Cr. A nanoindenter was used to measure the film hardness under the testing conditions of 2 mN applied load of nanoindentation, 5 s loading and unloading, indentation depth less than 50 nm, and each measurement value using the average of six tests. A ball-on-disk tester was used to evaluated the sliding tribological behavior in ambient atmpsphere under the testing conditions of 2 N normal load, 0.65 ms^{-1} sliding speed, sliding distance of 800 m, using a ϕ6 mm Al_2O_3 ball as a counterpart and using ϕ45 mm M2 high-steel sample deposited with Cr-DLC as a disc. The intrinsic stresses σ in the films were

Copyright © 2012. Nova Science Publishers, Incorporated. All rights reserved.

Diamond-Like Carbon Films, Nova Science Publishers, Incorporated, 2012. ProQuest Ebook Central,

analyzed by measuring the radius of curvature of the Si substrate with an optical profilometer after the deposition of the corresponding film. Then, the measurements were further processed using the following Stoney's equation [55].

$$\sigma = \frac{1}{6R}\frac{E}{(1-v)}\frac{d_{sub}^2}{d} \quad (1)$$

where: E, v, and d_{sub} are Young's modulus, Poisson's ratio, and thickness of the substrate, respectively; and d is the film thickness. The radius R of curvature of the reference wafer before deposition was measured and taken as R_1. After deposition, the R was taken as the relative substrate radius of curvature and was calculated as $R=R_1R_2/(R_1-R_2)$ in which R_1 and R_2 are the radii of curvatures before and after depositions, respectively.

3. Results

As shown in Table 2 indicating the main parameter, Cr atomic percentage and grain size in eight DLC films, the mid-frequency dual-magnetron system is a successful tool to produce the Cr-DLC films with a variety of chromium contents, spanning from 5 at% to 36 at%. The atomic percent of chromium element exhibits a increasing tendency with the value increase of Cr magnetron current. The Cr magnetron current is a major effective factor for controlling the Cr at%.

Table 2. Main deposition parameter, Cr atomic percentage and grain size for eight Cr-DLC coated samples

Film number	Cr magnetron current (A)	Cr (at%)	Cr-containing grain size (nm)
1	**1.2**	**5.4**	**17.6**
2	**2.1**	**8.3**	**18.4**
3	**2.8**	**10.6**	**23.6**
4	**3.2**	**15.3**	**26.9**
5	**4.3**	**21.6**	**34.8**
6	**5.2**	**25.7**	**48.7**
7	**8.5**	**30.8**	**53.6**
8	**11.8**	**35.4**	**73.2**

Base pressure: 2×10^{-3} Pa; Ar^+ sputtering cleaning: 4 Pa, -600 V(duty ratio: 70%), 10 min; deposition: pressure: 0.3 Pa, -120 V (duty ratio 50 %), chamber temperature less then 100 ^oC.

Copyright © 2012. Nova Science Publishers, Incorporated. All rights reserved.

Diamond-Like Carbon Films, Nova Science Publishers, Incorporated, 2012. ProQuest Ebook Central,

But the Cr atomic percentage couldnot be precisely set only by controlling the current in that the combination of pressure, substrate bias voltage and substrate temperature also affects the atomic precent in a certain degree.

The XRD spectra show a majority of amorphous characteristic by means of "amorphous peaks" and some chromium broadening peaks. The amorphous characteristic is a typical character of DLC film, and the peak broadening may be attributed to the smaller Cr-containing grain size, i.e., the crystallites are dispersed in the amorphous matrix [56,57]. The following Scherrer formula [58] is used to determine the size of Cr crystals in a direction normal to its crystallographic plane:

$$D = \frac{K \cdot \lambda}{B_{1/2} \cdot \cos\theta} \tag{2}$$

where: λis the X-ray wavelength of CuKα radiation and equal to 0.154 nm; $B_{1/2}$ is fullwidth at half maximum of the peak and θ is Bragg angle. Calculation based on the measured $B_{1/2}$ gives the mean grain-sizes of the Cr-containing nanoparticles, as shown in Table 2. The microstructure of Cr-DLC consists of a mixture of an amorphous carbon with a chromium-containing nanocrystalline, and the grain size increases with increasing Cr content. One reason is that the formation of chromium-containing nanocrystallites disperses an amorphous carbon network (DLC), favoring constant re-nucleation of chromium-containing nanoparticles as the Cr content increases.

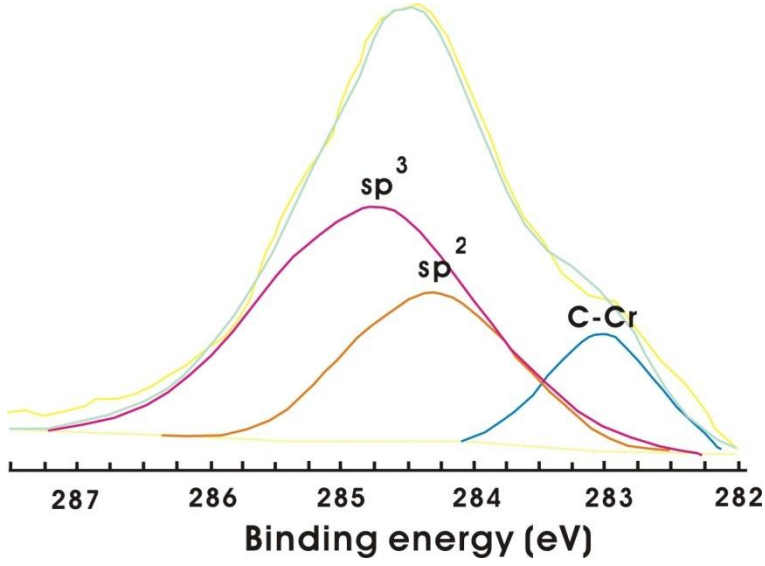

Figure 18. High-resolution C 1s spectrum of Cr-DLC with 8.3 at% Cr content.

Since the percentage of carbon (C) couldnot be detected with accuracy by EDS and XRD, the Cr-DLC films were analyzed using XPS. Figure 18 shows a high-resolution C 1s XPS spectrum from a Cr-DLC film with 8.3 at% Cr, exhibiting a major peak at a binding energy around 284.5 eV and a shoulder around 283 eV. The C 1s peak can be deconvoluted into

Copyright © 2012. Nova Science Publishers, Incorporated. All rights reserved.

Diamond-Like Carbon Films, Nova Science Publishers, Incorporated, 2012. ProQuest Ebook Central,

three components with binding energies 283, 284.3, and 284.8 eV corresponding to Cr–C [59], sp^2 C–C [60], and sp^3 C–C [61,62], respectively. The shoulder around 283 eV can also be further deconvoluted into four components with binding energies 283.1, 282.9, 282.8 and 282.6 eV corresponding to Cr_7C_3, Cr_3C_2, Cr_2C_3 and CrC, respectively. As the Cr content increases, XPS spectra indicate (i) the relative intensity of shoulder peak increases which suggests some Cr combines with C to from Cr-rich carbide while the rest Cr is incorporated in the C network of DLC; (ii) the binding energy of the shoulder peak tends to approach the low limit of 283 eV which means the Cr combines with C to partly transform the Cr-rich nanoparticles into a CrC phase.

As shown in Figure 19 indicating the hardness and intrinsic stress (compression stress) varied with Cr contents, increasing with Cr content, the hardness value of the Cr-DLC films presents a sudden increasing to a maximum value, approximately 43 GPa for the 8.3 at% Cr, and then tends to a gradual decrease to a minimum value, approximately 22 Gpa the 35.4 at% Cr; whereas the instrinsic stress value shows a gradual increase on the whole from 1034 MPa the 5.4 at% Cr to 2458 MPa the 35.4 at% Cr. Suitable addition of chromium, especially for the 8.3 at% Cr, leads a significant increase in the hardness and a simultaneous decrease in the intrinsic stress for the hardest of the Cr-DLC films. The dependence of the hardness and the instrinsic stress on the Cr content is complex. Hardness of non-hydrogenated DLC films results from a balance between the formation of sp^3 hybridization owing to local increases in mass density of the film and lattice relaxation owing to thermal spikes [63]. The addition of Cr to the growing film results in two competing effects: (i) The larger size of Cr atoms when compared with C atoms leads to a greater increase in local density and in intrinsic stress of the Cr-DLC films; and (ii) the presence of multiple charged ions, C^{m+} and Cr^{n+} ions with various chemical charge states, in the plasma stream leads to a greater energy transfer to the film growth, which induces softeneing. The final effect on the film may be a compromise between the above two effects.

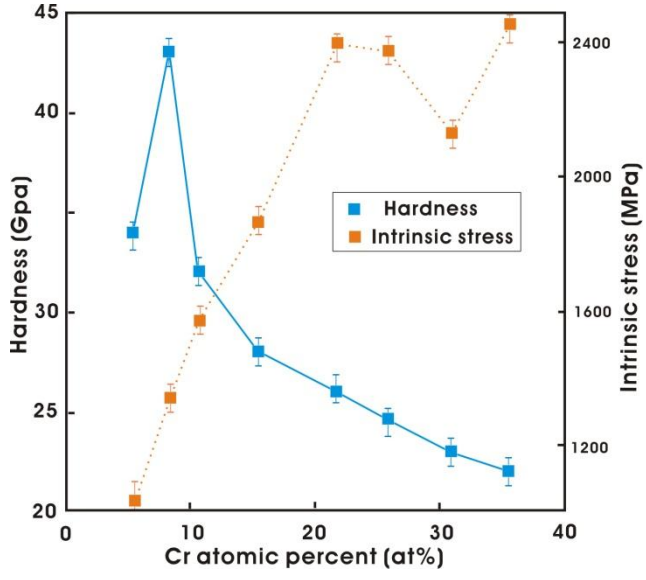

Figure 19. Hardness and intrinsic stress of Cr-DLC film as a function of Cr content.

Copyright © 2012. Nova Science Publishers, Incorporated. All rights reserved.

Diamond-Like Carbon Films, Nova Science Publishers, Incorporated, 2012. ProQuest Ebook Central,

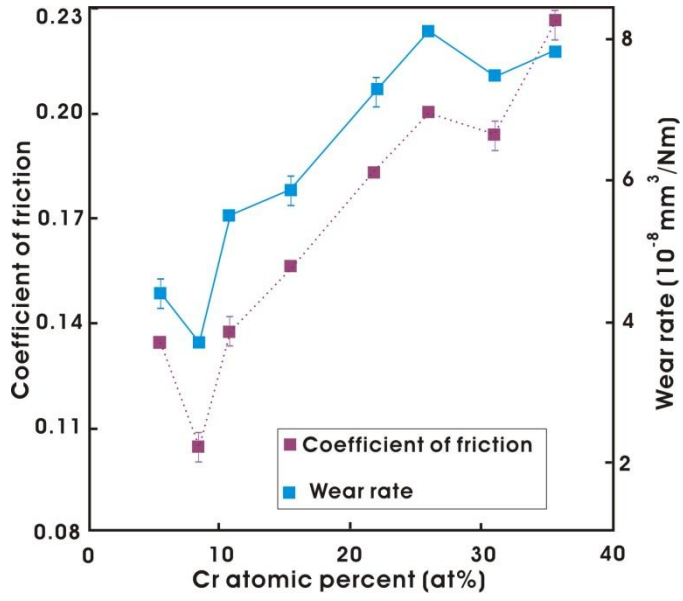

Figure 20. Coefficient of friction and wear rate of Cr-DLC films as a function of Cr content.

Figure 20 compares steady-state μ (COF, coefficient of friction) and wear rate (calculated after 800 m of sliding distance) of the Cr-DLC films as a function of Cr content. The steady-state μ refers to the COF after stabilization. The COF curves show that the COF of all films initially rises, then drops and later increases slowly, before stabilizing to a steady-state μ. The steady state μ of the films varies in range of 0.10~0.23 and basically tends to increase with the increase of Cr content. This can be attributed to the presence of the hard Cr/C particles that can remain in the wear track causing continuous disruption in the graphitized layer. Also, the Cr incorporated into the C network is also expected to interfere with the formation of low shear sp^2 C bonds. Graphitization results in the presence of a low shear strength layer at the sliding interface producing low friction. The wear rate shows an increasing tendency on the whole from 3.6 to 8.3 10^{-8} mm^3/Nm by increasing incorporation of Cr. Nevertheless, all wear rates are low and within the same order of magnitude of 10^{-8} mm^3/Nm. The Cr-DLC film with the 8.3 at% Cr possesses both the lowest COF, approximatelyμ=0.1, and the lowest wear rate, approximately 3.6 10^{-8} mm^3/Nm, which is attributed to its superhard characteristic. The reason for a sudden decrease in two curves in Figure 20 for the Cr-DLC film with the 30.8 at% Cr still needs a further investigation, which may be involved with its intrinsic stress.

4. Conclusion

The influence of Cr content and Cr-containing nanograin size on the microstructure, mechanical and sliding tribological behavior of the Cr-DLC films in the mid-frequency dual-magnetron was investigated. Such influence on the properties was attributed to the variation of Cr-content and the formation of Cr/C nanoparticles in the DLC matrix. Within a certain range of the Cr content and the nanograin size, the intrinsic compressive stresses and the COF of the Cr-DLC film were reduced whilst its hardness was increased.

Copyright © 2012. Nova Science Publishers, Incorporated. All rights reserved.

Diamond-Like Carbon Films, Nova Science Publishers, Incorporated, 2012. ProQuest Ebook Central,

REFERENCES

[1] J. Robertson. *Mat. Sci. Eng R.*. 2002, 37, 129-281.
[2] M.Chhowalla. *Diam. Relat. Mater*. 2001, 10, 1011-1016.
[3] Sam Zhang, Hong Xie. *Surf. Coat Technol*. 1999, 113, 120-125.
[4] Y.Lifshitz. *Diam. Relat. Mater*. 1999, 8, 1659-1676.
[5] J. Qi, K.H. Lai, C.S. Lee, I. Bello, S.T. Lee, J.B. Luo, S.Z. Wen. *Diam. Relat. Mater*. 2001, 10, 1833-1838.
[6] P.J.Kelly, R.D.Arnell. *Vacuum*. 2000, 56, 159-172.
[7] Sam Zhang, Xuan Lam Bui, Yongqing Fu. *Surf. Coat Technol*. 2003, 167, 137-142.
[8] J. Stallard, D. Mercs, M. Jarratt, D.G. Teer, P.H. Shipway. *Surf. Coat Technol*. 2004, 177/178, 545-551.
[9] S.Yang, D.G. Teer. *Surf. Coat Technol*. 2000, 131, 412-416.
[10] M. Jarratt, J. Stallard, N.M. Renevier, D.G. Teer. *Diam. Relat. Mater*. 2003, 12, 1003-1007.
[11] M. Stuber, S. Ulrich, H. Leiste, A. Kratzsch, H. Holleck. *Surf. Coat Technol*. 1999, 116–119, 591-598.
[12] Kwang-Ryeol Lee, Kwang Yong Eun, Inyoung Kim. *Thin Solid Films*. 2000, 377/378, 261-268.
[13] R.D.Arnell, P.J.Kelly, J.W.Bradley. *Surf. Coat Technol*. 2004, 188/189, 158-163.
[14] Yamamoto Kazuhiro, Watanabe Toshiya, Wazumi Koichiro, et al. *Diam Relat Mater*. 2001, 10, 895-899.
[15] Xiang Yu, Xu Zhang, Cheng-biao Wang, et al. *Vacuum*. 2004, 75, 231-236.
[16] Wei Zhang, Akihiro Tanaka , Koichiro Wazumi , Yoshinori Koga. *Diam. Relat. Mater*. 2002, 11, 1837-1844.
[17] J. Musil, P. Baroch, J. Blcek, K.H. Nam, J.G. Han. *Thin Solid Film*. 2005, 475(1-2), 208-218.
[18] R.D. Arnell, P.J. Kelly, J.W. Bradley. *Surf. Coat Technol*. 2004, 188–189, 158-163.
[19] U. Heister, J. Krempel-Hesse, J. Szczyrbowski, G. Teschner, J. Bruch. *Vacuum*. 2000, 59, 424-430.
[20] J.W. Bradley, H. Backer, P.J. Kelly, R.D. Arnell. *Surf Coat Technol*. 2001, 135, 221-228.
[21] D. Grimanelis, S. Yang, O. Bohme , E. Roman , A. Alberdi. *Diam. Relat Mater*. 2002, 11, 176-184.
[22] U. Krause, M. List, H. Fuch. *Thin Solid Films*. 2001, 392, 196-.
[23] J. Stallard, D. Mercs, M. Jarratt, D.G. Teer, P.H. Shipway. *Surf. Coat. Technol*. 177-178 (2004) 545-551.
[24] Martin Misina. *Surf. Coat Technol*. 2003, 169-170, 53-56.
[25] D. Luca, A. W. Denier van der Gon, V. Anita, M. W. G. Ponjee. *Vacuum*. 2001, 61, 163-167.
[26] P.J. Kelly, R.D. Arnell, *Vacuum*, 2000, 56, 159-176.
[27] Xiang Yu, Chengbiao Wang, Gongwu Jiang, Haisheng Liu, Meng Hua. *Vacuum*. 2004, 72, 461-466.
[28] Zhang Wei, Tanaka Akihiro, Wazumi Koichiro, Koga Yoshinori. *Diam. Relat Mater*. 2002, 11, 1837-1844.
[29] V. Felmetsger, P. Laptev. *Vacuum*. 2004, 74, 403-408.

Copyright © 2012. Nova Science Publishers, Incorporated. All rights reserved.

Diamond-Like Carbon Films, Nova Science Publishers, Incorporated, 2012. ProQuest Ebook Central,

[30] D. Camino, A.H.S. Jones, D. Mercs, D. G. Teer. *Vacuum*. 1999, 52, 125-131.
[31] S. Logothetidis, C. Charitidis, M. Gioti, Y. Panayiotatos, M. Handrea. *Diam. Relat. Mater*. 2000, 9, 756- 760.
[32] Kelly P. J., Arnell D. *Vacuum*, 2000, 56, 159-172.
[33] R.D. Arnell, P.J. Kelly, J.W. Bradley. *Surf. Coat Technol*. 2004, 188-189, 158-163.
[34] M. Sasaki, Y. Kozukue, K. Hashimoto, K.Takayama. *Vacuum*. 2004, 74, 455-459.
[35] D. L. Baptista, F. C. Zawislak. *Diam. Relat. Mater*. 2004, 13, 1791- 1801.
[36] C. D. Joon, K. W. Hoe, J. S. Moon. *Vacuum*. 2004, 72, 445-451.
[37] S.Yang, D.G.Teer. *Surf Coat Technol*. 2000, 131, 412-418.
[38] I.Ahmad, P. D.Maguire, P. Lemoine. *Diam. Relat. Mater*. 2004, 13, 1346- 1439.
[39] Lungu Cristian Petrica, Iwasaki Kunihiko, Kishi Katsuhiro. *Vacuum*, 2004, 76, 119-126.
[40] R. Prioli, M.Chhowalla, F. L. Freire. *Diam. Relat. Mater*. 2003, 12, 2195- 2202.
[41] J. Robertson. *Mat. Sci. Eng. R*. 2002, 37(4-6), 129-281.
[42] S. Zhang, Y. Q. Fu, H. J. Du, X. T. Zeng. *Surf Coat Technol*. 2003, 162(1),42-48.
[43] Peter C.T. Ha, D.R. McKenzie, M.M.M. Bilek. *Surf. Coat Technol*. 2007, 201(15), 6734-6736.
[44] T. Iseki, H. Mori, H. Hasegawa, H. Tachikawa K. Nakanishi. *Diam. Relat. Mater*. 2006, 15(4-8), 1004-1010.
[45] J. Barriga, M. Kalin, K. Van Acker, K. Vercammen, A. Ortega and L. Leiaristi. *Wear*. 2006, 261(1), 9-14.
[46] W. J. Yang, T. Sekino, K. B. Shim, K. Niihara and K. H. Auh. *Thin Solid Films*. 2005, 473(2), 252-258.
[47] K. Baba, R. Hatada, Y. Tanaka. *Surf. Coat Technol*. 2007, 200(19-20), 8362-8365.
[48] C.W. Moura e Silva, J.R.T. Branco, A. Cavaleiro. *Thin Solid Films*. 2006, 515(3), 1063-1068.
[49] E. Liu, B. Blanpain, X. Shi, J. P. Celis, H. -S. Tan. *Surf. Coat Technol*. 1998, 106(1),72-80.
[50] X. Yu, C. B. Wang, Y. Liu, D. Y. Yu. *Plasma Sci. Technol*. 2006, 8(3): 337-343.
[51] X.Yu, Y. Liu, C. B. Wang, X. C. Lu, D. Y. Yu, *Vacuum*. 2005, 80(4), 324-331.
[52] X. Yu, C. B. Wang, Y. Liu, D. Y. Yu, Z. Q. Fu. *Surf. Coat Technol*. 2006, 200(24), 6765-6769.
[53] Y. Pauleau, F. Thièry. *Surf. Coat Technol*. 2004, 180-181, 313-322.
[54] V. Singh, J.C. Jiang, E.I. Meletis. *Thin Solid Films*. 2005, 489(1-2), 150-158.
[55] X. Yu, C. B. Wang, Y. Liu, D. Y. Yu, *Diam. Relat. Mater*. 2006, 15(9), 1223-1227.
[56] H. Windischmann, K. J. Gray. *Diam. Relat. Mater*. 1995, 4(5-6), 837-842.
[57] S. Hussain, A.K. Pal. *Appl. Surf. Sci*. 2007, 253(7), 3649-3657.
[58] Masahito Ban, Takeshi Hasegawa, Sadao Fujii, Junzo Fujioka. *Diam Relat Mater*. 2003, 12(1), 47-56.
[59] G. S. Wu, X. Q. Zeng, S. S. Yao, X. M. Wang. *Mater. Lett*. 2007, 61(19-20), 4019-4022.
[60] H. Goretzki, P. Vonrosenstiel, S. Mandziej, Z. Fresenius. *Anal. Chem*. 1989, 333, 451.
[61] S. K. Pal, J. Jiang, E. I. Meletis, *Surf. Coat Technol*. 2007, 201(18), 7917-7923.
[62] Š. Meškinis, M. Andrulevičius, S. Tamulevičius, V. Kopustinskas. *Vacuum*. 2006, 80(9), 1007-1011.
[63] R Monteiro. *Annu. Rev. Mater. Res*. 2001, 31, 111-137.

Copyright © 2012. Nova Science Publishers, Incorporated. All rights reserved.

Diamond-Like Carbon Films, Nova Science Publishers, Incorporated, 2012. ProQuest Ebook Central,

In: Diamond-Like Carbon Films
Editor: Yuto S. Tanaka
ISBN: 978-1-61324-791-4
© 2012 Nova Science Publishers, Inc.

Chapter 8

A DIAMOND-LIKE CARBON FILM APPLIED AS AN ALIGNMENT LAYER FOR LCDS

Yoshimine Kato
Department of Materials Science and Engineering,
Kyushu University, Fukuoka, JAPAN

ABSTRACT

Diamond-like carbon (DLC) films have been applied as an alignment layer for liquid crystal displays (LCDs). There are two ways to align the DLC films for liquid crystals (LC). One way is to use non-contact alignment processes on DLC such as ion beam (IB) or linearly polarized UV light. The other way is to use novel self-aligned DLC film. No alignment processes such as rubbing or atomic beam bombardment or UV irradiation on DLC are necessary. In other words, DLC itself is self-aligned for LC as deposited. In the first section, a DLC film which uses an additional alignment process is described, and in the second section a self-aligned DLC film without an alignment process is described.

The DLC films which are used with non-contact alignment processes were deposited by chemical vapor deposition (CVD) or reactive DC magnetron sputtering on indium tin oxide (ITO) transparent electrodes on a glass. For this alignment process the DLC films can contain no or some hydrogen. The mechanism of liquid crystals (LC) alignment appears to be due to the C=C π bonds (sp^2) orientation of the alignment layer. Therefore, with the non-contact alignment processes π bonds on the DLC surface remain more in one direction. As a result, LC aligns on the DLC films. Many amorphous, transparent, and electrically insulated films were investigated, and DLC films were the first to be optimized.

On the other hand, the self-aligned DLC films were deposited without hydrogen by using a DC magnetron in-line sputtering system only. The LC director alignment direction seems to be parallel to the substrate movement that is parallel to the magnetic field of the cathode and perpendicular to the plasma track line on the target during the in-line sputtering. The alignment mechanism of this DLC film seems to be related to the DLC crystalline structure that relates to the anisotropy of the π bonds orientation.

Copyright © 2012. Nova Science Publishers, Incorporated. All rights reserved.

Diamond-Like Carbon Films, Nova Science Publishers, Incorporated, 2012. ProQuest Ebook Central,

1. INTRODUCTION

LCDs have been widely used as flat panel displays for personal computers, TVs, projectors, game toys, watches, cellular phones, and portable displays for electronic goods, etc. For twisted nematic (TN) and in-plane switching LCDs it is necessary to align the LC, and the rubbing method has been used for many decades. For an alignment layer usually a polymer, such as polyimide (PI), is used and mechanically rubbed with a cloth-covered roller. Using this contact rubbing process in manufacturing causes problems, such as creating particles, causing electrostatic discharges, rubbing tracking, and rubbing cloth maintenance.

Recently, new methods of non-contact alignment have been proposed instead of rubbing, such as amorphous alignment [1], polarized UV irradiation [2], atomic beam bombardment [3-7], and plasma treatment [8]. For example, a diamond-like carbon (DLC) film was used as an alignment film instead of a polymer film, along with a non-contact alignment method using an Ar atomic beam or polarized UV light [6]. Oblique angle deposition of alignment films for LC has been also studied for decades [9-10].

From the near edge X-ray absorption fine structure (NEXAFS) study, it was found that the C=C π bonds (sp^2) orientation is related to LC alignment [11]. It is well known that IB bombarded PI surface mimics the surface of DLC which contains both sp^2 and sp^3 bonds. The replacement of PI film by a simple dry processed film was advantageous from a cost point of view. Many amorphous, transparent, and electrically insulated films were investigated, and DLC films were the first to be optimized for TN and inplane switching display technologies used in LCDs [4, 5].

The first section describes the use of DLC films as an alignment layer instead of a polymer film with a new non-contact alignment method using an Ar IB, and linearly polarized UV light. Deposition conditions and the characteristics of the DLC film used as the alignment film for LCDs are discussed. Ar IB and UV conditions are also described.

In the next section, it is demonstrated that a sputtered DLC film works as an alignment layer for LC without any additional alignment process such as rubbing or IB bombardment or UV irradiation. This self-aligning film fabrication process was performed using an in-line type DC magnetron sputtering tool with only Ar gas without H_2, and a carbon target. The alignment properties are observed by using a test cell examination and the V-T curve measurement [12].

2. DLC FILMS USING ION BEAM OR UV LIGHT NON-CONTACT ALIGNMENT PROCESS

DLC films were applied as an alignment layer for LCDs instead of a conventional polymer alignment film. DLC films can be aligned with non-contact alignment methods using an Ar atomic beam or polarized UV light. The deposition conditions for the DLC films, such as total pressure, power, electrode gap, and gas mixture ratio were carefully studied and optimized. Alignment of liquid crystals was created by exposing the substrate to 257nm polarized UV light and the directional bombardment of an Ar ion beam onto the DLC film. By using this non-contact alignment method, high quality large area LCD panels can be successfully fabricated. The resulting LCDs showed higher quality front-of-screen

Copyright © 2012. Nova Science Publishers, Incorporated. All rights reserved.

Diamond-Like Carbon Films, Nova Science Publishers, Incorporated, 2012. ProQuest Ebook Central,

characteristics than those obtained by the conventional thick polymer rubbing method particularly with respect to the lack of the rubbing tracks.

2.1. Experiment

DLC films used as alignment layers were deposited by either a parallel plate capacitive coupled plasma enhanced chemical vapor deposition (PECVD) or a reactive DC magnetron sputtering tool. For test samples, the DLC films were deposited on a glass substrate containing indium tin oxide (ITO) transparent electrodes. For actual large size LCDs, the film was deposited on both the color filter glass and the thin film transistor (TFT) array substrate. The film thickness was varied from about 2 to 20 nm thick.

For PECVD deposition, similar to a conventional diamond-like carbon (DLC) deposition for hard disks, the substrates were placed on a RF powered cathode. Methane (CH_4) and 10% helium-based acetylene (C_2H_2) gas were used as precursors. Power density was varied from 14.4 to 180.4 mW/cm^2 and the substrate temperature was kept at room temperature. The operating pressure was varied from 2.7 to 27 Pa, and the electrode gap was varied from 60 to 130 mm. The gas mixture ratio of He/H_2/CH_4 or H_2/C_2H_2 was also varied. These deposition parameters were carefully studied and optimized. The cathode self-bias voltage ($-V_{dc}$) was recorded during the process.

The sputtering deposition was performed in a conventional DLC deposition method similar to those used to coat hard disks. A sintered graphite plate was used as a target and a mixture of Ar and H_2 gases were used. The power density was varied from 0.62 to 3.1 W/cm^2 and the substrate temperature was varied from room temperature to 250ºC. The operating pressure was varied from 0.1 to 2.0 Pa. The gas mixture ratio of H_2/Ar was also varied from 0 to 1.0.

Following the DLC film deposition, the alignment process for liquid crystals was performed using both the directional bombardment of an Ar IB onto the DLC film at an angle of 15 to 70 degrees [4-5], and using the linearly polarized UV photo alignment process [2]. For the UV photo alignment, 257nm linearly polarized deep UV laser light with an energy density of 20mW/cm^2 was irradiated normal to the sample surface. The UV dosage was varied by changing the exposure time. For an IB alignment a Kaufman-type ion source was used for creating an Ar ion beam with an accelerating voltage of 50-700 eV. A tungsten filament neutralizer was used to neutralize the Ar ion beam. The total Ar flow rate was varied from 3 to 30 sccm. To create the alignment for liquid crystals the DLC film coated glass substrate was scanned beneath the Ar beam with a scan speed of 2-100 mm/sec. Faraday-cup probes were used to measure the ion beam profile. Figure 1 shows the schematic drawing of the ion beam source and the substrate.

For analysis of the DLC film, the resistivity, optical transmittance, stress, hardness, Fourier transform infrared spectroscopy (FTIR) characteristics, Ramann spectra and H content were measured. The resistivity measurement was done in the film plane using a high-resistivity meter (YHP 4329A) with a ring-shaped electrode. The optical transmittance of the film was determined by integrating the transmittance spectrum from 380 to 780 nm. The H contents were measured using Rutherford backscattering spectrometry (RBS) and forward recoil elastic scattering (FRES) of 2.3 MeV $^4He^+$ ions. X-ray photoemission spectroscopy

Copyright © 2012. Nova Science Publishers, Incorporated. All rights reserved.

Diamond-Like Carbon Films, Nova Science Publishers, Incorporated, 2012. ProQuest Ebook Central,

(XPS) and Time-of-Flight Secondary Ion Mass Spectrometry (TOF-SIMS) were used to measure the impurity element in the film.

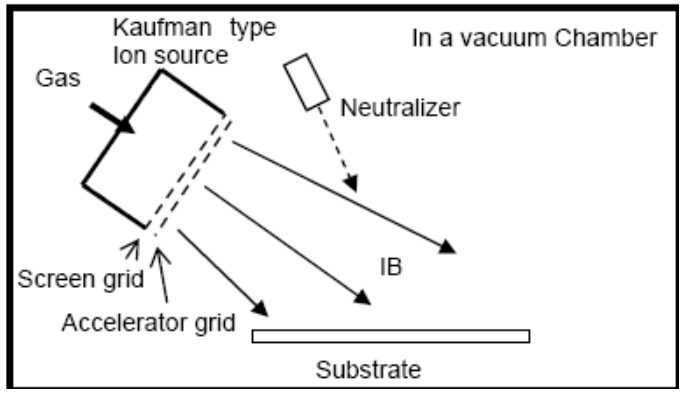

Figure 1. Schematic drawing of an ion beam source and a substrate in a vacuum chamber.

For observation of the surface topography, atomic force microscopy (AFM) was used. The film thickness was determined by transmission electron microscopy (TEM) cross-sectional photograph, measurement of the step height and by calculation from the optically measured transmittance and reflectance (wavelength = 190-1000 nm) of the film, which were obtained by using an nandk analyzer. The alignment property on the DLC film was analyzed by NEXAFS spectroscopy [11, 13] and LC alignment was characterized by fabricating conventional LC test cells and LCDs.

After the DLC films were deposited and the alignment process was performed on the glass substrates, spacer balls were spread on the surface. Then, the two substrates were glued face to face and LC was injected in-between. The anchoring energy (AE) and pretilt angle (PA) were measured with a method described elsewhere [14].

2.2. Results and Discussion

2.2.1. PECVD and Sputtered DLC Films

Since the DLC alignment film is deposited on both the color filter glass and a TFT array glass, its transmittance is important as a display. For PECVD films, as shown in Figure 2, transmittance mostly depends on power density and not much on other parameters. As the power density becomes higher the transmittance becomes lower for both C_2H_2 and CH_4 gases. This transmittance in Figure 2 is normalized for 10 nm film thickness. Therefore, it is important to keep the power density lower in order to obtain a high transmittance CVD film. It is interesting to note that the resistivity of the film exhibits the same tendency as the transmittance as shown in Figure 2. The resistivity decreases as the power density increases for both C_2H_2 and CH_4 gases.

The transmittance and sheet resistance variation relates to the hydrogen incorporation in the film as shown in Figure 3(a). This does not relate to the gas type either CH_4 or C_2H_2. Hydrogen content in the film is higher when the power density is lower as shown in Figure

Copyright © 2012. Nova Science Publishers, Incorporated. All rights reserved.

Diamond-Like Carbon Films, Nova Science Publishers, Incorporated, 2012. ProQuest Ebook Central,

3(b), thus hydrogen incorporation in the film is higher when the deposition rate of the carbon is lower; therefore, the film transmittance becomes higher.

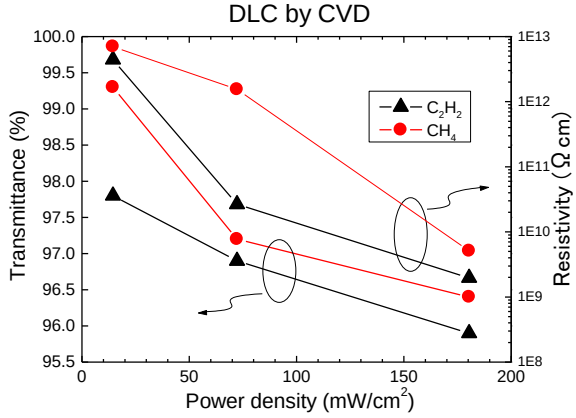

Figure 2. Transmittance and resistivity vs. power density for CVD film. Transmittance and resistivity is higher for CH_4.

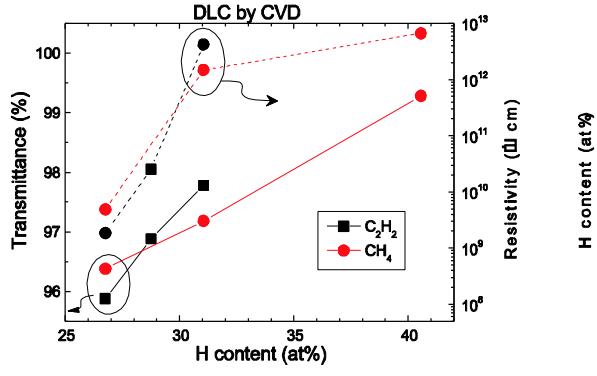

(a)

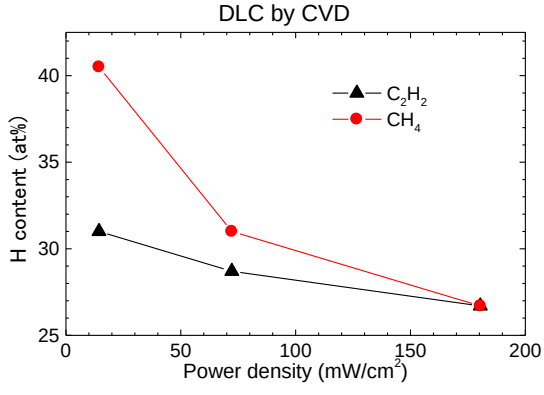

(b)

Figure 3. Hydrogen content variation of CVD films. (a) Hydrogen content effect on transmittance and resistivity of the film. (b) Hydrogen content in the film vs. power density.

Copyright © 2012. Nova Science Publishers, Incorporated. All rights reserved.

Diamond-Like Carbon Films, Nova Science Publishers, Incorporated, 2012. ProQuest Ebook Central,

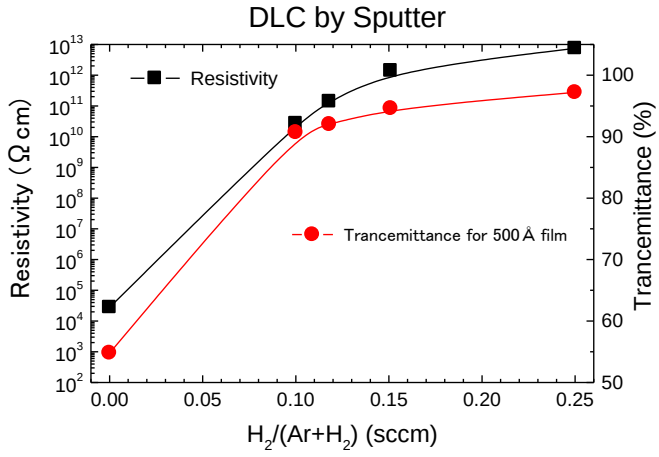

Figure 4. H content during sputtering vs. resistivity and transmittance and of the film.

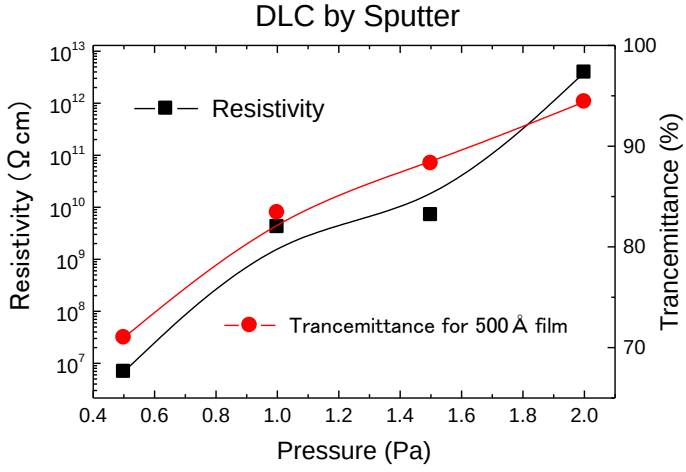

Figure 5. Total pressure during sputtering vs. resistivity and transmittance of the film.

This appears to be the same for the resistivity, as the H content increases the number of sp^2 π bonds in the film decreases; therefore, the conduction related to sp^2 bonding also decreases. As shown in Figure 2, using CH_4 results in higher film transmittance consistent with a higher H/C ratio than in the case for C_2H_2 gas. It is apparent that this is due to the C and H mole fraction difference between CH_4 and C_2H_2 gases, CH_4 contains more H per C atom. Other parameter such as electrode gap had minimal influence on the film characteristics.

For sputtered films, the transmittance of the film also increases with the H content in the film, the result of adding more H_2 gas during the sputtering. As the H_2/Ar gas ratio increases, the resistivity of the film also increases as shown in Figure 4. Therefore, the transmittance and resistivity of the film are related to the H content in the film consistent with the CVD deposited films. The sputtered DLC film contained about 30 at% (atomic percent) H when $H_2/Ar + H_2$ was 0.25. This can also be realized by increasing the pressure in the chamber during sputtering as shown in Figure 5. Both transmittance and resistivity increase with total

Copyright © 2012. Nova Science Publishers, Incorporated. All rights reserved.

Diamond-Like Carbon Films, Nova Science Publishers, Incorporated, 2012. ProQuest Ebook Central,

pressure, however, the substrate temperature did not have much influence. This can be explained by the large hydrogen incorporation in the film as the H_2 partial pressure increases.

The stress of DLC films also varies with the operating pressure during the sputter or CVD deposition process as shown in Figure 6. As the total pressure in the deposition chamber increases, we found that the compressive stress in the film decreases. The effect was observed in both the CVD and sputter deposited films. This effect is the well known, "peening effect", result of the inverse relationship between the energy of the species impinging on the substrate during the deposition and the process pressure. As the pressure is decreased, the increasing energy of the impinging species results in a denser film which exhibits and increasing compressive stress. In order to maximize the film adhesion, it is important to have lower compressive stress in the films.

Figure 7 shows a cross-sectional TEM image of the sputtered DLC film on a glass substrate. It shows that the DLC film is quite uniform through out the viewing area. Adhesion to the glass was well enough when the stress of the film was less than around 1-2 x 10^9 dyn/cm^2 , and passed so-called the Scotch tape pealing test.

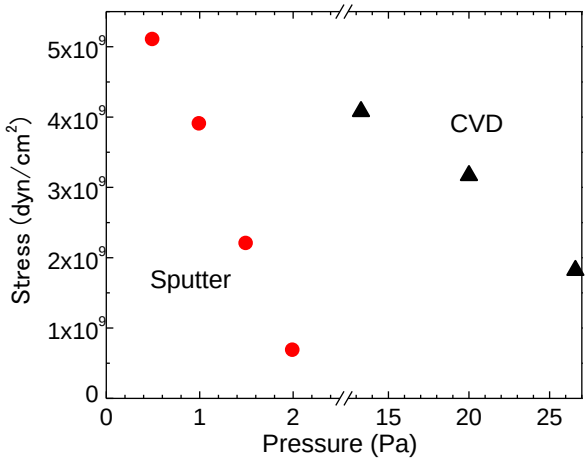

Figure 6. Compressive stress of DLC film vs. total pressure during the sputtering and CVD process.

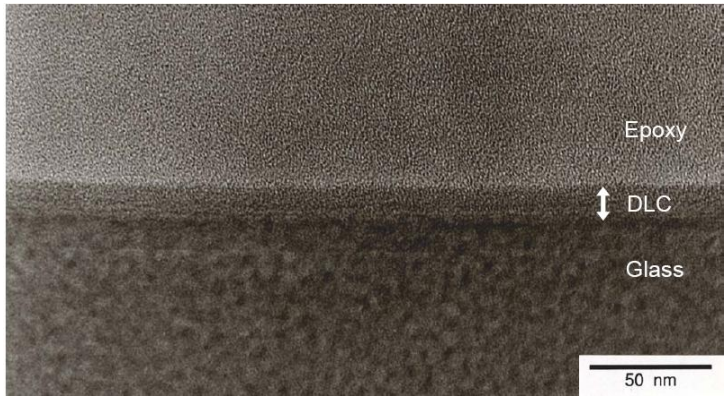

Figure 7. Cross-sectional TEM image of the sputtered DLC film on a glass substrate.

Copyright © 2012. Nova Science Publishers, Incorporated. All rights reserved.

Diamond-Like Carbon Films, Nova Science Publishers, Incorporated, 2012. ProQuest Ebook Central,

2.2.2. UV Photo-Alignment

The DLC film displays alignment characteristics for LC by exposing linearly polarized UV light on the film. The anchoring energy (AE) increases with the UV dosage as shown in Figure 8. However, the absolute value of the AE is quite small even when the UV intensity is high compared with PI aligned with the UV light. This may be due to the initial random state of the C=C π bonds (sp^2) network in the DLC film, such that the C=C bonds parallel to the polarized UV light are mostly destroyed; therefore, the LC aligns in the direction perpendicular to the polarized light along the C=C bonds. However, some of the C=C bonds perpendicular to the polarized UV light are also destroyed because there is no anisotropy in the absorption of the DLC film, thus the AE is not large enough.

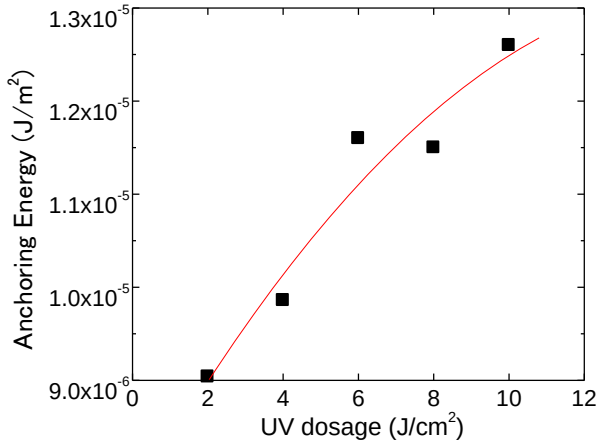

Figure 8. Anchoring energy of a photo-aligned DLC film using linearly polarized UV light.

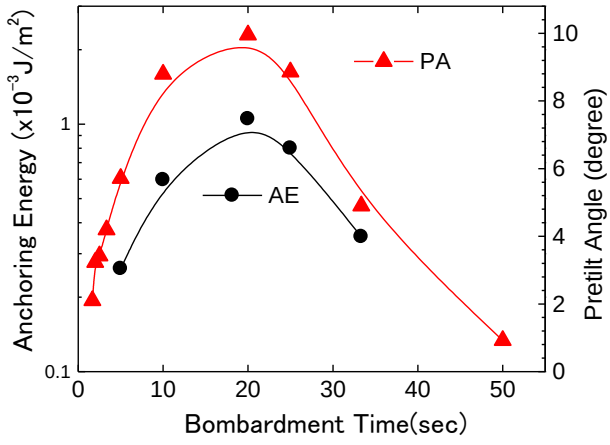

Figure 9. Anchoring energy (AE) and pretilt angle (PA) for an atomic beam aligned DLC film vs. bombardment time.

On the other hand, PI has anisotropy in absorbing the UV light and the PI molecules' main chain parallel to the polarized UV light have a larger absorption than those perpendicular to the polarized light [2]. Therefore, large anisotropy in the C=C bonds occurs on the PI surface and its anchoring energy is higher.

Copyright © 2012. Nova Science Publishers, Incorporated. All rights reserved.

Diamond-Like Carbon Films, Nova Science Publishers, Incorporated, 2012. ProQuest Ebook Central,

2.2.3. Ion beam alignment

Anchoring energy for LC varies with the ion beam conditions such as incident angle, accelerator voltage, beam current and voltage, gas flow rate, total pressure, and IB dosage. In particular, IB dosage is directly related to AE and PA as shown in Figure 9. It is similar to the UV photo alignment: as the IB dosage increases, it is believed that the C=C bond anisotropy increases due to bond-breaking, with IB along the incident direction, resulting in an increase in AE. However, when the ion dose becomes too large, the C=C bond anisotropy is destroyed and the AE starts to degrade. The same phenomenon occurs for the PA. The anchoring energy at the maximum is large enough for conventional LCDs such as twisted nematic and in-plane switching active mode displays. High quality, large area LCD panels can be fabricated without any rubbing tracks.

3. NOVEL DLC FILMS WITHOUT ANY ALIGNMENT PROCESS

The novel DLC films without H deposited by using a DC magnetron in-line sputtering system have shown sufficient self-alignment properties towards LC. From the observations of the test cells, the LC director was aligning parallel to the substrate movement direction of the in-line sputtering system. The alignment property of the DLC films has been demonstrated by a contrast ratio value of the test cells close to 200. It appears that the DLC film may have anisotropic structure that is interacting with LC to align.

3.1. Experiments

The DLC film was deposited by using a conventional in-line DC magnetron sputtering tool, which are similar to one mentioned in the last section, on a glass substrate coated with ITO transparent electrodes. A 5 x 25 inch sintered graphite plate was used as a target with conventional magnets and only Ar gas was introduced in a chamber. The glass substrate was scanned in front of the C target while Ar ions were sputtering the target as shown in Figures 10(a) and (b).

The film thickness was varied from 3 to 20nm and the power density was varied from 0.62 to 3.1 W/cm^2. The substrate temperature was kept at room temperature and the operating pressure was varied from 0.1 to 2.0 Pa. For comparison, a parallel plate capacitive coupled PECVD film was also tested with CH_4 or 10% helium-based C_2H_2 gas as a precursor. The film thickness was determined by using an optical instrument (nandk Analyzer 1280 made by nandk Technology, Inc., USA) that measures transmittance and reflectance of the film (wavelengths = 190-1000 nm) and then calculates the film thickness.

Liquid crystal test cells were fabricated by gluing two glass substrates coated with the DLC alignment film face to face and injecting twisted nematic (TN) LC (Merck MJ971189) with chiral pitches of 18μm or 100μm between glasses. The optical birefringence Δn of LC was about 0.094 and the test cells gap was about 5 μm. Both glasses were glued as alignment easy axes to become orthogonal such as for conventional TN cells. Then the optical cells were heated above the nematic-isotropic (NI) point and cooled down to become set in the amorphous alignment state.

Copyright © 2012. Nova Science Publishers, Incorporated. All rights reserved.

Diamond-Like Carbon Films, Nova Science Publishers, Incorporated, 2012. ProQuest Ebook Central,

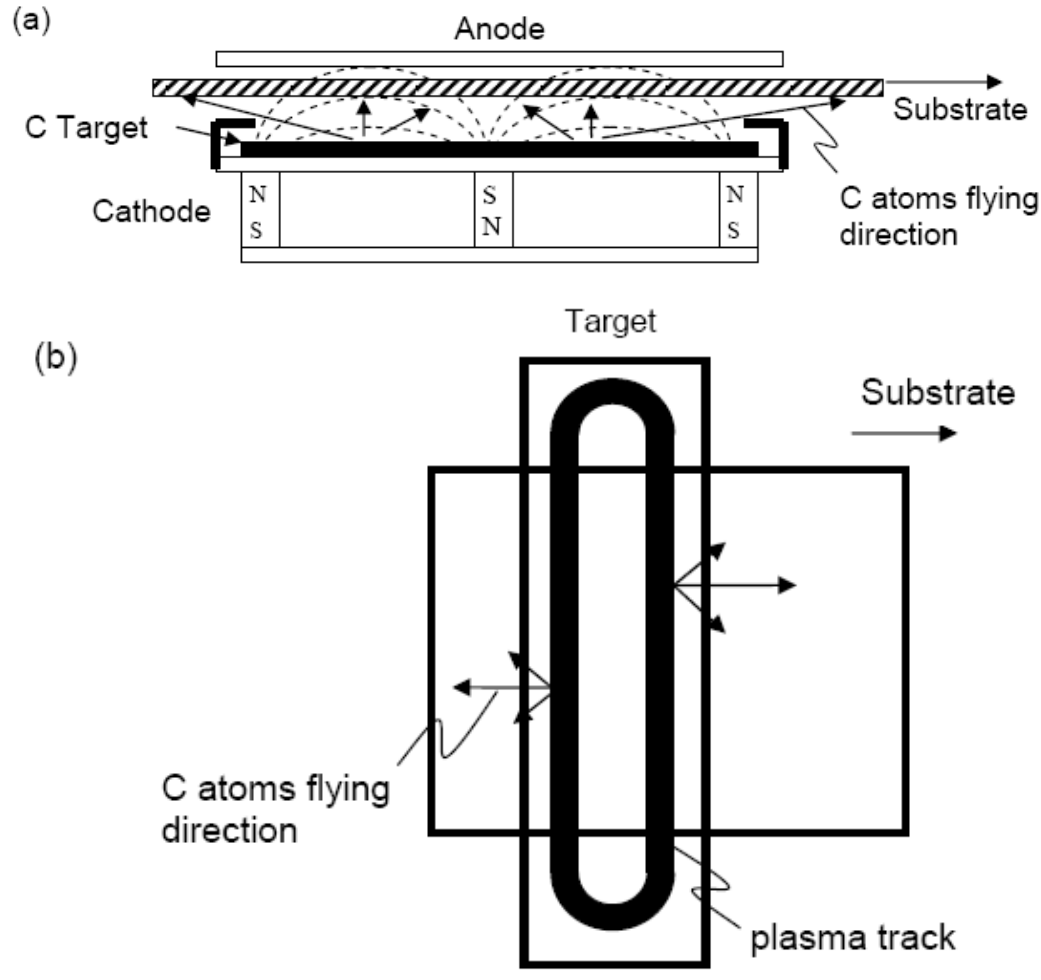

Figure 10. Schematic figure of a DC magnetron in-line sputtering apparatus. (a) Cross-section and (b) facing a carbon target.

In addition, as a comparative experiment, two kinds of test cells were fabricated in a similar way with PI films (SE-7492, Nissan Chemical Industries) with and without a rubbing process. The rubbing was done by rotating a cylinder wrapped with velvet cloth. When the LC molecules were not aligned, the LC molecules are randomly aligned relative to an alignment film, and the twist angles were determined according to the chiral pitches. All color pictures of the test cells were taken when the cells were placed between parallel polarizers using a white fluorescent light source. The optical characteristics of the alignment films were observed by measuring the applied voltage vs. transmittance (V-T) curves, contrast ratios, anchoring energies, and pretilt angles [14]. Optical transmittance was measured by using luminance meter (Prichard, Kyokko) with a white fluorescent light source. For this measurement the test cells were placed between crossed Nicols polarizers and the visible wavelength between 380-780nm was integrated.

Copyright © 2012. Nova Science Publishers, Incorporated. All rights reserved.

Diamond-Like Carbon Films, Nova Science Publishers, Incorporated, 2012. ProQuest Ebook Central,

3.2. Results and Discussion

3.2.1.Optical Characteristics

It was found that the sputtered DLC film without H has a self-alignment property for LC. The LC director alignment direction seems to be parallel to the substrate movement that is parallel to the magnetic field of the cathode and perpendicular to the plasma track line on the target as shown in Figure 10(b) during the sputtering. In order to test the alignment properties, different chiral pitches of LC were examined. Chiral pitches of 100 μm and 18μm LC were injected in the cells for Figs. 11(a) and (b), respectively. DLC alignment directions of the test cells were placed orthogonal so that it makes 90° TN. Figures 11(a) and (b) show photographs of the LC test cells placed between parallel polarizers at room temperature. The transmitted color change depends on the transmittance axes of the polarizers and the alignment angle of the cell. Both transmittance axes and alignment (director) axes are shown in Figure 11. The test cells were rotated about 45° form the dark state. For Figure 11(b) since the chiral pitch is 18μm, the LC twists about 90°; therefore, the cell looks purple-blue as in the case for a conventional 90° TN LC cell. Since the birefringence of LC Δn is designed such that the first minimum value corresponds to a wavelength of 550 nm, green light is absorbed and the LC device appears bluish magenta color when observed with the parallel Nicols polarizers. This can be realized from the following equation of transmittance for 90° TN LC placed between parallel polarizers [14].

$$I = \frac{\sin^2(\pi / 2\sqrt{1+u^2})}{2(1+u^2)} \tag{1}$$

where $u = 2\Delta nd / \lambda$, Δn is the birefringence of the liquid crystal, d is the cell gap thickness and λ is the wavelength of the incident light.

For the cell with the chiral pitch of 100μm shown in Figure 11(a), the LC twist only 18° in the 5μm cell gap. Even though it has 18° twist angle the cell is colored in purple-blue similar to that as shown in Figure 11(b). In this case visible light ranging from 380 nm to 780 nm generally transmits through parallel Nicols polarizers and the LC device should not colored. This means that the DLC film is acting as an alignment film by itself without any particular alignment process being carried out. Therefore, 90° TN was achieved even LC itself has twist angles of 18°.

Moreover, by rotating the cell devices between the crossed Nicols polarizers, it was confirmed by the color change that the LC are aligned in a mono domain. The transmitted color change depends on the extinction axes of the polarizers and the alignment angle of the cell. When the LC molecules are not aligned and in the amorphous state, the color does not change with the angle. In this way, it is confirmed that the LC molecules were aligned by the DLC film. This shows that the DLC film already has a structure with the alignment properties at the as-deposited stage. As for a reference, test cells with a conventional rubbed PI alignment film was observed in the same way and looked the same as the ones shown in Figure 11 (a) and (b).

In order to confirm the above experiment, next, the test cells were made with PI layers without any rubbing alignment process for comparison. The test cells were heated up above

Copyright © 2012. Nova Science Publishers, Incorporated. All rights reserved.

Diamond-Like Carbon Films, Nova Science Publishers, Incorporated, 2012. ProQuest Ebook Central,

the NI temperature to become set in the amorphous alignment state. When PI is not rubbed, LC is not aligned and angle of twist is determined only by the chiral dopant. Similarly, chiral pitches of 100 μm and 18μm LC were also injected in the cells for Figures 12(a) and (b), respectively.

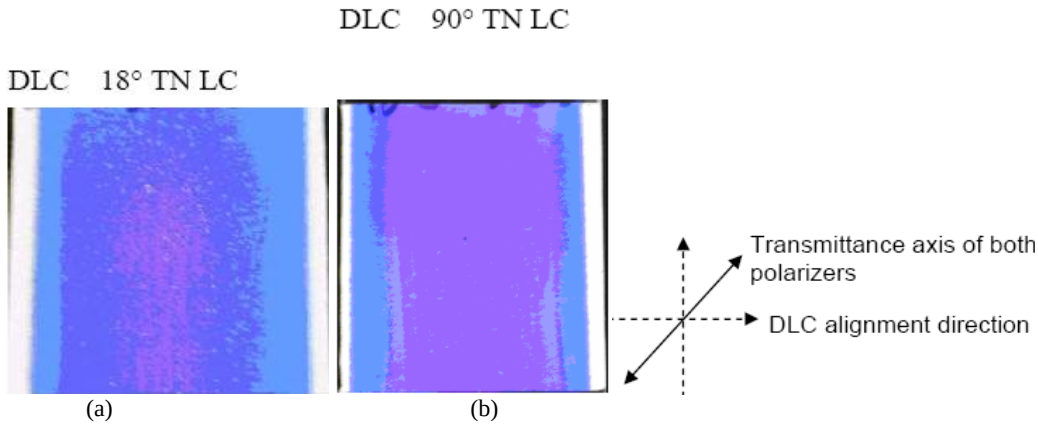

Figure 11. Photographs of LC test cells using DLC self-alignment film without any additional alignment process. The cells were between the parallel Nicols polarizers. Twist angles of the LC were (a) 18° and (b) 90°.

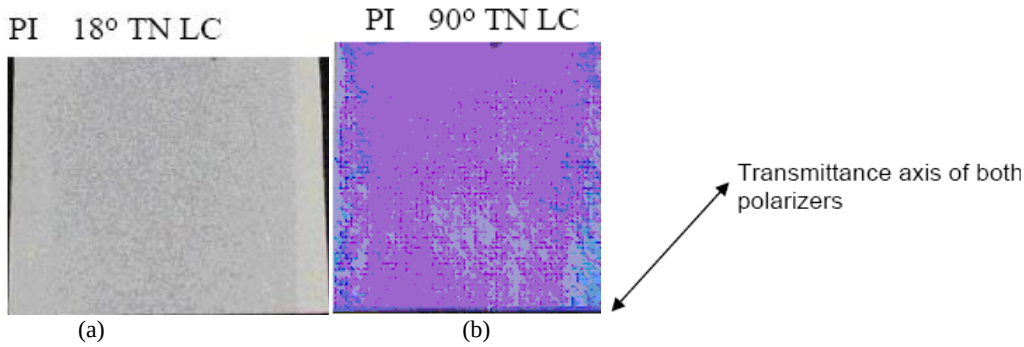

Figure 12. Photographs of LC test cells using a PI layer without a rubbing alignment process between the parallel Nicols polarizers. Twist angles of amorphous TN LC were (a) 18° and (b) 90°.

Therefore, LC twist 18° and 90° for Figures 12(a) and (b), respectively. For Figure 12(a) visible light ranging from 380 nm to 780 nm generally transmits through parallel Nicols polarizers, thus the LC device is not colored and looks nearly gray. On the other hand, for the chiral pitch of 18μm, the LC twists about 90°, so the cell looks purple-blue as shown in Figure 12(b). When the PI film does not have the proper alignment property, the LC molecules have twisted angles of about 90° as in the case of Figure 12(b). Since the birefringence of LC, Δn, is designed such that the first minimum value corresponds to a wavelength of 550 nm, green light is absorbed and the LC device appears bluish magenta color when observed through the parallel Nicols polarizers. Since the alignment condition is in amorphous state, the test cell color did not change even it was rotated between the polarizers.

Copyright © 2012. Nova Science Publishers, Incorporated. All rights reserved.

Diamond-Like Carbon Films, Nova Science Publishers, Incorporated, 2012. ProQuest Ebook Central,

3.2.2. Electro-Optical Characteristics

For comparison of the PI, DLC, and ITO films without any alignment process, the V-T characteristics were measured for each test cells as shown in Figures 13(a) and (b). As seen in Figure 13(a), V-T characteristics of the DLC films are better than those of ITO or PI films without rubbing, and closer to that of the conventional PI rubbed film. Low brightness for the DLC films (without H) is due to lower transmittance of the film itself (see Section 3.3) compare to those of PI or ITO films. The LC molecules were subjected to amorphous alignment by heating the test cells to 130°C and 160°C, and the samples thus obtained are denoted as DLC 130 and DLC 160, respectively. The characteristic for the conventional PI film with alignment processes is also shown for reference. The DLC alignment films show no disclination lines and contrast ratios (CRs) was about 200. A chiral pitch of 18μm LC was used for the test cells shown in Figures 13(a) and 13(b), thus the twist angles of LC were about 90º.

Note that in the amorphous alignment cell using PI, there exist grains with a size of a few tens of micrometers, for which the alignment orientation is slightly different from each other. This causes deterioration of the blackness level, so some light leakage was observed as seen in the curves of Figure 13(b). This is not observed in cells where rubbing was done in a single direction. The light leakage is attributed to disclination lines generated at the grain boundaries. However, the LC cell using the DLC film had deterioration of the blackness level, and the disclination lines were not observed even in microscopic observations. In other words, the LC device exhibited the characteristics equivalent to the one subjected to a PI alignment process in a single direction electro-optically.

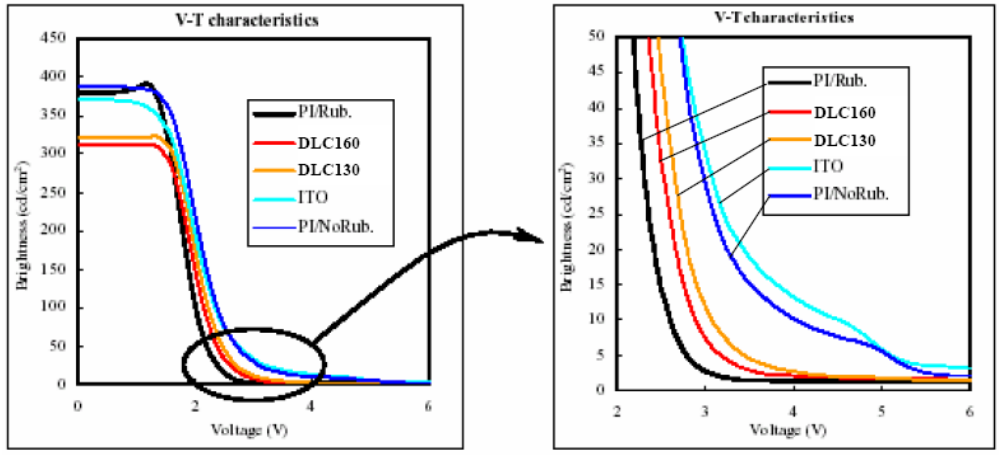

(a) (b)

Figure 13. (a) Transmittance vs. applied voltage characteristics. (b) Magnified and rescaled portion of Figure 13(a). Twist angles of the LC were 90°.

The CRs at 5 and 6 volts are also summarized in Table 1. The contrast ratio at 5V is less than 100 for the samples where PI and ITO were used without an alignment process. On the other hand, the LC test cells using the DLC films have good alignment properties with values close to 200. This indicates that the contrast ratio is high enough for practical use, although the DLC films still have lower CRs compare with conventional rubbed PI which are around 300. This appears to be due to a still lower azimuthal anchoring energy of the DLC film.

Copyright © 2012. Nova Science Publishers, Incorporated. All rights reserved.

Diamond-Like Carbon Films, Nova Science Publishers, Incorporated, 2012. ProQuest Ebook Central,

Table 1. Contrast ratios (CRs) at 5 and 6 volts of the test cells with PI, DLC, and ITO films without alignment process. Conventional PI rubbed film CR is shown as a reference

	DLC130	DLC160	ITO	PI/NoRub.	PI/Rub.
CR (@ 6V)	206	232	118	194	301
CR (@ 5V)	193	194	64	71	299

3.2.3. DLC Film Conditions

Varying the DLC thickness did not affect the alignment quality. Figure 14 shows photographs of the test cell alignment properties between the parallel Nicols polarizers with a distribution of the DLC film thickness from 3 to 20nm. The relation between the transmittance axes of the polarizers and the alignment (director) angle of the LC is the same as shown in Figure 11. In this case the DLC film was deposited in a state where the substrate was not moving, but stopped in the in-line sputtering chamber. In Figure 14, LC molecules having a chiral pitch of 100 μm, thus having 18° twisted angles, were used. The coloring characteristics, alignment quality, were hardly changed in spite of the differences in the film thickness and are almost the same for each cell. Accordingly, this indicates that the alignment of LC occurs only at the very surface of the DLC film and does not depend on film thickness. This also shows that the DLC film will also have sufficient allowance for variations in the film thickness at the time of manufacturing.

It is interesting to note that no alignment property was observed when H is contained in the film during the sputtering deposition. The H-contained DLC film was deposited by sputtering with the same conditions but in an atmosphere containing H_2. Then, the test cell was fabricated using the DLC film without any alignment process. LC having a chiral pitch of 18 μm was injected to fabricate the test cells in a method similar to the previous samples, thus making this sample comparable. In addition, another sample was fabricated by using a DLC film deposited by CVD as an alignment film without any rubbing process, thus making some similar comparative test cells. Figures 15(a) and (b) show pictures of the optical characteristics of the test cells. Figure 15(a) is a result of the case where the DLC film containing about 30 at% of H was used as an alignment film fabricated by the DC magnetron sputtering method. Figure 15(b) is a result of the case where the DLC alignment film containing H fabricated by the CVD method. As seen in Figs. 15(a) and (b), both of cells look non-uniform grayish color partially owing to the flow alignment. The flow alignment did not disappear by heating up above the clearing temperature. It was found that the DLC film containing H did not show the alignment property even when fabricated not only by the DC sputtering method but also by the CVD method.

It is known that when the DLC film contains H, the film becomes amorphous like and results in terminating sp^2 bonded networks [15]. Therefore, the alignment for LC appears to be due to the DLC crystalline anisotropy which occurs only during the sputtering deposition process without H.

Copyright © 2012. Nova Science Publishers, Incorporated. All rights reserved.

Diamond-Like Carbon Films, Nova Science Publishers, Incorporated, 2012. ProQuest Ebook Central,

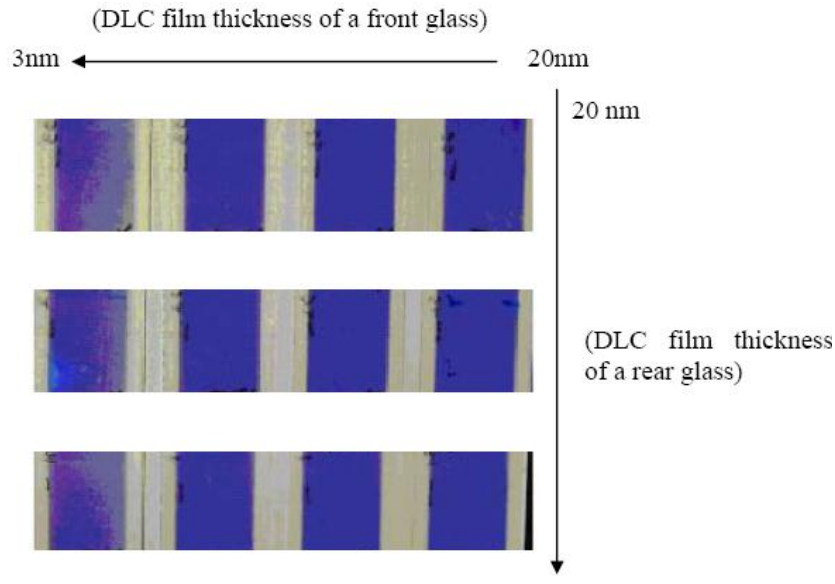

Figure 14. Photograph of the test cells under the parallel polarizers with different DLC alignment film thickness. A twist angle of the LC was 18°. The transmittance axes and alignment (director) axes are the same as shown in Figure 11.

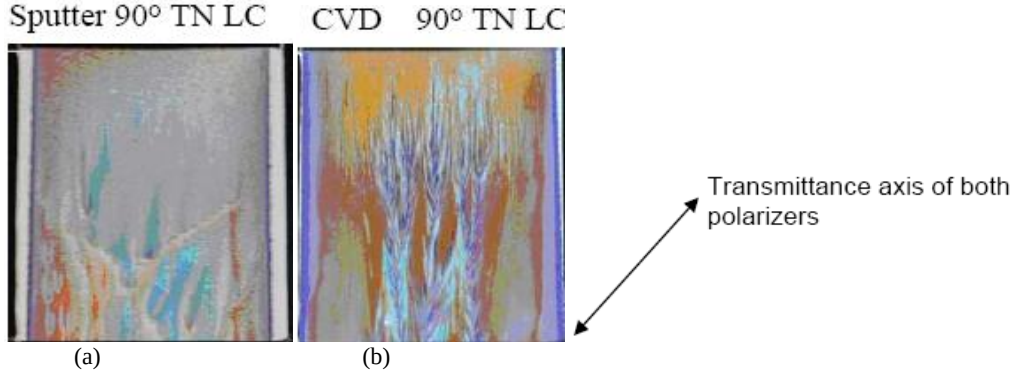

Figure 15. Photographs of LC test cell using H contained DLC alignment film without any alignment process. DLC was deposited by using (a) a sputtering tool and (b) a CVD system. A twist angle of LC was 90° for both samples. The transmittance axes of both polarizers are shown.

The alignment characteristics of DLC is considered to be along the substrate movement direction which is also parallel to the magnetic field of the cathode and also perpendicular to a plasma track on the target as shown in Figure 10(b) for the in-line sputtering system. When the carbon atoms impinge the substrate with shallow angles as shown in Figure 10(a), it is known that they form nano-columner structure along the direction that the carbon atoms came from due to a shadowing effect [16]. This is similar to the oblique angle deposition that the anisotropy of the deposited materials causes the alignment for LC [9-10]. It was also reported that the fraction of sp^2 carbon is large for the shallow angle deposition [17]. According to the study of LC alignment mechanism on PI, LC appear to align and adsorb to PI through π bonds interaction [11]. Therefore, LC seem to align due to this π bonds of the DLC film as

Copyright © 2012. Nova Science Publishers, Incorporated. All rights reserved.

Diamond-Like Carbon Films, Nova Science Publishers, Incorporated, 2012. ProQuest Ebook Central,

well. The magnetic field from the cathode of the magnetron sputtering system may also relate to this crystalline anisotropy. However, more study is necessary to clarify the effect of magnetic field to the DLC crystalline anisotropy.

3.2.4. LC Adsorbability to the DLC Film

The LC adsorbability to the DLC film also appears to be large enough compared with the conventional PI film from the measurement of the interface NI point temperature (a temperature that LC to become an amorphous alignment condition) which was confirmed to be above the limit of measurement temperature of 160 °C, while the interface NI temperature was around 130 °C to 140 °C for the conventional PI films. As for a reference the bulk NI temperature for the same LC was measured to be about 80 °C. This phenomenon may also be due to the strong π bond interaction between LC and DLC film. For example, it has also been reported that DLC film has strong adsobability to DNA which also has π-bonds [18]. These results imply that organic molecules such as liquid crystals or DNA which have π bonds can be strongly adsorbed to DLC film or carbon materials and can be aligned in a certain direction.

4. SUMMARY

Firstly, a DLC film has been used as an alignment layer for LCDs successfully using non-contact alignment method such as linearly polarized UV and IB alignment methods. The DLC film was deposited on LCD glass by CVD using C_2H_2 gas or CH_4 gas, and by DC reactive sputtering with a carbon target and mixture of Ar and H_2 gases. Hydrogen content in the film is strongly related to the film characteristics such as transmittance, resistivity and stress. Hydrogen content can be controlled by the power density for CVD deposition and Ar/H_2 ratio for sputter deposition. The operating pressure strongly influences the film resistivity and stress for both CVD and sputtering deposition. Considering those parameters an optimized DLC film for LCDs fabrication was developed. Alignment of liquid crystals was performed using 257nm polarized UV light, and the directional bombardment of an Ar IB onto the DLC film. By using this non-contact IB alignment method, rubbing track free, high quality, large area LCD panels were successfully fabricated.

Secondly, the in-line sputtered DLC film was used as a self-aligned film for LC. The self-aligned DLC film was deposited on a glass substrate by an in-line DC magnetron sputtering using a carbon target. It has been demonstrated that a DLC film can be used as an alignment layer for LC without using any alignment process. It was found that the self-aligned DLC film can be deposited by the sputtering system only with Ar gas and without H_2 gas. The alignment properties were observed with the test cells placed between a pair of parallel and crossed Nicols polarizers. From the observations of the test cells, it seems that the LC director was aligning along the DLC nano-columner structure growing direction which is considered to be aligning parallel to the substrate movement direction. It seems to be that sp^2 bonds of this nano-columner structure are interacting with LC molecules to align. From the measurements of the contrast ratios, it was also shown that the quality of the alignment is good enough for practical use. It is also demonstrated that the DLC alignment film has sufficient allowance for variations in the film thickness.

Copyright © 2012. Nova Science Publishers, Incorporated. All rights reserved.

Diamond-Like Carbon Films, Nova Science Publishers, Incorporated, 2012. ProQuest Ebook Central,

ACKNOWLEDGMENT

This work was done when author was in IBM and would like to thank all my colleagues; Y. Nakagawa, Y. Saitoh, H. Satoh, H. Kamiya, S. Odahara, A. Makita, K. Sakai, T. Nakamura, M. Hasegawa, P. Chaudhari, J. Doyle, S. A. Lien, A. Callegari, J. Ritsko, M. Samant, and J. Stohr for their great help and discussions.

REFERENCES

[1] Y.Toko, T. Sugiyama, K. Katoh, Y. Iimura and S. Kobayashi, *J. Appl. Phys*. 74 , (1993) 2071.

[2] Hasegawa M. and Taira Y. J. Photo. Sci. and Tech. 8 (1995) 241-244; *Conference Record of the 1994 International Display Research Conference and International Workshops on Active Matrix LCDs and Display Materials* 1994 P213.

[3] P. Chaudhari, J. Lacey, A. Lien and J. Speidell, *Jpn. J. Appl. Phys*. 37 (1998) L55.

[4] P. Chaudhari, J. Lacey, J. Doyle, E. Galligan, S. Lien, A. Callegari, G. Hougham, N. Lang, P. Andry, R. John, K. Yang, M. Lu, C. Cai, J. Speidell, S. Purushothaman, J. Ritsko, M. Samant, J. Stohr, Y. Nakagawa, Y. Katoh, Y. Saitoh, K. Sakai, H. Satoh, S. Odahara, H. Nakano, J. Nakagaki, and Y. Shiota, *Nature* 411 (2001) 56.

[5] Y. Nakagawa, Y. Kato, Y. Saitoh, K. Sakai, H. Satoh, K. Wako, S. Odahara, N. Nakamura, J. Nakagaki, H. Nakano, P. Chaudhari, J. Lacey, J. Doyle, E. Galligan, S. Lien, A. Callegari, G. Hougham, P. Andry, R. John, M. Lu, C. Cai, J. Speidell, S. Purushothaman, J. Ritsko, M. Samant, and J. Stohr, *SID '01 Dig*. (2001) 1346.

[6] Y. Kato, Y. Nakagawa, Y. Saitoh, H. Satoh, S. Odahara, M. Hasegawa, P. Chaudhari, J. Doyle, S. Lien, A. Callegari, J. Ritsko, M. Samant, and J. Stohr, *Proceedings of the 22nd International Display Research Conference*: Euro Display '02, pp.525-529 (2002).

[7] J. P. Doyle, P. Chaudhari, J.L. Lacey, E.A. Galligan, S.C. Lien, A.C. Callegari, N.D. Lang, Lu M, Y. Nakagawa, H. Nakano, N. Okazaki, S. Odahara, Y. Katoh, Y. Saitoh, K. Sakai, H. Satoh, Y. Shiota, Ion beam alignment for liquid crystal display fabrication, *Nuclear Instruments and Methods in Physics Research Section B-Beam Interactions with Materials and Atoms Vol.*206, pp.467-471 (2003).

[8] Yaroshchuk, Kravchuk, A. Dobrovolskyy, L. Qiu, O. D. Lavrentovich, Planar and tilted uniform alignment of liquid crystals by plasma-treated substrates, *Liquid Crystals* 31 (2004) 859.

[9] J.L. Janning, Thin film surface orientation for liquid crystals, *Appl. Phys. Lett*. 21 (1972) 173.

[10] D. Armitage, Alignment of liquid-crystals on obliquely evaporated silicon-oxide films, *J. of Appl. Phys*. 51 (1980) 2552.

[11] J. Stöhr, M. G. Samant, J. Lüning, A. C. Callegari, P. Chaudhari, J. P. Doyle, J. A. Lacey, S. A. Lien, S. Purushothaman, and J. L. Speidell, Liquid Crystal Alignment on Carbonaceous Surfaces with Orientational Order, **Science** 292 (2001) 2299.

[12] Y. Kato , H. Kamiya, and Y. Saitoh, A diamond-like carbon film as a self-alignment layer for LCDs, *Diamond and Related Materials* 16 (2007) 296–301.

Copyright © 2012. Nova Science Publishers, Incorporated. All rights reserved.

Diamond-Like Carbon Films, Nova Science Publishers, Incorporated, 2012. ProQuest Ebook Central,

[13] Y. Momoi, J. Stohr and M. G. Samant, in Proceedings of SID ’97, p. 73 (1997).
[14] Y. Saitoh, A. Lien, *Jpn. J. Appl. Phys*., 39 (2000) 1743.
[15] N. Cho, K. Krishnan, D. Veirs, M. Rubin, C. Hopper, B. Bhushan, and D. Bogy, Chemical-Structure and Physical-Properties of Diamond-like Amorphous-Carbon films prepared by magnetron sputtering, *J. of Mater. Res*. 5 (1990) 2543.
[16] M. Q. Ding, A. F. Myers, W. B. Choi, R. D. Vispute, S. M. Camphausen, J. Narayan, J. J. Cuomo, J. J. Hren and J. Bruley, Field emission from amorphous diamond coated Mo tip emitters by pulsed laser deposition, *J. Vac. Sci. Technol*. B: 15 (1997) 840.
[17] M. Park, S. M. Camphausen, A. F. Myers, P. T. Barletta, V. Sakhrani, L. Bergman, R. J. Nemanich, and J. J. Cuomo, “Raman Scattering of Tetrahedrally Bonded Amorphous Carbon Deposited at Oblique Angles”, *Mater. Lett*. 41, (1999) 229.
[18] K. Takahashi, M. Tanga, O. Takai, H. Okamura, DNA preservation using diamond chips, *Diamond and Related Materials* 12 (2003) 572.

Copyright © 2012. Nova Science Publishers, Incorporated. All rights reserved.

Diamond-Like Carbon Films, Nova Science Publishers, Incorporated, 2012. ProQuest Ebook Central,

INDEX

#

3D images, 76

A

absorption spectra, 115
accelerator, 7, 189
accounting, 47
acetone, 122, 153, 158, 160, 168, 174
acetylene gas, 27, 28, 31
activation energy, 68
adaptation, 42
adhesion, viii, ix, 63, 67, 96, 121, 122, 149, 151, 152, 154, 156, 157, 158, 159, 162, 164, 166, 172, 173, 187
adhesion force, 158
adhesion strength, ix, 151
adhesions, 158
adhesive interaction, 135
adhesive properties, 166
adsorption, 28, 36, 120
AFM, 3, 4, 75, 76, 84, 85, 168, 169, 184
alters, 85
aluminium, 14
ambient air, 120, 154, 168, 171
amplitude, 23, 70, 147, 148
anchoring, 184, 188, 189, 190, 193
anisotropy, x, 181, 188, 189, 194, 195
annealing, 41, 45, 46, 48, 49, 50, 52, 53, 54, 55, 56, 57, 58, 59, 68, 73, 74
annihilation, 59
argon, 3, 28, 49, 99, 102, 113, 122, 154, 162, 168
articulation, 120
artificial heart valve, 35, 36
atmosphere, 30, 31, 49, 122, 154, 168, 194
atomic distances, 43, 56
atomic force, 168, 184
atoms, 22, 26, 42, 44, 46, 47, 51, 52, 54, 56, 57, 58, 59, 65, 68, 72, 81, 82, 85, 97, 101, 102, 121, 142, 152, 177, 195
attachment, 21, 23
attribution, 51

B

background noise, 148
backscattering, 123, 183
band gap, 40, 57, 60, 67, 68, 72, 73, 89
bandwidth, 125
barriers, 49, 79
base, 3, 75, 76, 79, 84, 122, 153, 161
beams, vii, 39
behaviors, 115
Beijing, 151, 153, 160
Belarus, 1, 7, 8, 36
bending, 73, 79, 100
benefits, 40
bias, 3, 5, 7, 25, 26, 27, 29, 36, 98, 99, 100, 101, 102, 103, 104, 105, 112, 122, 152, 153, 154, 155, 156, 157, 158, 159, 160, 161, 162, 164, 166, 167, 168, 170, 174, 176, 183
binding energies, 29, 56, 177
binding energy, 3, 51, 55, 56, 81, 176
biocompatibility, 96
biomedical applications, 67, 121
birefringence, 189, 191, 192
body fluid, 121
Boltzmann constant, 28, 87
bonding, ix, 37, 48, 64, 67, 68, 73, 89, 96, 101, 102, 104, 110, 115, 121, 125, 151, 173, 186
bonds, viii, ix, x, 4, 5, 18, 19, 29, 30, 45, 52, 56, 59, 66, 85, 95, 96, 102, 103, 104, 105, 106, 109, 112, 115, 116, 120, 121, 128, 129, 135, 137, 178, 181, 182, 186, 188, 195, 196
bone, 36

Copyright © 2012. Nova Science Publishers, Incorporated. All rights reserved.

Diamond-Like Carbon Films, Nova Science Publishers, Incorporated, 2012. ProQuest Ebook Central,

boron, viii, 47, 63, 68, 73
Brazil, 119
breakdown, 60, 127, 160
Brno, 149

C

cables, 120
candidates, 54
carbides, 42
carbon, vii, viii, ix, x, 2, 3, 5, 6, 7, 14, 15, 16, 17, 18, 19, 21, 22, 23, 24, 26, 27, 28, 29, 30, 31, 36, 37, 38, 39, 40, 41, 42, 43, 44, 45, 46, 47, 48, 49, 50, 51, 52, 54, 56, 57, 58, 59, 60, 63, 64, 65, 68, 70, 72, 73, 81, 83, 85, 95, 96, 98, 101, 102, 103, 104, 106, 109, 111, 114, 119, 120, 121, 122, 125, 126, 135, 142, 144, 148, 149, 151, 152, 154, 156, 166, 168, 170, 173, 176, 181, 182, 183, 185, 190, 195, 196, 197
carbon atoms, viii, 3, 7, 14, 22, 43, 49, 50, 54, 57, 58, 63, 65, 68, 81, 104, 121, 135, 195
carbon film, vii, 21, 26, 30, 37, 38, 43, 45, 68, 96, 109, 149, 156, 197
carbon materials, 196
carbon nanotubes, 70, 72
carbon-rich phases, vii, 39, 41, 49, 51, 59
catalytic activity, 125
catastrophic failure, 172
cathodic arc plasma deposition, vii, 1
cathodic arc processes, vii, 1
ceramic, 2, 3, 37, 43
chemical, viii, ix, x, 26, 27, 29, 36, 40, 41, 44, 47, 48, 49, 55, 59, 60, 63, 64, 66, 73, 74, 96, 98, 102, 115, 119, 120, 121, 122, 123, 125, 130, 131, 137, 151, 173, 174, 177, 181, 183
chemical bonds, 29
chemical inertness, viii, ix, 36, 63, 66, 96, 120, 130, 137, 151, 173
chemical properties, 121
chemical reactions, 56
chemical stability, 40, 60
chemical vapor deposition (CVD), vii, viii, x, 1, 26, 28, 31, 34, 35, 36, 64, 74, 95, 97, 98, 99, 107, 112, 113, 116, 122, 152, 181, 183, 184, 185, 186, 187, 194, 195, 196
chemicals, 120
China, 151
chromium, x, 131, 151, 153, 156, 173, 175, 176, 177
clarity, 49
classification, vii, 39, 42
cleaning, 3, 79, 153, 160, 167, 175
cleavage, 46
cluster model, 104, 111
clusters, 30, 48, 49, 50, 51, 52, 54, 56, 57, 58, 60, 64, 65, 66, 68, 74, 75, 82, 83, 85, 104, 105, 122, 136
coatings, ix, 6, 14, 15, 16, 19, 21, 27, 29, 31, 34, 36, 37, 67, 68, 120, 121, 130, 135, 137, 141, 142
collisions, 29, 31, 36, 142
color, 183, 184, 190, 191, 192, 194
combined effect, 83, 87
commercial, vii, 1, 120
compatibility, 40, 47, 49, 158
compliance, vii, 39, 40, 41, 42, 43, 46, 47, 50, 58, 59
composition, viii, 20, 29, 39, 40, 41, 47, 48, 49, 50, 51, 52, 55, 57, 59, 64, 152
compounds, 40, 47, 50, 98, 173
compression, 177
computer, 22, 77, 126
condensation, 104
conduction, 68, 73, 83, 89, 186
conductivity, viii, 63, 66, 68, 89, 128
conductor, 3
configuration, 8, 12, 13, 42, 76, 115, 121, 146, 153, 160, 161, 166, 174
confinement, 57
construction, 166
consumption, 58
contamination, 37, 44, 81
contradiction, 44
cooling, 45, 99, 112
coordination, 44, 97
copper, 7, 8
correction factors, 78
correlation, 49, 58, 71
correlations, viii, 95, 96, 97, 102, 107, 110, 111, 112, 154
corrosion, ix, 119, 120, 121, 125, 127, 128, 129, 130, 131, 136, 137
cost, 66, 73, 182
covalent bond, 42
cracks, 171, 172
critical value, 142
crystalline, vii, ix, x, 41, 42, 45, 46, 48, 50, 54, 57, 59, 82, 119, 121, 122, 137, 148, 181, 194, 196
crystalline diamond (CD), ix, 119, 121
crystallinity, 67, 98
crystallites, viii, ix, 48, 95, 96, 105, 107, 110, 111, 112, 120, 131, 176
crystals, x, 103, 126, 176, 183, 197
CVD technique, vii, 1, 28, 31
cycles, 31, 32, 131, 132, 133

D

decay, 21, 48
decomposition, 6, 27, 30, 41, 97, 98, 101, 105

Copyright © 2012. Nova Science Publishers, Incorporated. All rights reserved.

Diamond-Like Carbon Films, Nova Science Publishers, Incorporated, 2012. ProQuest Ebook Central,

deconvolution, 5, 18, 30
defects, 17, 41, 49, 54, 56, 59, 73, 89, 130, 154, 162, 168
deformation, 5, 156
degradation, viii, 63, 67, 73, 120
degradation process, 120
demonstrations, 46
deposition, vii, viii, ix, x, 1, 3, 5, 14, 15, 17, 19, 26, 27, 28, 29, 30, 31, 34, 36, 37, 43, 45, 48, 49, 66, 68, 74, 75, 79, 82, 84, 95, 96, 97, 98, 99, 100, 101, 102, 104, 105, 106, 110, 113, 119, 120, 121, 122, 141, 142, 144, 146, 149, 151, 152, 153, 154, 156, 159, 160, 161, 166, 167, 168, 170, 174, 175, 182, 183, 185, 187, 194, 195, 196, 198
deposition rate, 3, 27, 28, 30, 31, 36, 66, 75, 98, 156, 170, 185
depth, 4, 5, 51, 55, 56, 101, 146, 147, 148, 162, 170, 174
destruction, 27, 29
detection, 102, 114
diamond-like carbon (DLC), viii, 95, 120, 152, 173, 182, 183
dielectric constant, 67, 83
dielectric strength, viii, 63, 66
dielectrics, 41, 60, 67
diesel engines, 34
diffraction, 22, 43, 44, 45, 46, 47, 57, 82, 125, 148
diffusion, 50, 56, 58, 74, 76
direct current (DC), vii, 1
direct measure, 111
discharges, 14, 23, 144, 182
discs, 158
disorder, 43, 111, 125, 136
dispersion, 57
displacement, 2, 9, 12, 13, 41, 162
dissociation, 29, 51
distilled water, 126, 131
distortions, 136
distribution, 15, 16, 22, 23, 24, 25, 26, 30, 51, 136, 148, 149, 194
distribution function, 25, 26
divergence, 14
DLC films., viii, ix, x, 5, 19, 21, 36, 38, 63, 73, 74, 83, 85, 89, 121, 122, 123, 127, 131, 136, 151, 158, 159, 171, 173, 174, 177, 181
DNA, 196, 198
donors, 73
dopants, 68
doping, viii, x, 63, 68, 73, 83, 121, 151, 152, 155
dosage, 183, 188, 189
double bonds, 109
drawing, 183, 184
ductility, x, 151, 174
durability, 96, 98

E

editors, 38
electric charge, 17
electric field, 17, 69, 70, 71, 72, 73, 74, 77, 79, 83, 86, 87
electrical conductivity, 43, 68, 89, 128
electrical fields, 19, 121
electrical properties, 64, 68
electrochemical impedance, 128, 129
electrodes, x, 2, 3, 75, 127, 181, 183, 189
electrolyte, 127, 129
electromagnetic, 21
electron, vii, viii, 14, 21, 22, 25, 26, 27, 43, 44, 46, 47, 54, 55, 63, 64, 66, 67, 68, 69, 70, 71, 72, 73, 77, 79, 83, 85, 95, 97, 98, 99, 100, 101, 102, 105, 112, 121, 122, 128, 142, 143, 148, 154, 162, 168, 174
electron cyclotron resonance, 122
electron diffraction, 43, 44, 46, 47
electron microscopy, 162
electron-beam-excited plasma (EBEP), viii, 95, 98
electronic structure, 49, 73
electrons, 7, 11, 12, 14, 26, 48, 56, 69, 70, 71, 72, 73, 82, 87, 89, 121, 142, 160
emission, vii, viii, 6, 21, 22, 23, 24, 25, 26, 29, 39, 48, 49, 50, 51, 54, 60, 64, 67, 68, 69, 70, 71, 72, 73, 74, 76, 77, 78, 79, 82, 83, 85, 86, 87, 88, 89, 142, 143, 198
emission field, 73
emitters, 48, 67, 72, 198
endurance, 173
energy, vii, 1, 15, 18, 19, 21, 22, 23, 24, 25, 26, 27, 28, 29, 32, 33, 41, 46, 51, 55, 56, 68, 69, 70, 81, 83, 96, 97, 102, 105, 114, 125, 126, 142, 149, 154, 159, 164, 174, 177, 183, 184, 187, 188, 189, 193
energy consumption, 27
energy density, 183
energy transfer, 177
engineering, viii, 64, 121
environment, ix, 120, 135, 136, 137
equilibrium, vii, 19, 39, 40, 41, 43, 47, 59
equipment, 120, 146
erosion, 3, 6, 120
ESR, 55
etching, 40, 47, 48, 50, 55, 56, 85, 97
evaporation, 3, 152
evidence, 5, 15, 54, 57, 58, 170, 171
evolution, 52, 53
excitation, 22, 27, 128

Copyright © 2012. Nova Science Publishers, Incorporated. All rights reserved.

Diamond-Like Carbon Films, Nova Science Publishers, Incorporated, 2012. ProQuest Ebook Central,

experimental condition, 55
exposure, 81, 183
extinction, 191
extraction, 120

F

fabrication, v, vii, 1, 34, 39, 41, 47, 60, 92, 182, 196, 197
face-centered cubic carbon, vii, 39
Fermi level, 70, 73, 74, 79, 83, 85, 89
FFT, 148
filament, 74, 122, 142, 144, 149, 183
fillers, 120
film thickness, 5, 16, 72, 73, 96, 99, 113, 146, 147, 168, 175, 183, 184, 189, 194, 195, 196
filters, 37
financial, 137
financial support, 137
fluctuations, 21
fluid, 74
fluorine, viii, 63, 68, 85, 121
foils, 14, 30
food, 121, 131
food industry, 131
force, 31, 86, 87, 147, 148, 171, 172
formation, viii, 4, 5, 18, 19, 21, 29, 31, 32, 33, 36, 40, 41, 42, 43, 44, 45, 46, 47, 48, 49, 50, 52, 54, 56, 57, 58, 59, 67, 75, 79, 83, 84, 95, 115, 122, 135, 176, 177, 178
formula, 99, 102, 113, 176
fracture toughness, 147, 149
free energy, ix, 41, 54, 127, 141, 142, 145
free surface energy, 144
friction, viii, ix, x, 19, 21, 31, 32, 33, 34, 63, 66, 67, 96, 119, 120, 121, 122, 131, 132, 133, 135, 137, 151, 152, 154, 158, 159, 164, 166, 171, 172, 173, 178
FTIR, 50, 183
fullerene, 48, 49

G

geometrical parameters, 144
geometry, 10, 86, 123
germanium, 35, 36
glasses, viii, 63, 189
glioma, 36
glow discharge, 97
glycol, 145
grain boundaries, 72, 74, 193
grain size, ix, 85, 120, 131, 149, 174, 175, 176
graph, 86
graphite, vii, viii, 1, 2, 3, 4, 6, 7, 20, 21, 23, 30, 31, 43, 44, 45, 48, 50, 51, 56, 59, 64, 65, 66, 81, 95, 96, 98, 103, 105, 107, 110, 111, 112, 121, 122, 126, 148, 153, 156, 158, 173, 183, 189
graphite macroparticles, vii, 1, 7
growth, ix, 19, 26, 30, 31, 36, 51, 54, 58, 59, 66, 73, 85, 141, 142, 154, 159, 177
growth mechanism, 58, 66
growth rate, 26, 31
guidance, 19

H

hardness, vii, viii, ix, 1, 5, 6, 21, 31, 36, 37, 44, 45, 63, 66, 67, 96, 97, 98, 101, 102, 107, 110, 112, 113, 114, 115, 119, 121, 122, 125, 141, 144, 146, 147, 148, 151, 152, 155, 158, 159, 164, 166, 169, 173, 174, 177, 178, 183
heat conductivity, 45
height, 70, 71, 72, 77, 79, 83, 168, 184
helium, 183, 189
hemisphere, 72
heterogeneity, 68
hexagonal lattice, 46, 47
hexane, 122
high energy of plasma particles, vii, 1
history, 171, 172
homogeneity, 5
HRTEM, 81, 82, 83, 148, 149
human, 36
humidity, 120
hybridization, viii, 56, 63, 66, 67, 89, 174, 177
hydrofluoric acid, 84
hydrogen, vii, viii, x, 1, 22, 23, 29, 44, 63, 64, 65, 95, 96, 97, 98, 101, 102, 104, 106, 107, 108, 109, 110, 111, 112, 113, 114, 115, 116, 122, 126, 142, 152, 153, 156, 159, 160, 166, 181, 184, 187
hydrogen atoms, 23, 65, 101, 104, 109
hydrogen bonds, 126
hydrophilicity, 145
hydrophobicity, 145

I

ideal, 106
identification, 48
image, 4, 27, 32, 33, 35, 69, 71, 84, 126, 149, 155, 169, 170, 187
image analysis, 126
images, 81, 82, 123, 129, 130, 134, 148, 154, 155, 162, 163, 168, 169

Copyright © 2012. Nova Science Publishers, Incorporated. All rights reserved.

Diamond-Like Carbon Films, Nova Science Publishers, Incorporated, 2012. ProQuest Ebook Central,

immersion, 128
implants, 36
improvement function, 34
impulses, 21, 28, 30
impurities, 56, 144, 153, 168
indentation, 5, 31, 37, 101, 114, 146, 147, 148, 174
India, 63, 92
indium, x, 181, 183
indium tin oxide (ITO), x, 181, 183
induction, 10, 12, 14, 15, 21
industries, 131, 142
industry, vii, ix, 1, 34, 119, 131
information processing, ix, 141
infrared spectroscopy, 183
inhibition, 120
inhibitor, 120
inhomogeneity, 57, 83
initiation, 129
insertion, viii, 95, 112
insulators, 60
integrated circuits, 48, 50
integration, 10
integrity, 159
interface, 34, 48, 49, 59, 70, 74, 121, 142, 145, 146, 147, 149, 152, 158, 170, 178, 196
interfacial layer, 164, 168, 170
interference, 52
iodine, viii, 63, 68
ion beam (IB), x, 181
ion bombardment, 45, 104, 153, 154, 156, 159, 161, 168, 171
ion implantation, vii, 39, 40, 41, 46, 47, 49, 50, 59, 62
ions, vii, ix, 1, 3, 5, 7, 11, 12, 14, 15, 16, 21, 22, 23, 26, 27, 28, 31, 43, 44, 45, 46, 47, 50, 51, 52, 55, 56, 57, 58, 59, 96, 97, 99, 105, 119, 129, 131, 137, 142, 160, 164, 177, 183, 189
ion-synthesized films, vii, 39
IR spectra, 102, 114, 115
iron, 32, 33
irradiation, 41, 42, 43, 45, 58, 59
islands, 59

J

Japan, 36, 37, 95

L

lasers, 60
lattice parameters, 43, 45
lattices, 42, 47, 58
lead, 54, 58, 67, 73, 141
leakage, 193
lens, 35
lifetime, 21, 41
light, 21, 23, 36, 39, 40, 41, 48, 54, 59, 60, 69, 111, 146, 182, 183, 188, 190, 191, 192, 193
light transmission, 36
light-emitting diodes, 60
linear dependence, 14, 31
liquid crystals, x, 181, 182, 183, 196, 197
liquid crystals (LC), x, 181
liquids, 126, 142
localization, 49
low temperatures, 73
lubricants, 34
luminescence, vii, 28, 29, 39, 40, 47, 48, 49, 51, 58
Luo, 179
lying, 78, 85, 87

M

machinery, 120
magnetic field, x, 6, 7, 8, 9, 10, 12, 13, 14, 15, 160, 181, 191, 195
magnetization, 6, 14
magnets, 189
magnitude, 7, 14, 17, 28, 68, 127, 131, 147, 165, 166, 178
majority, 104, 172, 173, 176
management, 155, 170
manufacturing, 34, 73, 142, 182, 194
mass, 14, 15, 96, 131, 177
materials, vii, viii, ix, 1, 5, 36, 38, 39, 40, 41, 47, 64, 65, 66, 67, 69, 70, 72, 73, 87, 96, 119, 120, 121, 141, 142, 149, 195
matrix, vii, viii, 3, 25, 30, 39, 48, 49, 52, 54, 57, 63, 64, 67, 68, 74, 79, 81, 82, 83, 85, 104, 121, 122, 130, 152, 155, 164, 176, 178
matter, 65, 101
measurement, 3, 5, 74, 144, 145, 147, 148, 149, 155, 162, 168, 171, 174, 182, 183, 184, 190, 196
measurements, 25, 26, 43, 55, 56, 68, 76, 77, 99, 101, 113, 114, 123, 126, 128, 132, 133, 145, 146, 170, 175, 196
mechanical properties, viii, ix, 5, 63, 64, 68, 119, 122, 147, 152, 164, 165, 166
mechanical stress, 58, 144
media, 67
median, 148
medical, 6, 36, 121
medicine, 6, 34, 36, 149
melting, 40, 41, 144
melting temperature, 40

Copyright © 2012. Nova Science Publishers, Incorporated. All rights reserved.

Diamond-Like Carbon Films, Nova Science Publishers, Incorporated, 2012. ProQuest Ebook Central,

memory, 60
metal-containing DLC (Me-DLC), ix, 151, 173
metals, viii, 3, 42, 63, 97
metastable materials, vii, 1
meter, 183, 190
methanol, 75, 84
methodology, 37
microcrystalline, 72, 74, 98, 103, 105
microelectronics, 67
microhardness, 152, 154, 155, 156, 158, 159, 162, 163, 166, 167, 171, 174
micrometer, 6, 77
microscope, 17, 77, 102, 154, 168, 174
microscopy, 31, 162, 168, 184
microstructure, viii, 49, 73, 83, 95, 102, 111, 112, 128, 152, 154, 168, 176, 178
microstructures, 75, 174
mixing, 122
models, 41, 72, 73
modulus, 5, 6, 37, 100, 146, 147, 148, 175
mold, 34, 35
moldings, 166, 173
mole, 186
molecules, 24, 25, 27, 29, 31, 48, 188, 190, 191, 192, 193, 194, 196
molybdenum, 32, 142
momentum, 70
Moon, 92, 139, 180
morphology, ix, 3, 75, 84, 123, 141, 144, 148, 154, 159, 162, 168, 169, 172, 173
Moscow, 38, 55, 56, 91
multilayered structure, 159, 166, 169, 170, 172, 173
multiplier, 10

N

nanocrystals, 40, 48, 49, 50, 51, 52, 54, 56, 57, 58, 59, 60
nanoindentation, 5, 6, 174
nanometer, 6, 16, 66
nanometer scale, 16, 66
nanometers, 4, 36
nanoparticles, 37, 48, 58, 122, 123, 176, 177, 178
nanophases, 48, 57
nanorods, 86
nanostructured materials, 148, 149
nanostructures, vii, 39, 40, 47, 49, 50, 51
nanowires, 86
neutral, 7, 14, 24
next generation, 66
NIR, 68
nitrides, 42
nitrogen, viii, 41, 42, 54, 63, 68, 73, 76, 83, 96, 97, 98, 114, 121, 122, 153, 160, 168, 174
non-hydrogenated DLC films, vii, 1, 177
non-linear optics, 60
nucleation, 58, 122, 176
nuclei, 58
nucleus, 6, 58

O

obstacles, 26, 120
oil, 34, 74, 120
operating costs, 120
opportunities, 36
optical properties, viii, 40, 49, 63, 67, 68
optoelectronics, vii, 39, 40
organic solvents, 67
oxidation, viii, 40, 48, 49, 63, 115, 120
oxygen, 22, 30, 32, 33, 42, 44, 50

P

palladium, 28
parallel, x, 72, 75, 86, 99, 112, 181, 183, 188, 189, 190, 191, 192, 194, 195, 196
pathways, 68
permeability, 9, 36
personal computers, 182
petroleum, ix, 119, 120, 131
phase diagram, 40, 64
phase transformation, vii, 39, 41, 42
phase transitions, 52
phosphorous, viii, 63, 68
photoelectron spectroscopy, 3
photoemission, 183
photographs, 191, 194
photoluminescence, viii, 48, 64
photonics, vii, 39
physical properties, 121, 155, 169, 173
pitch, 76, 77, 191, 192, 193, 194
PL spectrum, 50, 53
plastic deformation, 5
plasticity, 148
platinum, 127
point defects, 41
polar, 126, 145
polarization, ix, 26, 119, 127, 128, 137
polyimide, 182
polymer, 27, 59, 85, 182
polymer films, 59
polymorphism, 59
porosity, 144

Copyright © 2012. Nova Science Publishers, Incorporated. All rights reserved.

Diamond-Like Carbon Films, Nova Science Publishers, Incorporated, 2012. ProQuest Ebook Central,

precipitation, 54, 57, 120
preservation, 198
pressure gauge, 74
prevention, 34
principles, 3, 8
probability, 3, 19, 40, 70
probe, 14, 21, 22, 24, 25, 26, 27, 86
process control, 155, 170
profilometer, 175
project, 8
prosthesis, 120
protection, ix, 67, 120, 127, 128, 131, 137, 166
protective coating, 67, 98
pulse discharge, 7
pulsed arc method, vii, 1, 29
pumps, 74
purity, 80, 153, 160
pyrolysis, 43

Q

quality improvement, 152
quantum confinement, 49, 50, 51
quartz, 75
quasi-equilibrium, 14, 47

R

radial distribution, 56
radiation, 21, 23, 29, 41, 45, 54, 56, 59, 125, 176
radiation damage, 54
radicals, 27, 29, 31, 36
radio, 79, 99, 112, 122
radius, 7, 9, 10, 11, 12, 14, 15, 54, 58, 71, 72, 100, 175
raman scattering spectroscopy, ix, 120, 123, 128, 137
raman spectra, 5, 18, 19, 20, 21, 30, 96, 103, 105, 111, 125
raman spectroscopy, 3, 29, 37, 50, 102, 136, 155, 168, 169
reactions, 27, 57
reality, 14
reasoning, 20
recombination, 45, 49, 54, 58
recombination processes, 54
reconstruction, 42
recovery, 49, 58
refractive index, 144, 145
relaxation, viii, 68, 95, 116, 177
reliability, vii, 1, 25
requirements, vii, 1, 146
researchers, 13, 48, 130, 149, 159
resistance, viii, ix, 5, 34, 63, 119, 121, 125, 127, 128, 129, 131, 132, 136, 137, 149, 152, 155, 158, 169, 184
resolution, 56, 148, 176
response, 146, 148
rings, 43, 104
Romania, 141
room temperature, 28, 36, 45, 79, 100, 123, 126, 128, 131, 183, 189, 191
roughness, ix, 31, 32, 36, 73, 75, 84, 85, 120, 123, 124, 137, 153, 154, 160, 162, 168
Russia, 3, 39, 54, 55, 56, 60

S

salinity, 120
sapphire, 60
saturation, 25, 26
scanning electron microscopy, 168
scattering, ix, 48, 51, 102, 109, 114, 120, 123, 125, 128, 137, 183
school, 60
science, 37, 62, 142, 149
semiconductor, 40, 73
semiconductors, 41, 42
sensing, 146
sensitivity, 23, 25, 44, 148
shape, 6, 30, 76, 86, 126, 136, 145
shear, 127, 132, 135, 178
shear strength, 132, 178
showing, 5, 114, 155, 169, 170
silicon, vii, viii, 4, 5, 31, 32, 33, 39, 40, 41, 42, 43, 45, 46, 47, 48, 49, 50, 51, 52, 54, 56, 57, 58, 59, 60, 75, 79, 84, 86, 95, 96, 97, 98, 113, 114, 115, 116, 121, 146, 149, 197
silicon nanocrystals, 40, 56, 58, 59
silver, viii, 36, 38, 63, 76, 79
sine wave, 160, 166
skeleton, 42, 111
skewness, 30
smoothness, 21, 135, 155, 169
sodium, 127
solar cells, viii, 60, 64
solid surfaces, 69
solidification, 41
solubility, 58
solution, ix, 41, 57, 75, 84, 120, 127, 128, 129, 131, 132, 133, 134, 135, 136, 137
species, 40, 51, 55, 59, 79, 125, 187
spectral component, 22
spectroscopic techniques, 54
spectroscopy, ix, 21, 29, 50, 54, 55, 102, 120, 123, 128, 137, 183, 184

Copyright © 2012. Nova Science Publishers, Incorporated. All rights reserved.

Diamond-Like Carbon Films, Nova Science Publishers, Incorporated, 2012. ProQuest Ebook Central,

spin, 55
stability, viii, 49, 54, 63, 73, 127, 178
standard deviation, 114, 124, 133, 135, 136
state, 21, 25, 41, 47, 55, 59, 131, 132, 133, 144, 155, 170, 173, 174, 178, 188, 189, 191, 192, 194
states, 44, 48, 49, 56, 73, 74, 177
statistics, 71
steel, ix, 7, 19, 21, 31, 32, 33, 68, 74, 76, 86, 96, 97, 119, 120, 121, 122, 123, 127, 128, 129, 130, 131, 132, 133, 134, 135, 136, 137, 142, 152, 153, 160, 166, 167, 169, 171, 172, 173, 174
stimulus, 41
stoichiometry, 49, 52
storage, 23, 26, 67, 148
stress, vii, viii, 26, 36, 54, 63, 67, 68, 89, 95, 96, 97, 98, 100, 101, 102, 107, 108, 109, 110, 111, 112, 113, 114, 115, 116, 127, 152, 155, 156, 166, 169, 173, 177, 178, 183, 187, 196
stretching, 103
structural defects, 73
structural transformations, vii, 39
structure, x, 3, 6, 18, 20, 25, 36, 37, 38, 41, 42, 43, 45, 46, 47, 49, 50, 51, 52, 55, 57, 58, 59, 65, 66, 68, 70, 71, 72, 73, 74, 81, 82, 97, 101, 104, 107, 109, 123, 135, 136, 142, 148, 149, 151, 154, 155, 156, 159, 164, 166, 169, 170, 171, 173, 181, 182, 189, 191, 195, 196
substitution, 42, 46, 47
substrate, viii, ix, x, 3, 5, 14, 15, 16, 17, 19, 23, 24, 25, 26, 27, 28, 29, 31, 32, 33, 34, 35, 36, 43, 45, 48, 59, 63, 66, 67, 73, 75, 76, 77, 97, 98, 99, 100, 101, 112, 113, 119, 121, 122, 128, 130, 131, 135, 142, 143, 146, 147, 152, 153, 154, 155, 156, 157, 158, 159, 160, 162, 164, 166, 167, 168, 169, 170, 171, 172, 173, 174, 175, 176, 181, 182, 183, 184, 187, 189, 191, 194, 195, 196
substrates, ix, 19, 26, 28, 30, 59, 68, 73, 75, 79, 84, 99, 100, 121, 122, 123, 149, 151, 152, 153, 162, 166, 168, 170, 173, 183, 184, 189, 197
sulfur, 73, 83, 120
sulfur dioxide, 120
Sun, 92, 93, 138
surface area, 75, 85
surface energy, 126
surface layer, 20
surface modification, 97
symmetry, 8, 15, 30, 142
synthesis, vii, viii, ix, 38, 39, 40, 42, 43, 45, 47, 48, 49, 50, 52, 55, 56, 58, 59, 64, 75, 76, 79, 80, 84, 85, 144, 151, 173

T

tangent angle, 145
target, x, 59, 80, 152, 153, 154, 156, 157, 159, 160, 161, 162, 164, 166, 167, 168, 170, 181, 182, 183, 189, 190, 191, 195, 196
techniques, vii, 39, 40, 47, 48, 50, 121, 148, 152, 174
technologies, ix, 141, 142, 182
technology, vii, 1, 3, 14, 34, 36, 37, 40, 47, 48, 49, 50, 62, 67, 142, 143, 144, 146, 149, 159
temperature, viii, 21, 22, 23, 24, 25, 26, 28, 40, 41, 42, 43, 45, 46, 47, 49, 54, 58, 59, 63, 66, 68, 71, 75, 76, 77, 79, 82, 85, 87, 88, 89, 122, 154, 162, 174, 175, 176, 183, 187, 189, 192, 194, 196
temperature annealing, 40, 49, 54
temperature dependence, 54
tension, 75
TEOS, 75, 76
terminals, 75
testing, 26, 31, 36, 146, 162, 173, 174
thermal energy, 26, 69, 144
thermal expansion, 14, 36, 100
thermal stability, viii, ix, 26, 59, 63, 151
thermal treatment, 48, 52, 59
thermodynamic equilibrium, 41, 71
thin film layers, 144
thin films, vii, viii, 37, 70, 73, 75, 76, 79, 84, 85, 95, 96, 97, 98, 99, 100, 101, 102, 104, 105, 107, 108, 109, 110, 111, 112, 113, 114, 115, 116, 144, 146
thrombocyte, 6
tin, viii, x, 63, 68, 181, 183
tin oxide, x, 181, 183
titanium, viii, 36, 63
topology, 21
total energy, 27
toys, 182
tracks, 31, 32, 33, 158, 162, 164, 183, 189
training, 149
trajectory, 6, 15
transformation, 21, 41, 42, 43, 44, 56, 59, 96, 116, 173
transformations, vii, 39, 41, 42
transistor, viii, 64, 183
transition metal, 21
transmission, 51, 87, 102, 148, 184
transmission electron microscopy (TEM), 27, 34, 51, 52, 57, 148, 184, 187
transparency, viii, 63, 66, 68, 96
transport, 7, 8, 14, 15, 16, 17, 19, 37, 68, 129
treatment, 48, 182
trial, 159, 166
tribology, 19
tumors, 36

Copyright © 2012. Nova Science Publishers, Incorporated. All rights reserved.

Diamond-Like Carbon Films, Nova Science Publishers, Incorporated, 2012. ProQuest Ebook Central,

tungsten, 34, 68, 69, 142, 183
tungsten carbide, 34
tunneling, 68, 69
TVA, v, ix, 141, 142, 143, 144, 145, 149
twist, 190, 191, 192, 193, 195

U

uniform, 3, 13, 15, 16, 71, 82, 153, 160, 187, 194, 197
USA, 34, 62, 92, 189
UV irradiation, x, 181, 182
UV light, x, 181, 182, 188, 196

V

vacancies, 41, 45
vacuum, ix, 2, 3, 6, 7, 8, 9, 17, 21, 26, 27, 28, 29, 30, 31, 32, 33, 34, 36, 37, 38, 43, 44, 66, 67, 69, 70, 74, 75, 76, 79, 83, 122, 141, 142, 144, 153, 160, 166, 184
valence, 121
valve, 75, 84
vapor, 3, 28, 29, 31, 48, 97, 121, 122
variations, 100, 102, 104, 107, 110, 114, 158, 159, 171, 194, 196
vector, 9, 10, 12, 14, 15, 16, 19
velocity, 6, 14, 17, 19, 23, 26
velvet, 190
vibration, 25, 103
Vickers hardness, 173

W

watches, 182
water, 1, 2, 7, 99, 112, 120, 126, 145
wave vector, 19
wavelengths, 45, 50, 54, 146, 189
wear, viii, ix, 20, 21, 32, 33, 34, 63, 66, 67, 120, 121, 131, 135, 136, 137, 149, 152, 154, 155, 158, 159, 162, 166, 168, 169, 171, 173, 178
wettability, 149
wetting, 127
wide band gap, 121, 125
windows, 36, 67
workers, 68

X

x-ray diffraction (XRD), 49, 125, 126, 174, 176
x-ray photoelectron spectroscopy (XPS), 3, 4, 29, 51, 55, 56, 57, 80, 81, 83, 174, 176, 184

Y

yield, 5, 57, 156

Copyright © 2012. Nova Science Publishers, Incorporated. All rights reserved.

Diamond-Like Carbon Films, Nova Science Publishers, Incorporated, 2012. ProQuest Ebook Central,